# Comparative analysis of fine and nanoparticles for cellular uptake, oxidative stress and genomic damage in human lung cells

Inaugural Dissertation for the Degree of
Doctor of Natural Science
Dr. rer. nat.

A Thesis Presented to
The Faculty of Biology and Geography
University of Duisburg-Essen
Germany

Presented by
**Kunal Bhattacharya**
from Lucknow, India

March, 2008

Die der folgenden Arbeit zugrunde liegenden Experimente wurden in der Arbeitgruppe ‘In-vitro- und Molekulare Toxikologie’ am Institut für Hygiene und Arbeitsmedizin der Universität Duisburg–Essen, durchgeführt.

1. Gutachter:

2. Gutachter:

3. Gutachter:

Vorsitzender des Prüfungsausschusses:

Tag der mündlichen Prüfung: 1.10.2008

Dedicated to my Parents

The following publications were written during my doctoral tenure at the Institute of Hygiene and Occupational Medicine, University of Duisburg–Essen, and are partially attached to this thesis:

- Dopp, E., Yadav, S., Ansari, F.A., Bhattacharya, K., von Recklinghausen, U., Rauen, U., Rödelsperger, K., Geh, S., Rahman, Q. (2005). ROS-mediated genotoxicity of asbestos-cement in mammalian lung cells in vitro. *Part. Fibre Toxicol.* **2**, 9.

- Bhattacharya, K., Dopp, E., Kakkar, P., Jaffery, F.N., Rahman, I., Jaurand, M.C., Rahman, Q. (2005). Biomarkers in risk assessment of asbestos exposure. *Mutat. Res.* **579**(1-2), 6-21.

- Bhattacharya, K., Alink, G.M., Dopp, E. (2007). Oxidative stress and changed gene expression profiles in fiber-/particle-induced carcinogenesis. *Int. J. Hum. Gen.* **7**(1), 1-21.

- Bhattacharya, K., Cramer, H., Zimmermann, U., Yadav, S., Geh, S., Shi, T., Shokouhi, B., Schins, R., Rahman, Q., Rettenmeier, A.W., Dopp, E. (2008). Cyto- and genotoxic effects of natural and surface-treated ultrafine titanium particles in mammalian cells. *J. Tox. Environ. Health*. (In press)

## Abbreviations

| | |
|---|---|
| µg /cm² | Microgram per centimetre square |
| µm | Micrometer |
| µM | Micromolar |
| $^1O_2$ | Singlet oxygen |
| 8-OHdG | 8-hydroxyl–2-deoxyguanosine |
| AAS | Atomic absorption spectroscopy |
| ANOVA | Analysis of variance |
| Approx. | Approximately |
| APS | Aerodynamic particle sizer |
| As(III) | Arsenic trivalent |
| As(V) | Arsenic pentavalent |
| $Ca^{2+}$ | Calcium |
| cDNA | Complementary desoxyribonucleic acid |
| $CO_2$ | Carbon dioxide |
| CPC | Condensed particle counter |
| cRNA | Complementary ribonucleic acid |
| Cu(II) | Copper divalent |
| DCF | 2',7'-dichlorofluorescein |
| DEP | Diesel exhaust particles |
| DFG | Deutsche forschungsgemeinschaft |
| D-KSFM | Defined keratinocyte serum free medium |
| DMA | Differential mobility analyzer |
| DMPO | 5,5-dimethyl-pyrroline-N-oxide |
| DNA | Desoxyribonucleic acid |
| EDX | Electron dispersive X-ray analysis |
| ELISA | Enzyme linked immunosorbent assay |
| EMEM | Earl's modified Eagle medium |
| EPR | Electron paramagnetic resonance |
| ER | Endoplasmic reticulum |
| FACS | Fluorescence-assisted cell sorting |
| Fe(II) | Iron divalent |
| $Fe_2O_3$ | Ferric oxide |
| FeAsS / $FeAs_{0.9}S_{1.1}$ / $FeAs_{1.1}S_{0.9}$ | Natural arsenopyrite mineral |
| Fig | Figure |
| G | Grams |
| GO | Gene ontology consortium |
| h | Hours |
| $H_2$DCFDA | 2',7'-Dichlorodihydrofluorescein diacetate |
| $H_2O$ | Water |

| | |
|---|---|
| µg /cm² | Microgram per centimetre square |
| $H_2O_2$ | Hydrogen peroxide |
| $H_2SO_4$ | Sulphuric acid |
| HBSS | Hank's buffer saline solution |
| HOCL | Hypochlorous acid |
| HPLC | High pressure liquid chromatography |
| ICP-MS | Inductively coupled plasma mass spectrometry |
| kDa | Kilodalton |
| keV | Kiloelectron volts |
| l/min | Litres per minute |
| LMPA | Low melting Agarose |
| M | Molar |
| $M^2/g$ | Meter square per grams |
| $mg/m^3$ | Milligram per cubic meter |
| $Mg^+$ | Magnesium |
| mins | Minutes |
| mM | Millimolar |
| mRNA | Messenger ribonucleic acid |
| NADPH | Nicotinamide adenine dinucleotide phosphate-oxidase |
| NfκB | Nuclear factor kappa B |
| ng | Nanograms |
| nm | Nanometer |
| O | Oxygen |
| $O_2$ | Molecular dioxygen |
| $O_2^{\bullet-}$ | Superoxide radicals |
| $O_3$ | Ozone |
| $^oC$ | Degree centigrade |
| $OH^\bullet$ | Hydroxyl radicals |
| $ONOO^\bullet$ | Peroxynitrite |
| OSHA | Occupational safety and health administration |
| OTM | Olive tail moment |
| p | Probability Value |
| PAH | Polycyclic aromatic hydrocarbons |
| PBS | Phosphate buffer saline |
| PEL | Permissible exposure limits |
| PHEM | Piperazine-N-bis |
| PI | Propidium iodide |
| PM | Particulate matter |
| $PM_{10}$ | Mass of particles ≤ 10 µm mass median aerodynamic diameter |
| $PM_{2.5}$ | Mass of particles ≤ 2.5 µm mass median aerodynamic diameter |
| ppm | Parts per million |

| | |
|---|---|
| µg /cm² | Microgram per centimetre square |
| PSLT | Poorly soluble, low-toxicity |
| RF | Radiofrequency |
| $RO^{\bullet}$ | Alkoxyl radicals |
| $RO_2^{\bullet}$ | Peroxyl radicals |
| rpm | Rotation per minute |
| RT | Room temperature |
| S | Sulphur |
| sec | Seconds |
| SEM | Scanning electron microscope |
| Si | Silica |
| SMPS | Scanning mobility particle sizer |
| $SO_2$ | Sulphur dioxide |
| TEM | Transmission electron microscopy |
| $TiO_2$ | Titanium dioxide |
| TLV | Threshold limit value |
| TNS | Trypsin neutralizing solution |
| Tris - EDTA | Tris–ethylenediaminetetraacetic acid |
| TWA | Time weighted average |
| UV | Ultra violet |
| W | Watt |
| w/v | Weight by volume |
| WCE | Whole cell extract |
| WTC | World trade centre |
| x g | Time multiplied by gravity |

## CONTENT

# 1 INTRODUCTION

## 1.1 Particle-inflicted health risks

Experience attained through the vast array of investigations related to the impact of exposure to ambient air particulates on the human respiratory system had demonstrated injuries and reactions such as asthma, alveolitis, pneumoconiosis, fibrosis, emphysema and cancer. The earliest reported case for ambient air pollution-related deaths comes from December 1930 when during a 5-day fog episode 63 people died in the Meuse valley, Belgium (Nemery *et al.,* 2001). A modest rise in ambient air particle mass concentration, measured as the mass of particles ≤10 µm mass median aerodynamic diameters ($PM_{10}$), has demonstrated exacerbation of respiratory diseases (Chestnut *et al.,* 1991; Pope III, 1991) and excess of human mortality (Schwartz and Marcus, 1990). Furthermore, the $PM_{10}$ along with $PM_{2.5}$ (particulate size–2.5 µm) have been observed to elevate incidences of cardiovascular diseases and related mortalities (Boldo *et al.,* 2006; Pope III *et al.,* 2002). Most recent evidence of adverse health effects of over-exposure to ambient air particulate matters comes from the survivors of the catastrophic terrorist attack and demolition of the World trade centre towers (WTC) leading to a release of high volume of $PM_{2.5}$-sized particulate matter in the ambient air (Gavett, 2003). WTC health registry had reported that out of 5,226 people caught directly in the dust and debris from the collapsed WTC towers more than half (56.6%) of the survivors were experiencing new or worsening respiratory symptoms and burning sensation in their hearts after the attacks (Brackbill *et al.,* 2006). Several studies had reported an increase in the toxicity of the particles with decrease in their size (Monteiller *et al.,* 2007; Oberdörster *et al.,* 1994).

Scientific and industrial attainments within the last few years had led to discoveries which were far beyond the imagination of mankind half a century ago. Globally, scientists are still discovering the unique properties of daily used materials at sub-micrometer range (a billionth meter) domain. These materials known as ‘nanoparticles’ have found their utility in everyday life of people as components of cosmetics such as toothpastes and sunscreens, sanitary-ware coatings, in medical applications such as biomaterials, sustained cancer drug delivery vehicle, magnetic resonance imaging, etc. (Nel *et al.,* 2006).

However, these interesting developments in the field of nanotechnology had also increased the concerns about the impact of these nanosize particulate matters on human health following occupational and non-occupational exposures. These unique nanoparticles are abundant in the ambient air. But their contribution to the particulate mass is almost negligible (Vinzents *et al.,* 2005). Mechanistically, nanoparticles are important because of the adverse health effects they might cause by their large surface area, chemical composition, capability to induce inflammation and to translocate into the circulation passing through the nasal nerves into the brain (Oberdörster *et al.,* 2004; Kreuter *et al.,* 2002). Inside the lungs they have the capacity to deposit as higher fraction within the alveolar region (Donaldson *et al.,* 2001; Donaldson and Tran, 2002; Nemmar *et al.,* 2002; Nemmar *et al.,* 2004). These nanoparticles can also penetrate through the dermis when there is flexing (Tinkle *et al.,* 2003) or breaking of the epithelial layer of the skin, through the hair follicles and stratum corneum (Warheit *et al.,* 2007) and through the gastrointestinal tract (Bockmann *et al.,* 2000; Kreyling *et al.,* 2002; Semmler *et al.,* 2004) (Fig. 1).

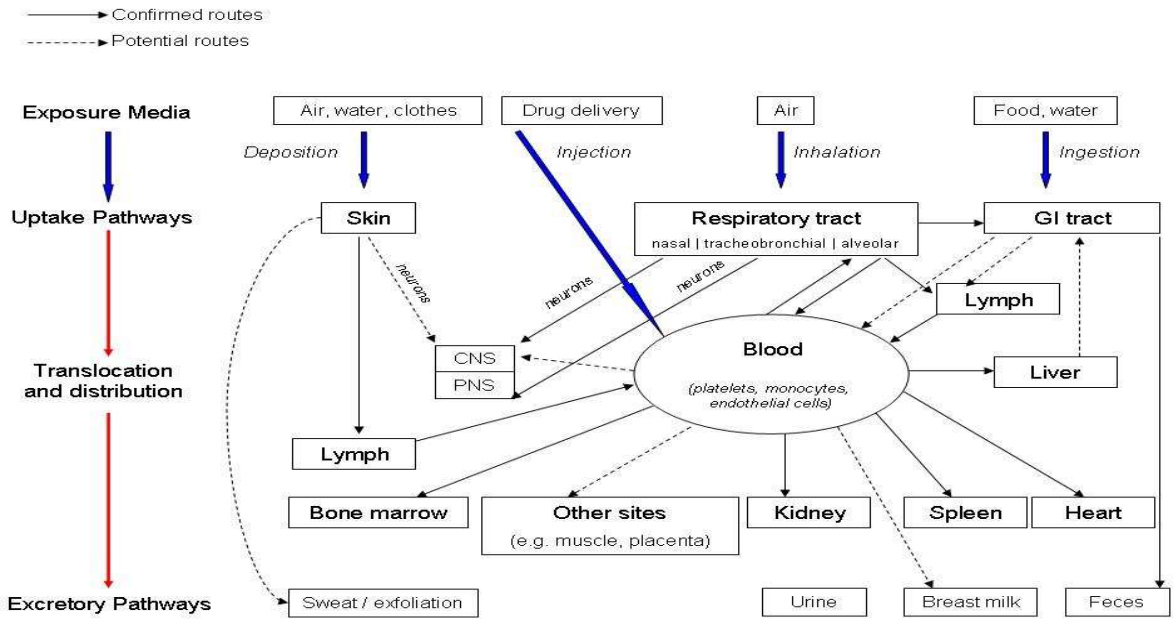


**Figure 1:** Biokinetics of nanoparticles. While many uptake and translocation routes have been demonstrated, others still are hypothetical and need to be investigated. Largely unknown are translocation rates as well as accumulation and retention in critical target sites and their underlying mechanisms. Figure obtained from Oberdörster *et al.* (2005a).

Nanoparticles had also been observed to cause cardiovascular diseases such as thrombosis (Calderon-Garciduenas *et al.,* 2004; Nemmar *et al.,* 2003) and altered heart rates (Campen *et al.,* 2003). Nanoparticles also have the ability to induce prothrombic changes on the endothelial surface of the hepatic microvessels (Khandoga *et al.,* 2004), aggregation of blood platelets (Nemmar *et al.,* 2004) and reaching the liver after their penetration into the circulatory system through gastrointestinal tract (Bockmann *et al.,* 2000).

### 1.2 Ambient air particulate matter characteristics

Particulate matters (PM) with respect to size can range from a few nanometers to several micrometers and are generally described under total suspended particles (TSP) coarse, fine and nanoparticles. The coarse fractions ($PM_{10}$) are relatively large particles with diameters around 2.5–10 µm, mainly derived from soils, crusted materials and through mechanical wear processes, such as drilling, crushing and grinding. The fine fraction ($PM_{2.5}$) is composed of particles with an aerodynamic diameter of approximately 0.1–2.5 µm and includes carbonaceous materials and secondary aerosols. They are mostly derived directly or indirectly from combustion of fossil fuels and automobile engines (Chang *et al.,* 2007; Lee *et al.,* 2007). Nanoparticles ($PM_{0.1}$) have a diameter less than 0.1 µm can be produced artificially from industrial processes (Evans *et al.,* 2007), natural sources and automobile exhausts. These nanoparticles are mainly composed of carbon and salts, mainly ammonium sulphate and ammonium nitrate (Lee *et al.,* 2007).

Most particles obtained from the ambient atmosphere lie in the range from 0.05 to 0.2 µm. However, the relative occurrence of all the three particle fractions at different locations and under diverse air pollution circumstances is largely unknown. Presently, no personal sampler can measure particles with a diameter of less than 0.1 µm (Borm *et al.,* 2006).

Three major properties of the particles that affect their toxicity are–

a) **particle size**
b) **particle surface charge**
c) **particle surface composition**

Particle size - It has been suggested that particle size and number are more important than the mass in producing biological effects. This has been related to the availability of large surface area of the smaller particles. It is estimated that a mass of a single 1 µm size particle is equivalent to the mass of 1000 0.1 µm size particles. While, the surface of the same mass of 0.1 µm particles is 10 times that of a single 1 µm size particle (Salvi *et al.,* 1999).

It had been hypothesized that the small size and high surface area of the nanoparticles have been hypothesized to assist in their direct binding to the proteins. The consequences following the binding of proteins on the nanoparticle surface can be quite different from the events when the same protein binds to larger particles. Nanoparticles bound to proteins may become more portable and through protein metabolism might gain access to sites which larger particles would not be able to reach (Colvin and Kulinowski, 2007; Donaldson *et al.,* 2004). Furthermore, enhanced protein degradation on the large surface area of the nanoparticles can also lead to their functional alterations which would be highly improbable on the relatively smaller surface area of the larger particles (Borm and Kreyling, 2004; Kreyling *et al.,* 2004).

Particle surface charge (Zeta potential) – The physical and chemical property of a material is determined by the type of motion its electrons are allowed to execute. This motion is determined by the space in which the electrons are confined to due to the forces they encounter. Once the electrons are bound in an atom or in a molecule, its motion becomes highly confined and quantisation sets in. In semiconductors, excitation involves the separation of electrons and holes (charge carriers) by distances that encompass a number of molecules or ions making up the lattice. Such a distance is known as Bohr radius, is on a nanometer scale. The minimum energy required to separate the charge carriers is known as the band gap energy. Based on the above presumption when the size of the particle decreases, it reduces

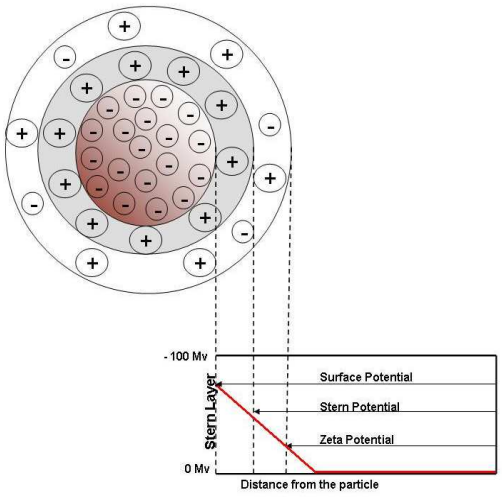


**Figure 2:** Decreasing level of electrical potential around the particle with increasing distance

the space in between the charge carriers of the particles to move and thus additional quantum confinement is imposed on their motion. This leads to an increase in the band gap energy, the electrons kinetic energy and the density of the charge carriers within and at the nanoparticle surface (El-Sayed, 2001). Zeta potential is the electrical potential that exists at the "shear plane" of a particle, at some small distance from its surface (Fig. 2). Zeta potential units are *mV*. The value of 25 mV can be taken as the boundary that separates low-charged surfaces from highly-charged surfaces.

Therefore, as the particles grows smaller, their proportion of atoms on the surface increases relative to the proportion inside its volume (Borm *et al.,* 2006), thus altering the charge on their surface. Higher surface energy make these nanoparticles interact strongly and stick together. It is for this reason that the nanoparticles are never found naked or as individual entities. If nanomaterial building blocks have some parts of their surface sticky and other parts passive and non-sticky, then the random Brownian motion in the fluid can cause the blocks to stick together in defined ways to make larger structures (Borm *et al.,* 2006).

Schins *et al.* (2002a) found that coating pure quartz (DQ12) particles with aluminium lactate or polyvinylpyridine-N-oxide and altering the surface charge effectively reduced their uptake by the lung epithelial cells and the capacity to produce hydroxyl radicals as compared to the uncoated particles.

Particle surface composition - The surface composition of all the particles plays a very important role in enhancing their toxic potential. Particles can react with free radicals and/or antioxidants using the transition elements present on their surface as impurities and by chelating them in the surrounding region. The presence of ferrous / Fe(II) and cuprous / Cu(II) on the surface of a particle is a very crucial factor due to their involvement in the Fenton reaction (Barchowsky and O'Hara, 2003; Donaldson *et al.,* 2003; Fubini and Hubbard, 2003). Other transition metals such as zinc can trigger effects more directly by interacting with cellular proteins (Haase and Maret, 2005; Tal *et al.,* 2006). In particles such as quartz, surface reactivity plays a very important role in the production of reactive oxygen species (primary ROS) along with the overburden they create inside the lungs (Fubini *et al.,* 1990; Duffin *et al.,* 2001).

The role of the surface composition in the generation of reactive oxygen species (ROS) and causing oxidative stress are the most accepted mechanistic paradigm as a reason for the toxicity of these nanoparticles (Donaldson *et al.,* 2004; Oberdörster *et al.,* 2005b). Electron acceptor and donor active sites on the nanoparticles can cause its interaction with molecular dioxygen ($O_2$) by redox–cycling (Nel *et al.,* 2006). Electron capture can lead to formation of superoxide radicals ($O_2^{\bullet-}$), which through dismutation or Fenton chemistry can generate additional ROS (Bhattacharya *et al.,* 2007 – Appendix 11).

### 1.3 Particle-induced health effects based on size distribution

Both the fine and nanoparticles have been found to be associated with the development of adverse health effects (Lipfert and Wyzga, 1997; Schwartz, 1999).

#### Fine airborne particles

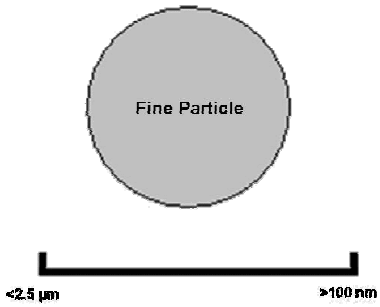


Previous studies performed in humans using radioactivity labelled particles had demonstrated that $PM_{2.5}$ exposure leads to 83% total lung deposition as compared to particles of size >2.5 µm which undergo 31 - 49% deposition. This suggested an inverse relationship between particle size and total lung deposition (Salvi and Holgate, 1999). Based on epidemiological studies it had been estimated that the mortality rate increases by 0.9% and death from a specific respiratory disease by 2.7% per increase of 10 µg/m$^3$ concentration of environmental particles ($PM_{2.5}$) (Pope III *et al.,* 2004).

According to the Deutsche Forschungsgemeinschaft the acceptable concentration of inhalable dust fraction (previously total dust) in a work place should not exceed 4 mg/m³. Similarly, maximum respirable fraction (previously fine particles) in a work place must not exceed the concentration of 1.5 mg/m³ (DGF, 2007).

All types of $PM_{2.5}$ particles tend to injure the lung tissue by causing overburden, subsequently resulting in an impaired alveolar clearance and influx of inflammatory cells (ILSI, 2000; Oberdörster, 2002). Persisting inflammatory reaction can cause a high level of oxidative stress within the surrounding lung tissue, stimulating the production of reactive oxygen species (ROS) also known as ‘Secondary ROS’ (Bhattacharya *et al.,* 2007 – Appendix 11). Damages due to the

presence of high amount of ROS can lead to the formation of tumours and cancers (Schwarze *et al.,* 2006). Individuals with pre-existing diseases, such as chronic obstructive pulmonary disease, asthma and already exhibiting trends of oxidative stress, tend to accumulate more particles in the airways as compared to normal lungs (Luo *et al.,* 2007). This makes them more susceptible to the particle induced inflammatory reactions even at concentrations below overload levels (Bonner, 2007).

Besides creating lung burden particles also tend to act as carriers for toxic substances such as polycyclic aromatic hydrocarbons (PAH) and catalyse their reactions with the biomolecules inside the cellular systems. Hematite fine particles coated with PAH had shown an enhancement in the production of ROS and genotoxicity as compared to the native particle and PAH, individually (Garry *et al.,* 2003; Gosset *et al.,* 2003).

As previously described presence of transition elements also play a very important role in enhancing the toxicity of particles. Epidemiological studies carried out in the Utah valley area of US, demonstrated a variation in the mortality and morbidity rate of people, which was closely correlated with the transient closure of a steel plant and the associated changes in the air pollution (Ghio *et al.,* 2004). Analysis of the ambient air samples collected during the activity of the steel plant from the Utah valley indicated a high metal content (iron, copper, lead, nickel and zinc among others) compared to the samples collected during to the closed time period of the steel plant (Ghio, 2004; Dye *et al.,* 2001 ).

*In vitro* studies performed with lung cells and extracts of the samples collected during different times of the steel plant activity produced significant effects with a high capacity to produce oxygen radical formation and cytokine expression (Frampton *et al.,* 1999). Treatment of the samples with iron chelator demonstrated decrease in the induction of inflammatory cytokines as compared to the untreated samples (Soukup *et al.,* 2000) suggesting a role of the iron content in the particles.

A similar study performed in the Eastern part of Germany demonstrated a high prevalence of respiratory disorders and allergic sensitization in children living near industrial sites compared to children without such exposure (Heinrich *et al.,* 1999). Decline in the pollution level led to a reduction in the respiratory symptoms of the children (Heinrich *et al.,* 2005). Later analysis revealed a higher level of metal and

particle content in the air near the industrial sites compared to the more rural area (Schaumann *et al.,* 2004).

**Nanoparticles**

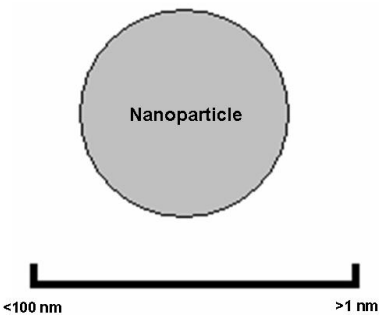


Not much is known about the exact mechanism utilized by the nanoparticles for causing toxicity. Speculations point towards a cumulative effect from the particle size, surface charge and presence of transition elements. There has been much focus on the role of nanoparticles in driving the toxicity of particulate air pollution (Seaton *et al.,* 1995). There is also no threshold limit set for ambient air concentration by the DFG commission.

Ferin *et al.* (1992) had stated that nanoparticles are more potent than $PM_{10}$ at driving inflammation and causing respiratory and cardiovascular health effects. *In vivo* and *in vitro* studies had also confirmed that nanoparticles such as carbon black, polystyrene beads nanoparticles are more toxic and inflammable than fine particles (Li and Karin, 1999; Brown *et al.,* 2000; Stoeger *et al.,* 2006). Epidemiological studies conducted by Pope III *et al.* (2004) had also demonstrated an increase in respiratory problems which were directly proportional to the increase in the number of ambient nanoparticles. Studies had suggested that nanoparticles are not inherently benign and they affect biological behaviour at the cellular, subcellular and protein levels (Colvin*,* 2003; Service, 2004; Nel *et al.,* 2006).

Rejman *et al.* (2004) had reviewed a number of different endocytic pathways for internalization of the nanoparticles, including phagocytosis, macropinocytosis, clathrin-mediated endocytosis and caveolae-mediated endocytosis. He observed that in the non-phagocytic cells (*in vitro*), internalisation of the particles through clathrin-coated pits prevailed for latex microspheres having a size of <200 nm, whereas with increase in size up to 500 nm, caveolae became predominant. The surface charge on the nanoparticle helps it to interact with native proteins and their direct uptake and translocation within the cell through a variety of active protein channels.

Another important aspect in the toxic potential of the nanoparticles is their capability to undergo photocatalytic degradation. Nanoparticles convert to a more toxic substance when they are not stable to photocatalysis and degrade to release

their toxic surface coating or expose their metallic core. Goniat *et al.* (2007) had studied *Escheria coli* bacteria, and observed damage to their desoxyribonucleic acid (DNA) from reactive oxygen species that were being produced from the photocatalytic reaction of titanium dioxide ($TiO_2$) nanoparticles. He had proposed a Fenton reaction for the production of the free radicals from the $TiO_2$ nanoparticles.

Involvement of metals in the generation of oxidative stress, as in the case of diesel soot nanoparticles, has been well established (Ball *et al.,* 2000). Transition elements have been reportedly involved in the redox cycling of quinones, a major organic species involved in the oxidative stress caused by ambient particles (Dellinger *et al.*, 2001; Squadrito *et al.*, 2001). Production of free radicals due to the high surface reactivity of these nanoparticles has been evident from the electron paramagnetic resonance (EPR) spectras obtained by spin-trap techniques (Vallyathan *et al.,* 1992; Schins *et al.,* 2002b; Knaapen *et al.,* 2002b). People exposed to nanoparticles occupationally, or, in parts with the ambient air $PM_{10}$, had been observed with increased inflammatory reactions (Wilson *et al.,* 2002). Chalupa *et al.* (2004) found that ambient air particles of nanosize range contribute more to the health effects in people exposed to them and its efficiency of causing inflammation increasing several folds in individuals having asthma (Duffin *et al.,* 2002).

Transition elements and nanoparticle surface have been observed to act synergistically in producing inflammation (Wilson *et al.,* 2002) and finally result in the pathway of oxidative stress-mediated cytokine gene transcription (Stone *et al.,* 2007). Intracellularly, different nanoparticles including ambient nanoparticles can also target mitochondria directly (Oberdörster *et al.,* 2005; Xiao *et al.*, 2003).

## 1.4 Mechanism of reactive oxygen species (ROS)-induced damage inside the lung tissue

The chemical definition of the ROS is ‘an atom or groups of atoms with one or more unpaired electrons’. ROS include superoxide ($O_2^{\bullet -}$), hydroxyl radicals ($^{\bullet}OH$), peroxyl radicals ($RO_2^{\bullet}$) and alkoxyl radicals ($RO^{\bullet}$). Additionally, the term is also used to describe certain non-radicals that are either oxidizing species or that can easily convert other radicals like ozone ($O_3$), hypochlorous acid (HOCL), peroxynitrite ($ONOO^{\bullet}$), singlet oxygen ($^1O_2$), and hydrogen peroxide ($H_2O_2$).

ROS can be derived from numerous sources *in vivo*. These include auto-oxidation, photochemical and enzymatic reactions of both endogenous compounds and various xenobiotics. The number of enzymes shown to be capable of generating ROS is large and includes cytochromes P450, various oxidases, peroxidases, lipoxygenases and dehydrogenases. The involvement of xenobiotics can be particularly important in the determination of the extent of ROS generated by these enzymes. Major source for the generation of hydroxyl radical (·OH) or the less reactive superoxide radical ($O_2 \cdot^-$) is from the mitochondrial oxidative metabolism and body's immune system cells responding to neutralize foreign substances. Environmental factors such as pollution, radiation, cigarette smoke and herbicides can also generate free radicals, acellularly. Therefore, biological systems are continuously interacting with free radicals arising either from metabolism or from environmental sources (Fig. 3).

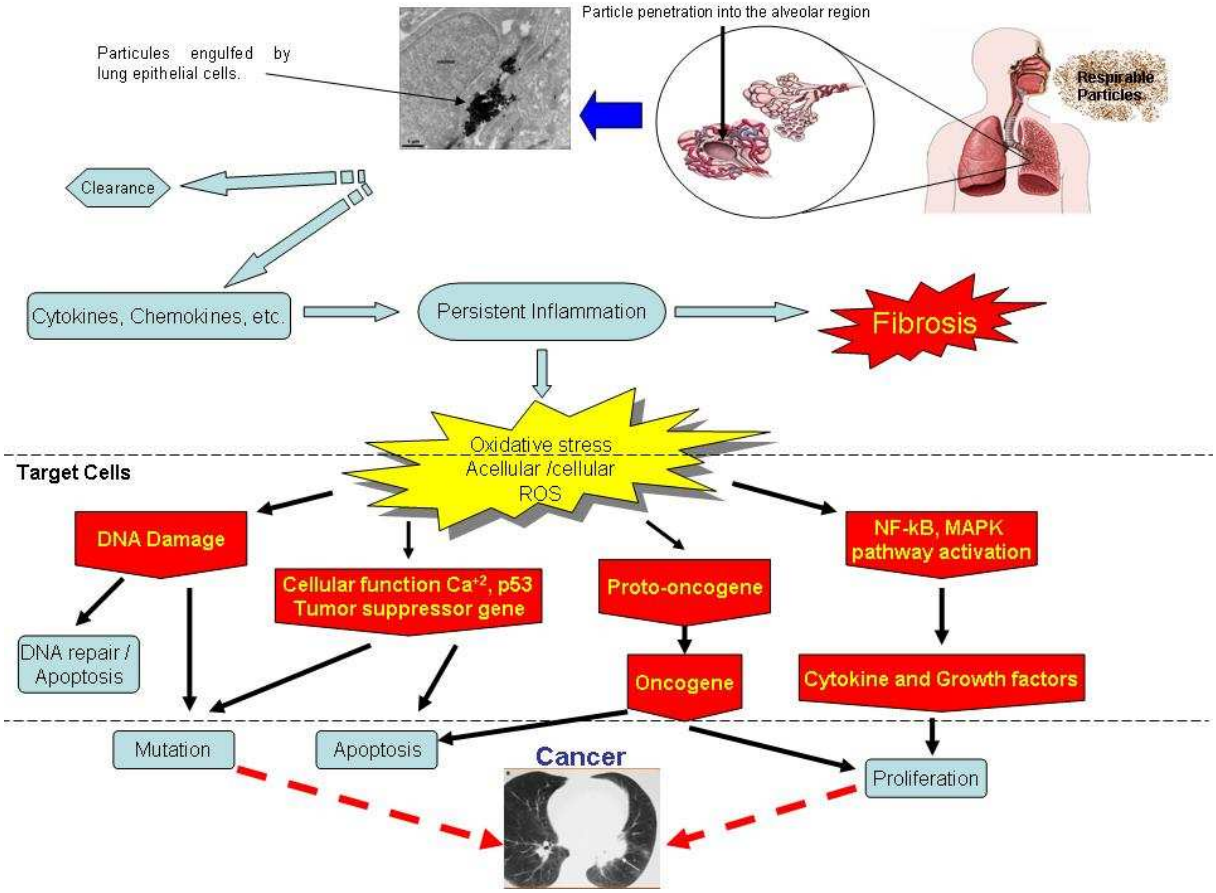


**Figure 3:** Particle induced interaction of reactive oxygen species with target molecules leading to cancer development.

Particulate matters can generate ROS by a) directly causing inflammatory reactions within the cells, b) through the chelation of the transition metals, such as

iron and copper from their surface, and c) interaction between the oxygen donors and acceptors present on the surface of the particles with molecular dioxygens (Nel *et al.,* 2006). These free radicals under excessive quantity can lead to oxidative stress and induction of apoptosis, mutations and cancer (Fig. 4).

Transition elements present on a particle surface can cause the conversion of the hydrogen peroxide ($H_2O_2$) to highly reactive hydroxyl radicals ($OH^{\bullet}$) inside a cellular system (Chance *et al.,* 1979). Fe(II) transition metals participate directly in the Fenton reaction, generating highly reactive hydroxyl radicals (Reaction 1). $O_2^{\bullet-}$ can act as an oxidant and facilitate $OH^{\bullet}$ production from $H_2O_2$ by releasing Fe(II) available from iron-sulphur cluster [4Fe.4S] containing enzymes for the Fenton reaction (Leonard *et al.,* 2004; Liochev *et al.,* 2002 ; Pekarkova *et al.,* 2001). $O_2^{\bullet-}$ has also been found to participate in the Haber-Weiss reaction (Reaction 2) and in the reduction of Fe(III), yielding Fe(II) and oxygen (Reaction 3) (Pekarkova *et al.,* 2001).

$Fe(II) + H_2O_2 \rightarrow Fe(III) + OH^{\bullet} + OH^-$ (Reaction 1)

$O_2^{\bullet-} + H_2O_2 \rightarrow O_2 + OH^{\bullet} + OH^-$ (Reaction 2)

$Fe(III) + O_2^{\bullet-} \rightarrow Fe(II) + O_2$ (Reaction 3)

Half-lives of all the ROS species can range from few minutes ($H_2O_2$), seconds ($RO_2^{\bullet}$) to about a nanosecond ($^{\bullet}OH$). $^{\bullet}OH$ radical is the most reactive ROS and can react with any biological molecule present in its vicinity.

Within every cell several neutralizing factors are present. These are broadly referred to as ‘antioxidants’. Antioxidants can prevent generation of free radicals by a) by chelating free metal ions, b) scavenging free radicals, c) by acting as a free radical chain reaction breakers. They can form a part of the redox antioxidant network and regulate gene expressions. Under normal physiological conditions the ratio between the cellular pro-oxidants and antioxidants is balanced.

Antioxidants had been broadly divided into 2 categories - a) antioxidants acting enzymatically and b) antioxidants acting non-enzymatically. Enzymatically acting antioxidants include catalase, peroxidases, methionine sulphoxide reductase, and superoxide dismutase (SOD). The non-enzymatic antioxidants include mainly small molecules, such as ascorbic acid, glutathione and uric acid. The term ‘oxidative

stress' was first coined by Sies (1986) referring to the imbalance that arises after exposure to oxidants changing the normal redox status of major tissue antioxidants.

Nel *et al.* (2006) had defined three levels of oxidative stress that affects the cell signalling, genetic outcome and the concluding result in different ways (Fig. 4). Triggering of the free radicals as a response to induction of stress in the cell can lead to lipid peroxidation, altered intracellular calcium level triggering signalling agents (stress related proteins) and gene expression (Fig. 1 – Bhattacharya *et al.,* 2007 – Appendix 11).

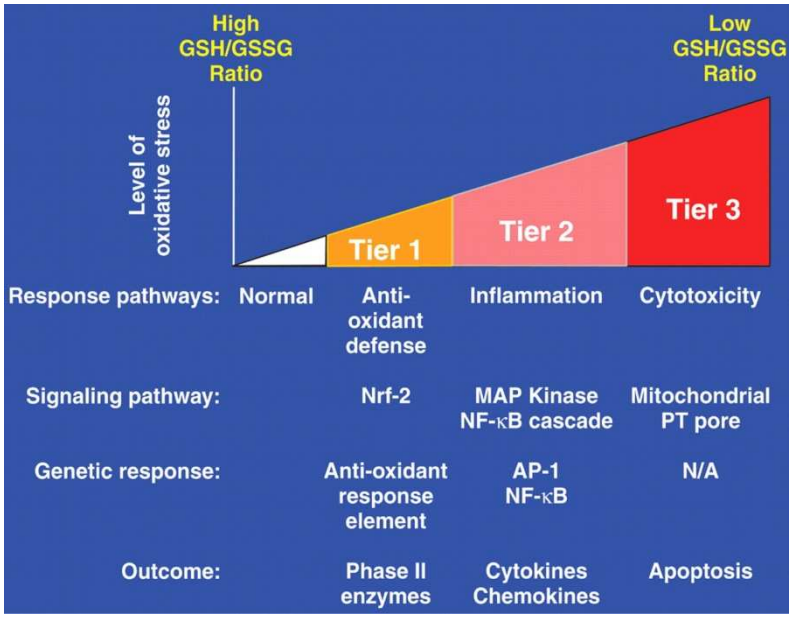


**Figure 4:** Hierarchical oxidative stress model. [Obtained from Nel *et al.* (2006)]. N/A means not applicable.

ROS can react with different biomolecules producing various by-products (lipids - isoprostanes, age pigment, or lipofuscin; proteins - carbonyl and nitrotyrosine derivatives; DNA causing its fragmentation and base oxidations such as 8-hydroxyl–2-deoxyguanosine [8-OHdG]). 8-OHdG are probably the most abundant base oxidation product in DNA having altered base-pairing properties, with adenine replacing cytosine in the daughter strands formed after replication of the affected DNA strand (Collins, 1999). Mineral dusts such as crystalline silica and $TiO_2$ can lead to ROS generation related to their physical dimensions and the surface-based radical generating properties of the particles (Geh *et al.,* 2006b). Modification of the particle surface clearly influence the ROS generation. Prahalad *et al.* (2001) had demonstrated that on exposing different particles to 2'-deoxyguanosine (dG), calf thymus DNA and human airway epithelial cells resulted in oxidative DNA damage

that was mediated by hydroxyl radical generation and was catalysed by water soluble transition metals. Transition metals such as Fe(III) in the absence of $O_2$ can also react directly with DNA producing oxidative DNA adducts (Reaction 4).

$DNA^{\bullet} + Fe(III) \rightarrow DNA_{OX} + Fe(II) + H^{+}$ (Reaction 4)

All redox–based antioxidants appear to interact with each other through the 'antioxidant network' comprised of non-enzymatic and enzymatic reactions. In this way antioxidants are recycled or regenerated by biological reductants. For example, bioflavonoids and polyphenols interact with the vitamin C radicals lengthening its lifetime (Fig. 5).

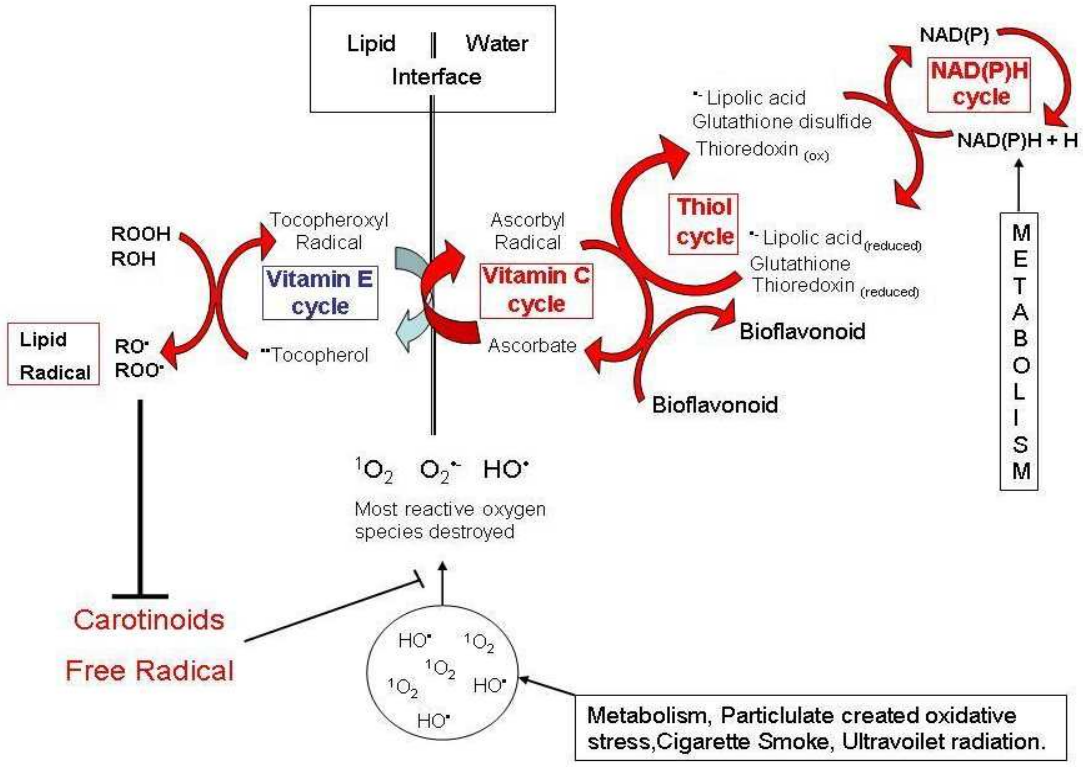


**Figure 5:** Antioxidant networking

Oxidative stress can weaken the strength of the entire endogenous antioxidant system. Redox active antioxidants from food or food supplements bolster this depleting antioxidant defences and help in preventing oxidative damage. Antioxidants can affect the gene expression in two general ways, either by changing the redox status of the cell, or directly by specific interactions with molecular targets in a manner partially independent of their antioxidant / radical–scavenging ability.

Cell signalling pathways are very sensitive to oxidants and cellular redox status changes. Hence, free radicals and antioxidants must regulate gene expression. Activation of the plasma membrane nicotinamide adenine dinucleotide phosphate-oxidase (NADPH oxidase), auto-oxidation of polyphenols or bioflavonoids and mitochondrial metabolism can lead to the generation of hydrogen peroxide ($H_2O_2$), sometimes referred to as a second messenger (Fig. 5). The presence of $H_2O_2$ in the cytosol changes the glutathione / glutathione disulfide ratio (important for cell signalling systems) and provides an oxidizing environment, which is needed for the binding of activated transcription factors such as nuclear factor kappa B (NfκB) and inhibits protein phosphatases, causing hyperphosphorylation of enzymes and proteins of cell regulatory processes. Any or all these events can modulate gene expression thus making the antioxidants critical components of cell growth, development, differentiation and function.

### 1.5 Intrinsic DNA damage repair mechanisms

Cells cannot function properly if DNA damage corrupts the integrity and of the genome do that the accessibility of essential information is no longer available. If the rate of DNA damage is greater than the repairing capacity, the cell can go through senescence (dormancy with no mitotic division), apoptosis (programmed cell death), or mutations leading to tumours and cancers (Fig. 6).

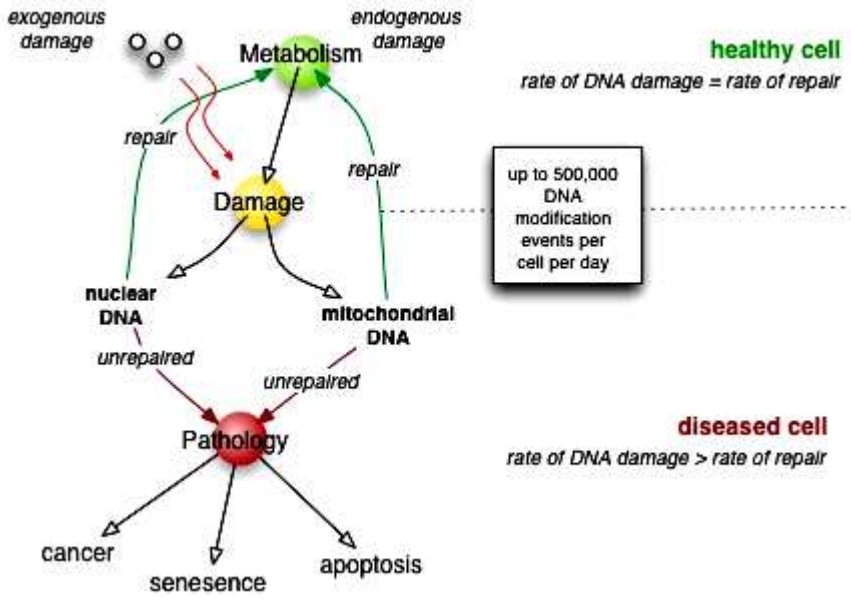


**Figure 6:** DNA damage related consequences

Image source: http://en.wikipedia.org/wiki/Image:Dnarepair1.jpg

A cell can identify the damaged DNA by its altered spacial configuration. Soon after the damage occurs, cell cycle check points are activated and they temporarily halt the cell cycle, giving time to the DNA damage repair mechanism to mend the damaged region. DNA damage check points occur at G1/S and G2/M boundaries (Camman *et al.,* 1994). An intra-S checkpoint also exists. Checkpoints activation is controlled by 2 master kinases ATM and ATR. ATM responds to DNA double-stranded breaks and disrupts chromatin structure (Bakkenist *et al.,* 2003), while ATR primarily responds to stalled replication forks. These kinases phosphorylated downstream targets in a signal transduction cascade, eventually leading to cell cycle arrest. TP53 is an important downstream target of ATM and ATR, as it is required for inducing apoptosis following DNA damage. At the G/S checkpoint TP53 functions by deactivating the CDK2/cyclin E complex. Similarly, at the G2/M checkpoint, TP21 mediates the deactivation of CDK1/ cyclin B complex.

Depending upon the type of damage inflicted on the DNA's double helical structure, a variety of repair mechanisms can get activated to restore the lost information. Under normal conditions if the damage occurs on a single strand the DNA utilizes the complementary / daughter strand to recover the original sequence. However, if the damage occurs on both the strands simultaneously, the cell uses an error prone recovery mechanism known as translesion synthesis.

Single-stranded repair mechanism – A defect in which the other strand is used as a template guide for correction of the damaged strand. For this purpose there is a base excision repair mechanism that removes the damaged nucleotide and replaces it with a new one complementary to the undamaged second nucleotide. It is of mainly two types –

a) Base excision repair – This repair mechanism is one of the major repair pathways and specially active in repair of the nucleotide damages as a result of oxidative insult, alkylation, hydrolysis, or deamination (Risom *et al.,* 2005). The base is removed with glycosylase and ultimately replaced by repair synthesis with DNA ligase. NTHL1 and OGG1 are some of the important enzymes involved in the removal of the oxidized DNA bases (8-OHdG) (Klungland *et al.,* 1999).

b) Mismatch repair – It is responsible for the correction of errors that occur during replication, formation of heteroduplexes and secondary structures such as imperfect palindromes (Bishop *et al.,* 1985). Mismatches can also be the result of deamination of 5-methylcytosine to uracil, which escapes detection and removal by uracil N-glycosylase, resulting in G-T mismatch. Neither direct repair nor excision repair deals with mismatched bases. These processes have no mechanism to distinguish between the correct parental strand and the strand containing the misinformation. The mismatch repair system is a mechanism consisting of enzymes that are responsible for the excision of the defective patch, followed by repair synthesis and ligation (Yu *et al.,* 1999).

Double-stranded repair mechanism – Defects occurring on both the strands simultaneously as a result of oxidative stress are repaired by this mechanism (Demple and Harrison, 1994). Two types of repair mechanisms exist under this category –

a) Non – homologous end joining (NHEJ) – In this a specialized DNA ligase forms a complex with the co-factor XRCC4 and directly joins the two ends (Wilson *et al.,* 1997). To guide an accurate repair, NHEJ relies on short homologous sequences called microhomologies present on the single-stranded tails of the DNA ends to be joined. If those overhangs are compatible, repair is usually accurate (Moore and Haber, 1996; Boulton and Jackson, 1996; Wilson and Lieber, 1999; Budman and Chu, 2005). NHEJ can also induce mutations during repair. Loss of damaged nucleotides at the break site can lead to deletions and joining of mis-matching termini forms translocations. NHEJ is specially important before the cell has replicated its DNA, since there is no template available for repair by homologous recombination. Several NHEJ backup pathways are present in the higher eukaryotes (Wang *et al.,* 2003).

b) Homologous repair – It requires an identical or nearly identical sequence to be used as a template for break repair. The enzymatic machinery responsible for this repair precess is nearly identical to the mechanism responsible for the chromosomal crossover during meiosis. The pathway allows the damaged

chromosome to be repaired using a sister chromatid (available in G2 after DNA replication) or a homologous chromosome as a template. Double-stranded breaks caused by a replication mechanism (topoisomerase) attempting to synthesize across a single-stranded break or unrepaired lesion cause collapse of the replication fork and are typically repaired by recombination

## 1.6 Particles of interest

### 1.6.1 Hematite (fine and nanoparticles)

Deposits of hematite exist in Brazil, Sweden, Germany, Norway, England, Spain, New Zealand and in the Midwest and West of the USA. The sedimentary deposits in the Lake Superior region of the US are the world's largest, producing 0.7 million tones annually.

Hematite is a mineral appearing as metallic gray, red gray or red brown with a metallic lustre; it may even look more like a metal than a mineral when encountered in nature. The name hematite originates from the Greek word for blood, *Haema,* which refers to the dark red colour of the mineral's streak.

Hematite crystals are members of the trigonal system group, which is a subset of the hexagonal system (Fig. 7). The chemical formula of hematite is ferric oxide ($Fe_2O_3$).

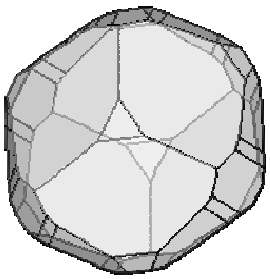

**Figure 7:** Crystalline structure of hematite

***Areas of occupational exposure***

Occupational exposure to hematite particles occur while working in iron mining, crushing, rolling industries and foundries in which metal strips are subjected to agitation with the consequent production of rust and iron scale dust. A survey in the Sheffield steel foundry between 1955 and 1960 revealed that the average prevalence of siderosis among welders and burners in the fettling and grinding shops was 17.6 percent (Gregory, 1970). People working in boiler scaling industries were

involved in the cleaning of fireboxes, flues and water-tubes in enclosed spaces of the boiler of ships, factories and power stations. Indirectly, workers using hematite particles for polishing of silver and steel are also exposed to this specific dust particle.

***Toxicological analysis***

Siderosis may occur alone in workers who pulverize and mix natural mineral pigments of hematite as well as those engaged in their uses (Das *et al.,* 1983). A threshold limit value of 1.5 mg/m$^3$ has been established for ferric oxide fine particles by DFG (2007).

The macroscopic appearance of the pulmonary pleura is marbled in a deep brick red colour after hematite exposure. This is due to their deposition of the iron ore in the pleural lymphatics similar to the black pigmentation seen in the pleura of coal miners. The cut surface of the lungs reveals grey to rust-brown coloured macules (*macula*, a stain or mark) from 1 to 4 mm in diameter which are impalpable and do not stand up from the surface in contrast to silicotic nodules.

In their microscopic appearances the fundamental lesions consist of a perivascular and peribronchiolar aggregation of dark pigmented iron oxide particles, which are present in macrophages and extracellularly in alveolar spaces and walls where they are mostly perivascular. Slight reticulin proliferation may be present but there is no collagenous fibrosis; and intra- and extra-cellular collections are also seen sub-pleurally and infiltrating interlobular septa.

Experiments performed with hematite particles had demonstrated that they were unable to induce tumours in rats (Pott *et al.,* 1974). Similarly, in freshly isolated rat microsomes from short- and long-term exposures hematite fine-sized particles failed to induce any lipid peroxidation (Fontecave *et al.,* 1990). Studies done with coated fine-sized hematite particles verified that these particles only act as enhancers of oxidative stress for other substances such as polycyclic aromatic hydrocarbons within the cells (Garry *et al.,* 2003; Garry *et al.,* 2004).

Hematite nanoparticles are mainly used as the magnetic layer of storage devices in computers, as well as pigments for paints, etc. Recently, Fe(III) nanoparticles are used in nanomedicines for drug targeting cancer cells (Kumar *et al.,* 2007) and for labelling and tracking target cells using imaging techniques like

magnetic resonance (Lewin *et al.,* 2000). Hence, people were exposed to higher amounts of nanoparticles with these techniques than under normal conditions.

Seaton *et al.* (2005) had shown that the commuters and workers of the London underground train system take a high risk of exposure to particulate matter of size <PM 2.5. They found that 64–71% of the dust contained iron oxide. Furthermore, they estimated that on an average a driver of the underground system might be getting exposed to 210 µg/$m^3$ and the station staff to 190 µg/$m^3$ of this dust everyday. In contrast to the fine sized hematite particles, the nanoparticles had been demonstrated to induce toxic effects in growing neuronal cells by reducing their viability and capacity (Pisanic *et al.,* 2007).

### 1.6.2 Arsenopyrite ash particles

The name arsenopyrite, or arsenical pyrites, is derived from the German *arsenikalisk Kies* (King, 2002). Arsenopyrite is the most common mineral containing ferric, arsenic and sulphur. It is the main commercial source of sulphur and arsenic.

It is the principal mineral of the arsenopyrite group, of which there are five recognized members. The group has the general formula FeAsS. The members may be monoclinic or orthorhombic. The chemistry of naturally occurring arsenopyrite varies from $FeAs_{0.9}S_{1.1}$ to $FeAs_{1.1}S_{0.9}$. The ratio of Fe: (As + S) is 1: 2. The variation is due to environment-related changes of temperature and pressure. The structure of arsenopyrite is basically a derivative from the marcasite structural type, in which half of the S is replaced by As. It has been shown that arsenopyrite, although appearing to have orthorhombic symmetry is composed of twinned monoclinic individuals (Fig. 8).

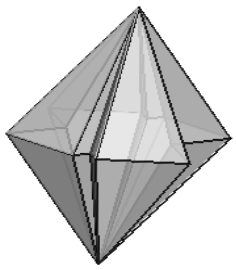

**Figure 8:** Crystalline structure of arsenopyrite

***Areas of occupational exposure***

Arsenopyrite ash particles used here were sulphur industry residues that had been disposed off after the extraction of sulphur dioxide ($SO_2$) from the natural mineral particles. For this purpose it is roasted at very high temperature under aerobic conditions (Fig. 9). The arsenopyrite ash produced from this process is disposed outside on open grounds before getting utilized for other purposes such as in road building and house constructions. The workers involved in moving these industrial residues were exposed during these processes.

***Toxicological analysis***

Not much data are available on the toxicological analysis of these arsenopyrite ash particles. Even though, arsenopyrite as a mineral (FeAsS) has been implicated in the conversion of arsenic content into As(III) via various biological (Dopson *et al.*, 2001) and spontaneous chemical reactions. As(III) is released into the ground water system and causes its contamination. This is a great problem in several developed and developing countries like India, Bangladesh (Joshi *et al.,* 2003), China (Liu *et al.,* 1996) and Finland (Lahermo *et al.,* 1998). There is no threshold limit value established individually for the arsenopyrite ash particles in ambient air by DFG commission.

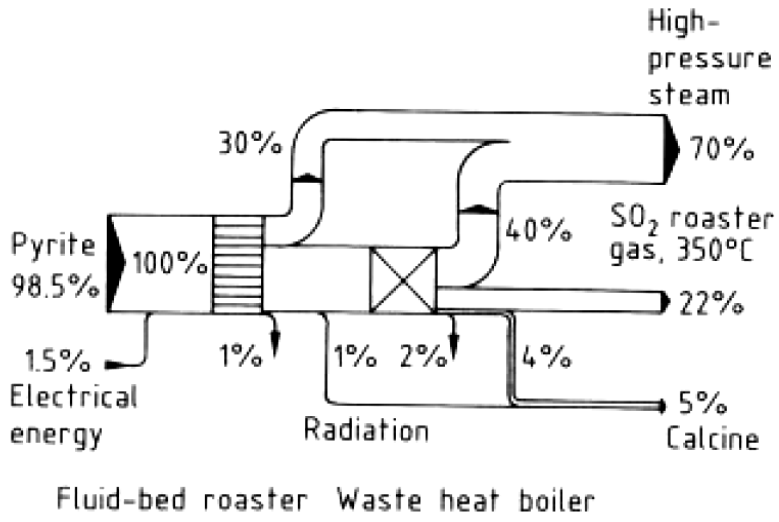


**Figure 9:** Industrial energy flow diagram for the roasting of natural arsenopyrite minerals producing $SO_2$ and arsenopyrite ash residue.

$2FeS_2 \longrightarrow 2FeS + S_2\,(g)$

$\Delta H = +\ 293$ kJ/mol (Reaction 5)

$S_2\,(g) + 2SO_2 \longrightarrow 2SO_2$

$\Delta H = -\ 723$ kJ/mol (Reaction 6)

$2FeS + 3\ O_2 \longrightarrow 2FeO + 2SO_2$

$\Delta H = -\ 948$ kJ/mol (Reaction 7)

$2\ FeO + 0.5\ O_2 \longrightarrow Fe_2O_3$

$\Delta H = -\ 282$ kJ/mol (Reaction 8)

---

$2FeS_2 + 5.5\ O_2 \longrightarrow Fe_2O_3 + 4\ SO_2$

$\Delta H = -\ 282$ kJ/mol (Reaction 9)

### *1.6.3 Titanium dioxide nanoparticles*

Titanium dioxide ($TiO_2$), also known as titanium(IV) oxide or titania, is the naturally occurring oxide of titanium. It has several isoforms of which anatase is the most commercially used type. Anatase consists of a tetragonal crystal system with the crystalline structure varying from typically acute dipyramidal to highly modified obtuse pyramidal or tabular and less commonly to prismatic (Fig. 10).

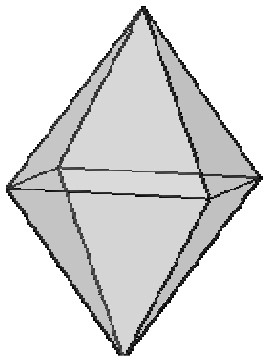

**Figure 10:** Crystalline structure of titanium dioxide

### *Areas of occupational exposure*

No parameter for the average ambient air concentration of $TiO_2$ nanoparticles have been set by any concerned agency. For the finer particles American conference of governmental industrial hygienists (ACGIH) has assigned $TiO_2$ a threshold limit value of 10 mg/m$^3$ (total dust) as a time weighted average for a normal 8 h workday and a 40 h workweek (American Conference of Governmental Industrial Hygienists,

1992). DFG commission (2007) had set the ambient air concentration value for $TiO_2$ fine particles at 1.5 mg/m³.

Occupational exposure to $TiO_2$ nanoparticles can occur during manufacturing / use of these particles as pigments for paints, varnishes, enamels, lacquers and paper coatings to impart whiteness, opacity and brightness. Exposures can also occur from the use in cosmetics such as in sunscreens, dusting powder, ointments and from radioactive decontamination of the skin.

***Toxicological analysis***

Titanium dioxide ($TiO_2$) is considered under the category of poorly soluble, low-toxicity (PSLT) particles (American Conference of Governmental Industrial Hygienists, 1992). The toxicity of the $TiO_2$ nanoparticles had been found to be based on the dosage levels and retention time of the particles within the organs. Recent studies indicate that $TiO_2$ nanoparticles are also toxic to eco-relevant species (i.e., *Escherichia coli*, Daphnia) (Adams *et al.,* 2006) and mammals (Warheit *et al.,* 2006, 2007). Turkez *et al.* (2007) found that $TiO_2$ nanoparticles were able to cause genotoxic effects by causing sister chromatid exchange and micronucleus formation in human white blood cells.

Wang *et al.* (2007) also observed an increase in cytotoxicity, micronucleus formation and genetic mutation on exposing human lymphoblastoid cells to high doses of $TiO_2$ nanoparticles in an *in vitro* culture. Rahman *et al.* (2002) demonstrated an induction of micronucleus and apoptotic bodies in Syrian hamster embryo cells after an exposure to $TiO_2$ nanoparticles. Taira *et al.* (2006) observed an increase in oxidative stress in the macrophage like RAW264 cells leading to an arrest of their cellular proliferation, to a high production of super oxide dismutase and to an increased expression of tumour necrosis factor – alpha. While fine $TiO_2$ particles are generally considered to be inert, their nanosize counterparts can be highly photoreactive in the presence of ultraviolet (UV) light (Serpone *et al.,* 2001). $TiO_2$ nanoparticles can produce $^{\cdot}OH$ radicals, $H_2O_2$ and $O_2^{\cdot-}$ when exposed to UV light (Clechet *et al.,* 1979). Previously, we had studied the effects of exposure to natural anatase and surface modified (vanadium pentoxide-coated) $TiO_2$ nanoparticles in Chinese hamster lung fibroblast cells (V79) *in vitro*. We found no cyto- and genotoxicity induction in the cells after the particle exposure for both short and long term periods in case of the natural anatase $TiO_2$ as compared to the surface-modified

$TiO_2$. The oxidative stress being induced by the natural particles was also very low (statistically insignificant) as compared to the coated $TiO_2$ particles (Bhattacharya *et al.,* 2008 – Appendix 11).

### 1.6.4 Quartz (DQ12) fine particles

Quartz or silicon dioxide ($SiO_2$) is formed from silica and oxygen under conditions of increased heat and pressure. It is the most common mineral found on the surface of the earth occurring crystalline and amorphous forms. A significant component of many igneous, metamorphic and sedimentary rocks, this natural form of silicon dioxide is found in an impressive range of varieties and colours. There are three primary polymorphs: quartz (Fig. 11), tridymite and cristobalite, with quartz being the most commonly found form (Peretz *et al.,* 2006).

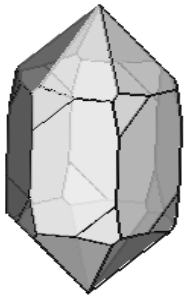

**Figure 11:** Crystalline structure of pure quartz (DQ12).

***Areas of occupational exposure***

Occupational exposure to quartz can occur during the manufacturing of coloured flint, fibreglass and ceramics. Other occupational exposures can occur in agriculture and horticultural industries during its use in the production of soil additives, top dressings, root dressings and composts and in the building industry for brick facing, flooring compounds and screeds together with acoustic thermal and fire proofing insulation boards. According to National Institute for Occupational Safety and Health (NIOSH) an estimated 1.7 million workers in United States are exposed to quartz occupationally (NIOSH, 2002).

***Toxicological analysis***

The International Agency for Research on Cancer (IARC) and the DFG commission had declared crystalline silica as carcinogenic to humans (Group 1) (IARC, 1997; DFG, 2007). Still it is one of the most used and profitable mineral in industry. Occupational exposure to respirable silica is associated with different diseases including reduced lung function, chronic obstructive pulmonary disease and the established pneumoconiosis – silicosis, in various forms (Peretz *et al.,* 2006). Under normal conditions, however, a person is never exposed to the pure form of silica. Inhalation of a silica mixture by rats led to the formation of fibrosis only when the silica content was 20% or more in the mixture (Ross *et al.,* 1962). Similarly, Nagelschmidt (1960) observed an increase in the silicotic changes with massive fibrosis in the lungs of the workers when the dust concentration exceeded 18%. Another study dealing with the occurrence of silicosis and other health effects in workers occupationally exposed to silica dust demonstrated a significant development of diseases (McDonald *et al.,* 2005). One study had further shown that in the case of DQ12 exposure at a constant surface area, particles with an average diameter of 5 to 11.2 µm were more fibrotic than those of size 1 µm after ensuring corresponding deposition and clearance rate (Wiessner *et al.,* 1989).

The surface properties of quartz have been found to play a significant role in causing its toxicity. Surface properties of quartz are associated with ROS formation (Schins *et al.,* 2002b). Studies performed with different surface modifications of the quartz particles using grinding, etching or coating had demonstrated a significant difference in ROS production using the electron paramagnetic resonance technique (Vallyathan *et al.,* 1988; Vallyathan *et al.,* 1991; Fubini *et al.,* 1990, Fubini *et al.,* 1995). Studies carried out with intratracheal instillation of quartz in rats have demonstrated an enhanced formation of 8-OHdG lesions in the lungs providing evidence for the direct involvement of ROS in causing DNA damage (Yamano *et al.,* 1995; Nehls *et al.,* 1997; Seiler *et al.,* 2001).

**Aim of this study**

This study has been designed to analyze and answer several paradigms surrounding the potential toxicity of fine and nanoparticles in human lung cells and also try to elucidate the underlying mechanism utilized by them. Therefore, this study will try to look into and answer the following queries -

- Effect of the different fine and nanoparticles size distribution on their uptake and translocation inside the lung epithelial cells.
- Toxic effects of the particles having the same/different chemical compositions and size distributions, measured by cyto- and genotoxicity assays in lungs epithelial and fibroblast cells *in vitro*.
- Capability of the particles to generate acellular reactive oxygen species following oxidizing and reducing condition treatments, with special emphasis on the Fe(III) content and size distribution of the particles.
- Cellular response to different fine and nanoparticle exposure through the generation of intracellular reactive oxygen species in the epithelial cells.
- Formation of 8-hydroxy-2-deoxyguanosine adducts in the genomic DNA of lung cells due to different fine and nanoparticles exposure and the resulting oxidative stress.
- Up-regulation of DNA damage repair genes and related mechanisms as a response to the genomic damage induced by particles, through oxidative stress.

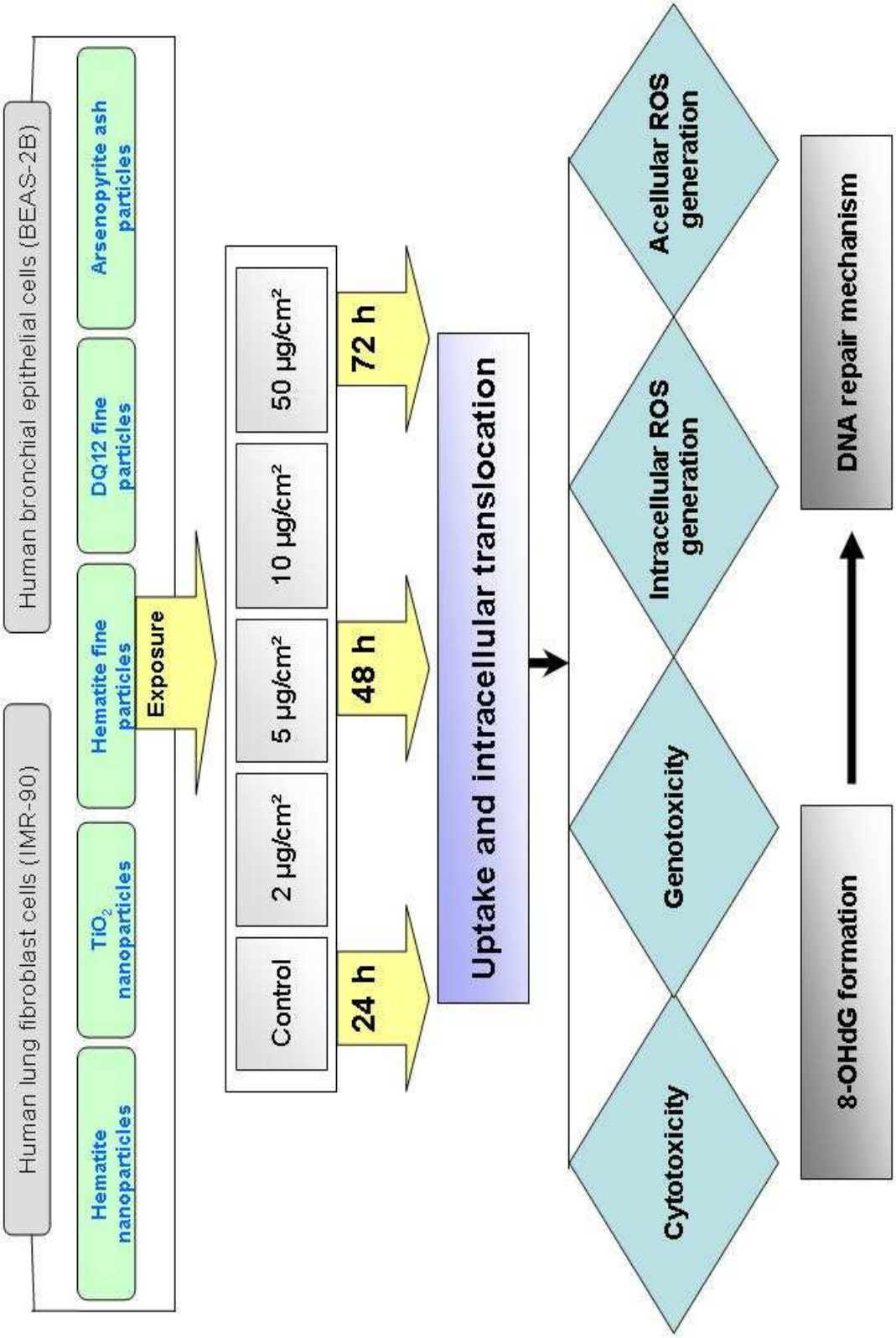
Human lung fibroblast cells (IMR-90)
Human bronchial epithelial cells (BEAS-2B)
Hematite nanoparticles
TiO2 nanoparticles
Hematite fine particles
DQ12 fine particles
Arsenopyrite ash particles
Exposure
Control
2 µg/cm²
5 µg/cm²
10 µg/cm²
50 µg/cm²
24 h
48 h
72 h
Uptake and intracellular translocation
Cytotoxicity
Genotoxicity
Intracellular ROS generation
Acellular ROS generation
8-OHdG formation
DNA repair mechanism

# 2. MATERIALS AND METHODS

## 2.1 Particle source

The hematite fine and nanoparticles were bought from Sigma-Aldrich GmbH. Arsenopyrite ash particles were recieved as a gift from PVS Chemicals Germany GmbH, Kelheim, and sieved through a steel mesh to the required size at the Institute of Energy and Environmental Technology, Duisburg, Germany. DQ12 fine and $TiO_2$ nanoparticles were obtained from Deutsche Montan Technology GmbH and from Degussa GmbH, Germany, respectively.

## 2.2 Cell culture

***Primary human lung fibroblasts (IMR-90)***

The human diploid fibroblast strain IMR-90 was developed by Nichols *et al.* (1977) from the lungs of a 16 weeks old female foetus. The cells were obtained from the American type culture collections (Catalogue no.– CCL-186™) (Figure 12).

Th cells were grown in Earl's Modified Eagle's Medium (EMEM) supplemented with 2 mM glutamine, 1% non-essential amino acids, 10% foetal bovine serum (FBS) and 0.5% gentamycin. The cell cycle varied with conditions of the cells from 1 to 3 days (24 – 72 h).

For passaging, of the cells old medium was removed and the cells were washed with phosphate buffer saline solution (PBS) free from calcium ($Ca^{2+}$) and magnesium ($Mg^{+}$). The cells were then exposed to a low concentration of trypsin (0.25%) for 30 sec followed by incubation for 10 min in 37℃. The cells were then resuspended in the complete medium (EMEM) and counted with a haemocytometer. They were then plated into new culture flasks. The cultures were maintained in humid condition at 37ºC temperature and with 5% $CO_2$.

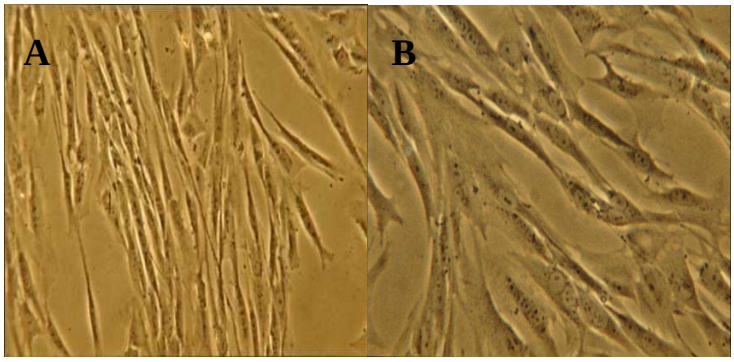


**Figure 12:**
A - Low magnification (x100)
B - High magnification (x400)

***SV-40 virus-transformed human bronchial epithelial cells (BEAS-2B)***

Reddel *et al.* (1995) created a non-tumorigenic immortalized human bronchial epithelial cell line by transforming it with SV40 virus and with an activated c-Ha-ras (EJ-ras) oncogene. The cells were obtained from the European collection of cell cultures (Catalogue no.– 95102433) (Figure 13).

The cells were grown in defined keratinocytes serum free medium (D-KSFM) supplemented with special epithelial cells growth supplements (1 ml) and 0.5% gentamycin. The cell cycle varied with conditions of the cells from 1 to 3 days.

For passaging, old medium was removed and the cells were washed with Hanks buffered saline solution (HBSS). Cells were then exposed to a low concentration of trypsin (0.05%) for time period of 20 sec and followed by incubation for 10 min in 37℃. The cells were further exposed to a trypsin neutralizing solution (TNS) and incubated for another 10 min with TNS at 37℃. The cells were then centrifuged for 5 min (1000 rpm) and the supernatant was removed. Cell pellet was resuspended in D-KSFM and plated into new culture flasks. The cultures were maintained in a humid condition at 37ºC temperature and with 5% $CO_2$.

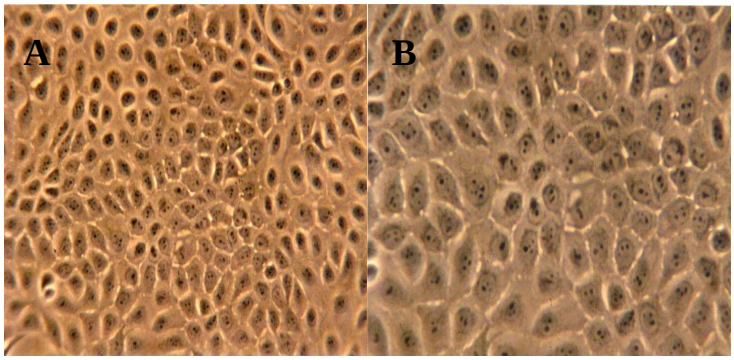


**Figure 13:**
A- Low magnification (x100)
B- High magnification (x400)

**2.3 Particle size analysis**

***Scanning mobility particle sizer (SMPS)***

The SMPS classifies aerosol particles based on their size and counts using a condensation particle counter. A defined charge distribution of the particles was achieved by a bipolar charger ($Kr^{85}$) prior to the classification in the DMA (Differential mobility analyzer). All particles were fractionated on the basis of their electrical mobility by scanning the voltage of the inner cylinder of the DMA. Particle size distribution was calculated using the particle counts per mobility class and the known particle charge distribution. SMPS covered a size range of 14 to 750 nm mobility

diameters with a resolution up to 64 channels per decade with a long DMA (aerosol flow-0.3 l/min, sheath flow-3.0 l/min, scan time-240 sec).

***Aerodynamic particle sizer (APS)***

The APS detects and classifies airborne particles in the range from 0.5 to 20 µm with a resolution of 32 channels per decade. The particle size classification by the APS was based upon their time of flight between two laser beams. The aerosol was drawn through a nozzle and all particles were accelerated according to their aerodynamic mobility, with larger particles being slower than smaller particles.

Size distributions obtained with the SMPS (based on electrical mobility) were converted to aerodynamic particle size distribution using suitable particle densities and after removing the particles from the aerosol droplets generated from distilled water for the final data analysis.

## 2.4 Scanning electron microscopy (SEM) and electron dispersive X-ray analysis (EDX)

SEM creates images by focusing a high-energy beam of electrons onto the surface of a sample and detecting signals from the interaction of the incident electrons with the sample's surface. The types of signals gathered in a SEM can vary and include secondary electrons, characteristic X-rays and back-scattered electrons. In a SEM these signals come not only from the primary beam impinging upon the sample, but also from other interactions within the sample near the surface. SEM is capable of producing high-resolution images of a sample surface in its primary use mode and secondary electron imaging. Due to the manner in which this image is created, SEM images produce a great depth of field yielding characteristic three-dimensional appearance useful for understanding the surface structure of a sample.

Characteristic X-rays are emitted when the primary beam, typically in the range 10-20 keV causes the ejection of inner shell electrons from the sample and are used to tell the elemental composition of the sample. The back-scattered electrons emitted from the sample may be used alone to form an image, or in conjunction with the X-rays characterized for each atomic number, presents clues to the elemental composition of the sample. It is a technique used for identifying the elemental composition of the specimen. The EDX analysis system works as an integrated

feature of a scanning electron microscope (SEM) and cannot operate on its own without the latter (Fig. 14).

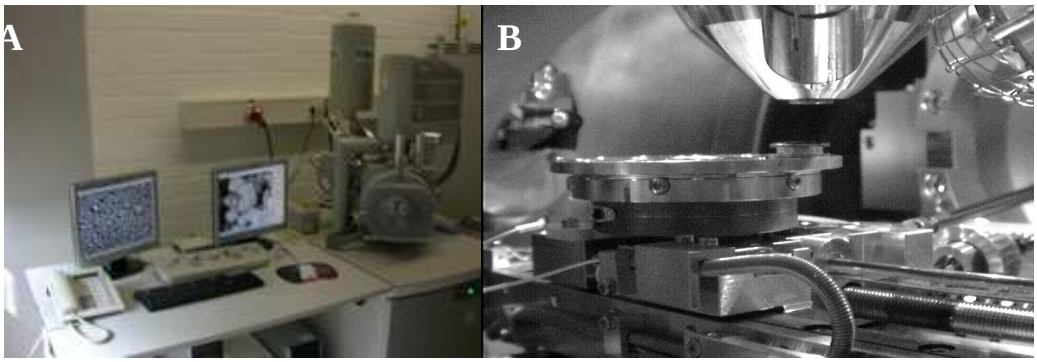


**Figure 14:** Complete setup of the SEM integrated with electron dispersive X-ray analysis (EDX), B- Sample loading stage

For the EDX analysis and imaging dry particle samples were mounted on the stage of the SEM and bombarded with a high-energy electron beam. The resulting X-rays emitted from the samples and images acquired were analyzed with the help of software to detect the individual elements present in the sample, as well as the morphology of particles.

### 2.5 Inductively coupled plasma mass spectrometry (ICP-MS)

ICP-MS instrument consists of concentric tubes located inside a copper coil that is connected to a radiofrequency (RF) generator (Fig. 15). The plasma is generated at the end of the quartz torch via a tesla spark and maintained by using a high frequency electromagnetic field. The RF flowing through the copper coil induces oscillating magnetic fields. Electrons and ions flow at rapid acceleration rates while passing through the oscillating electromagnetic field. These accelerated electrons and ions were further ionized by collision with non-ionized Argon gas (Meyers, 2000).

For the analysis of the arsenopyrite sample, 5 g of powder were added to 50 ml of PBS and incubated on a flatbed shaker (1 cm throw) at 300 rpm RT for (i) 1 h and (ii) 50 h. Following incubation, extracts were filtered (0.45 µm pore) and divided into two 20 ml portions, one of which was adjusted to physiological pH (i.e. pH 7.4) with NaOH (Table 1). These extracts were incubated at room temperature for up to

24 h and analyzed by high pressure liquid chromatography (HPLC) / ICP-MS at 0 h, 1 h, 5 h and 24 h with regard to arsenic speciation and concentration.

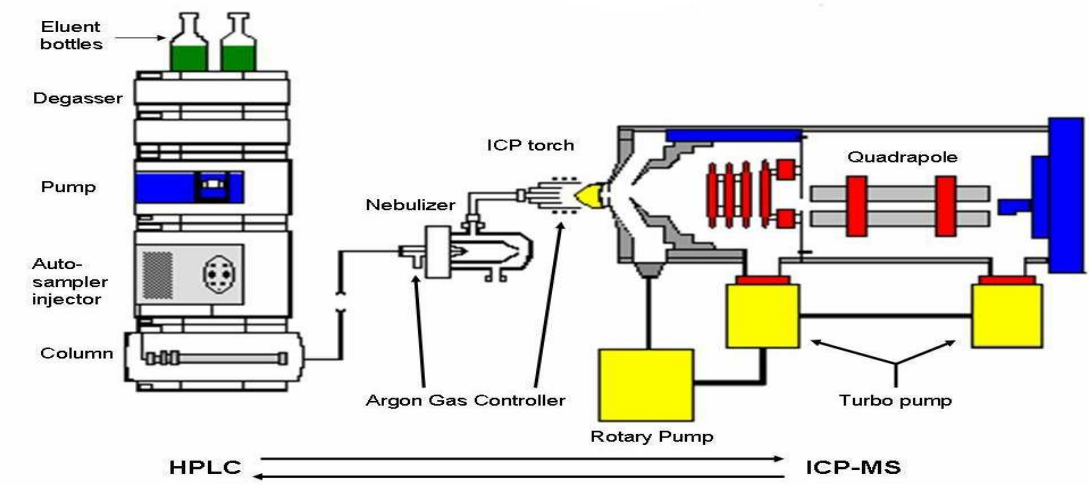


**Figure 15:** Schematic of a typical ICP-MS instrument (modified from original drawing of European Virtual Institute for Speciation Analysis)

**Table 1:** Adjustment of pH of the particle suspension

| Samples | Volume (ml) | Initial pH | Adjusted pH |
|---|---|---|---|
| **1 h extract pH 7.4** | 20 | 6.2 | 7.4 |
| **50 h extract pH 7.4** | 20 | 5.8 | 7.4 |

The HPLC method of Raab *et al.* (2005) was used, i.e. Hamilton PRP-X-100 column, mobile phase 15 mM ammonium carbonate pH 8.0 (= 2 g/l), flow rate 1 ml/min. The injection loop volume was adjusted to 10 µl. The arsenic concentrations in the extracts were determined by inductively coupled plasma-mass spectrometry (ICP-MS). The ICP-MS was operated at 1580 W rf-power, with argon flows of 15 l/min (plasma gas), 0.76 l/min (carrier gas) and 0.41 l/min (auxiliary gas). The outlet of the HPLC was connected directly to the Babington nebulizer and routed through a double-pass Scott-type spray chamber maintained at 2°C. The signals for 34 S (500 ms), for 56 Fe (500 ms) and for 75 As (1000 ms) were monitored. Furthermore, the signal at m/z 77 (500 ms) was monitored in order to control chloride interference. The arsenic standards (0.2 ppm, 0.6 ppm, 1 ppm) of $As_i$(III) ($As_2O_3$) and $As_i$(V)

($Na_2AsHO_4$) were prepared in Seralpure water and diluted to working concentrations in mobile phase and a HPLC/ICP-MS chromatograms was recorded (Fig. 16)

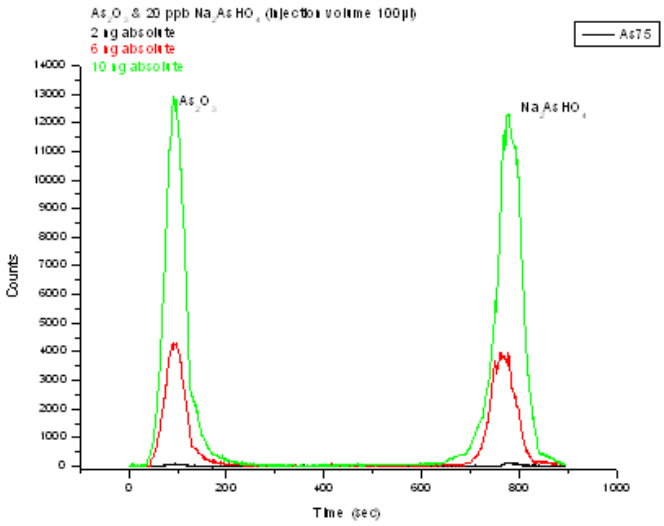


**Figure 16:** Signal detection peaks for $As_2O_3$ and $Na_2AsHO_4$ in HPLC/ ICP-MS analysis

## 2.6 Determination of total iron content in the particles

A spectrophotometric technique was used for analyzing the total iron content of the particles as described by Pyenson *et al.* (1945) with minor modifications specified by the Deutsche industrienorm (DIN: 38 406).

Iron standards were prepared using $FeCl_3$ (Appendix 4 [1]). Sulphuric acid ($H_2SO_4$) was adjusted to a final concentration of 1.84 g/ml at RT. Two millilitres of adjusted $H_2SO_4$ was mixed with required amounts of different standards to convert all of the Fe present to Fe (III). The final volume of these standard solutions was adjusted to 100 ml with MilliQ $H_2O$. Fifty ml of each standard solution were taken into an Erlenmeyer flask and 5 ml of potassium peroxodisulphate were added. This mixture was boiled until approximately 20 ml were left (approx. time – 40 min, temperature – 150$^oC$). Five ml of ammonium acetate (buffer) and 2 ml of hydroxylammonium chloride were added to the remaining mixture to convert all of the Fe(III) to Fe(II), and the final volume was adjusted to 98 ml with MilliQ $H_2O$. Finally, 2 ml of 1,10-phenanthroline chloride were added, and after 15 min absorbance was measured at 510 nm. A standard curve was prepared from a scatter plot having a regression coefficient of more than 99%.

For measuring the total iron content in the particles, 70 mg of each was suspended in 20 ml of $H_2O$. Five ml of aqua regia were added to the suspension and

heated at 70 – 90℃ (not boiling). The solution was evaporated till only 2 ml of final volume were left. Two ml of concentrated $H_2SO_4$ were added to this mixture to convert all of the Fe present to Fe(III) (Reaction 10). Conversion of the solution to a milky white colour was observed. Heating was further continued till the suspension turned to creamy white. Twenty ml of $H_2O$ were added to this precipitate and stirred till a clear solution was obtained. The solution was diluted to a final amount of 0.714 mg / 100 ml. It was filtered through a 0.45 micron filter and to 50 ml of this solution 40 ml of ammonium acetate (buffer) were added. Two millilitres of hydroxylammonium chloride (Reaction 11), each followed by 2 ml of 1,10-phenanthroline chloride (Reaction 12), were added to the solution while stirring. The reaction is shown below. After 15 min the absorbance of the final solution was measured at 510 nm.

$$Fe_2O_3 + 3\ H_2SO_4 \rightarrow Fe_2(SO_4)_3 + 3\ H_2O \qquad \text{(Reaction 10)}$$

$$2\ Fe^{+3} + 2\ NH_2OH + 2\ OH^- \rightarrow 2\ Fe^{+2} + N_2 + 4\ H_2O \qquad \text{(Reaction 11)}$$

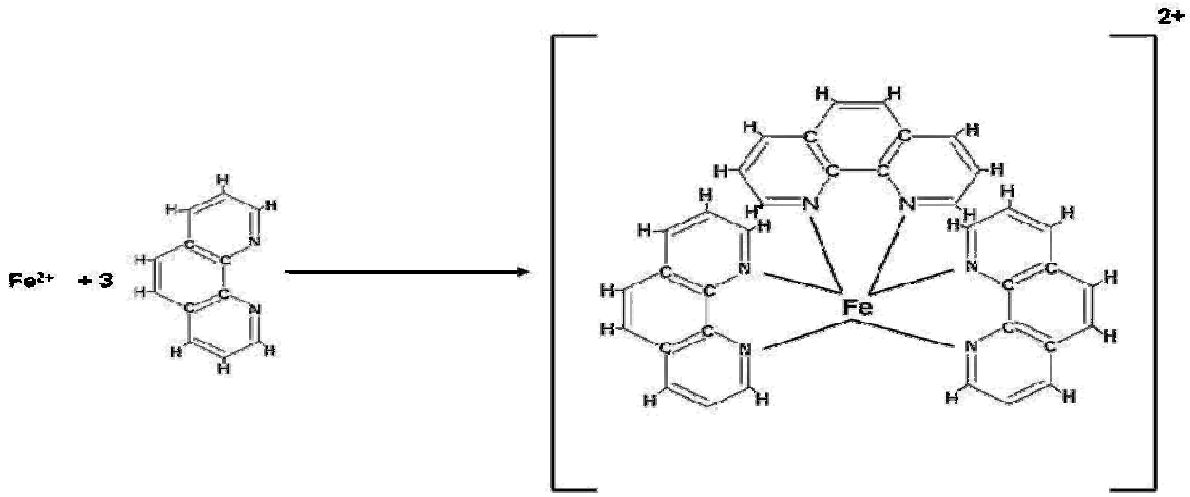


(Reaction 12)

For measuring the absolute amount of Fe(III) present in the samples, 50 mg of the particles were suspended in 100 ml of MilliQ $H_2O$ and stirred for 1 h under anaerobic condition. After 1 h the suspension was filtered through a 0.45-micron filter. Twenty millilitres of filtrate were taken and mixed with 5 ml of ammonium acetate. While stirring 2 ml of hydroxylammonium chloride were added to the solution along with 2 ml of 1,10-phenanthroline chloride. This mixture was still for 15 min, and then the absorption spectra were measured at 510 nm.

## 2.7 Transmission electron microscopy (TEM)

TEM is a microscopy technique whereby a beam of electrons is transmitted through an ultrathin specimen, interacting with the specimen as it passes through. An image is formed from the electrons transmitted through the specimen, magnified and focused by an objective lens. It appears on an imaging screen, a fluorescent screen in most TEMs, or it is detected by a sensor such as a CCD camera.

BEAS-2B cells were plated at 10 millions per 75 $cm^2$ flask and pre-incubated for 24 h prior to the exposure. An exposure to particles was applied thereafter at a concentration of 10 $\mu g/cm^2$ for 48 h. After lapse of the time period all the cells were washed with PBS and trypsinized. They were then fixed in 4% paraformaldehyde and 0.1 % in 0.1 M PHEM buffer (pH 6.9) for 45 min at room temperature followed by a 3 h fixation in 4% paraformaldehyde alone. After 2 washes in 0.1 M PHEM, free aldehyde groups were neutralized by 50 mM glycine in 0.1 M PHEM. The cells were rinsed with PBS, released from the plastic surface with a Teflon edge in PBS containing 1% gelatine and pelleted in Eppendorf tubes. Each pellet was then resuspended in warm 10% gelatine and recentrifuged (Appendix 4 [2]).

After 20 min incubation on ice, gelatine-embedded pellets were released from the tubes and sliced into ~1 $mm^3$ square pieces using a razor blade. On a rotator the blocks were infiltrated in 2.3 M sucrose in PBS at 4℃ overnight and then mounted onto copper pins. All samples were shock-frozen and stored in liquid nitrogen. The mounted samples were trimmed with an Ultracut UCT and a Cryotrim 45° diamond knife at 90℃. Ultra-thin sections of 65 nm thickness were cut using a diamond knife at 120℃, were picked in 2% methyl cellulose / 2.3 M sucrose (1 part / 1 part) and were placed on formvar-coated grids. Remaining gelatine in the samples was removed by putting the grids on PBS for 20 min at 37℃. Cryosections were then washed four times in distilled water and finally contrasted and sealed in 3% uranyl acetate / 2% methyl cellulose (1.5 parts / 8.5 parts). All images were then acquired using a transmission electron microscope.

### 2.8 Trypan blue assay

Trypan blue is a vital dye. The reactivity of Trypan blue is based on the fact that the chromophore is negatively charged and does not interact with the cell unless the membrane is damaged. Therefore, all cells, which exclude the dye, are viable. The cell viability percentage is calculated by the formula

$$\frac{\text{Total number of white cells}}{\text{Total number of white and blue cells counted}} \times 100$$

Approximately, one million cells (80% confluent) were plated and pre-incubated for 24 h prior to the exposure. Before exposing the cells to the particles the old medium was replaced by a fresh one. Then the cells were exposed to the different concentrations of the particles for different time periods. One blank measurement having cells without exposure was taken for each time period as a negative control.

After elapse of the exposure time the media along with the particles were removed. The cells were washed twice with 2 ml of pre-warmed PBS. Then the cells were trypsinized (0.05 % trypsin) for 30 – 45 sec depending upon the type of cell used (IMR-90 / BEAS-2B cells). After trypsinization, the cells were incubated for 10 – 15 min in 37℃. They were resuspended in 300 µl of PBS mixed with Trypan blue (0.5%) in a 1:1 ratio and kept in an incubator for 4 min at 37ºC and in humid condition. Immediately after the lapse of incubation time the cells are counted with a haemocytometer, and the cell viability was calculated.

All the experiments were conducted in duplicates and the statistical significance was analyzed with one-way ANOVA, using the Holm–Sidak method and pair-wise analysis. A $p < 0.05$ was considered to be statistically significant effect.

### 2.9 Fluorescence assisted cell sorting (FACS)

Cell death can either be the consequence of a passive, degenerative process known as necrosis, or an active process known as apoptosis. Apoptosis is a highly regulated pathway that has significant importance in normal developmental

processes as well as many diseases. It ultimately leads to death, which can take from some minutes to many hours. ‘Early stages’ of apoptosis are characterized by changes in the mitochondrial membrane potential and cell membrane asymmetry with the transportation of phosphatidylserine to the membrane surface (but does not increase the cell permeability). ‘Late apoptosis’ stages are characterized by DNA fragmentation and loss of cell membrane permeability. In general, apoptotic cells shrink (and can break up into smaller apoptotic bodies) and have characteristic nuclear changes that are visible under an electron microscope.

Necrosis, unlike apoptosis, is not a step-wise, controlled phenomenon. It is caused by a disruption of the cell by physical or chemical means. ‘Primary necrotic’ cells have relatively normal looking nuclei but their cell membranes (and organelle membranes) are fragmented. With time, ‘secondary necrosis’ takes place during which there is organelle (including nuclear) disruption and swelling of the cells, eventually bursting them (and releasing inflammation inducers).

The FACS analysis technique is based upon the detection of the events of apoptosis and necrosis depending upon the changes induced in the plasma membrane of the cells. The analysis is done using two different dyes – annexin V and propidium iodide. Annexin V is a 35 kDa $Ca^{2+}$ dependent phospholipids-binding protein that has a high affinity for phosphatidylserine. This dye therefore binds to the cells going through the apoptotic phase and exposing this protein. However, annexin V cannot differentiate between early and late apoptosis, as in both these stages phosphatidylserine is on the outer side of the membrane. Therefore, a second dye propidium iodide (PI) is used to detect the late apoptosis. PI is an intercalating agent and a fluorescent molecule with a molecular mass of 67 kDa. It is generally, impermeable through the cell membrane and, therefore, excluded from viable cells. In the late apoptotic cell, the membrane looses its impermeability leading a quick penetration by the PI inside the cell.

PI and annexin V also help in the detection of the primary and secondary stages of necrosis. During the primary stage of necrosis, even though the cell looses its membrane permeability, its symmetry does not change therefore, only PI is able to penetrate the cell membrane and stain the nucleus. During the secondary stage of necrosis, the cell membrane and organelles completely disintegrate, getting stained by both annexin V and PI in this process. Therefore, based on the differential staining

of the cells apoptosis and its different stages along with necrosis can be easily distinguished. The early apoptotic cells are detected when they are annexin V positive and PI negative, primary necrotic cells are annexin V negative and PI positive and the late apoptotic / secondary necrotic cells are both annexin V and PI positive (Fig. 17).

For the analysis, IMR-90 cells were plated and pre-incubated for 24 h before the exposure. The cells were exposed to hematite nanoparticles along with hematite fine, DQ12 fine and arsenopyrite ash particles, respectively at a concentration of 10 µg/cm$^2$ and for a time period of 24 h. After the lapse of the exposure time the cells were washed with PBS, trypsinized and then treated with 2.5 µl PI and 5 µl annexin V-FITC for 30 mins at 4ºC in the dark. Later, the cells were fixed with 1% paraformaldehyde overnight to remove the background fluorescence level from the cells itself. Finally, the cells were analyzed using FACS Calibur, and the results were analyzed by CELL-Quest software.

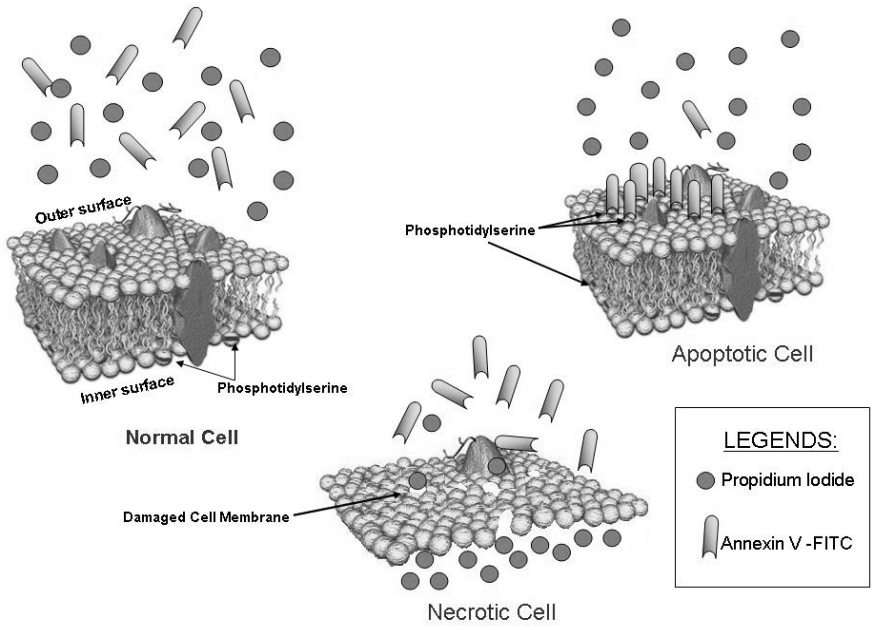


**Figure 17:** Interaction of the annexin V-FITC and propidium iodide with normal, apoptotic and necrotic cells.

Statistical analysis was performed by comparing the values obtained from the exposed cells with negative control cells. Student's t-test was performed, and a p of <0.05% was considered significant.

## 2.10 Alkaline comet assay

Alkaline comet assay, also known as the 'single cell gel electrophoresis' (SCGE), is a sensitive and rapid technique for quantifying and analyzing DNA damage in individual cells such as double- and single-strand breaks and alkali-labile sites in the living cells (Collins, 2004). The Swedish researchers Östling and Johansson developed this technique in 1984 (Ostling *et al.*, 1984). Singh *et al.* (1988) later modified this technique as the alkaline comet assay. The resulting image that is obtained resembles a 'comet' with a distinct head and tail. The head is composed of intact DNA, while the tail consists of damaged (single-stranded or double-stranded breaks) or fragments of DNA (Fig. 18).

For the analysis by the comet assay, individual cells are embedded in a thin agarose gel on a microscope slide. All cellular proteins were then removed from the cells by lysing. The genomic DNA is allowed to unwind under alkaline/neutral conditions. Following the unwinding, the DNA undergoes electrophoresis, allowing the broken DNA fragments or damaged DNA to migrate away from the nucleus. After staining with a DNA-specific fluorescent dye, the gel is read for the amount of fluorescence in head and tail and the length of tail. The extent of DNA liberated from the head of the comet is directly proportional to the amount of DNA damage.

The olive tail moment (OTM) is one of the most exploited parameters calculated as a product of two factors: the percentage of DNA in the tail (tail percentage DNA) and the distance between the intensity centroids of the head (head mean) and the tail (tail mean) along the x-axis of the comet. It is calculated by the formula –

$$OTM = \frac{(\text{tail mean} - \text{head mean}) \times \text{tail percentage DNA}}{100}$$

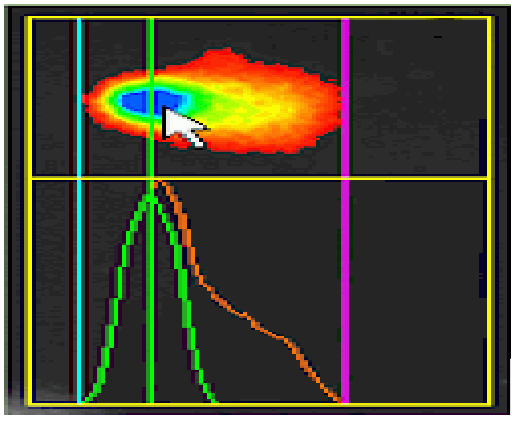

**Figure 18:** Screenshot of a Comet.

For the experiment, approx. one million cells were plated and pre-incubated 24 h before starting the exposure. The old medium was replaced by fresh one, and the cells were exposed to different concentrations of the particles for different time intervals. After lapse of the exposure time, cells were washed with PBS, trypsinized and counted using a haemocytometer. 0.75 % of low melting agarose (LMPA) was melted at 75℃ for and then pre-cooled to 37℃ foll owed by 15,000 cells suspended in it. An eight-well chamber is fixed onto a Gelbond™ film and ~45 µl cell suspension in LMPA is spread in one well. The LMPA was allowed to solidify for 5 min at 4℃, and then the chamber was removed carefully. The Gelbond™ was covered with a freshly prepared and pre-cooled lysis buffer and left at 4℃ overnight. On the next day, the Gelbond™ film was washed with aqua bidest and incubated for 15 min in a freshly prepared alkaline electrophoresis solution (RT; pH 12.7) for DNA unwinding (Appendix 4 [3]). Electrophoresis was run for 10–15 mins under conditions – 300 mA, 1.5 V/cm at 4℃. After completion of the electropho resis run time, the Gelbond™ film was treated with neutralisation solution (RT) for 30 min. The Gelbond™ film was then suspended in absolute $CH_3COOH$ for 2 h to dehydrate the LMPA gel. Gels were stored over night at 4℃ to let them dry completely and stored in the dark at 4 ℃ until stained with SYBR-Green nucleic acid stain. For staining the gels were covered with the dye for 20 min, rinsed with aqua bidest and put on a microscope slide.

Image analysis was performed using ‘Comet Assay IV’ software and Leica microscope attached to a CCD camera. Values of the OTM were automatically calculated by the software. All experiments were carried out twice in duplicate, and the statistical analysis was done using Student’s t-test.

### 2.11 Electron paramagnetic resonance (EPR)

The electron paramagnetic resonance (EPR) spectroscopy technique is used for studying chemical species having one or more unpaired electrons and a short life-span, such as free radicals or inorganic complexes possessing a transition metal ion. The basic physical concepts of EPR are based on the fact that an electron is a charged particle, which spins around its axis causing it to act like a tiny bar magnet. Technically, this property of the electron is known as a magnetic moment. The EPR measures this spin of the electrons using a spin trap such as 5,5-dimethyl-1-

pyrroline-N-oxide (DMPO), which forms a stable product (spin adduct) after reacting with the free radical.

DMPO reacts directly with the hydroxyl radicals ($OH^{\bullet}$) forming the product DMPO–OH (Reaction 13) or the decomposition of DMPO–OOH (Reaction 14), having a half-life of approximately 1 min in neutral media.

$DMPO + OH^{\bullet} \rightarrow DMPO–OH^{\bullet}$ (Reaction 13)

$DMPO + O_2^{\bullet -} + H_2O \rightarrow DMPO–OOH + DMPO–OH^{\bullet}$ (Reaction 14)

The generation of the hydroxyl radical by the particles (hematite fine, hematite ultrafine, arsenopyrite ash, DQ12 and $TiO_2$) at concentrations of 10 µg/cm$^2$ and 50 µg/cm$^2$ were measured with EPR under the following conditions:

1. treatment of the particles with $H_2O_2$
2. after treatment of the particles with ascorbic acid and $H_2O_2$
3. after treatment of the particles with whole cell extract and $H_2O_2$

**1. Treatment of the particles with $H_2O_2$**

The particles were suspended in a petri dish at a concentration of 50 µg/cm$^2$ and in the presence of 50 µl of 1M as DMPO spin trap (Appendix 4 [4]) and 120 mM $H_2O_2$. Dd$H_2O$ was used as negative control. The suspension was incubated for 1 h at 37ºC in a $CO_2$ incubator and the suspension was filtered through a 0.45 µm Acrodisc syringe filter. The filtrate was immediately transferred to a capillary and measured with an EPR spectrometer.

**2. After treatment of the particles with ascorbic acid and $H_2O_2$**

The particles were suspended in a petri dish at concentrations of 10 and 50 µg/cm$^2$, respectively in the presence of ascorbic acid (concentration – 2 µg/ml) followed by the addition of 50 µl of 1M DMPO spin trap (Appendix 4 [4]) and 120 mM $H_2O_2$. Dd$H_2O$ was used as negative control. The suspension was incubated for 1 h at 37º C in a $CO_2$ incubator and before measurement was filtered through a 0.45 µm Acrodisc syringe filter. The filtrate was immediately transferred to a capillary and measured with an EPR spectrometer.

**3. After treatment of the particles with whole cell extract (WCE) and $H_2O_2$**

The WCE was prepared with the BEAS-2B cells grown in the 175 $cm^2$ flask following the protocol of Wang *et al.* (2005). Approximately, one hundred million cells were taken for the preparation of the WCE. The cells were trypsinized, collected and washed with cold PBS one time. They were centrifuged at 1500 rpm for 5 min at 4°C. The cell pellet was then washed and suspended in a hypotonic buffer. The cells were freeze-fractured by quick freezing at minus -80°C (liquid nitrogen) and thawing at 37°C in a water bath (about 2 min) for three times. Precaution was taken to completely submerge tubes containing the cells into liquid nitrogen, because it snap-freezes them and then the tube was immediately put into a 37℃ water bath to thaw it. Subsequently, the mixture was incubated at 4°C for 30 min on a rotating platform in KCl at a concentration of 500 mM and then centrifuged (14,000 rpm) at 4°C for 40 min, then the supernatant was removed and frozen at -20°C.

Final concentration of the protein in WCE was measured using the Bradford method (Dye – Coomassive Blue G-250 in acidic solution) and following the company protocol (Bio-Rad Protein Assay). In short, protein standards of 500 µg/ml, 400 µg/ml, 300 µg/ml, 250 µg/ml, 200 µg/ml, 100 µg/ml and 50 µg/ml were prepared. 10 µl of these standards and the probes were mixed with 200 µl of the dye reagent and mixed for 15 min at room temperature. Measurement was taken using a plate reader at 570 nm absorbance. A standard curve was drawn from the standard measurements using which the amount of protein in the WCE was determined to be approx. 450 µg/ml (Appendix 4 [4]– Fig. 46).

The particles were suspended in a Petri dish at concentrations of 10 and 50 µg/$cm^2$, respectively along with 250 µl of WCE followed by the addition of 50 µl of 1M DMPO as spin trap (Appendix 4 [4]) and 120 mM $H_2O_2$. Dd$H_2O$ was used as negative control. The suspension was incubated for 1 h at 37º C in a $CO_2$ incubator and the suspension was filtered through a 0.45 µm Acrodisc syringe filter. The filtrate was immediately transferred to a capillary and measured with an EPR spectrometer.

All the EPR spectra measurements were recorded at RT and the instrument was set to: magnetic field 3360 G, sweep width 100 G, scan time 30 sec, modulation amplitude 1975 G, receiver gain 1000. Quantification was done by accumulation of three different spectra each averaging three different scans. All four peaks were the

amplitude. Outcomes were expressed as the total amplitude in arbitrary units (EPR units) (Shi *et al.*, 2003).

### 2.12 2',7'- Dichlorodihydrofluorescein diacetate ($H_2$DCFDA)

2',7'-dichlorodihydrofluorescein diacetate ($H_2$DCFDA) is a fluorogenic probe commonly used to detect intracellular generation of reactive oxygen species (ROS). This principle behind the detection of ROS using this dye is based upon the initial de-acetylation of $H_2$DCFDA by cellular esterase forming the oxidant-sensitive compound, 2',7'-dichlorodihydrofluorescein ($H_2$DCF). $H_2$DCF reacts rapidly with ROS, generating the highly fluorescent 2',7'-dichlorofluorescein (DCF) (Bass *et al.*, 1983). After excitation of DCF at 485 nm, the level of fluorescence emitted is measured at 535 nm. An increased fluorescence level is an indication of an increased amount of ROS. Desferoxamine was used as a chelating agent to observe reduction in intracellular ROS generation. This metal chelator forms complexes predominantly with Fe(II) ions resulting in the formation of ferrioxamine. Chelation occurs on a 1:1 molar basis, so that 1 g desferoxamine theoretically can bind to 85 mg ferric iron.

For experiment one million cells were plated in a 12.5 $cm^2$ flask and pre-incubated for 24 h. The old media was then replaced by a fresh one and the cells were exposed to the particles at different concentrations for different time intervals. Metal chelator desferoxamine treatment was given to the cells at the final concentration of 100 µM concurrent to the particle exposures. After the lapse of exposure time cells were washed and suspended in 3 ml of PBS. They were exposed to a working solution of $H_2$DCFDA at the final concentration of 10 µM for 20 min and incubated at 37℃. The PBS and the dye were then re moved, and the cells were trypsinized with a low concentration of trypsin (0.05 %) and reincubated for 10 min. Finally, 200 µl of PBS/ HBSS were transferred into the culture flask and the cells were resuspended in it. This suspension was taken into a 96-well plate and immediately measured with an enzyme-linked immunosorbent assay (ELISA) plate reader set at an excitation wavelength of 485 nm and an emission wavelength of 535 nm.

For the analysis of the effects from transition elements (if present on the surface of the particles) in the generation of intracellular ROS, the metal chelator desferoxamine was added to the cells at a final concentration of 100 µM, concurrent

to the particle exposure. All the other parameters of the experiment were kept the same as had been mentioned previously.

All experiments were performed twice in duplicates, and for statistical analysis Student's t-test was applied.

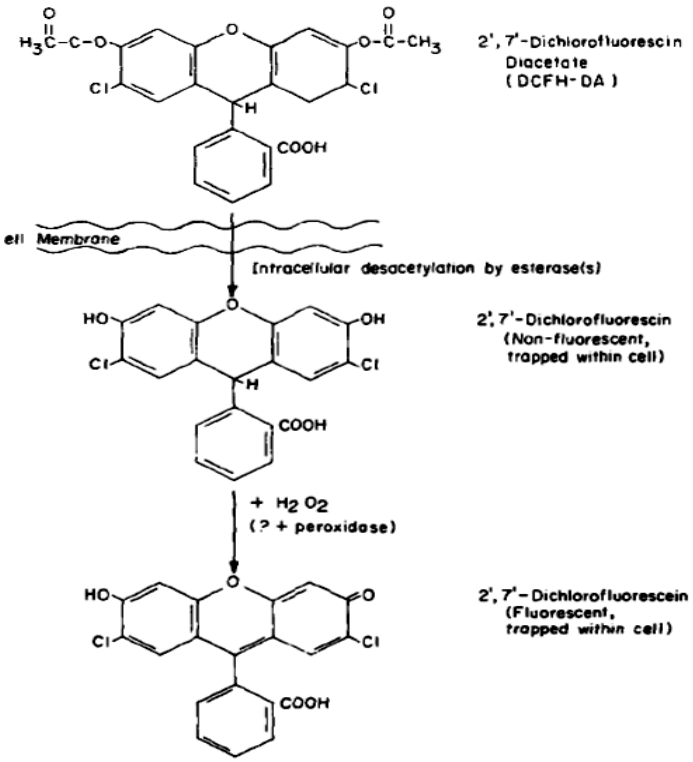


**Figure 19:** Chemical reaction of 2',7'-dichlorodihydrofluorescein diacetate intracellularly (Bass *et al.*, 1983)

## 2.13 8-Hydroxyl-2-deoxyguanosine (8-OHdG) detection by the enzyme-linked immunosorbent assay (ELISA) technique

Free radicals have an affinity to damage the DNA bases leading to their modifications. Of these, 8-OHdG with a hydroxyl group at the eight position of guanine is formed easily and abundantly by oxidative stress (Yamamoto *et al.*, 1992) (Fig. 20). Therefore, 8-OHdG had been used as an oxidative stress marker. During DNA synthesis, 8-OHdG can mismatch with adenine (A) instead of cytosine (C), causing the conversion (GC → AT) of the guanine (G) and cytosine (C) into adenine (A) and thymidine (T) and finally mutagenesis or carcinogenesis.

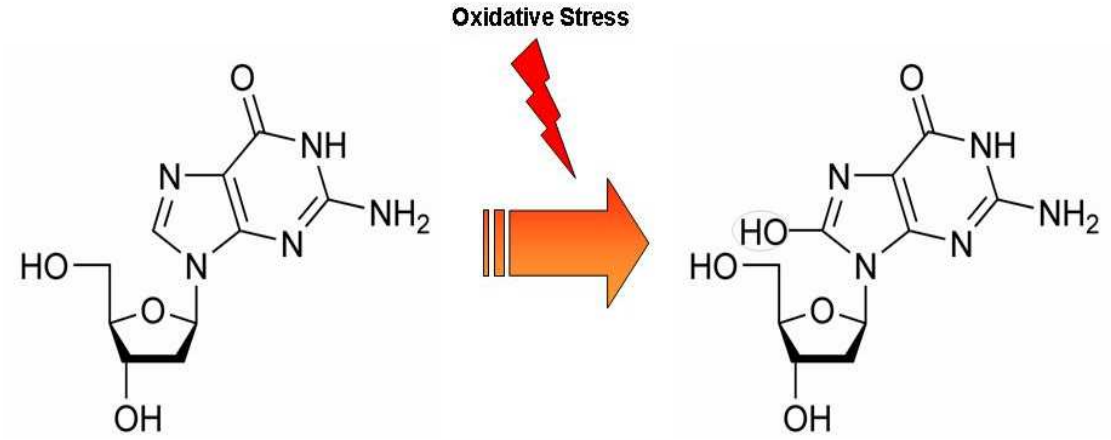


**Figure 20:** Structure of 8-hydroxyl-2-deoxyguanine.

The protocol used for the isolation of DNA from the IMR-90 cells without the formation of 8-OHdG adducts was adopted from the work of Helbock *et al.* (1998). Two million cells were plated and incubated in a 25 $cm^2$ flask and pre-incubated for 24 h, followed by exposure to the particles (hematite and $TiO_2$ nanoparticles and hematite, DQ12 fine and arsenopyrite ash particles) at concentrations of 5 and 10 µg/cm² for a period of 24 h. At the lapse of time period the cells were washed with luke-warm PBS and trypsinized. They were further incubated for 10 min by 37℃ and collected by centrifugation in 1 ml of PBS. The cell pellet was separated from the supernatant and resuspended in 500 µl of cell lysis solution followed by centrifugation at 10,000 x g for 20 sec. The supernatant with the cell debris was removed, and the pellet formed from the nuclei was treated once more with cell lysis solution followed by centrifugation. The cell nuclei pellet was resuspended in 200 µl of enzyme reaction buffer with 4 µg of RNAse A and incubated for 10 min at 37ºC. 10 µl of proteinase K (739 µg/ml) was added to this solution and re-incubated at 37ºC for 1 h with mixing at regular intervals. 300 µl of sodium iodide solution was added to the solution and mixed gently. It was followed by the addition of 500 µl of 100% 2-propanol, gently mixing it by inverting the tube several times. The solution was centrifuged at 10000 x g for 10 min, and the supernatant was removed. The precipitate was mixed with 1 ml of 2-propanol 40 % (w/v) at a temperature of -80ºC and centrifuged at 10000 x g for 5 min. One ml of ethanol 70 % (w/v) was added to the precipitate and the sample was centrifuged for 5 min. The precipitate was vaccuum dried for 3 mins and resuspended in 100 µl of Tris-EDTA buffer.

To check the purity of the DNA and its final concentration in suspension, absorbance of the DNA solution was measured at 260 and 280 nm, respectively.

| Purity of DNA = absorbance at 260 nm : absorbance at 280 nm |
|---|

The ratio obtained from the above formula demonstrated by pure DNA typically should be between 1.8 and 1.85.

For the concentration of DNA in Tris-EDTA buffer the absorbance was measured at 260 nm and calculated by the formula -

| Concentration of DNA = absorbance at 260 nm x 50 µg/ml x dilution rate |
|---|

For the measurement of 8-OHdG using an ELISA kit 200 µg of DNA extract were suspended in 135 µl of $H_2O$. 15 µl of 200 mM sodium iodide and 6 units of nuclease-P1 were then added to the DNA solution and incubated for 30 min to 1 h at 37ºC after argon substitution.

15 µl of 1 M Tris-HCl buffer (pH 7.4) and 2 units of alkaline phosphatase were added to the solution and incubated for 30 min – 1 h at 37ºC after argon substitution. To remove all macromolecules and enzymes the hydrolysates were filtered through Millipore microcon YM-10 at 14000 rpm for 10 min.

For ELISA following the protocol of company all the buffers were brought to room temperature. 50 µl of the standards (0.5 ng/ml, 2 ng/ml, 8 ng/ml, 20 ng/ml, 80 ng/ml, and 200 ng/ml) and the DNA samples of the exposed cells were applied onto the wells. The 50 µl primary antibody was applied to the wells followed by shaking and kept overnight (4ºC) after sealing it with an adhesive strip. On the next day the solution in the well was thrown away followed by removal of the residue by tapping onto absorbent towels several times. The assay plates were then washed with 250 µl of wash buffer 3 times. One hundred µl of the secondary antibody was then added to the wells and the assay plate was sealed tightly with an adhesive tape and incubated for 1 h (room temperature). After the lapse of time the washing steps followed to remove the excess primary antibodies was followed. One hundred µl of chromatic solution (3,3,5,5-tetramethyl-benzidine) were added to the wells followed by incubation for 15 min RT in dark. The chromatic solution had changed to blue colour.

The reaction was stopped by adding 100 µl of a reaction terminating solution (2M $H_2SO_4$) to the wells, and the absorbance was measured at 450 nm (reference wavelength – 620 nm). The standard curve was used to determine the amount of 8-OHdG present in the samples.

### 2.14 Microarray analysis

With certain exceptions, every cell of the body contains a full set of chromosomes and identical genes. Only a fraction of these genes are expressed at a certain time. 'Gene expression' is the term used to describe the transcription of the information contained within the DNA (the repository of genetic information) into messenger ribonucleic acid (mRNA) molecules that are then translated into the proteins to perform most of the critical functions of cells.

The kinds and amounts of mRNA produced by a cell provide an insight into how the cell responds to its changing needs. Microarray is used to analyze this information by creating complementary DNA (cDNA) libraries out of the expressed mRNAs and which are then converted to complementary RNA (cRNA) hybridized with special fluorescent dyes. These cRNAs are detected with different nucleic acid probes chemically printed onto a substrate / chip, which can be made out of glass, nylon or quartz and analyzed using special microarray software. The analysis consists of 2 parts: a) basic fluorescence intensity quality detection and background reduction, b) conversion of each spot into gene information and calculation of the fold up and down regulation by comparing the samples with control values.

For this assay 10 million IMR-90 cells were exposed to different particles (hematite fine and nanoparticles; arsenopyrite ash and Gypsum) at the concentration of 10 µg/cm$^2$ for 48 h. After the lapse of the time period the cells were washed to remove media and particles, trypsinized and treated with ice cold PBS. The cells were frozen at -20ºC stepwise and stored until further analysis.

Isolation of the total RNA was performed with 'Array Grade Total RNA-Isolation-Kit' from Superarray. In short, the frozen cells were thawed and taken into RNAse-free centrifuge tube and centrifuged at 1000 rpm for 5 min. The supernatant was removed and the pellet was resuspended in 350 µl of cell lysis buffer. Using a filter column the suspension was recentrifuged at 12000 rpm for 5 min and the supernatant was collected. Total RNA was precipitated with 70% ethanol and this

precipitate was separated from the ethanol by centrifugation. Salts from the RNA precipitate were removed by using a desalting buffer and centrifugation step. RNA was then washed with 3 respective wash buffers and centrifuged each time. Total RNA was eluted in 50 µl of RNAse free $H_2O$.

For measuring the quality and quantity of total RNA, 1 µl of RNA suspension was dissolved in 49 µl of Tris-EDTA buffer (pH 8.0) and the absorbance was recorded at 230, 260 and 280 nm. For determining the quality following ratios were analyzed:

i. 260 / 280 nm = 2.0

ii. 260 / 230 nm = 1.7

For measuring the quantity:

$A_{260}$ x 40 x 50 (dilution factor) = sample concentration (µg/ml)

'Dilution factor' is the ratio of solute (DNA) to solvent (Tris – EDTA) (1:50)

The samples were frozen at -20℃ till further analysis. cRNA was produced using the 'TrueLabeling-PicoAMP™ kit from Superarray and post-labelled with Cy3 and Cy5 dyes. For hybridization and microarray analysis the 'Oligo GEArray System' for DNA damage signalling in *Homo sapiens* from Superarray was used. The array membrane was soaked in deionized water as a prehybridization step, followed by adding the GEAhyb hybridization solution, heated to 60℃ after removing the deionized water and hybridized in an oven at 60℃ for 1 to 2 h with slow and continuous agitation. For preparing a hybridization mix, 2 µg of biotin-labelled cRNA target were then added to 0.75 ml of pre-warmed GEAhyb hybridization solution and kept at 60℃. This hybridization mix containing the labelled cRNA target is then added to the hybridization tube containing the membrane after removing the old hybridization buffer and is then hybridized overnight at 60℃ with continuous but slow agitation. On the next day the target hybridization mix from the hybridization tube was removed and stored at -20℃ for future use. The hybridized membrane was washed with wash-buffers and then treated for chemiluminescent detection. At RT 2 ml of GEAblocking solution Q at 37℃ were added to the hybridization tube containing the hybridized membrane and incubated for 40 min at RT. Later, the GEAblocking

solution-Q was discarded and the membrane wad treated with 2 ml of diluted AP-SA Buffer followed by further incubation. The membrane was finally washed four times with 4 ml 1X wash-buffer and rinsed with Oligo GEArray followed by 3 ml Buffer-G (supplied with the kit) and treated with 1 ml of CDP-Star chemiluminescent substrate. The tube was then rotated at room temperature in the hybridization oven for 2 to 5 min, and then the membrane was placed into a plastic sheet protector without any bubbles and the image acquisition was completed. The image analysis was performed using a specially designed web-based and completely integrated 'GEArray Expression Analysis Suite' from Superarray to do the data analysis.

The genes functions were classified according to the 'Human Genome Organisation' defined by 'Gene Ontology Consortium' (GO) (Bammler *et al.*, 2005) based upon the molecular function and involvement in biological processes. Only the up-regulated genes were analyzed for the detection of the probable DNA damages incurred by the cells on particle exposures.

# 3. RESULTS

## 3.1 Chemical and physical analysis of the particles

### 3.1.1 Particle size analysis

Hematite nanoparticles were found to have a size distribution of <100 nm = 39.6%, 100–500 nm = 60.3%, and >500 nm = 0.1%; hematite fine particles had a size distribution of 100-<500 nm = 23%, and 500 nm-2.5 µm = 77%; arsenopyrite ash particles had a size distribution of <100 nm = 37%, 100-<500 nm = 58%, 500 nm–2.5 µm = 0.3%, and 2.5 µm-<5 µm = 5% and finally, DQ12 fine had a size distribution of 100-<500 nm = 3% and 500 nm–2.5 µm = 95% (Fig. 21).

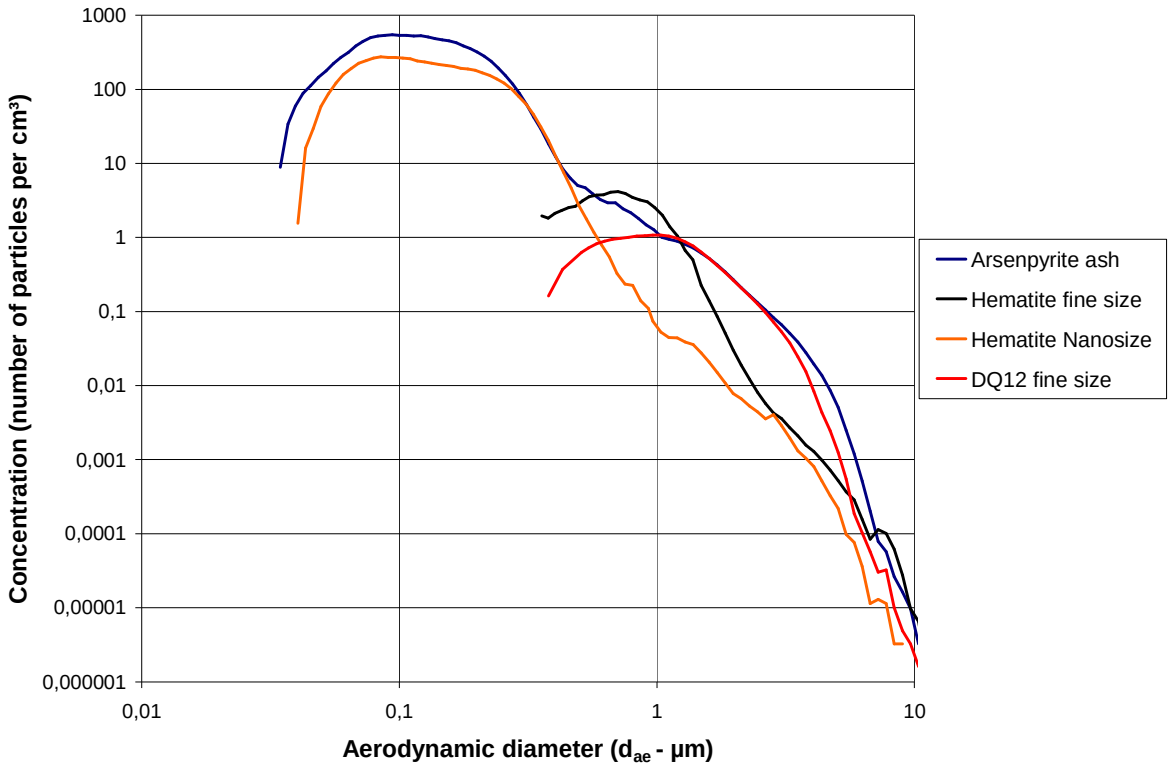


**Figure 21:** Graphical presentation of particle size distribution of the different particles

### 3.1.2 Morphological and elemental analysis of the particles by SEM and EDX

Depending upon the size distribution all particles were divided into the category of 'Nanoparticles' and 'Fine particles'.

#### 3.1.2.1 Nanoparticles

***Hematite***

Morphologically, these particles were found to be spherical in shape and size of these particles based on the scale provided in the SEM image indicated them to be under 100 nm diameter range (Fig. 22).

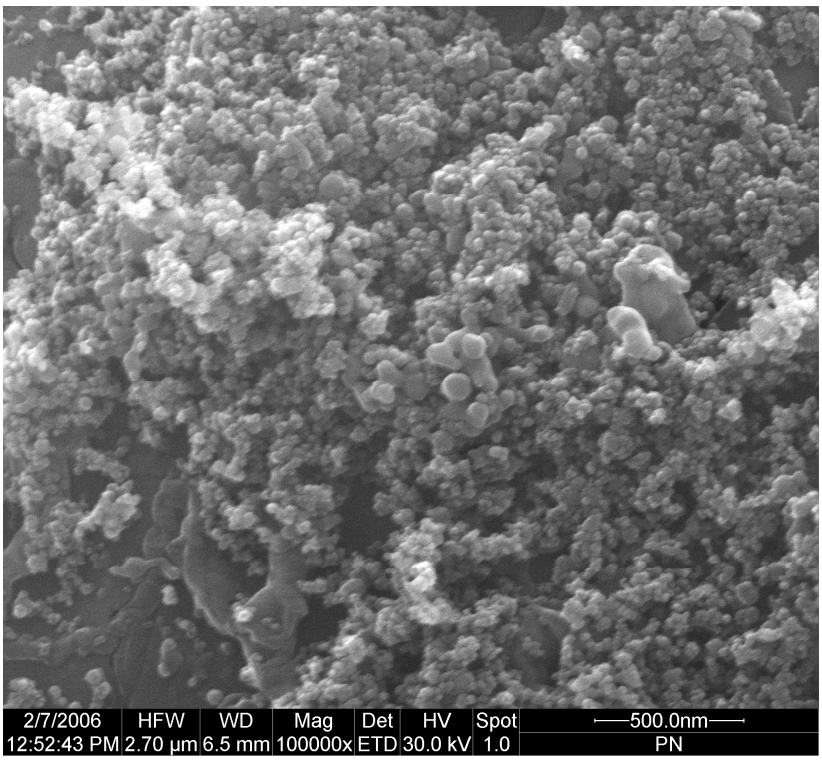


**Figure 22:** Scanning electron microscopic image of hematite nanoparticles

The elemental composition of the hematite nanoparticles obtained by EDX spectra analysis (Fig. 23) demonstrated that the particles contained 78.7% iron (Fe) and 21.3% oxygen (O) (Table 2). These nanoparticles were found free of any transition element.

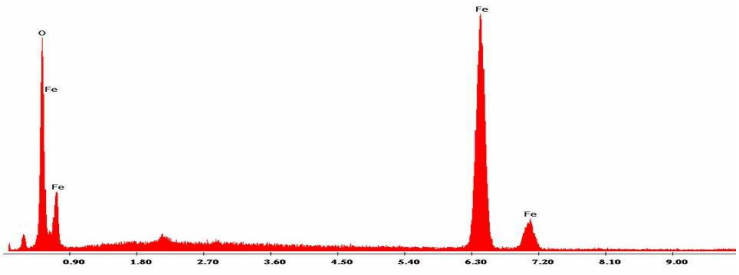


**Figure 23:** Spectra obtained by electron dispersive X-ray analysis of hematite nanoparticles

***Titanium dioxide ($TiO_2$)***

$TiO_2$ were found to be morphologically similar to the hematite nanoparticles as revealed by SEM. The obtained image also demonstrated that the majority of the nanoparticles were under the size range of 100 nm (Fig. 24).

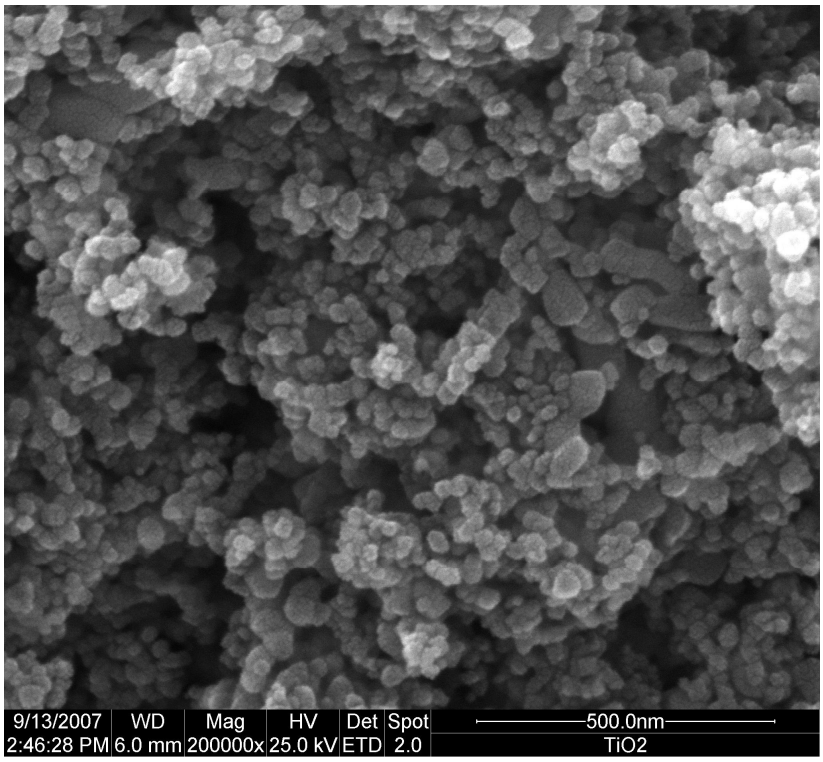


**Figure 24:** Scanning electron microscopic image of titanium dioxide particles

EDX spectra analysis (Fig. 25) revealed that the $TiO_2$ nanoparticles contained 56% titanium (Ti), 41% O and 3% carbon (C) elements (Table 2). An insignificant amount of carbon was also detected in the $TiO_2$ nanoparticles.

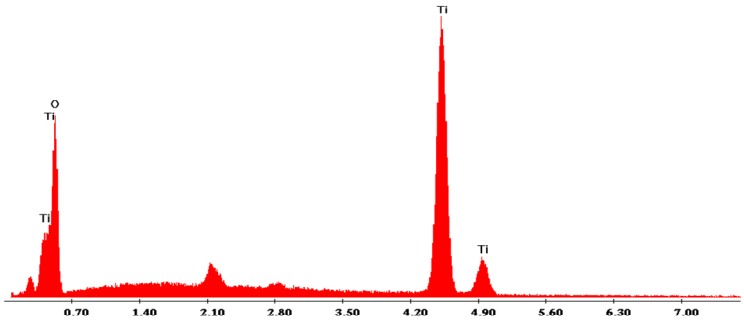


**Figure 25:** Spectra obtained from electron dispersive X-ray analysis of titanium dioxide nanoparticles

### 3.1.2.2 Fine particles

***Hematite***

Analysis of the SEM image demonstrated that the maximum number of hematite fine particles had a size between 500 nm and 2.5 µm. Morphologically, these particles were of heterogeneous form that is these particles had different shapes (Fig. 26).

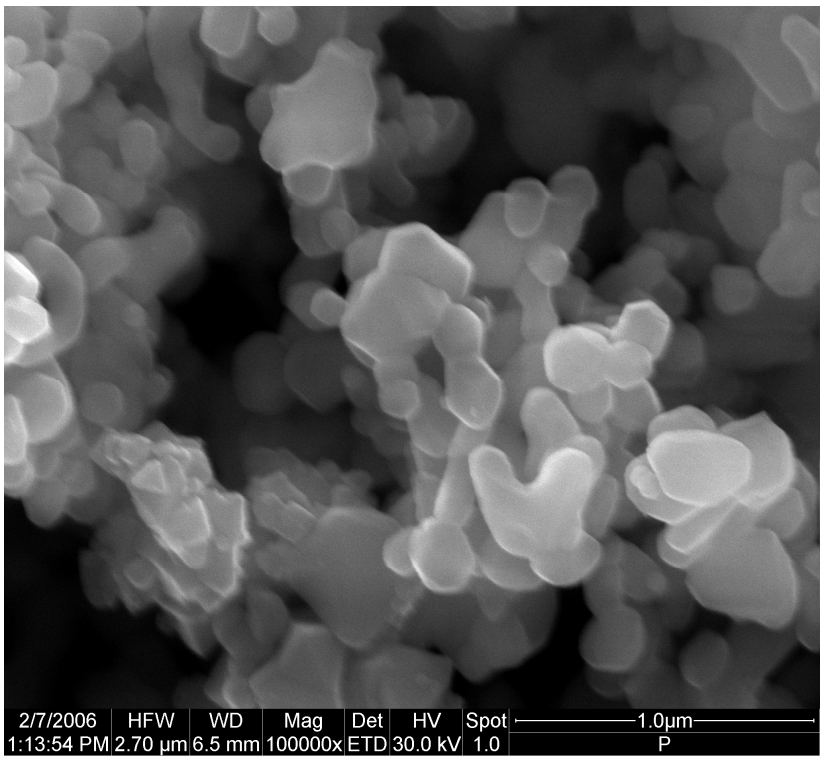


**Figure 26:** Scanning electron microscopic image of hematite fine particles

EDX spectra analysis (Fig. 27) demonstrated that the hematite fine particles contained 78.7% Fe and 21.1% O elements similar to the hematite nanoparticles. A small amount of silica (0.2%) was also found in the particles (Table 2).

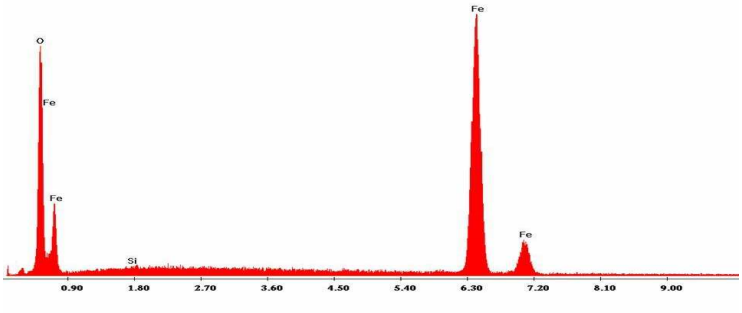


**Figure 27:** Spectra obtained from electron dispersive X-ray analysis of hematite fine particles

### *Quartz (DQ12)*

DQ12 fine particles were found to be heterogeneous in shape through SEM image analysis. These particles were found to have a size between 500 nm–2.5 µm confirming the results found through size distribution analysis (Fig. 28).

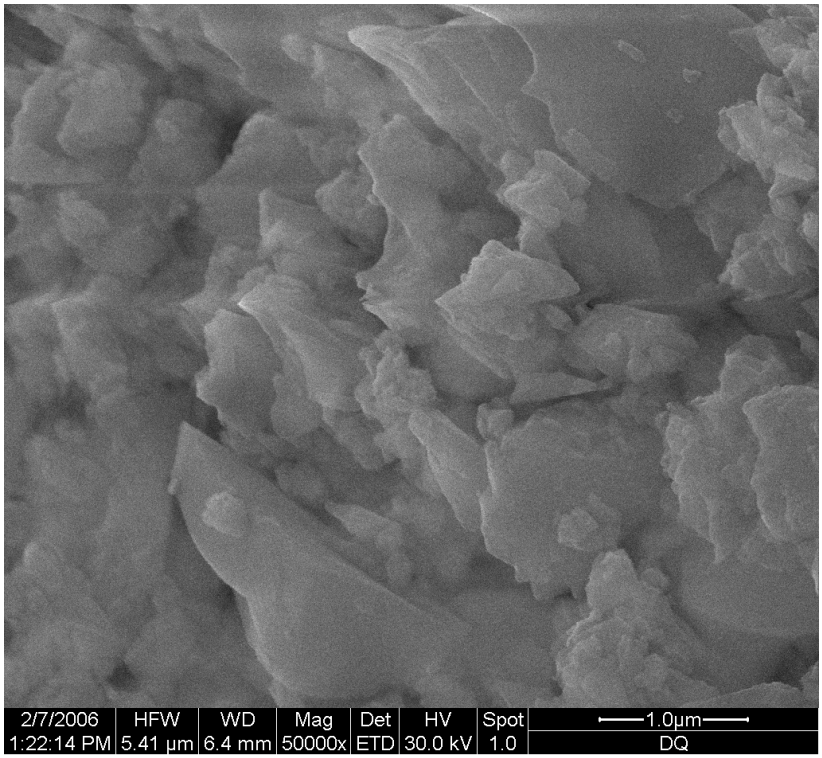


**Figure 28:** Scanning electron microscopic image of Quartz (DQ12) fine particles

EDX spectra analysis (Fig. 29) demonstrated the particles to be composed of 53% Si and 47% O elements. No transition element was traced in the particles (Table 2).

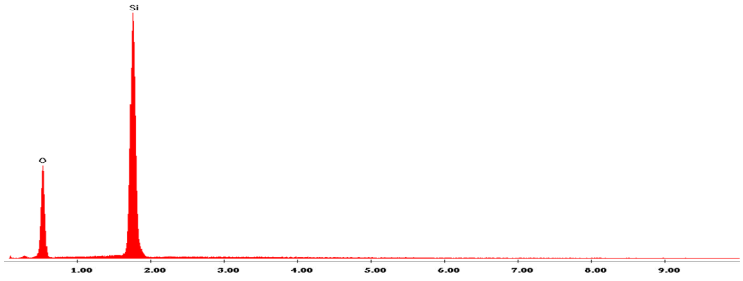


**Figure 29:** Spectra obtained from electron dispersive X-ray analysis of quartz (DQ12) fine particles

### *Arsenopyrite ash*

Arsenopyrite ash sample received from the sulphur processing company were found to contain particles between the size range of <100 nm-<10 µm as measured based on the SEM image scale (Fig. 30).

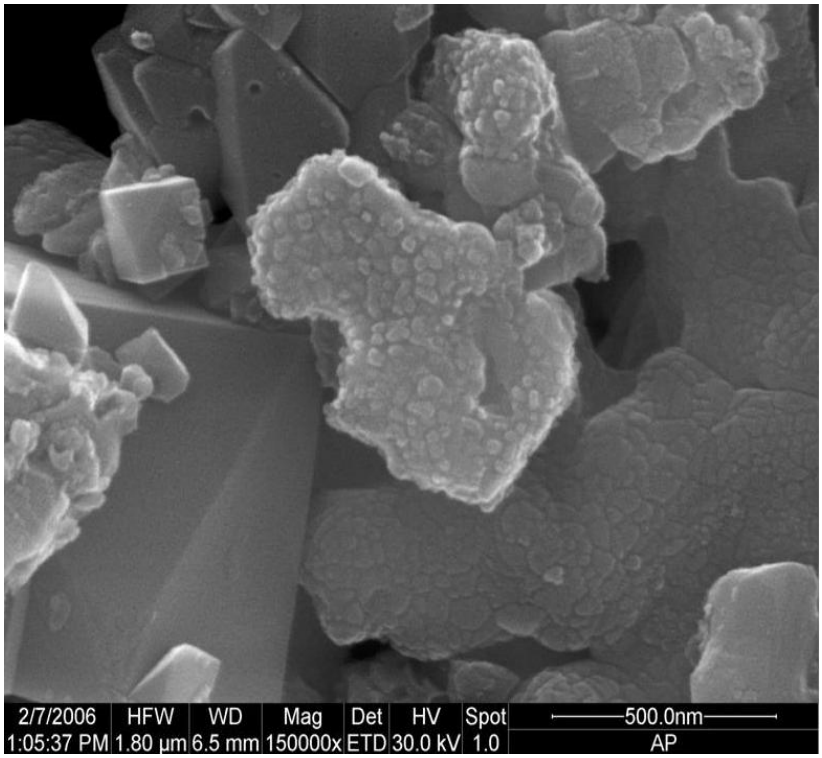


**Figure 30:** Scanning electron microscopic image of arsenopyrite ash particles

EDX analysis (Fig. 31) demonstrated that the arsenopyrite ash particles were a heterogeneous mixture of several elements. The major elements present were Fe – 43.9%, O – 25.2%, calcium (Ca) - 19.6%, and sulphur (S) – 13.9%. Arsenic (As) content of the particles was found to be as low as 0.62% (Table 2).

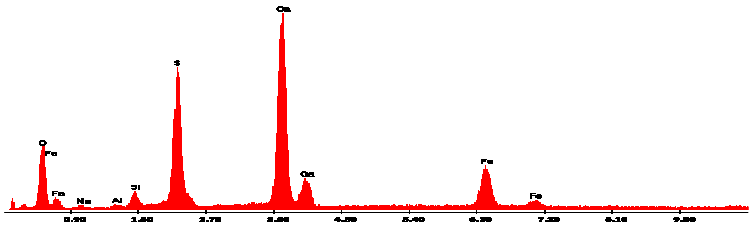

**Figure 31:** Spectra obtained from electron dispersive X-ray analysis of arsenopyrite ash particles

**Table 2:** Elemental composition of different particles determined by EDX

| **Hematite nanoparticles** | |
|---|---|
| Fe | 78.7 |
| O | 21.3 |
| **Titanium dioxide nanoparticles** | |
| **Elements** | **Weight %** |
| Ti | 56 |
| O | 41 |
| C | 3 |
| **Hematite fine particles** | |
| **Elements** | **Weight %** |
| Fe | 78.7 |
| O | 21.4 |
| Si | 0.2 |
| **DQ12 fine particles** | |
| **Elements** | **Weight %** |
| Si | 53 |
| O | 47 |
| | |
| **Arsenopyrite ash particles** | |
| **Elements** | **Weight %** |
| Fe | 43.9 |
| O | 25.2 |
| Ca | 19.6 |
| C | 18.3 |
| S | 13.9 |
| Si | 2.3 |
| Cl | 1.4 |
| K | 1 |
| Al | 0.8 |
| Na | 0.7 |
| Mg | 0.3 |
| As | 0.6 |

### 3.1.3 ICP-MS for arsenic detection and speciation

HLPC/ICP-MS analysis of the arsenopyrite ash particles gave a concentration of ≤1.58µg/100 mg arsenic present in the samples, and speciation revealed that the arsenic species was $As_2O_3$. Results provided by the company using arsenopyrite mineral for the production of Sulphur dioxide ($SO_2$) and creating arsenopyrite ash as a residue demonstrated an average presence of 23.13±17.82 µg arsenic per 100 mg of arsenopyrite ash residue. These results were obtained by atomic absorption spectroscopic (AAS) analysis of samples on a yearly basis (Appendix 5 - Fig. 47).

### 3.1.4 Determination of total iron content in the particles

All iron containing particles were found to have a similar amount of elemental iron present in them. Quantitatively, the total iron content per 0.4 mg of hematite fine, nanosize and arsenopyrite ash particles were amounted to 1.3 mM, 935 and 867 µM, respectively. No iron content was detected in the fine DQ12 fine and $TiO_2$ nanosized particles (Fig. 32).

No chelable amount of iron content in the particles was detected.

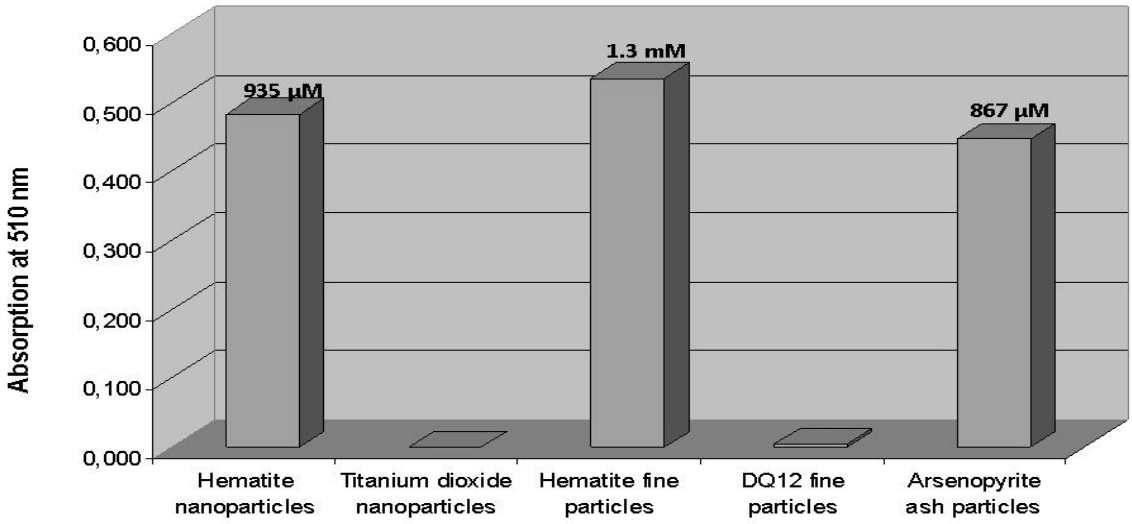


**Figure 32:** Total iron content of different particles determined by spectrometry

## 3.2 Reactivity of the particles towards cellular systems

IMR-90 cells (page 27) and BEAS-2B cells (page 28) were used for the experiments as these cells represent the first line of the lung cells to come in direct contact with the inhaled particulate matter.

### 3.2.1 TEM for uptake study of the particles

#### 3.2.1.1 Nanoparticles

***Hematite***

BEAS-2B cells (Fig. 33a) were taken to study the uptake and retention of different particles (page 34). Hematite nanoparticles were normally found in large

clusters inside the cells after their uptake. It was observed that when these particles were present in small clusters or as singly they were taken up by the process of micropinocytosis, as a small invagination on the outer cell membrane engulfing the nanoparticles was observed (Fig. 33b). Within 48 h the nanoparticles were found to be translocated to the peri-nuclear region of the cell moving inside the endoplasmic reticulum (ER) (Fig. 33c).

It was also observed that the nanoparticles taken up by micropinocytosis or, the ones separated from the large major cluster into smaller groups or single particles, crossed over into the cytoplasm either directly without any membranous covering or enclosed within a cytoplasmic vesicle (Fig. 33c and d).

Direct entry into the cytoplasmic region of the cell by a nanoparticle can only occur as a consequence of close interaction and coating of the nanoparticles with native proteins present on the cellular membrane or within the ER (Fig. 33c and d). It was observed that the particles present directly inside the cytoplasm were surrounded by several vesicle like structures (Fig. 33c).

*However, no particles were found to have penetrated any intracellular organelle such as nucleus or mitochondria.*

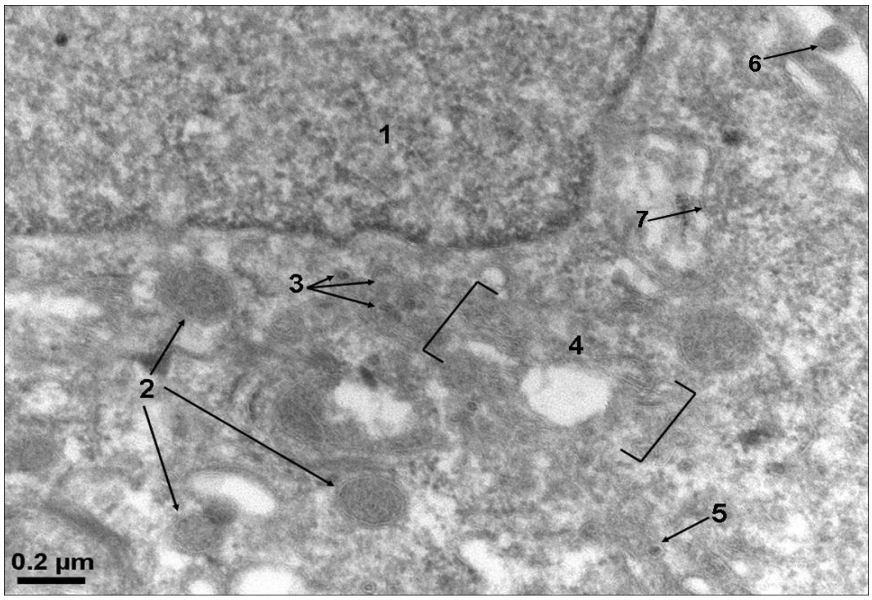


**Figure 33a:** Electron microscope images of a control cell illustrating the intracellular organelles of the BEAS-2B cell after cryo-sectioning

**Legends –** Nucleus – 1; Mitochondria – 2; Trans – Golgi apparatus – 3; Golgi apparatus – 4; Vesicles – 5; Filopodium – 6; Endoplasmic reticulum - 7

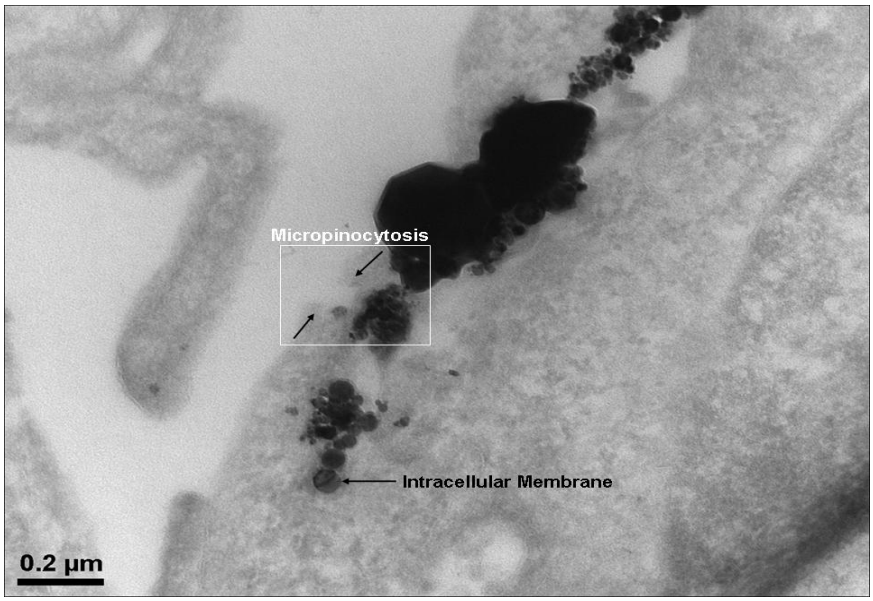


**Figure 33b:** A small cluster of nanoparticles inside the cytoplasm enclosed within the intracellular membrane

**White Box –** Micropinocytosis of nanoparticles

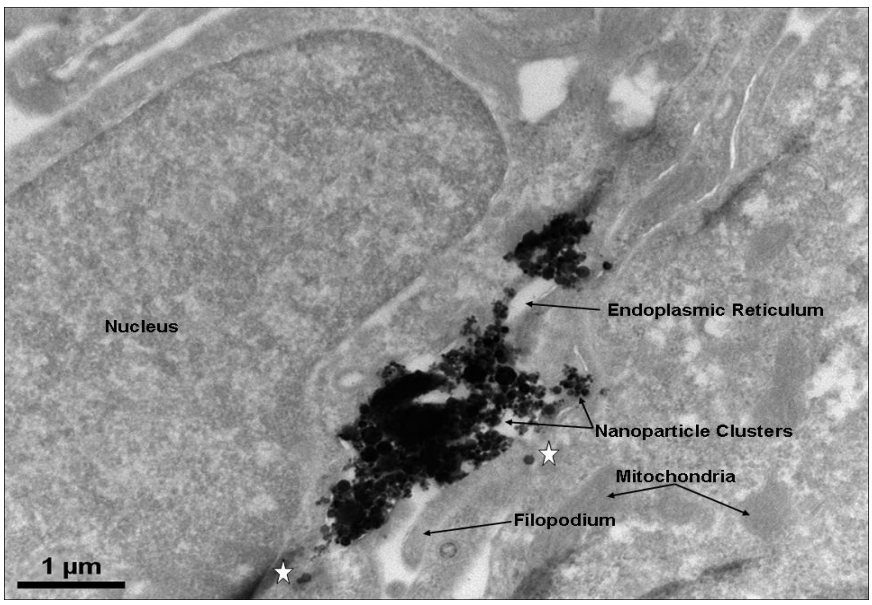


**Figure 33c:** Uptake of hematite nanoparticles using filopodium by the BEAS-2B cells as a large cluster of particle and their passage within the cells through the endoplasmic reticulum. The white stars represents a single or a small group of hematite nanoparticles broken from the main cluster and penetrating the cytoplasm of the cell

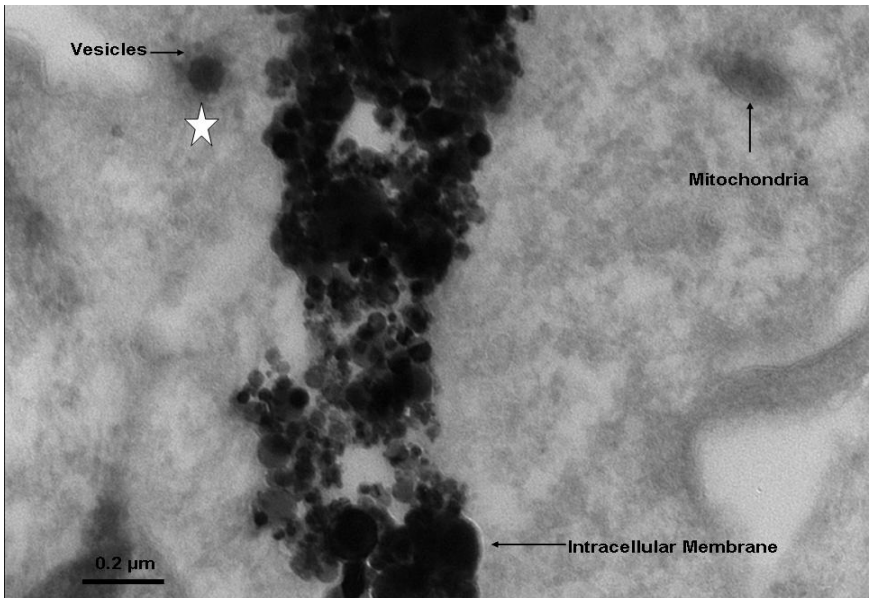


**Figure 33d:** A single large cluster of nanoparticles enveloped inside the endoplasmic reticulum. The white star represents a single nanoparticle directly present within the cytoplasm of the cell without any membrane covering and surrounded by vesicles

### 3.2.1.2 Fine particle

***Hematite***

For the uptake of hematite fine particles the BEAS-2B cells was found to be using filopodia, which assisted in the engulfment of the particles. Most of the hematite fine particles during and after uptake by the cells were observed to be grouped together in small agglomerates (Fig. 33e).

Following uptake most of the fine particles were translocated very close to the peri-nuclear region enclosed within the ER similar to the hematite nanoparticles (Fig. 33f). These fine particles were also found to be conspicuously surrounded by several mitochondria, a phenomenon not observable with hematite nanoparticles uptake and retention inside the cells. Some of these mitochondria were found at close proximity of the particles suggesting a direct interaction between these cell organelles and the particles (Fig. 33f and 32g).

***Arsenopyrite ash***

Arsenopyrite ash particles were also taken up in clusters by the BEAS-2B cells using filopodia, similar to the hematite particles (Fig. 33h). Some solitary particles were found surrounded by coated pits suggesting an endocytotic process (Fig. 33i).

Arsenopyrite ash particles were also found very close to the peri-nuclear region following their uptake by BEAS-2B cells, similar to the fate of the other particles. These particles were also conspicuously surrounded by mitochondria and

trans–Golgi vesicles, similar to the hematite fine particles, suggesting a close interaction between the particles and these cell organelles (Fig. 33j).

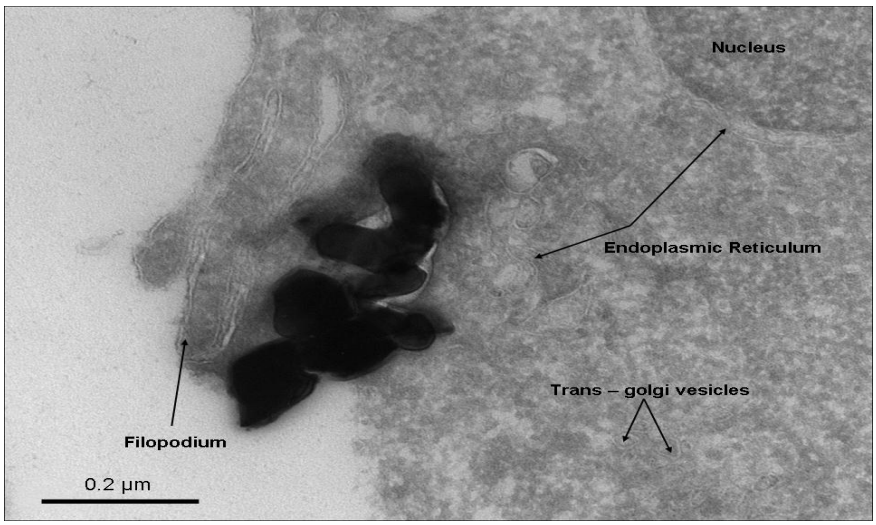


**Figure 33e:** Uptake of hematite fine particles with the help of filopodia appandages

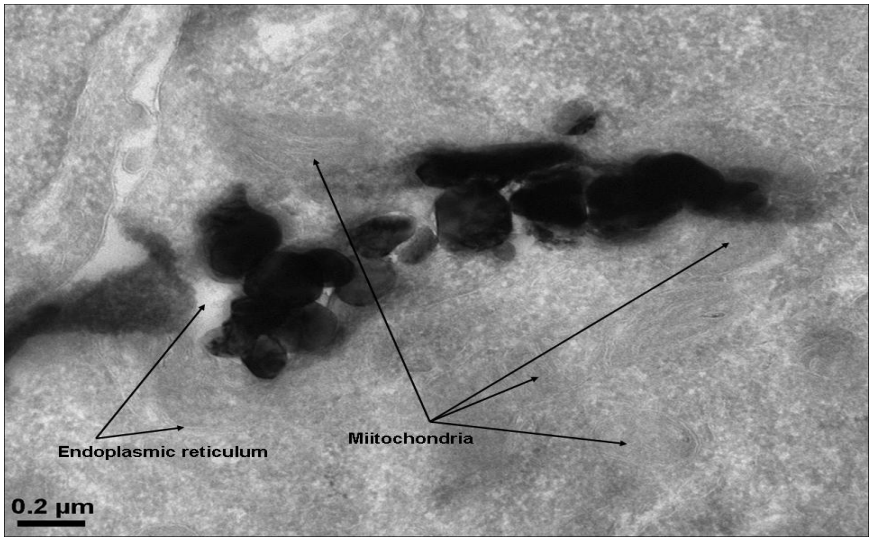


**Figure 33f:** Fine hematite particles were found enclosed within the endoplasmic reticulum, next to mitochondria and the nuclear membrane. The particles were seen to be present in clusters

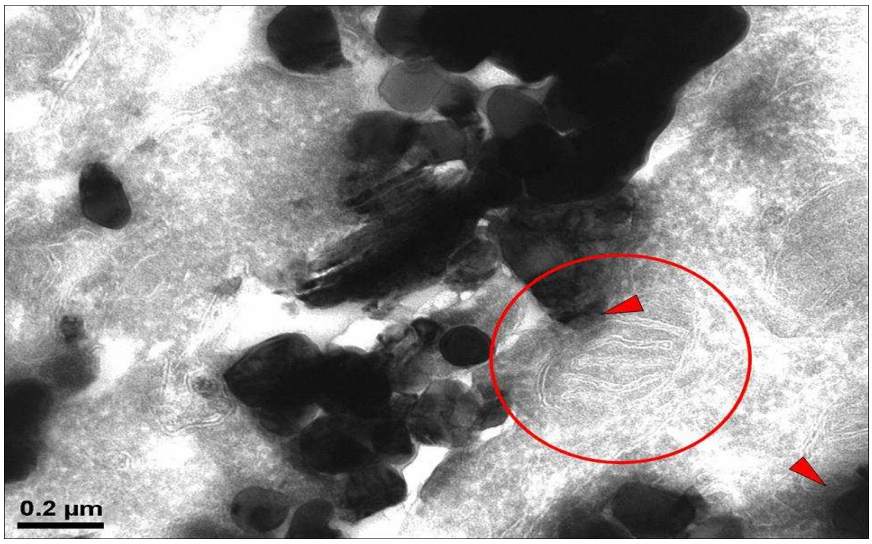


**Figure 33g:** Fine hematite particles enclosed within the endoplasmic reticulum surrounded by mitochondria

**Red arrow -** Illustrates possible point of close interaction between the particle and the mitochondria

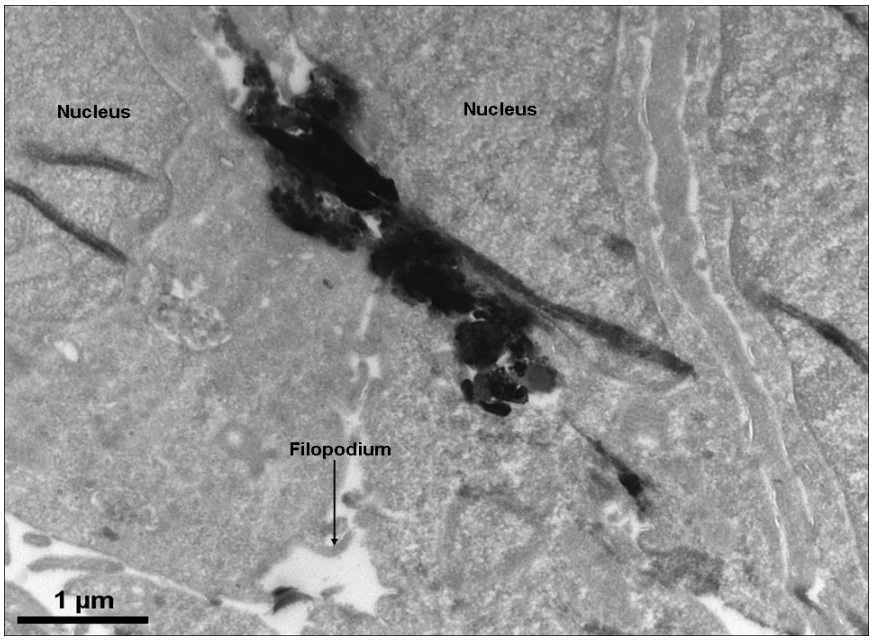


**Figure 33h:** Arsenopyrite ash particles enclosed within the endoplasmic reticulum after their uptake by the BEAS-2B cells using filopodium

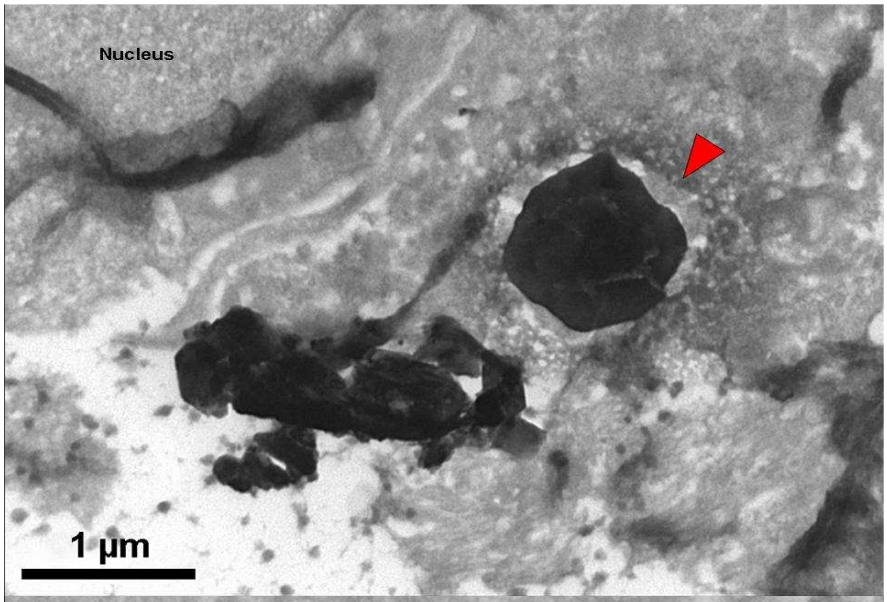


**Figure 33i:** Arsenopyrite ash particles enclosed within a coated pit after uptake

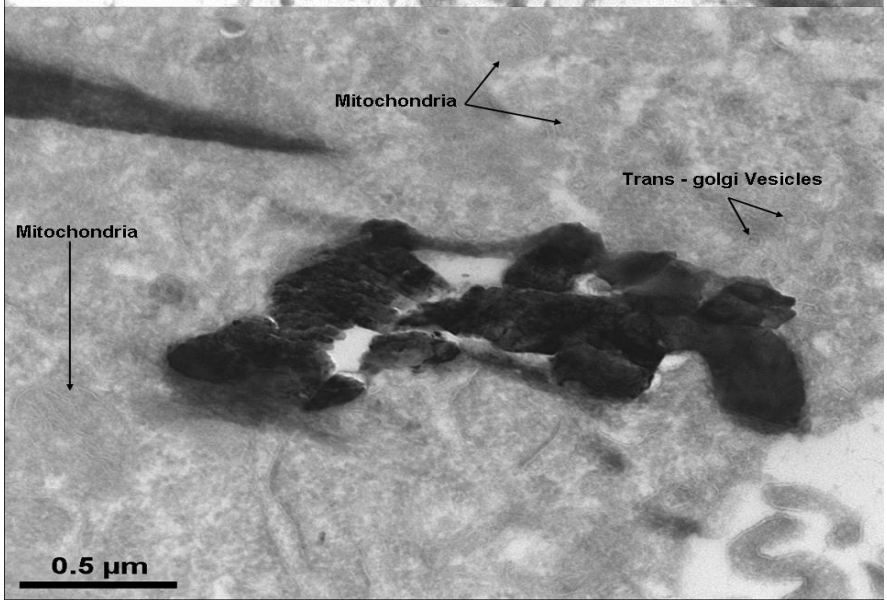


**Figure 33j:**Arsenopyrite ash particles surrounded by mitochondria and trans – Golgi vesicles

### 3.2.2 Cytotoxicity analysis using Trypan blue assay

#### 3.2.2.1 IMR-90 cells

***Nanoparticles***

***Hematite***

Exposure of the IMR-90 cells to hematite nanoparticles produced a statistically significant concentration dependent loss of cell viability ($p < 0.05$) at 24 and 72 h exposure. At 48 h a substantial recovery of cell viability was observed suggesting a possible population doubling in the cells.

***Titanium dioxide ($TiO_2$)***

$TiO_2$ nanoparticles exposure to the IMR-90 cells also resulted in a concentration-dependent loss of cell viability at 24 h. However, this effect was statistically significant only at a concentration of 50 µg/cm$^2$ ($p < 0.05$) as compared to the control (untreated cells). Similar to the hematite nanoparticles exposed IMR-90 cells a temporary recovery of cell viability was observed at 48 h. It was followed by the second statistically significant decrease in the cell viability ($p < 0.05$) at 72 h. The loss of cell viability found at the 72 h time point was not only higher in magnitude than that found at 24 h but also directly proportional to the increasing concentration of the nanoparticles (Fig. 34b).

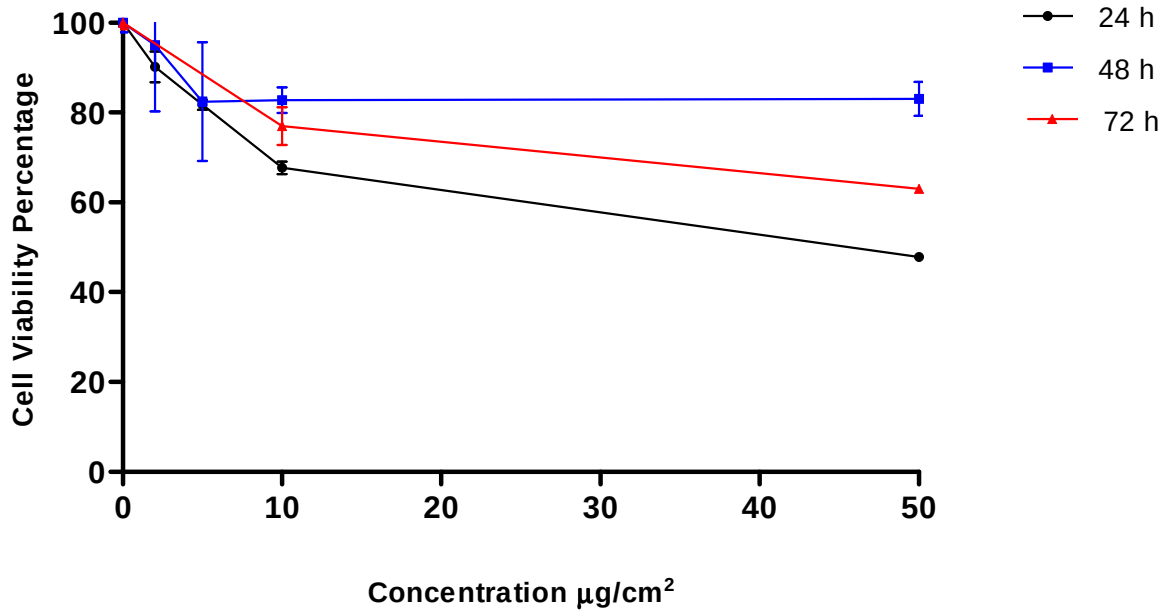


**Figure 34a:** IMR-90 cells exposed to hematite nanoparticles

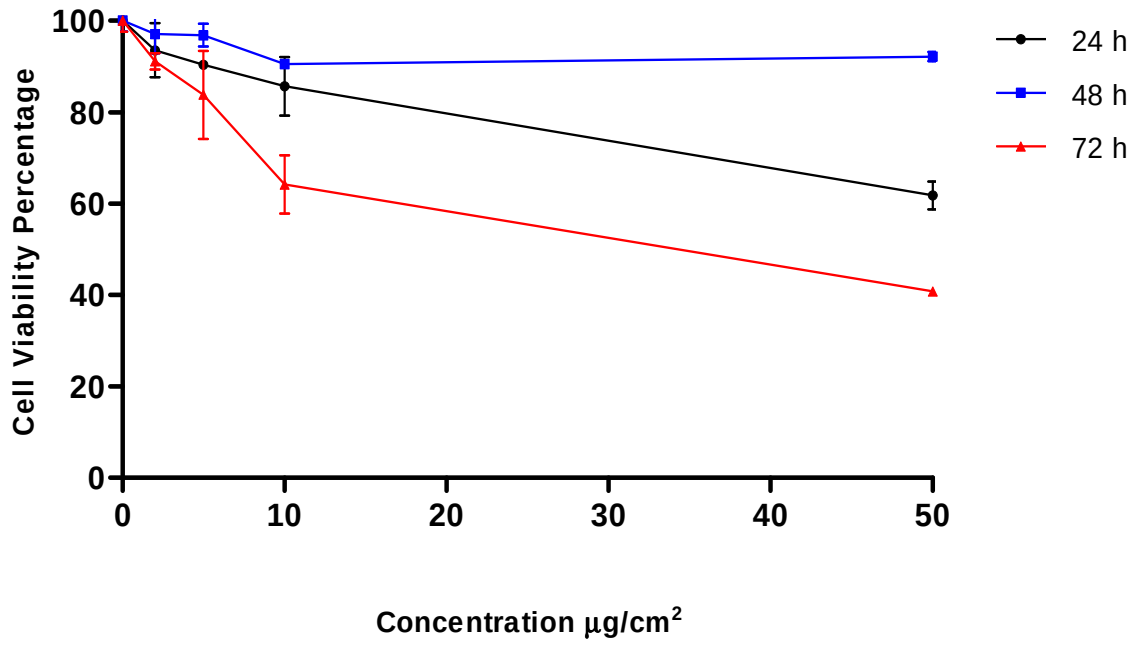


**Figure 34b:** IMR-90 cells exposed to titanium dioxide nanoparticles

***Fine particles***

***Hematite***

Exposure of IMR-90 cells to the hematite fine particles induced less cytotoxic effects as compared to the hematite nanoparticles-exposed cells. Loss of cell viability was found to be statistically significant at 24 h and at concentrations of 5 and 50 µg/cm² ($p < 0.05$). After 48 h exposure, except at 50 µg/cm² particle concentration where the loss of cell viability remained the same as of 24 h, a recovery was observed at all other particle concentrations applied. However, at 72 h exposure to the concentrations of 10 and 50 µg/cm² resulted in a statistically significant loss of cell viability again ($p < 0.05$) (Fig. 34c).

It was interesting to note that while till 10 µg/cm² particle concentration the loss of cell viability varied with time. At 50 µg/cm² particle concentration the loss of cell viability remained fairly stable and statistically significant at all time points. The results also pointed towards a significant difference in approach hematite fine and nanoparticles induced cytotoxicity.

***Quartz (DQ12)***

After 24 h exposure the IMR-90 cells showed a statistically significant decrease in cell viability only at the concentration of 2 and 5 µg/cm² ($p < 0.05$). After 48 h exposure, while the IMR-90 cells demonstrated a recovery in their cell viability at 2 and 5 µg/cm², a considerable loss was observed at the concentrations of 10 and 50 µg/cm². At the longest exposure time point of 72 h, all the cells exposed to 50 µg/cm² showed a constant decrease in their cell viability (Fig. 34d).

***Arsenopyrite ash***

Arsenopyrite ash particles were found to be least cytotoxic following their exposure to the IMR-90 cells. After 24 h exposure, even though the levels of cytotoxicity induced by the particles in IMR-90 cells at all the concentrations given (2, 5, 10 and 50 µg/cm²) remained low, these levels were found to be statistically significant ($p < 0.05$) compared to the negative control (untreated cell). Not much difference was found between the levels of cytotoxicity induced by particles at 24 and 48 h. Furthermore, at 48 h, only at the concentrations of 2 and 50 µg/cm² a statistically significant loss of cell viability was found ($p < 0.05$). At the 72 h exposure time point, a concentration-dependent loss of cell viability was also found, which was also statistically significant ($p < 0.05$) at the concentrations of 10 and 50 µg/cm² tested (Fig. 34e).

*Raw data of all the measurements are presented in Table 1 - Appendix 6.*

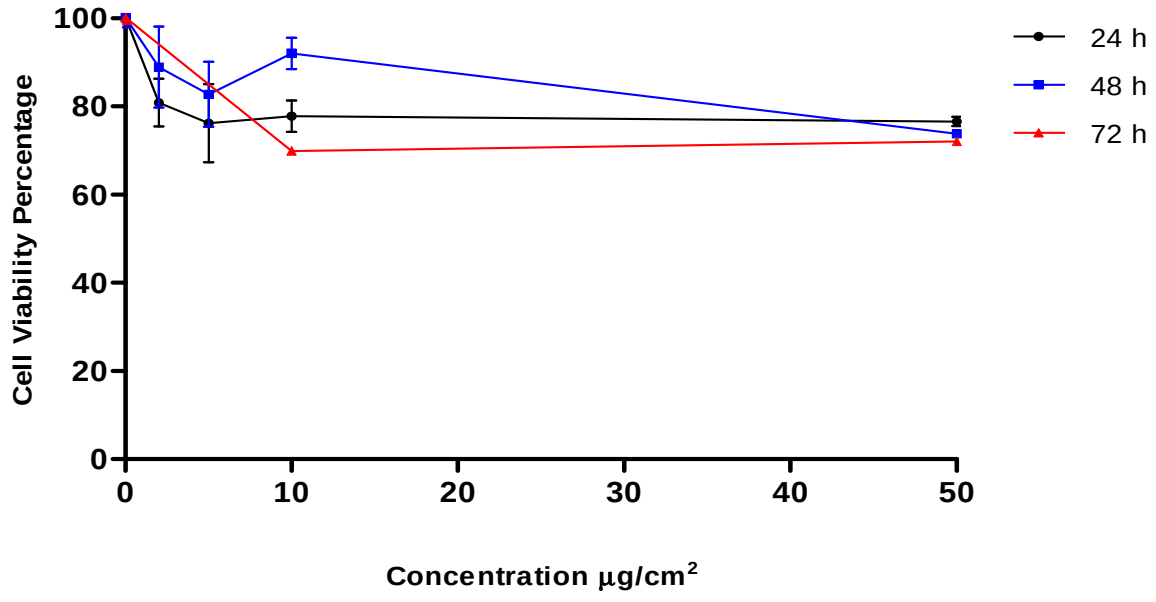

**Figure 34c:** IMR-90 cells exposed to hematite fine particles

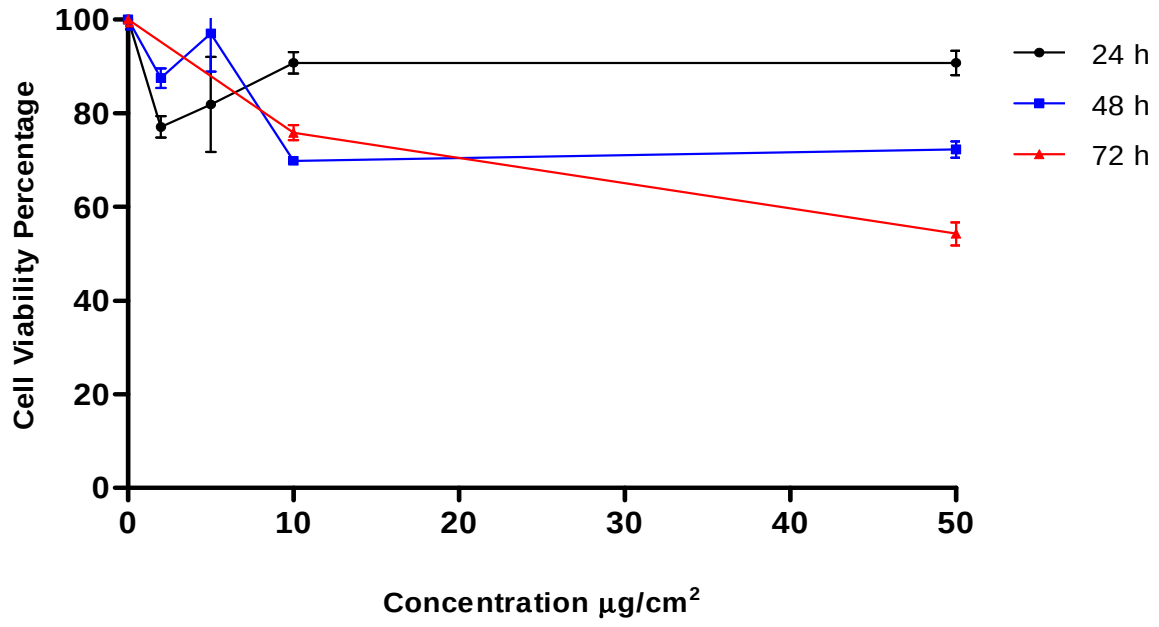


**Figure 34d:** IMR-90 cells exposed to DQ12 fine particles

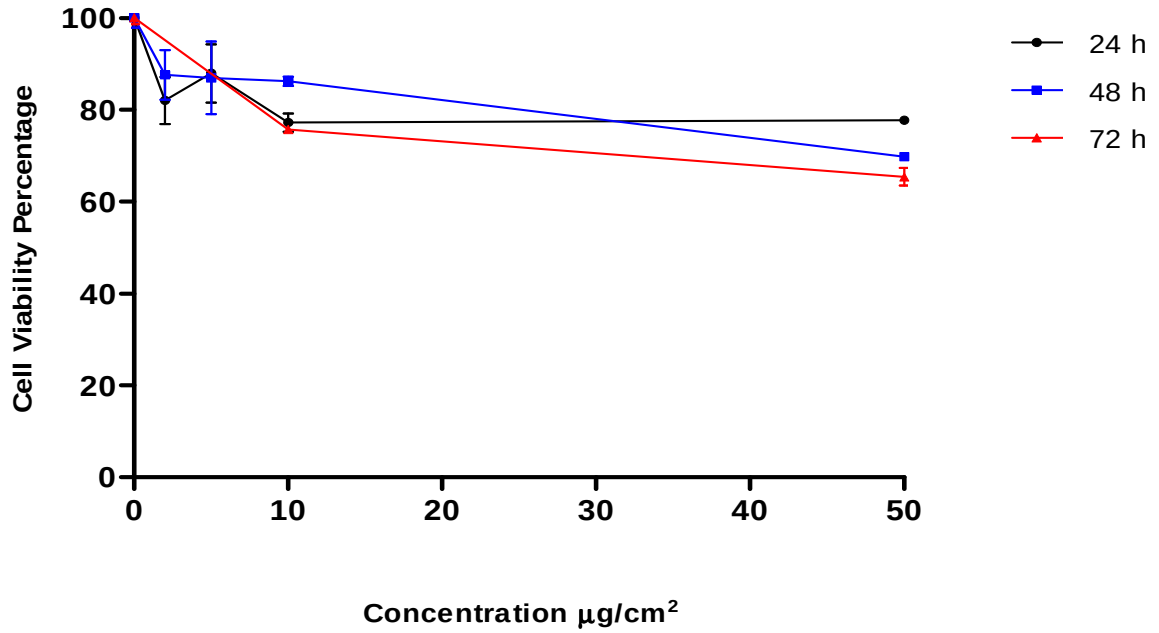


**Figure 34e:** IMR-90 cells exposed to arsenopyrite ash particles

### 3.2.2.2 BEAS-2B cells

***Nanoparticles***

***Hematite***

Exposure of the BEAS-2B cells to hematite nanoparticles at 24 h caused a concentration-dependent loss of cell viability, which was highest and statistically significant at 50 µg/cm² particle concentrations ($p < 0.05$). At 48 h, BEAS-2B cells exposed to particle concentrations of 2 and 5 µg/cm² showed a significant loss of cell viability. At the higher concentrations a recovery in the cell viability was also observed. Interestingly, loss of cell viability at all concentrations (2, 5, 10 and 50 µg/cm²) after 48 h exposure and at the concentrations of 10 and 50 µg/cm$^2$ after 72 h exposure were found to be statistically significant ($p < 0.05$) as compared to the control (untreated) cells (Fig. 34f). The results obtained were an average of two experiments done in duplicate.

***Titanium dioxide ($TiO_2$)***

$TiO_2$ nanoparticles were found to be completely non-cytotoxic in the BEAS-2B cells. Unlike to the effects observed in the IMR-90 no loss of cell viability was observed in the BEAS-2B cells at all the concentrations (2, 5, 10 and 50 µg/cm²) and the time points tested (24, 48 and 72 h) (Fig. 34g).

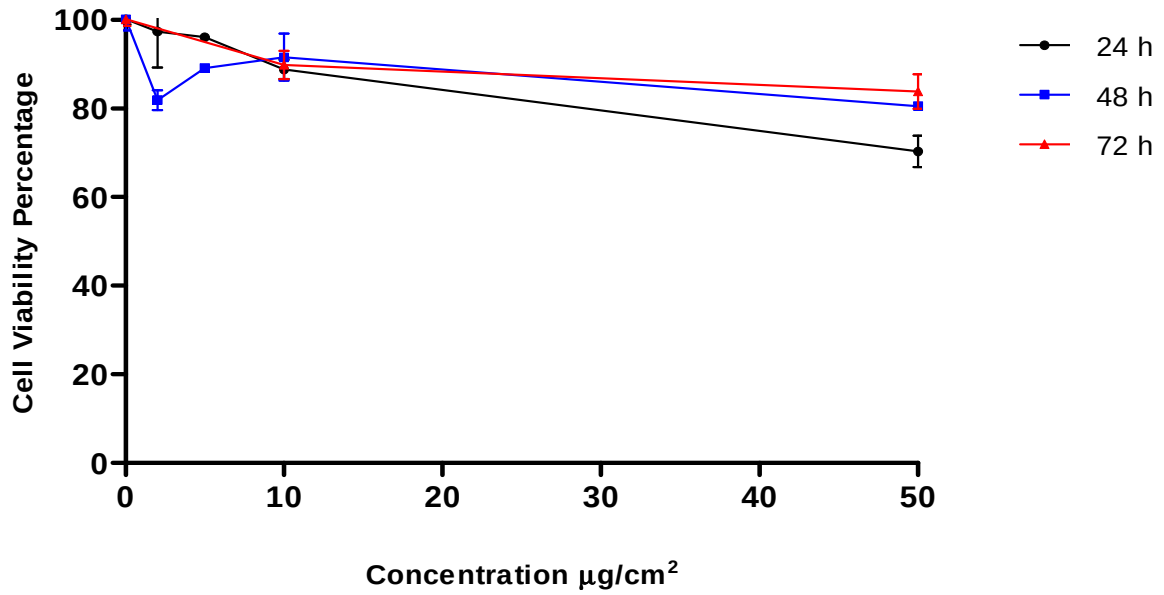

**Figure 34f:** BEAS-2B cells exposed to hematite nanoparticles

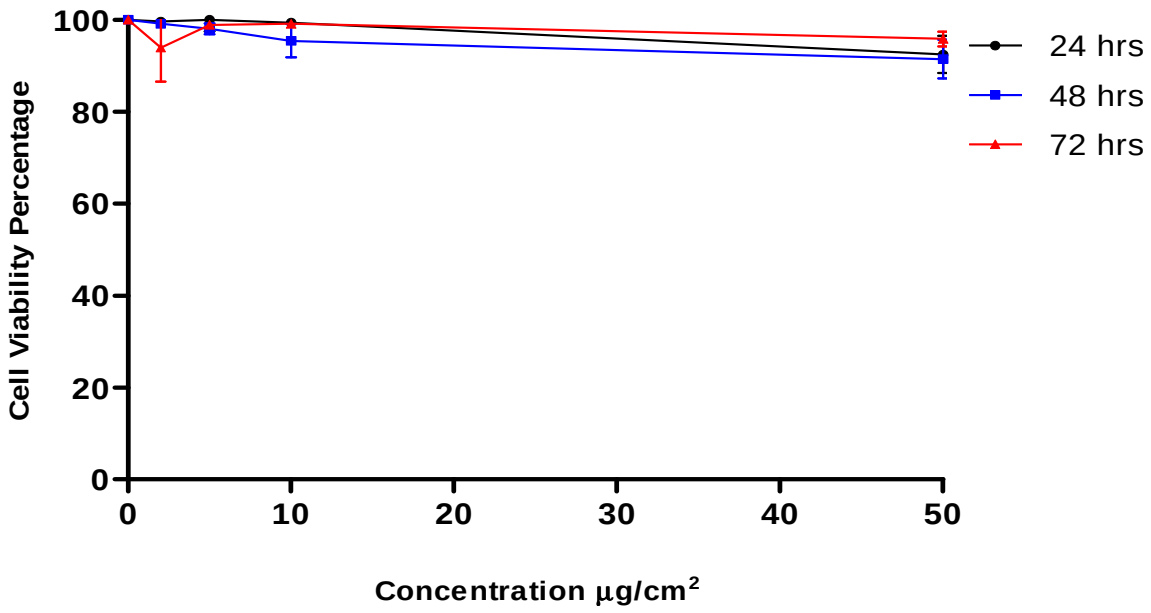


**Figure 34g:** BEAS-2B cells exposed to titanium dioxide nanoparticles

## ***Fine particles***

### *Hematite*

BEAS-2B cells exposed to hematite fine particles for 24 h showed a concentration-dependent loss of cell viability up to a concentration of 10 µg/cm². Loss of cell viability at the concentrations of 10 and 50 µg/cm² remained unaltered and statistically significant ($p < 0.05$). At 48 h, cytotoxicity due to particle exposure in the BEAS-2B cells was found elevated and also demonstrated a concentration-dependent loss of cell viability. However, similar to that observed at 24 h, the loss of cell viability at the concentrations of 10 and 50 µg/cm$^2$ was relatively constant. However, here both the concentrations were also found to cause a statistically significant ($p < 0.05$) loss of cell viability. At 72 h, the particles were found to have no cytotoxic effect at all concentrations tested, as the cell viability was found equal to that of the control (untreated) cells (Fig. 34h).

***Quartz (DQ12)***

DQ12 fine particles exposure to the BEAS-2B cells at 24 h led to a high loss of cell viability at the lower concentrations of 2 and 5 µg/cm², while it remained non-cytotoxic at the higher concentrations. After 48 h exposure the cells were found to have a concentration-dependent loss of cell viability till 10 µg/cm². Similar to the effects observed in the BEAS-2B cells exposed to hematite fine particles, the loss of cell viability at the 10 and 50 µg/cm² remained almost equal and statistically significant ($p < 0.05$). At 72 h, only at the concentration of 50 µg/cm² a statistically significant loss of cell viability was observed ($p < 0.05$) (Fig. 34i).

***Arsenopyrite ash***

Exposure of BEAS-2B cells to arsenopyrite ash particles induced a significant loss of cell viability at the time point of 24 h. This effect was found to be statistically significant ($p < 0.05$) at all concentrations tested (2, 5, 10 and 50 µg/cm²). A more prominent concentration-dependent loss of cell viability was observed after 48 h exposure. The effect was found to be statistically significant at the concentrations of 10 and 50 µg/cm² ($p < 0.05$). At 72 h, the cells showed a reduction in the level of cytotoxicity, which was found to be statistically significant at the concentrations of 10 and 50 µg/cm² (Fig 34j).

*Raw data of all the measurements are presented in Table 2 - Appendix 6.*

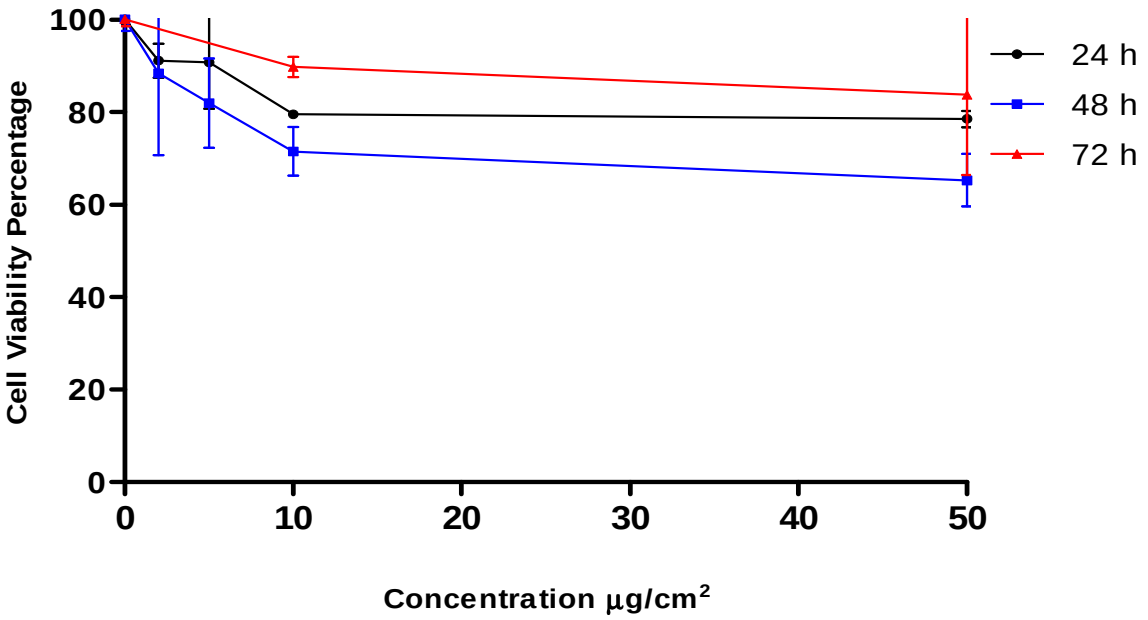


**Figure 34h:** BEAS-2B cells exposed to hematite fine particles

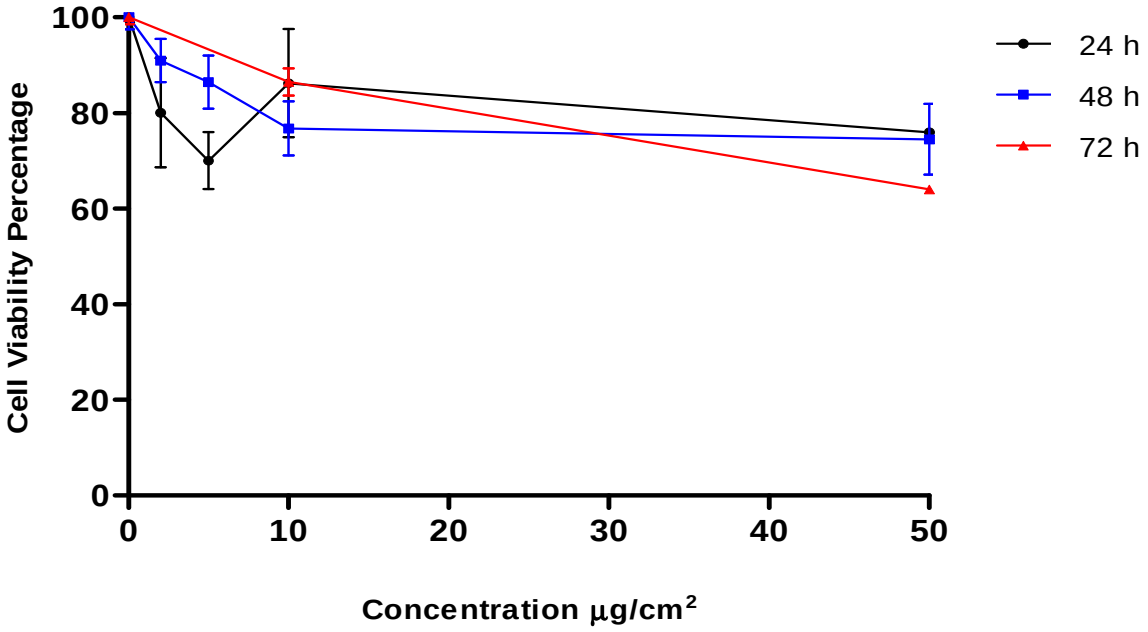


**Figure 34i:** BEAS-2B cells exposed to quartz (DQ12) particles

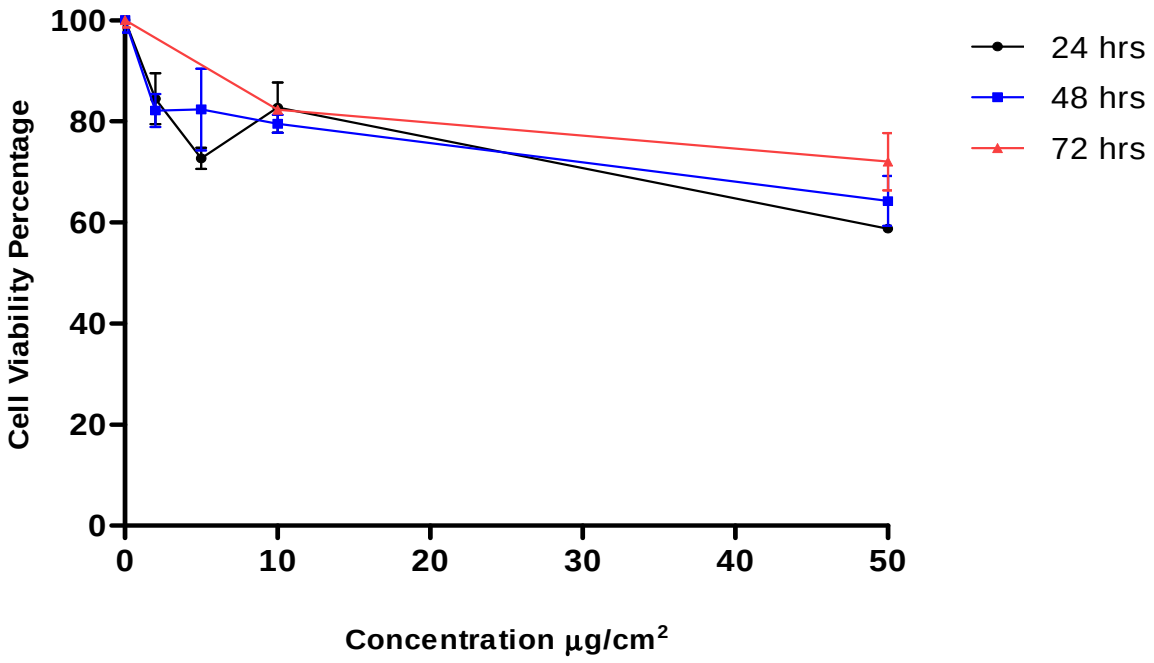


**Figure 34j:** BEAS-2B cells exposed to arsenopyrite ash particles

Unlike IMR-90, the BEAS-2B cells demonstrated a higher tolerance towards the particle cytotoxicity. Every particle was observed to have its own way of causing cytotoxicity. These effects were rather a cumulative effect of their physico-chemical properties, rather than an effect based upon the chemical composition. Reduction in the loss of cell viability at the 48 h time period found with different particle exposures seemed to be more related to the cell population doubling time of IMR-90 (25 – 30 h) and BEAS-2B (24 h) cells. The reduction in the number of dead cells due to nuclear fragmentation is also known as the process of 'cell blebbing'.

### 3.2.3 Apoptosis / necrosis study

Based on the cytotoxicity results, analysis of apoptosis / necrosis was conducted in the IMR-90 cells at the concentration of 10 µg/cm² and a time duration of 24 h. $TiO_2$ particles were not selected for this analysis, since they were found to be non-cytotoxic at the present concentration and time of exposure (Table–3).

The results obtained from the assay failed to reveal the pathway (apoptosis or necrosis) related to the loss of cell viability in the IMR-90 cells on exposure to the

particles. Most of the cells were found at the late apoptotic / secondary necrosis stage. The highest amount of late apoptotic cells were found following exposure to arsenopyrite ash particles followed by hematite fine and nanoparticles. The lowest number of late apoptotic cells was found on exposure to the DQ12 fine particles.

Among all the particles, hematite nanoparticles showed the most statistically significant result ($p < 0.001$) followed by arsenopyrite ash particles ($p < 0.05$) as compared to the negative control (untreated cells). The percentage of late apoptotic cells demonstrated by hematite and DQ12 fine particles was not found to be statistically significant. Late apoptosis / secondary necrosis had been related to the characteristic loss of cell membrane, nuclear disintegration and formation of apoptotic bodies.

**Table 3:** Apoptosis, primary necrosis and secondary necrosis/ late apoptosis was detected with flow cytometer after annexin V – FITC and propidium iodide staining.

| **10 µg/cm²**<br>**24 h** | **Viable** | **Apoptosis** | **Primary Necrosis** | **Late Apoptosis / Secondary Necrosis** |
|---|---|---|---|---|
| **Negative Control (Untreated cells)** | 74.02% ± 2.36 | 2.84% ± 1.51 | 2.48% ± 1.76 | 20.25% ± 1.21 |
| **Hematite (nanosize)** | 62.52% ± 3.48 | 0.04% ± 0.01 | 0.52% ± 0.57 | 36.89% ± 4.07 |
| **Hematite (fine)** | 40.54% ± 12.82 | 0.11% ± 0.14 | 0.11% ± 0.01 | 41.58% ± 37.61 |
| **DQ12** | 73.33% ± 17.52 | 0.4% ± 0.47 | 1.56% ± 0.82 | 24.47% ± 15.93 |
| **Arsenopyrite** | 47.97% ± 20.59 | 2.06% ± 1.23 | 3.18% ± 1.92 | 46.75% ± 17.42 |

### 3.2.4 Genotoxicity assay

#### 3.2.4.1 IMR–90 cells

***Nanoparticles***

***Hematite***

IMR-90 cells exposed to the hematite nanoparticles expressed the highest level of genotoxicity among all the particles applied. After 24 h exposure, statistically significant effects were observed at the concentrations of 5 µg/cm$^2$ ($p < 0.05$), 10 µg/cm$^2$ ($p < 0.001$) and 50 µg/cm$^2$ ($p < 0.01$). These effects after 48 h were found to be completely reduced. At 72 h, a mild and statistically significant effect at the concentration of 10 µg/cm² ($p < 0.01$) which however was very low as compared to the effects observed at 24 h exposure time (Fig. 35a).

***Titanium dioxide ($TiO_2$)***

IMR-90 cells exposed to $TiO_2$ nanoparticles revealed no DNA damaging effect. With this applied test system, $TiO_2$ was found to be non-genotoxic (Fig 35b).

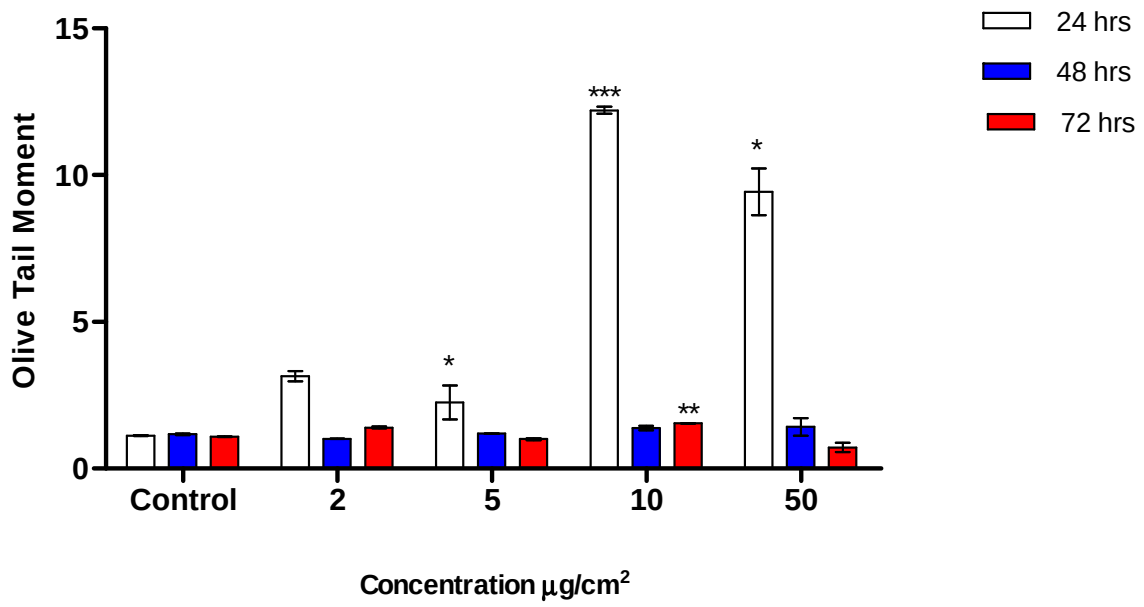


**Figure 35a:** Comet assay of IMR-90 cells exposed to hematite nanoparticles

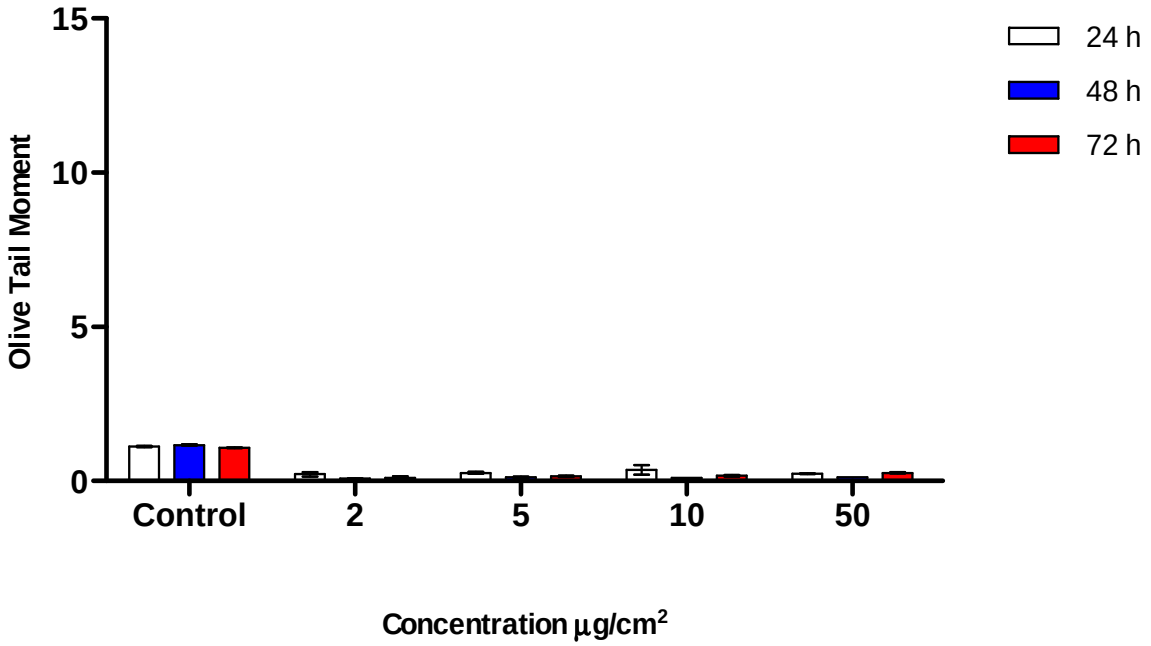


**Figure 35b:** Comet assay of IMR-90 cells exposed to titanium dioxide nanoparticles

***Fine particles***

***Hematite***

Exposure of IMR-90 cells to hematite fine particles induced a relatively strong effect. However, the observed effects were lower than that produced by hematite nanoparticles. The highest amount of genotoxicity was found at the concentrations of 10 µg/cm² ($p < 0.05$) and 50 µg/cm² measured after 24 h exposure. These genotoxic effects were found to be reduced to the control levels after 48 h exposure. A second strong and statistically significant genotoxic effect was observed after 72 h exposure. Statistically significant effects were found at the particle concentrations of 2 µg/cm² ($p < 0.05$), 5 µg/cm² ($p < 0.01$) and 10 µg/cm² ($p < 0.05$) (Fig. 35c). However, genotoxicity observed at 72 h were very low in magnitude as compared to those found after 24 h exposure.

***Quartz (DQ12)***

Exposure of IMR-90 cells to DQ12 particles produced a high and statistically significant level of genotoxicity only at concentrations of 10 and 50 µg/cm² and a time point of 24 h. Other concentrations applied at different time points were found to be

completely negative demonstrating a subdue genotoxic effect at the lower concentrations and longer time periods (Fig. 35d).

***Arsenopyrite ash***

Exposure to the arsenopyrite ash particles induced a slight but statistically significant genotoxic effect at the concentrations of 2, 10 and 50 µg/cm² ($p < 0.05$) after 24 h of particle exposure (Fig 35e). The particles were found non-genotoxic at other concentration applied and time points measured.

*Raw data of all the measurements are presented in Table 1 - Appendix 7.*

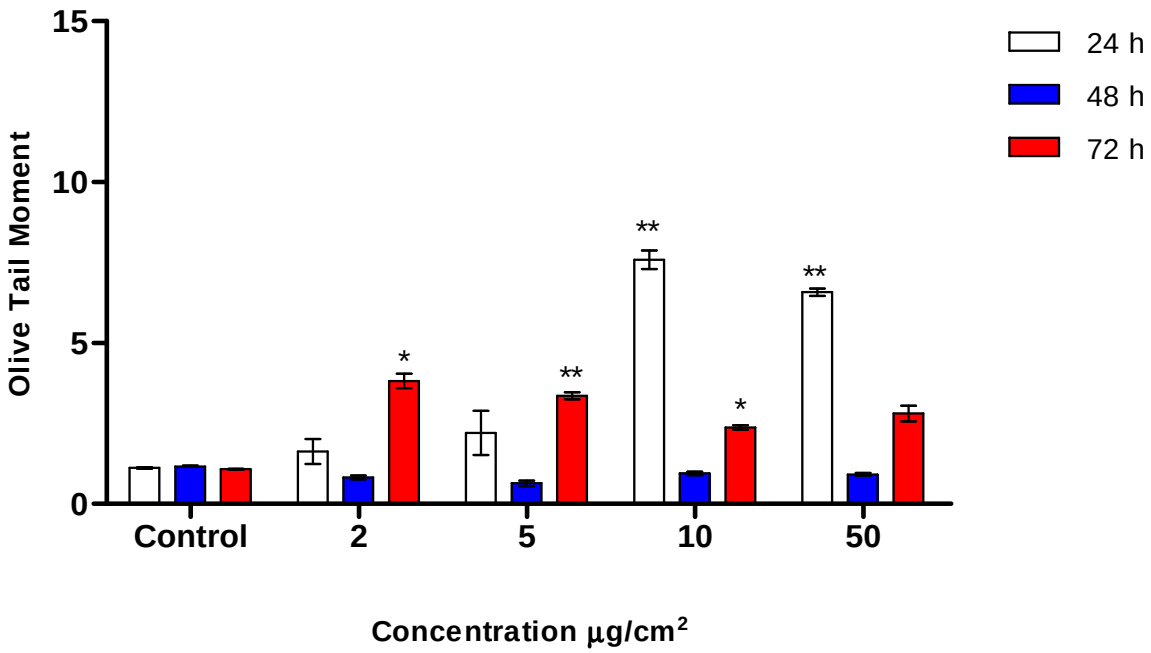


**Figure 35c:** Comet assay of IMR-90 cells exposed to hematite fine particles

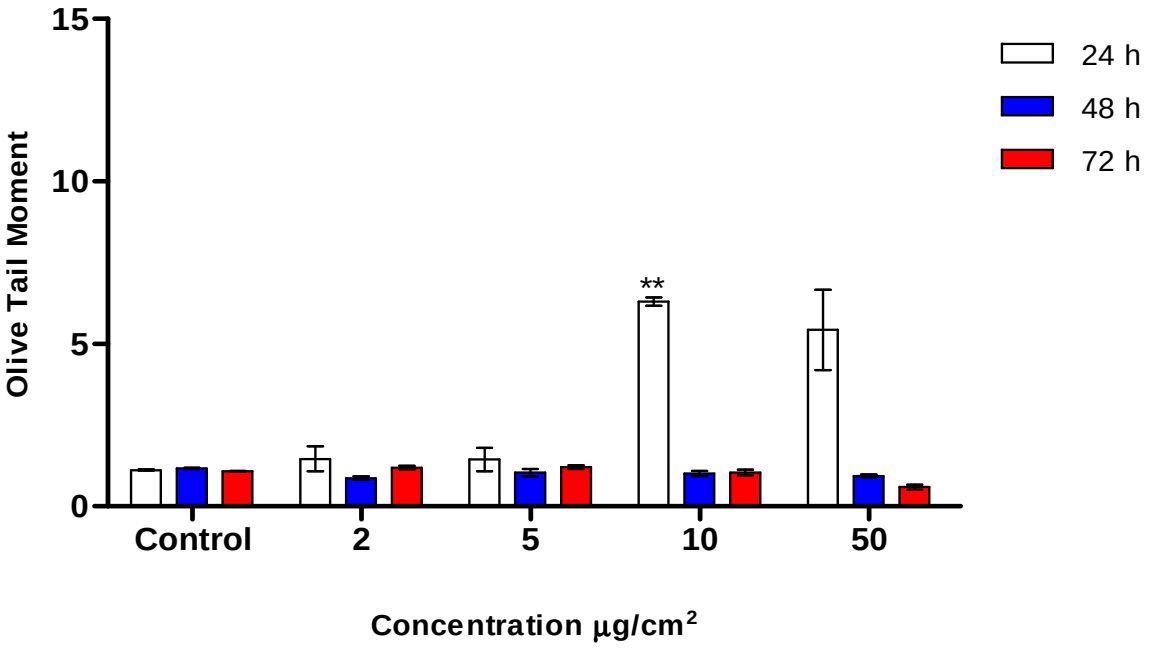


**Figure 35d:** Comet assay of IMR-90 cells exposed to quartz (DQ12) fine particles

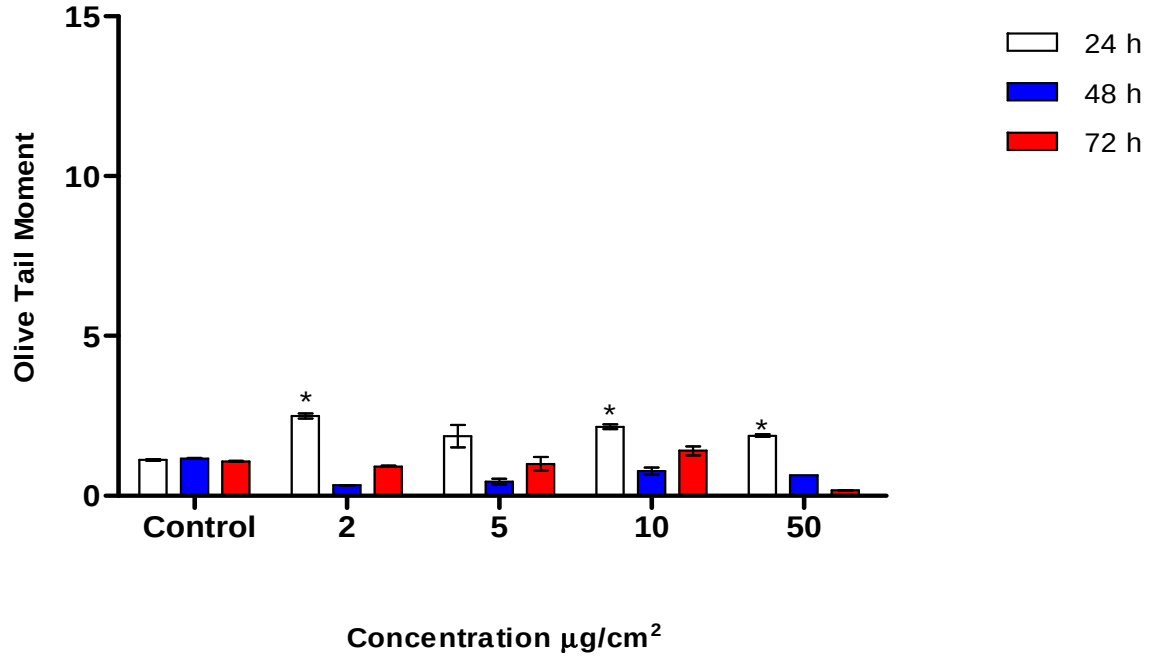


**Figure 35e:** Comet assay of IMR-90 cells exposed to arsenopyrite ash particles

### 3.2.4.2 BEAS-2B cells

***Nanoparticles***

***Hematite***

Exposure of BEAS-2B cells to hematite nanoparticles induced a genotoxic effect at 50 µg/cm² particle concentration after 24 and 72 h exposures. However, these effects were not found to be statistically significant. Genotoxicity induced by these particles in the BEAS-2B cells was also fivefold lower in magnitude as compared to the IMR-90 cells after exposure to the same particle concentrations and at the same time points (Fig. 35f).

***Titanium dioxide ($TiO_2$)***

$TiO_2$ particles proved to be completely non-genotoxic in this test system at all the concentrations and time points measured (Fig. 35g).

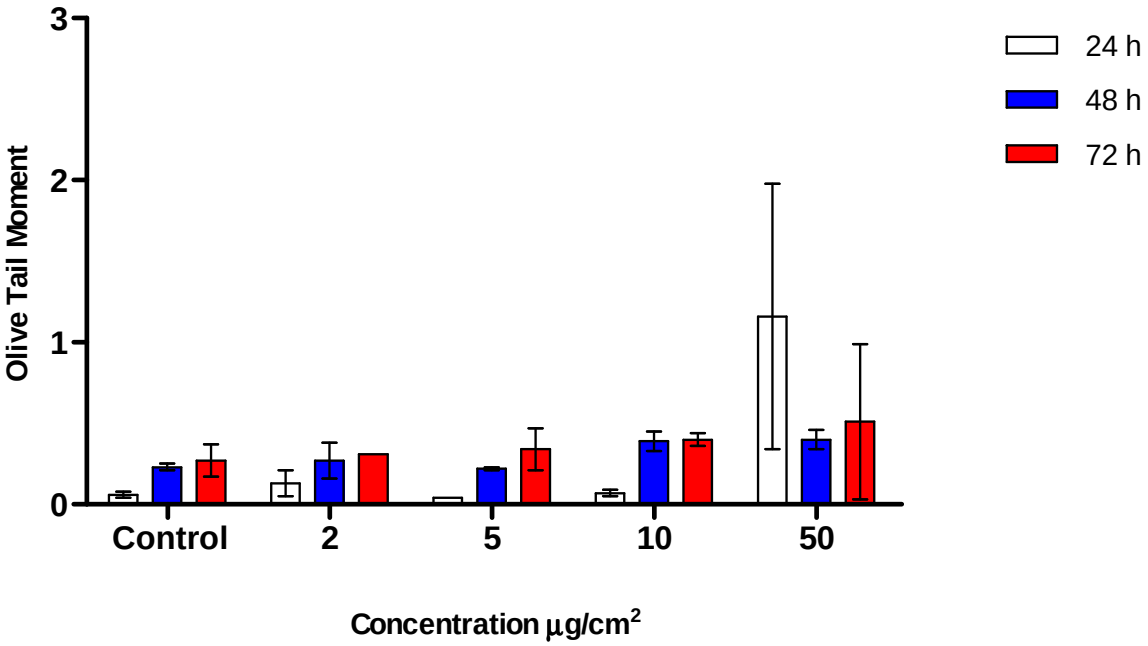


**Figure 35f:** Comet assay of BEAS-2B cells exposed to hematite nanoparticles

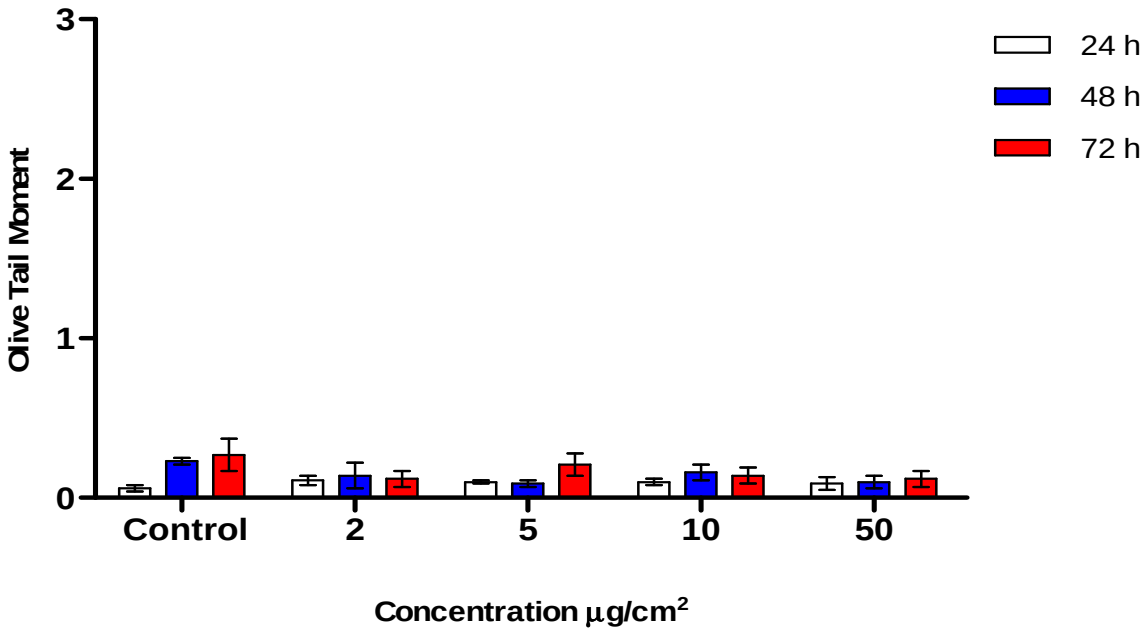


**Figure 35g:** Comet assay of BEAS-2B cells exposed to titanium dioxide nanoparticles

***Fine particles***

***Hematite***

Hematite fine particles induced strong genotoxic effects in the BEAS-2B cells at the concentrations of 2, 5 and 10 µg/cm² and the exposure time point of 24 h. Statistically significant genotoxic effect found at 5 µg/cm² particle concentration only ($p < 0.05$). These particles were found to be non-genotoxic at the other applied particle concentrations and longer exposure time points of 48 and 72 h (Fig. 35h).

***Quartz (DQ12)***

A negligible but statistically significant genotoxic effect as compared to the negative control was observed on DQ12 particle exposure at the concentration of 5 µg/cm² and 24 h time point. Highest genotoxic effect was observed on exposure to 50 µg/cm² particle concentration and long exposure time points of 48 and 72 h. But these effects were not found to be statistically significant (Fig. 35i).

***Arsenopyrite ash***

Arsenopyrite ash particles were found to be completely non-genotoxic in the BEAS-2B cells at all concentrations and time points measured (Fig. 35j).

*Raw data of all the measurements are presented in Table 2 - Appendix 7.*

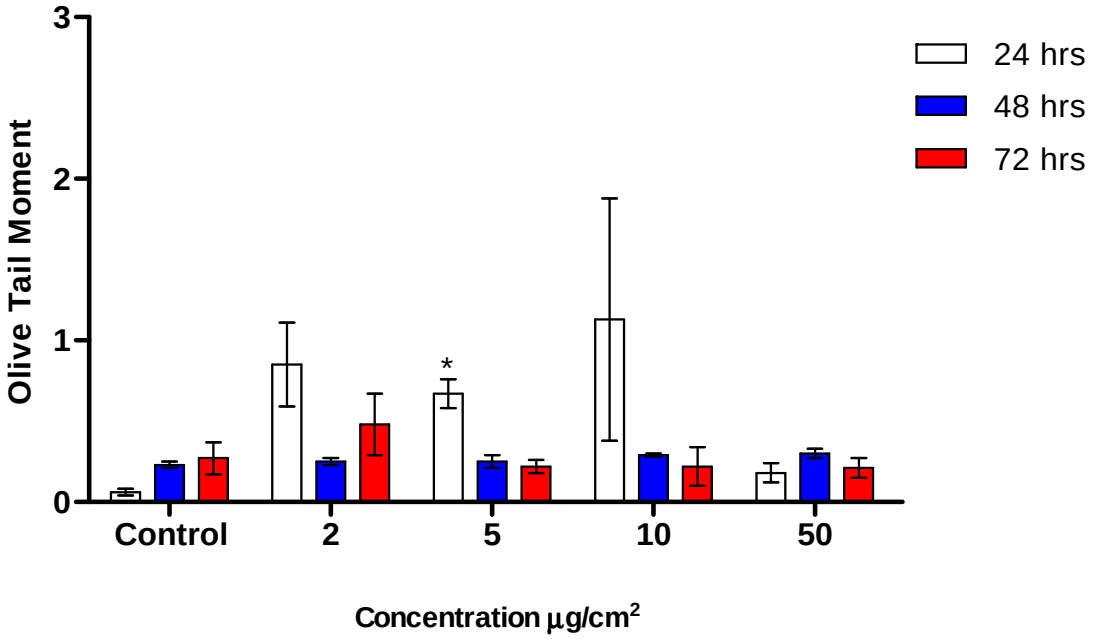


**Figure 35h:** Comet assay of BEAS-2B cells exposed to hematite fine particles

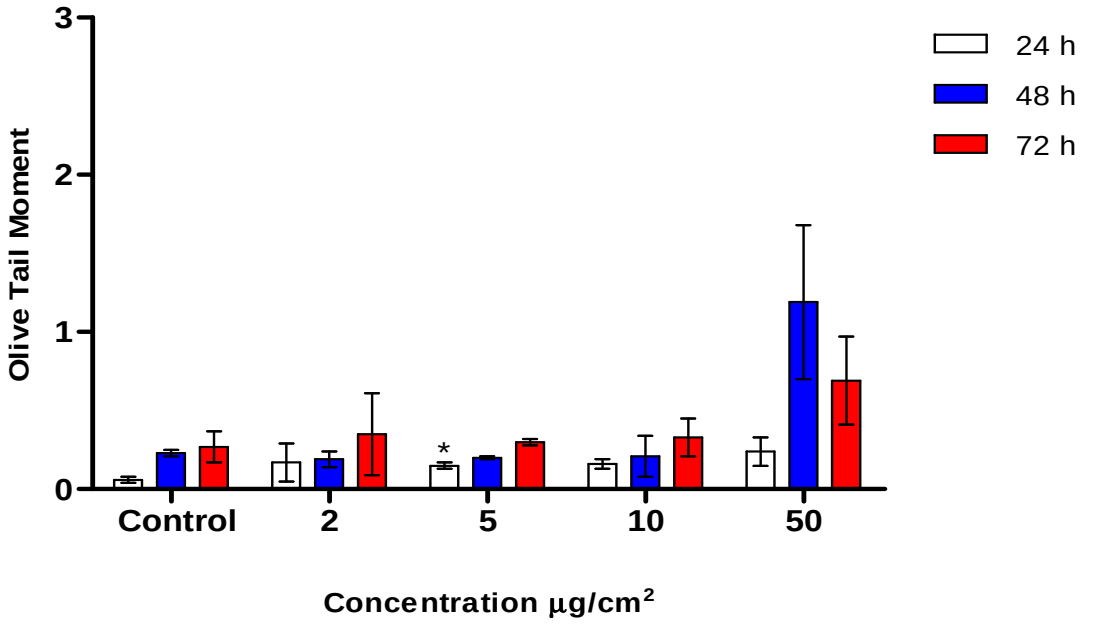


**Figure 35i:** Comet assay of BEAS-2B cells exposed to quartz (DQ12) fine particles

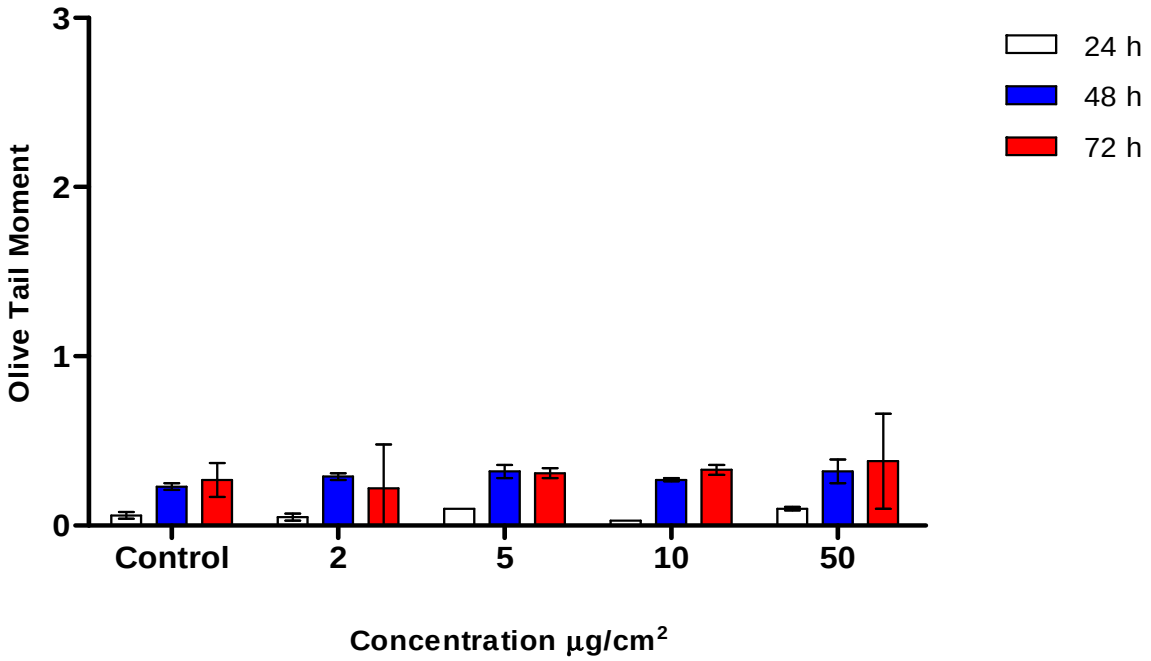


**Figure 35j:** Comet assay of BEAS-2B cells exposed to arsenopyrite ash particles

The genotoxicity analysis revealed that the two cell types responded differently to the same particle. BEAS-2B cells were found to be less susceptible to genotoxic effect from particle exposures as compared to the IMR-90 cells. While the $TiO_2$ nanoparticles remained non-genotoxic at all particle concentrations and time periods analyzed, iron containing fine and nanoparticles were most genotoxic at the concentrations of 10 and 50 µg/cm² and at the time point of 24 h. A reduction in DNA fragmentation was found at 48 h that might be related to the DNA repair mechanism acting during the normal cell cycle of 25 h in the case of the IMR-90 cells and 24 h in the case of BEAS-2B cells. The second effect observed at 72 h may be a cumulative effect from the deteriorated condition of the culture medium due to long term usage by the cells and a constant injury from the particles present in the cells.

### 3.2.5 Acellular ROS production under oxidizing and reducing conditions

Acellular ROS generation by the particles under oxidizing and reducing conditions at 37℃ and aerobic condition was analyzed using the electron paramagnetic resonance (EPR) technique (page – 40). For analyzing under oxidizing

condition the particles were treated with $H_2O_2$ to produce a replica of the condition they might face after internalization within bronchial phagocytic and epithelial cells.

The results indicated the highest acellular ROS generation was induced by arsenopyrite ash particles and the lowest by the hematite nanoparticles. DQ12, hematite fine particles and $TiO_2$ nanoparticles generated ROS in decreasing amounts. It may be noted that just the presence of Fe ions in the arsenopyrite ash particles cannot be held responsible for this high amount of acellular ROS generation, as the presence of significant amount of other transition elements was also observed from the EDX study. DQ12 had been implicated in a lot of studies to generate ROS with the help of its negative surface charge and trace elements present on the surface. Hematite fine particles were also found to produce high amounts of ROS, which gives a rise to the assumption that $H_2O_2$ reacted with Fe(III) producing large quantity of ROS under aerobic conditions and at 37℃. Furthermore, the reaction might occur on the surface of the iron containing particles as no chelable amount of Fe ions were found from the analysis using 1,10-phenanthroline chloride. $TiO_2$ nanoparticles also produced relatively small amount of acellular ROS. The hematite nanoparticles were found to generate the lowest amount of acellular ROS, even though it is chemically the same as the hematite fine particles. The result pointed towards a role played by the surface charge of these particles leading to their agglomeration them together in the liquid suspension medium. Therefore, in contrast to providing more surface area as compared to the fine particles for reaction, nanoparticles practically provided less surface area for the $H_2O_2$ radical ions to react (Fig. 36).

*Raw data of all the measurements are presented in Table 1 - Appendix 8.*

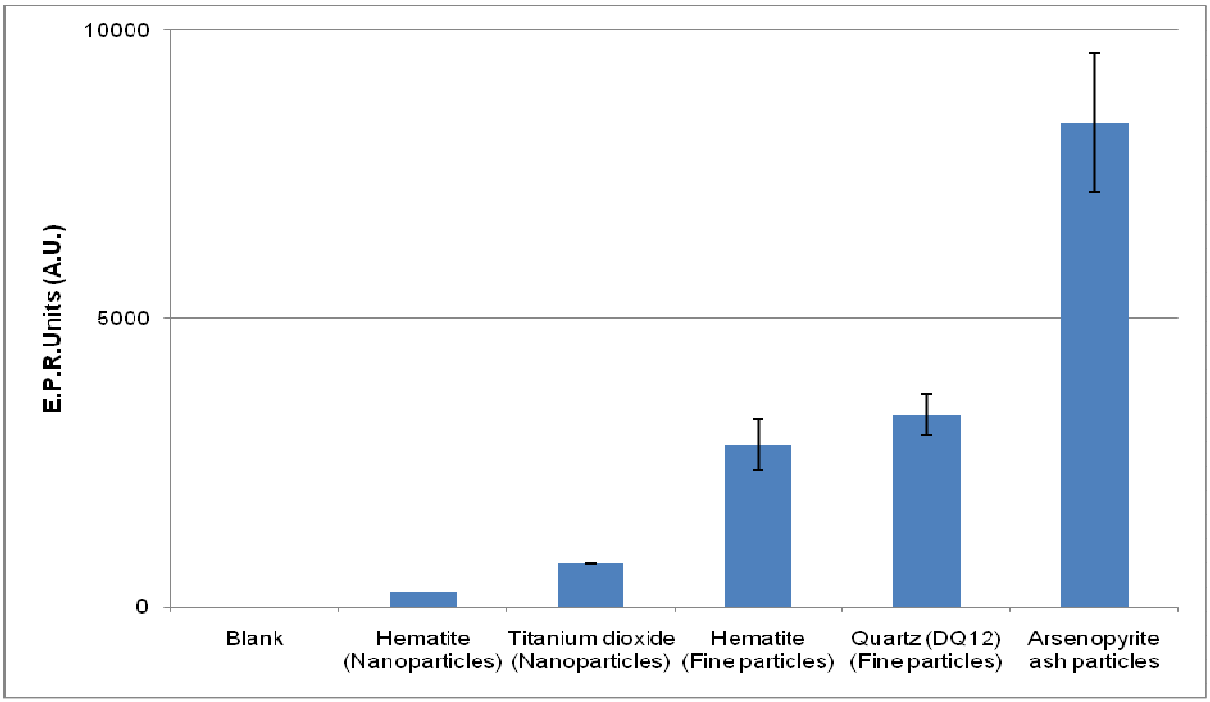


**Figure 36:** Acellular ROS production by different particles after treatment with $H_2O_2$ and spin trap – DMPO

Kim *et al.* (1998) had found that the pH of intracellular organelles such as, ER and Golgi apparatus can change between alkaline and acidic conditions depending upon the prevailing circumstances and in order to balance the pH between the intraorganelle space and the surrounding cytosol. Previously, we had found uptake of all the particles followed by a long-term retention of the fine particles inside the ER and the penetration by the hematite nanoparticles into the cytoplasmic region directly or indirectly. To observe a reduction of the Fe(III) ions present on the surface of the particles to Fe(II) under a biological reducing condition followed by Fenton reaction we pre-treated the particles with ascorbic acid or whole cell lysate followed by a treatment with $H_2O_2$.

The results obtained from exposing the particles to ascorbic acid and then to $H_2O_2$ under aerobic condition and at 37℃ demonstrated t hat both the arsenopyrite ash and hematite nanoparticles produced 100 x times more acellular ROS as compared to the amount produced by these particles on a single treatment with $H_2O_2$. Furthermore, both these particles produced ROS in a time- and concentration-dependent manner. Hematite fine particles also produced the double amount of acellular ROS after treatment with ascorbic acid and then with $H_2O_2$, but only at the 2

h time point. DQ12 and $TiO_2$ particles produced a constant amount of ROS that was equal to the amount being produced by them only with $H_2O_2$ treatment (Fig. 37).

These results demonstrated a complete conversion of hematite particle surface-bound Fe(III) ions into Fe(II) through a reducing reaction. It also pointed towards a possible alteration of the surface charge of the hematite nanoparticles minimizing the cluster formation inside the suspension medium and providing a larger surface area for the $H_2O_2$ to react. The same may hold true for the nanoparticle size fraction of the arsenopyrite ash particles also.

*Raw data of all the measurements are presented in Table 2 - Appendix 8.*

To understand this ROS producing mechanism by the particles under a more realistic reducing condition, the particles were treated with whole cell lysate and then with $H_2O_2$. The results demonstrated that even though the basic pattern of ROS production by the particles remained the same as found with their earlier treatment of ascorbic acid and $H_2O_2$, the quantity of acellular ROS generated was much lower. Hematite nanoparticles followed by the arsenopyrite ash particles were still found to produce the highest amount of ROS among all the particles. All the other particles including hematite fine particles either produced negligible amount of ROS or nothing at all (Fig. 38). A reason for this can be a strong binding and accumulation of the proteins freely available in the lysate to the particle due to surface charge and, thus limiting the space for the reducing agents present in the cell lysate to react with the particle surface. This result again points towards the role played by the higher surface area and charge on the particles in reacting with the radicals and other biomolecules.

*Raw data of all the measurements are presented in Table 3 - Appendix 8.*

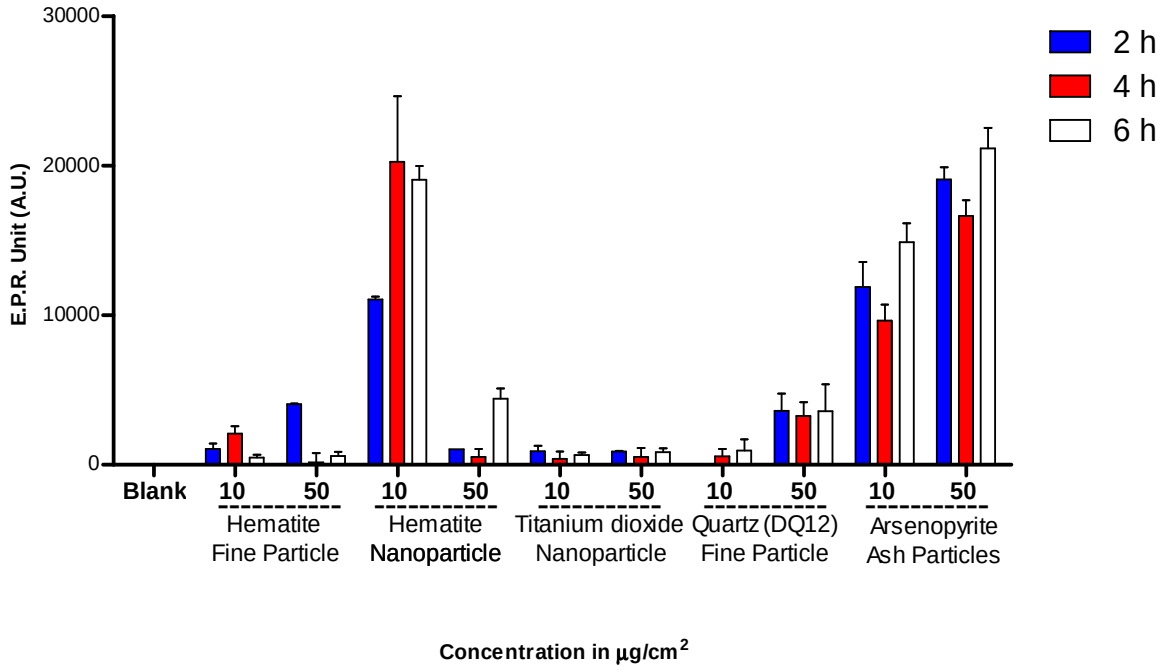


.

**Figure 37:** Acellular ROS measurement with the electron paramagnetic resonance (EPR) technique after treatment of the particles with ascorbic acid and $H_2O_2$

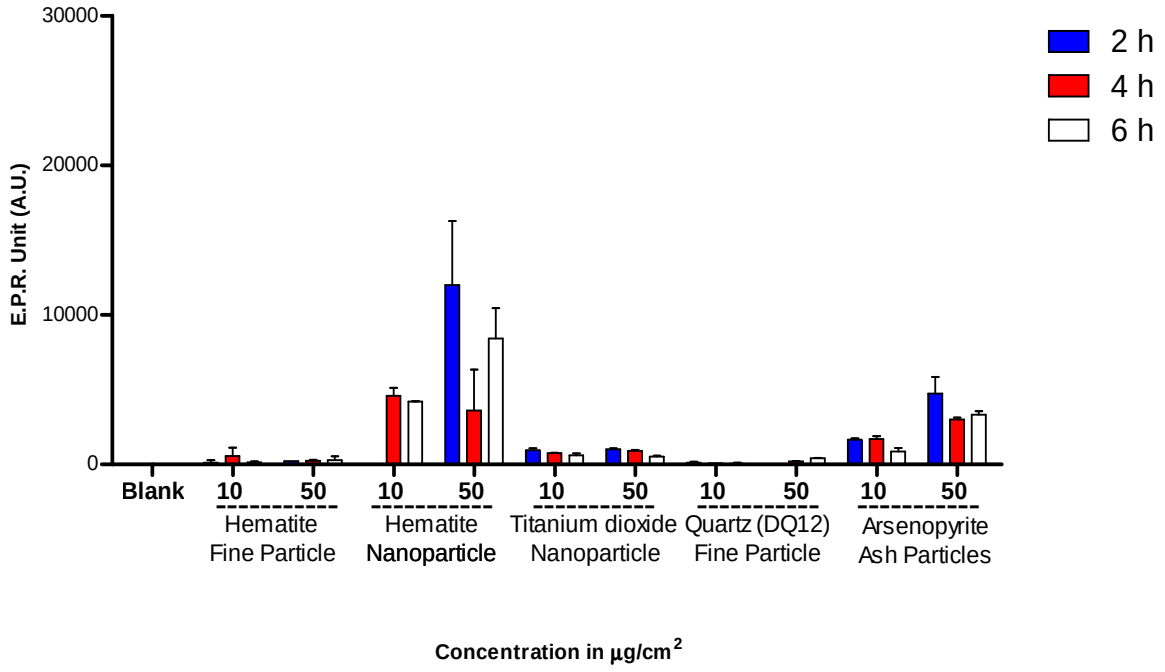


**Figure 38:** Acellular ROS measurement with the electron paramagnetic resonance (EPR) technique after treatment of the particles with whole cell lysate of BEAS-2B cells and $H_2O_2$

### 3.2.6. Intracellular ROS production

#### 3.2.6.1 Nanoparticles

***Hematite***

No generation of intracellular ROS was observed in the BEAS-2B cells at the short exposure time points of 1 and 6 h. Generation of intracellular ROS in the BEAS-2B cells started after 12 h exposure time with a slight time-dependent increase of the ROS level till 24 h. No difference in the ROS generation level was observed between 24 and 48 h. Generation of intracellular ROS by the BEAS-2B cells at particle concentrations of 2 and 5 µg/cm² and at the 12 h time point were found to be statistically significant ($p < 0.01$ and $< 0.05$, respectively) compared to the control (untreated cells) (Fig. 39a).

These results clearly point towards a late generation of intracellular ROS by the BEAS-2B cells following exposure to the particles. The possible mechanism being elucidated here might be correlated to the uptake and translocation of the particles inside the cells, where the reduction of Fe(III) to Fe(II) occurred initially after reacting with the antioxidant biomolecules and followed by intracellular generation of ROS thereafter according to the Fenton reaction.

***Titanium dioxide ($TiO_2$)***

$TiO_2$ nanoparticles prompted a spontaneous generation of intracellular ROS in the BEAS-2B cells. This was found to be directly proportional to the particles concentration applied to the BEAS-2B cells. Interestingly however the generation of intracellular ROS could not be related to the time of exposures. A statistically significant amount of intracellular ROS generation was observed after 1 h particle exposure at the concentrations of 2 µg/cm² ($p < 0.05$), 5 µg/cm² ($p < 0.05$), 10 µg/cm² ($p < 0.05$) and 50 µg/cm² ($p < 0.05$) and after 48 h particle exposure to the concentrations of 10 µg/cm² ($p < 0.05$) and 50 µg/cm² ($p < 0.01$). Highest ROS production was observed at the concentration of 50 µg/cm² and at the time point of 24 h, but it was found to be statistically insignificant due to the large standard deviation (Fig. 39b).

*Raw data of all the measurements are presented in Table 1 and 2 - Appendix 9.*

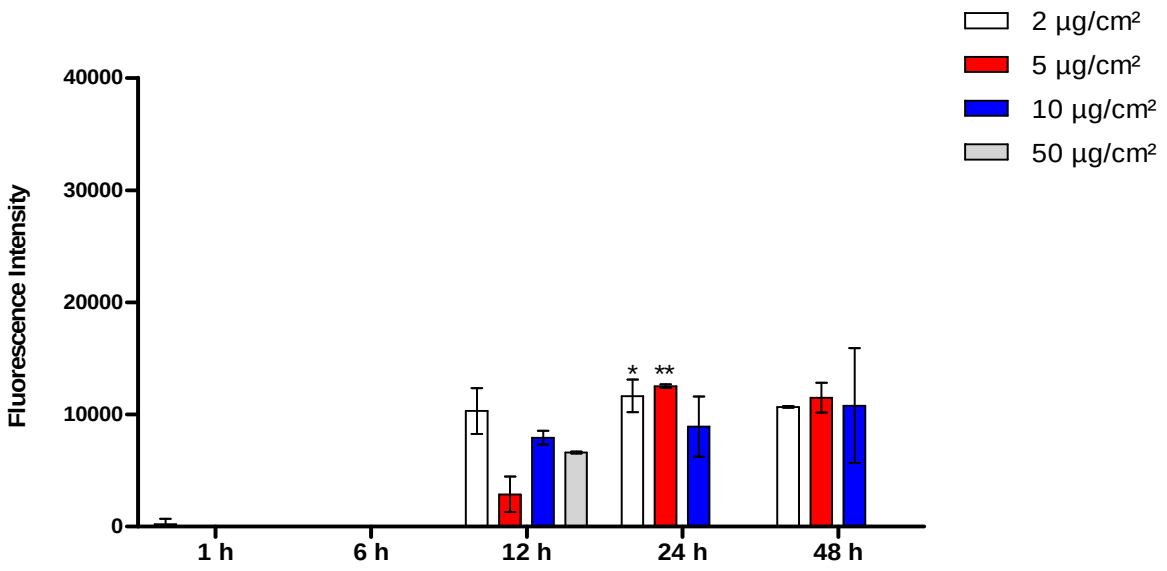


**Figure 39a:** Relative values of intracellular ROS measurement in BEAS-2B cells treated with hematite nanoparticles ($p < 0.05$ *; $< 0.01$ **)

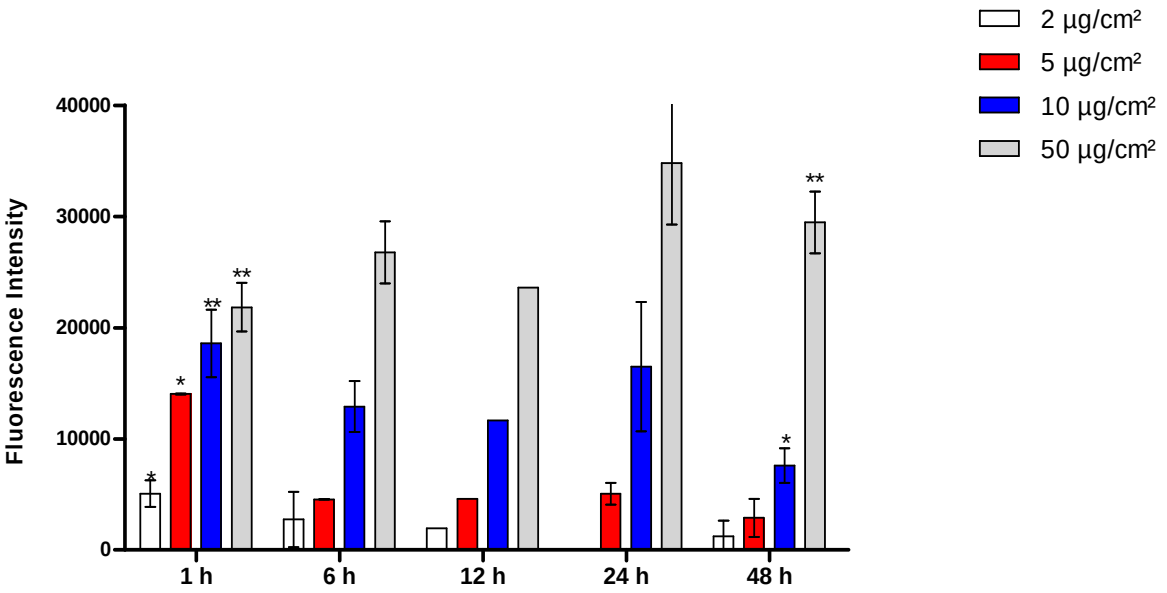


**Figure 39b:** Relative values of intracellular ROS measurement in BEAS-2B cells after treatment with titanium dioxide nanoparticles ($p < 0.05$ *; $< 0.01$ **)

### 3.2.6.2 Fine particles

***Hematite***

Exposure of BEAS-2B cells to hematite fine particles led to a spontaneous generation of intracellular ROS at all the particle concentrations applied. This intracellular ROS generation remained fairly stable till the particle exposure time point of 12 h. At the longer exposure time points of 24 and 48 h, the generation of intracellular ROS was found to get reduced. All particle concentrations at the exposure time points of 1 h generated statistically significant amounts of ROS (2, 5, 10 and 50 µg/cm²- $p < 0.05$). Similarly, after 6 h particle exposure to the BEAS-2B cells a statistically significant ROS generation was found (2, 5 and 50 µg/cm²- $p < 0.05$ and 10 µg/cm²- $p < 0.01$). The applied concentration of 5 µg/cm² ($p < 0.05$) generated a statistically significant amount of intracellular ROS at all exposure time points (12, 24 and 48 h) beside the shorter ones, while the 10 µg/cm² ($p < 0.05$) concentration generated a statistically significant amount of ROS only at the 12 h time point. (Fig. 39c).

***Quartz (DQ12)***

Exposure of the BEAS-2B cells to DQ12 fine particles led to a spontaneous and continuous generation of ROS. Immediately after exposure of the BEAS-2B cells to the particle at 1 h time point statistically significant generation of intracellular ROS was found at all concentrations applied (2, 5, 10 and 50 µg/cm² $p < 0.05$) as compared to the negative control (untreated cells). At the 6 h exposure time point applied particle concentrations of 5 and 10 µg/cm² were found to generate statistically significant amount of ROS intracellularly ($p < 0.05$). Highest amount of ROS generation was found at the particle concentrations of 5, 10 and 50 µg/cm² after 12 h exposure. Though intracellular ROS generated only at the applied concentration of 50 µg/cm² was found to be statistically significant ($p < 0.05$). Most statistically significant intracellular ROS generation was found at the exposure time point of 24 h where, both 5 and 50 µg/cm² particle concentrations generated intracellular ROS having a p of <0.01, followed by the applied particle concentration of 10 µg/cm² having a p of <0.05 (Fig. 40d)

***Arsenopyrite ash***

Exposure of the BEAS-2B cells to arsenopyrite ash particles led to a modest generation of intracellular ROS. An upward trend reaching the peak level at 24 h after exposure was found. Later measurement taken at the time point of 48 h showed a trend for reduction. It was interesting to find that as compared to the other particles, the lowest applied concentration of 2 µg/cm² generated the highest level of intracellular ROS at 24 h. A statistically significant generation of intracellular ROS was found only at the concentrations and time points of 10 µg/cm²- 6 and 12 h ($p < 0.05$), 2 µg/cm²- 24 h ($p < 0.05$), 5 µg/cm²- 48 h ($p < 0.05$) and 10 µg/cm²- 48 h ($p < 0.01$) (Fig. 39e).

*Raw data of all the measurements are presented in Table3, 4 and 5 - Appendix 9.*

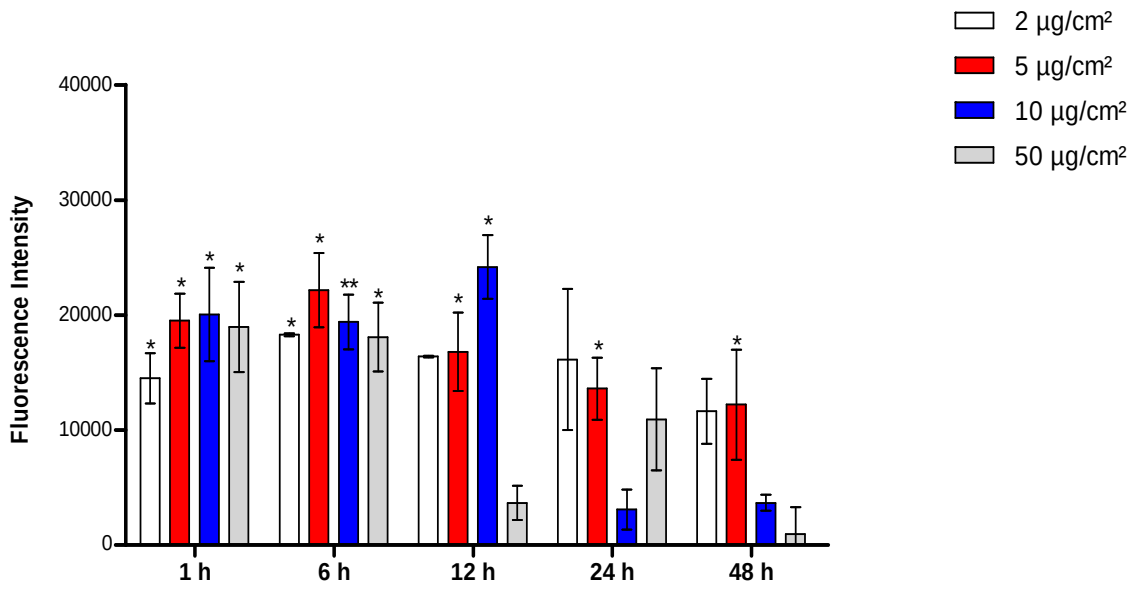


**Figure 39c:** Relative values of intracellular ROS measurement in BEAS-2B cells after treatment with hematite fine particles ($p < 0.05$ *; $< 0.01$ **)

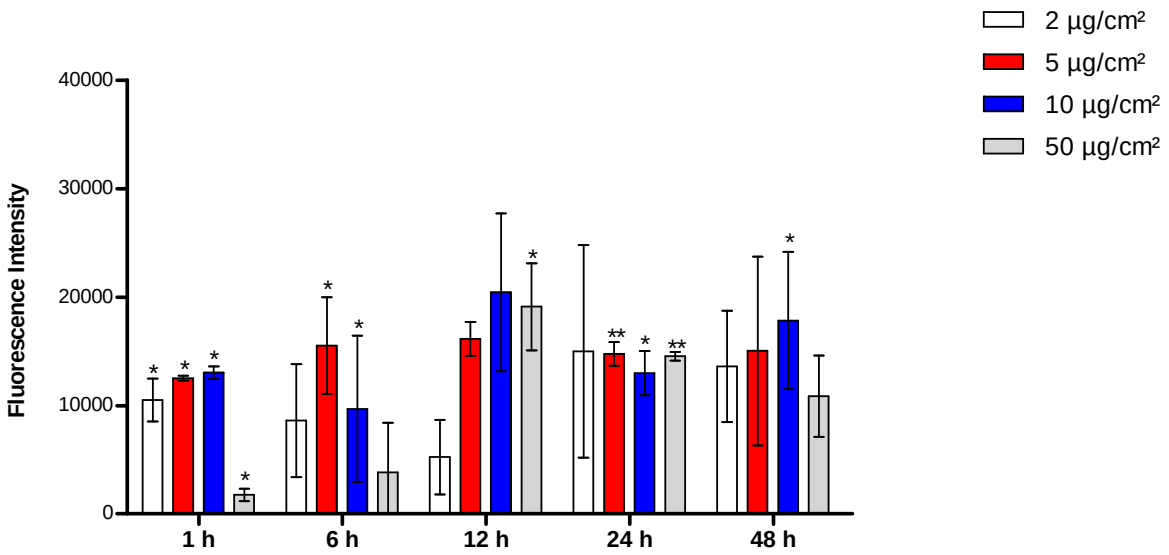


**Figure 39d:** Relative values of intracellular ROS measurement in BEAS-2B cells after treatment DQ12 fine particles ($p < 0.05$ *; $< 0.01$ **)

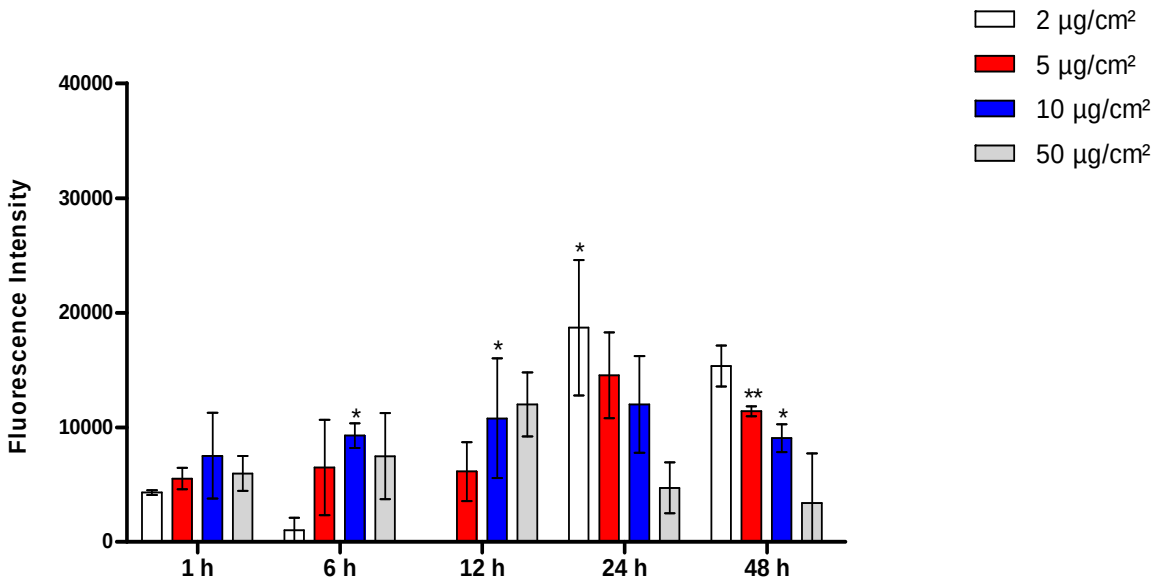


**Figure 39e:** Relative values of intracellular ROS measurement in BEAS-2B cells after treatment arsenopyrite ash particles ($p < 0.05$ *; $< 0.01$ **)

### 3.2.6.3 Desferoxamine treatment

***Nanoparticles***

The combined exposure of desferoxamine and nanoparticles to the BEAS-2B cells was found to be not effective enough in reducing the generation of intracellular ROS. On co-exposure with hematite and $TiO_2$ nanoparticles desferoxamine was only able to reduce intracellular ROS at the concentration of 5 µg/cm² and the time point of 12 h. The reduction observed with the application of 5 µg/cm² particle concentration of $TiO_2$ and desferoxamine was found to be statistically significant ($p < 0.05$) as compared to the intracellular ROS generated by the cells only on nanoparticle exposure. At all the other applied concentrations of particles and time points a co-exposure of desferoxamine led to a higher generation of intracellular ROS (Fig. 39f).

*Raw data of all the measurements are presented in Table 1 and 2 - Appendix 9.*

***Fine particles***

Co-exposure of BEAS-2B cells with different concentrations of fine particles and desferoxamine revealed a reduction of the ROS generation similar to that observed with nanoparticles. A reduction of the intracellular ROS generation was observed with hematite and DQ12 fine particles only at the applied concentrations of 5 and 10 µg/cm² and the exposure time point of 12 h. Only the reductions demonstrated by hematite fine particles (2 and 5 µg/cm²- 12 h time point) were found to be statistically significant ($p < 0.05$). At all other applied concentrations and exposure time points measured, an increase in the intracellular ROS generation level was observed (Fig. 39g).

*Raw data of all the measurements are presented in Table 3,4 and 5 - Appendix 9.*

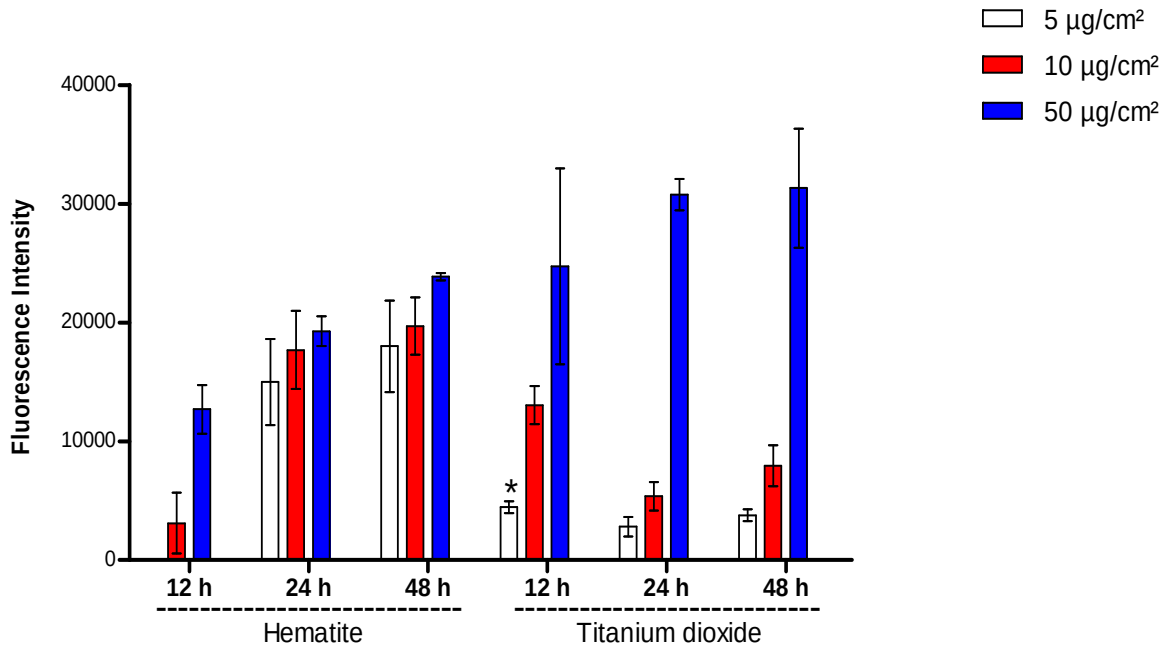


**Figure 39f:** Relative values of intracellular ROS measurement in BEAS-2B cells after co-exposure with different concentrations of hematite and $TiO_2$ nanoparticles and 100 µM desferoxamine ($p < 0.05$ *)

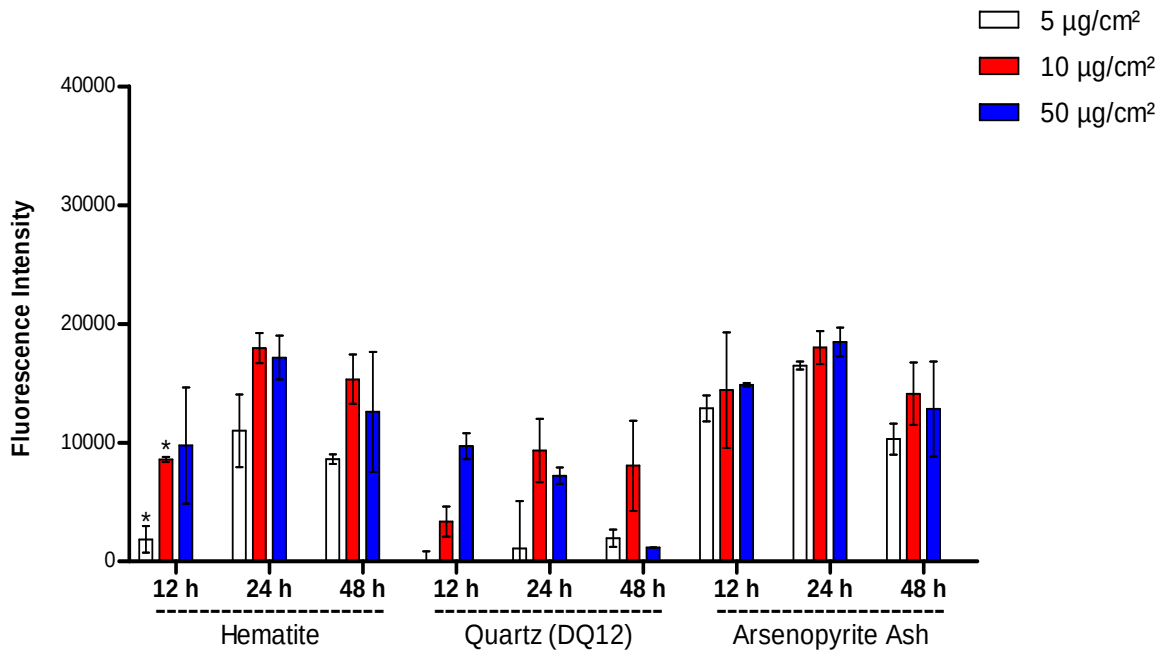


**Figure 39g:** Relative values of intracellular ROS measurement in BEAS-2B cells after co-exposure with different concentrations of fine particles and 100 µM desferoxamine ($p < 0.05$ *)

### 3.2.7 8-OHdG detection

Exposing the IMR-90 cells to different fine and nanoparticles for 24 h revealed that only hematite fine particles at the concentration of 10 µg/cm² and $TiO_2$ at the concentrations of 5 and 10 µg/cm² were capable of inducing 8-OHdGs. Quantitatively, it was found that hematite fine particles produced 0.1 ng/ml, and $TiO_2$ nanoparticles at the concentrations of 5 and 10 µg/cm² produced 1 and 1.1 ng/ml of 8-OHdG adducts, respectively. One ml of liquid suspension contained the whole genome extract from approx. 2 million cells (Fig. 40).

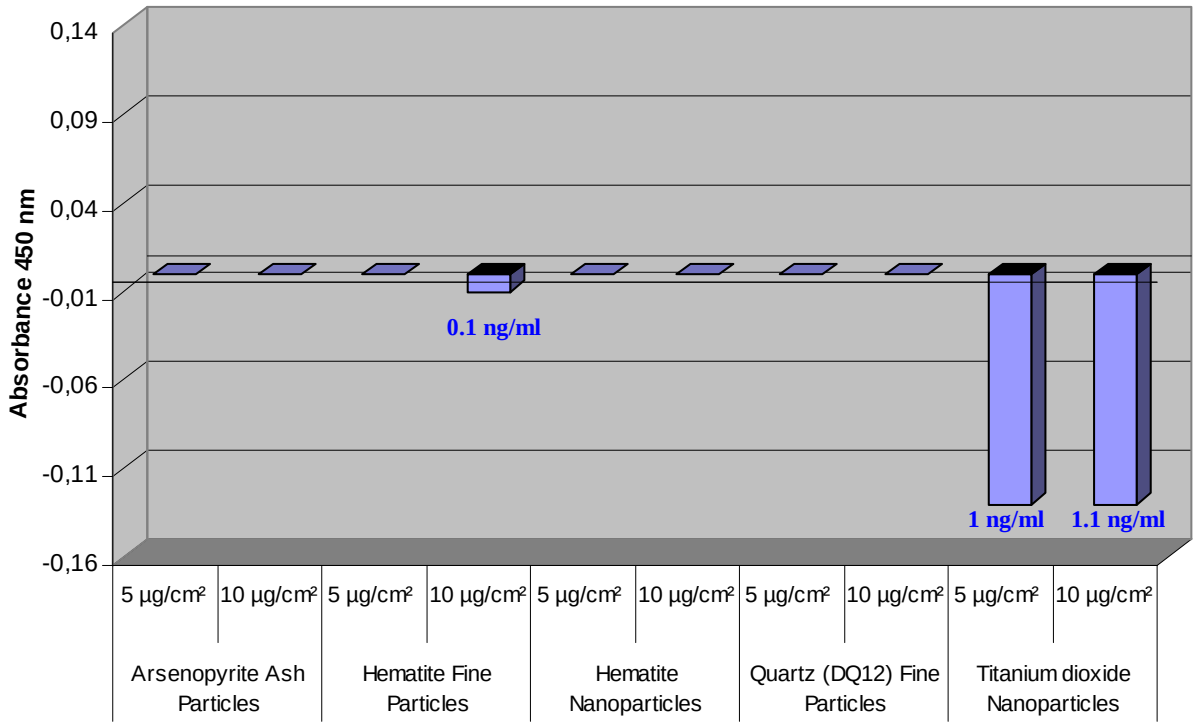


**Figure 40:** 8-OHdG adduct measurement in IMR-90 cells after treatment with different concentrations of particles for 24 hrs and measurement with ELISA at 450 nm absorbance

### 3.2.8 Microarray analysis for gene up-regulation on particle exposure

Exposure of IMR-90 cells to the hematite fine, arsenopyrite ash and gypsum particles at the concentration of 10 µg/cm² and the time point of 48 h led to an up-regulation of 50 and down-regulation of 40 genes for each particle. On grouping the up-regulated genes based upon particles the IMR-90 cells were exposed to 30 genes were found to be universally up-regulated after exposure to all the 3 particles. Eight genes were found to be up-regulated commonly on individual exposures to hematite fine and arsenopyrite ash particles. Similarly, 7 genes on individual exposures to

arsenopyrite ash and gypsum particles and 8 genes on individual exposures to hematite fine and gypsum particles were found to be common among the groups specified. In the cells exposed to hematite fine particles 3 unique genes and on exposure to DQ12 and arsenopyrite ash particles 5 unique genes each were found to be individually up-regulated (Fig. 41).

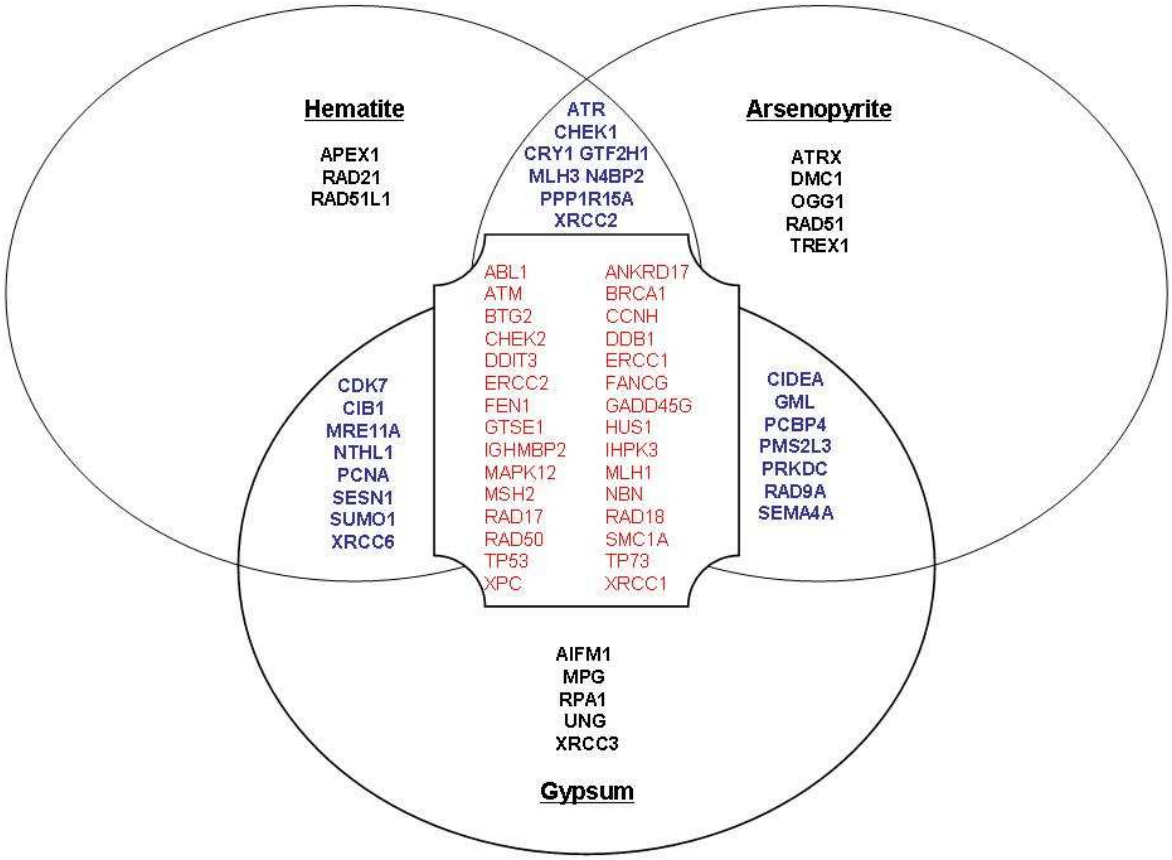


**Figure 41:** Venn diagram of up-regulated genes after exposure of the IMR-90 cells to 10 µg/cm² of hematite fine, arsenopyrite ash and gypsum fine particles for 48 h duration

After exposure to the hematite fine particles a total of 7 genes related to the function of regulating apoptosis (GO:0006915) were up-regulated. Similarly, 8 genes related to the function of cell cycle arrest (GO:0000077) and 5 genes related to cell cycle check point (GO:0007093) were found to be up-regulated. 15 genes were found up-regulated involved in the process of damaged DNA binding (GO:0003684). Four genes related to the function of base–excision repair (GO:0006284) and double-strand break repair (GO:0006302) each and 5 genes related to the process of mismatch repair (GO:0006298) were found up-regulated. Ten genes involved in

different processes of DNA damage repair mechanisms were also found up-regulated. The expression levels were obtained as fold increase between the particle exposed and negative control (untreated) cells (Table 4, 5 and 6; Fig. 42).

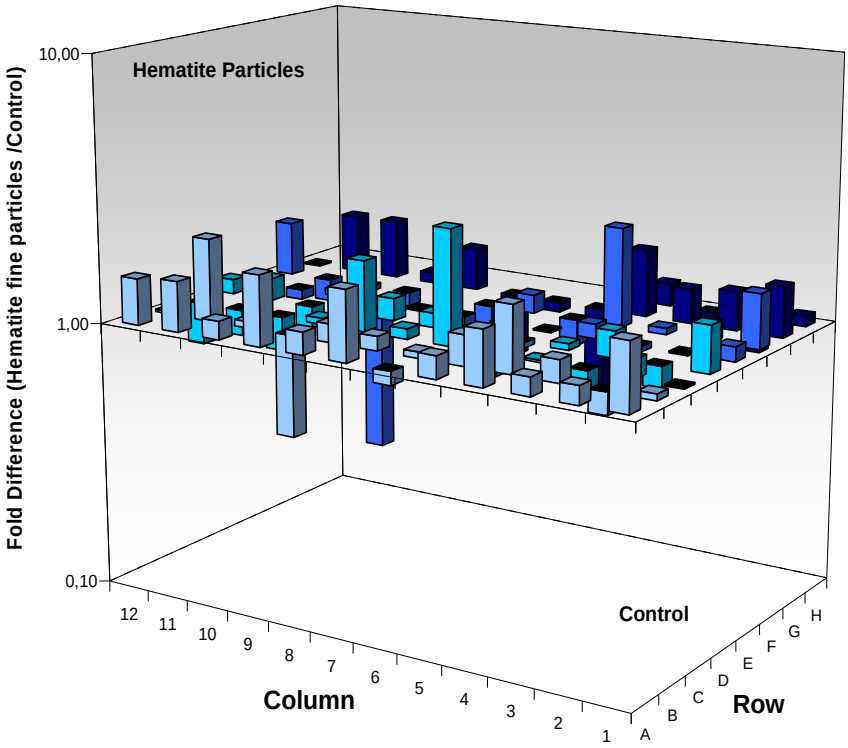


**Figure 42:** The 3D profile graphs the fold difference in expression of each gene between the two samples (hematite fine particles and negative control) in the 96-well format of the PCR array. Columns pointing up (with z-axis values > 1) indicate an up-regulation of gene expression, and columns pointing down (with z-axis values < 1) indicate a down-regulation of gene expression in the test sample relative to the control sample. The related name of genes is provided in Appendix 10 – Table 1.

Similarly, in the case of IMR-90 cells exposed to the arsenopyrite ash particle, 8 genes related to GO:0006915, 10 genes related to GO:0000077, 5 genes related to GO:0007093, 19 genes related to GO:0003684, 3 genes in GO:0006302, 6 genes in GO:0006298, and 8 genes involved in miscellaneous DNA repair processes were found to be up-regulated as compared to the negative control (untreated) (Table 4, 5 and 6; Fig. 43).

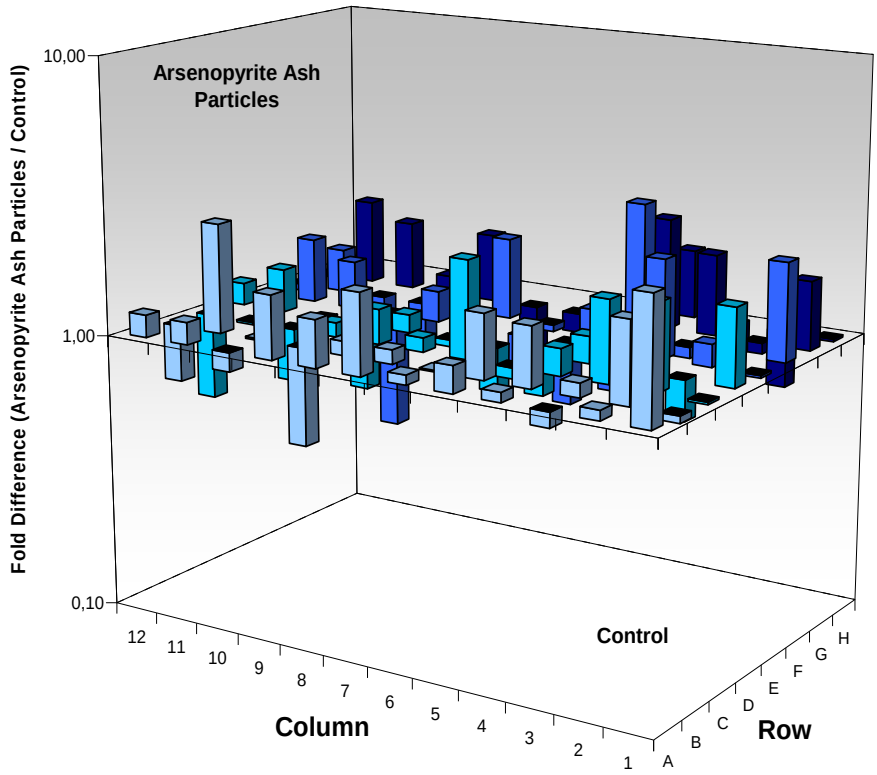


**Figure 43:** The 3D profile graphs the fold difference in expression of each gene between the two samples (arsenopyrite ash particles and negative control) in the 96-well format of the PCR array. Columns pointing up (with z-axis values > 1) indicate an up-regulation of gene expression, and columns pointing down (with z-axis values < 1) indicate a down-regulation of gene expression in the test sample relative to the control sample. The related name of genes is provided in Appendix 10 – Table 1.

In the IMR-90 cells exposed to the gypsum particles, 8 genes in GO:0006915 and GO:0000077 each, 4 genes in GO:0007093, 14 genes in GO:0003684, 4 genes in GO:0006284, 5 genes in GO:0006302 and GO:0006298, and 9 genes in miscellaneous DNA repair processes were found to be up-regulated as compared to the negative control (Table 4, 5 and 6; Fig. 44).

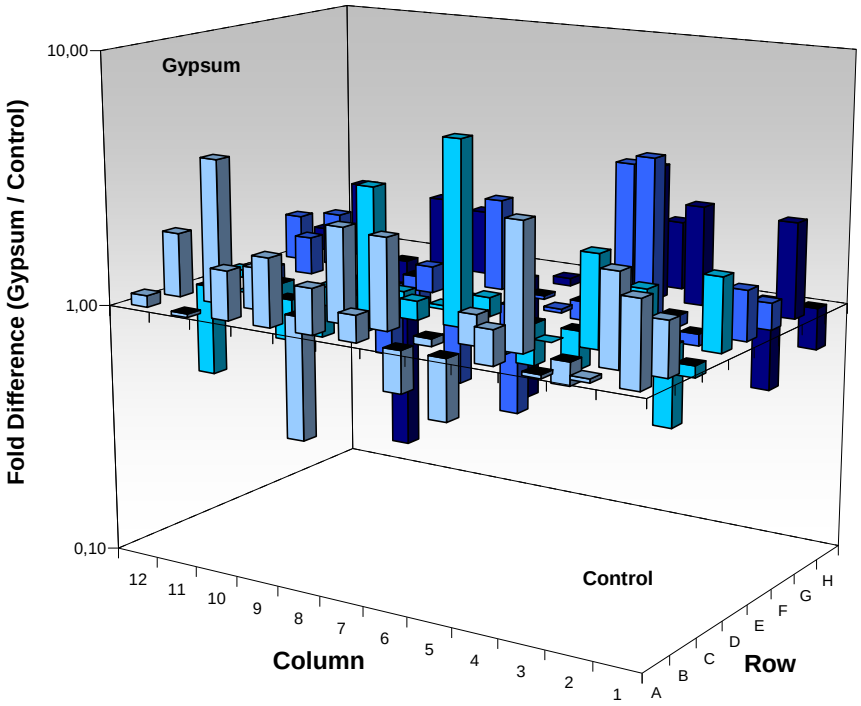


**Figure 44:** The 3D profile graphs the fold difference in expression of each gene between the two samples (gypsum particles and negative control) in the 96-well format of the PCR array. Columns pointing up (with z-axis values > 1) indicate an up-regulation of gene expression, and columns pointing down (with z-axis values < 1) indicate a down-regulation of gene expression in the test sample relative to the control sample. The related name of genes is provided in Appendix 10 – Table 1.

**Table 4:** Assortment of genes on the basis of their functions in DNA damage signalling and universally up-regulated in the IMR-90 cells after exposure to different particles individually

| | | | | | | |
|---|---|---|---|---|---|---|
| **Apoptosis Genes** | ABL1 | BRCA1 | GADD45G | IHPK3 | TP53 | |
| **Cell Cycle Genes** | | | | | | |
| Cell Cycle Arrest | CHEK2 | DDIT3 | GTSE1 | HUS1 | MAPK12 | RAD17 |
| Cell Cycle Checkpoint | BRCA1 | FANCG | SMC1L1 | TP53 | | |
| **DNA Repair** | | | | | | |
| Damaged DNA Binding | ANKRD17 | BRCA1 | DDB1 | ERCC1 | FANCG | FEN1 |
| | MSH2 | NBS1 | RAD18 | XPC | XRCC1 | |
| Double-strand Break Repair | FEN1 | RAD50 | | | | |
| Mismatch Repair | ABL1 | ANKRD17 | MLH1 | MSH2 | | |
| **Other Genes Involved in DNA Repair** | ATM | BTG2 | CCNH | ERCC2 | IGHMBP2 | |

**Table 5:** Grouping of genes assorted on the basis of their functions in DNA damage signalling and up-regulated in the IMR-90 cells after exposure to two different particles individually

| ***Hematite and Arsenopyrite ash*** | | | |
|---|---|---|---|
| **Apoptosis Genes** | PPP1R15A | - | - |
| **Cell Cycle Genes** | | | |
| Cell Cycle Arrest | CHEK1 | PPP1R15A | - |
| Cell Cycle Checkpoint | ATR | - | - |
| **DNA Repair** | | | |
| Damaged DNA Binding | GTF2H3 | N4BP2 | XRCC2 |
| Mismatch Repair | MLH3 | - | - |
| **Other Genes Involved in DNA Repair** | CRY1 | GTF2H1 | - |
| ***Hematite and Gypsum*** | | | |
| **DNA Repair** | | | |
| Base–excision repair | CIB1 | MRE11A | XRCC6B1 |
| Double-strand Break Repair | NTHL1 | - | - |
| **Other Genes Involved in DNA Repair** | CDK7 | PCNA | SUMO1 |
| ***Arsenopyrite ash and Gypsum*** | | | |
| **Apoptosis Genes** | CIDEA | GML | - |
| **Cell Cycle Genes** | | | |
| Cell Cycle Arrest | PCBP4 | RAD9A | - |
| **DNA Repair** | | | |
| Damaged DNA Binding | PMS2L9 | SEMA4A | - |
| Double-strand Break Repair | PRKDC | - | - |

**Table 6:** Grouping of genes assorted on the basis of their functions in DNA damage signalling and up-regulated in the IMR-90 cells after exposure to individual particle

| | **Hematite** | **Arsenopyrite ash** | **Gypsum** |
|---|---|---|---|
| **Apoptosis Genes** | RAD21 | - | PDCD8 |
| **DNA Repair** | | | |
| Damaged DNA Binding | RAD51L1 | DMC1<br>OGG1<br>RAD51 | XRCC3 |
| Base–excision repair | APEX1 | - | MPG<br>UNG |
| Double-strand Break Repair | RAD21 | - | - |
| Mismatch Repair | - | TREX1 | - |
| **Other Genes Involved in DNA Repair** | - | ATRX | RPA1 |

# 4. DISCUSSION

Aim of this study was to investigate the toxic behaviour of fine and nanosize iron-containing particles (hematite and arsenopyrite ash) along with fine sized quartz (DQ12) and $TiO_2$ nanoparticles in human lung cells *in vitro*. The factors taken into account for this analysis were: i) physico-chemical properties of the particles, ii) uptake of the particles by human lung epithelial cells followed by intracellular translocation, iii) capability of the particles to induce cyto- and genotoxicity in different lung cells, iv) primary and secondary ROS generation, and v) genomic damage caused by oxidative stress followed by an up-regulation of the DNA repair mechanisms.

## 4.1 Physico-chemical properties of the particles

Both the hematite and DQ12 fine particles were found within the size range of $PM_{2.5}$. A large percentage of the industrially generated arsenopyrite ash particles were in the size range of <500 nm. Interestingly, particles size distribution analysis of the hematite nanoparticles showed a high percentage of particles in the size range of 100-<500 nm even though they were certified by Sigma – Aldrich GmbH to contain a high percentage of $PM_{0.1}$. It was later confirmed by SEM image analysis that over 90% of the particle content belonged to $PM_{0.1}$. The size distribution analysis results using particle size analyzers therefore indicated towards formation of agglomerations by the nanoparticles inside liquid suspensions. Limbach *et al.* (2005) have related the property of nanoparticles to agglomerate in liquid to their high surface charge (zeta potential).

Both, hematite fine and nanoparticles showed a high percentage of Fe and O. Arsenopyrite ash particles were also found to contain the basic elements of Fe and O along with a high percentage of Ca and S and a small proportion of arsenic. The arsenic component present in the arsenopyrite ash particles was identified as being $As_2O_3$ by ICP-MS. Quantitatively, the amount of iron present in all three types of particles (hematite nanosized, fine and arsenopyrite ash) was found to vary minutely.

Due to the low concentration of $As_2O_3$ present in the arsenopyrite ash particles it was considered as non-toxic to the cells. Andrew *et al.* (2003) has found that $As_2O_3$

in a concentration of up to 5 µM did not cause any change in gene expression of BEAS-2B cells.

No chelable form of iron was found in the iron containing particles. This indicated that iron is present only in bound form. Both, DQ12 and $TiO_2$ particles turned out to be free of any iron contamination. The high content of Fe(III) in the iron-containing particles provided them with a high positive surface charge (He *et al.,* 2008). Furthermore, hematite ($Fe_2O_3$) is also known as a ferromagnetic particle due its property quality to get magnetized and to maintain this feature for some time (Woo and Lee, 2004). DQ12 fine and $TiO_2$ nanoparticles have been found to contain a negative surface charge (Nolan *et al.*, 1981; Ridley *et al.,* 2001).

Morphologically, only hematite and $TiO_2$ nanoparticles were found to be spherical in shape. All the other particles had a heterogenous form. It has been observed that the toxic potential of a particle is a collective consequence of all its physico-chemical properties (Salvi and Holgate, 1999).

### 4.2 Uptake and translocation of particles in BEAS-2B cells

Lung epithelial tissue forms the first line of innate immune defence against inhaled toxic substances and can produce inflammatory mediators (Helbock *et al.,* 1998), reactive oxygen species (Bammler *et al.,* 2005; Bayram *et al.,* 1998), and transcription factors such as, NFκB and activator protein-1 pathways (Nel *et al.,* 2001; Jimenez *et al.,* 2000). In order to reach for the mesenchymal region and blood capillaries of the lungs, particles have to cross through the epithelial tissue layer (Oberdörster *et al.,* 2005b).

The normal mode of transport for different particles has been observed to be through phagocytosis, micropinocytosis and clathrin–/caveolae–mediated endocytosis (Guilianelli *et al.,* 1993; Rejman *et al.,* 2004). In our study we found a filopodia-assisted engulfment of the fine particles and larger agglomerates of nanoparticles occurring in the BEAS-2B cells. Filopodia are slender cytoplasmic projections which extend from the leading edge of migrating cells. These appendages have also been found to act as points of adhesions by the cell to surface, cell to cell attachment and signalling (Lodish *et al.,* 2004). Recently, they had also been found involved in assisting the cells in food uptake by acting as

phagocytic tentacles (Kress *et al.,* 2007). Similar to our findings related to the uptake of nanoparticles, Stearns *et al.* (2001) have also demonstrated the uptake of $TiO_2$ nanoparticles as agglomerates within lung epithelial cells (A549). Single nanoparticle and small agglomerates of nanoparticles were also found to be taken up by micropinocytosis. Our study did not confirm findings from Churg *et al.* (1998). They have suggested that the nanoparticles were recognised and phagocytosed by the upper airway epithelium cells only as agglomerates. On some rare occasions single fine particles within the dimension of <1 µm were found to be taken up in coated pits signifying the presence of an endocytotic process by the BEAS-2B cells. Guilianelli *et al.* (1993) have also shown the uptake of hematite fine particles (<1 µm) by endocytosis in rabbit tracheal epithelial cells.

Following uptake and intracellular translocation occurring within the ER of epithelial cells all particles were found near to the peri-nuclear space. While the fine particles were retained securely inside the ER, nanoparticles were found to escape through the intracellular membrane into the cytoplasmic region of the cell. Recently, Park *et al.* (2008) have demonstrated the translocation of cerium oxide nanoparticles to the peri-nuclear region as agglomerated particles followed by their penetration into the cytoplasm directly and within vesicles, similar to our findings with the hematite nanoparticles.

The mechanism of nanoparticle translocation into the cytoplasm is still largely speculative. Geiser *et al.* (2005) have proposed that such type of translocation occurs through rapid binding of proteins onto the surface of the nanoparticles as soon as they come in contact with the surface of the cells or following phagocytosis by the cells (Linse *et al.,* 2007). The fate of these particles is then affected in terms of adhesion and residence time inside the epithelial cells and their penetration through the cell membrane. Another possible route for penetration by the nanoparticles is through the pores as suggested for the lung-blood barrier substance exchange (Conhaim and Rodenkirch, 1998; Hermans and Bernard, 1999). However, such a signal-mediated transport of nanoparticles has been demonstrated only in the case of 39 nm diameter gold particles in *Xenopus* oocytes (Pante e*t al.,* 2002). The third type of passive uptake not triggered by receptor–ligand interactions can be through the mechanism of Van der Waals forces, or by steric interactions related to the attractive

forces between the particles and surface molecules of the cell membrane (Rimai *et al.,* 2000).

In our uptake study, single nanoparticle and small agglomerates of hematite nanoparticles were translocated through the intracellular membrane of the ER with/without any membrane covering (vesicles). The nanoparticles passing into the cytoplasm enclosed within a vesicle represents a mechanism similar to the formation of the Golgi apparatus for the transportation of lipids and proteins from the endoplasmic reticulum to the different part of the cells. Direct translocation of hematite nanoparticles without any membranous covering into the cytoplasm suggested the role of one of the three mechanisms suggested by Geiser *et al.* (2005). They found the uptake of $TiO_2$ nanoparticles in rat lung epithelial cells similar to our findings. Oberdörster *et al.* (1992) have observed the translocation of ultrafine $TiO_2$ particles into the epithelial cells occurring within 24 h after intratracheal exposure to the rats. They have also observed that the uptake of nanoparticles was faster than their fine counterparts.

Agglomeration by both the iron-containing particles inside the cell was clearly visible in the TEM images. While, this characteristic of forming agglomerates by nanoparticles is well is related their high surface zeta potential (Borm *et al.,* 2000 and Limbach *et al.,* 2005). It was interesting to note the same effect in fine sized particles. Though the agglomerates formed by the fine particles were noticed to be quite small as compared to those formed by the nanoparticles. Guilianelli *et al.* (1993) had also observed formation of agglomerates by the hematite fine particles (<1 µm size) on the surface of rabbit tracheal epithelial cells.

Unlike the findings of Chen and von Mikecz (2005) and of Li *et al.* (2003) that the nucleus and the mitochondria of cells were penetrated by $SiO_2$ and ambient air nanoparticles, we found no nanoparticles penetrating these organelles in our study. The reason for the inability of the hematite nanoparticles to penetrate the cell organelles might the positive zeta potential or the type of cells used for our study. Chen and von Mikecz (2005) have studied the negatively charged $SiO_2$ for their translocation into the nucleus of epithelial cells. Li *et al.* (2003) have studied the translocation of ambient air nanoparticles into the mitochondria of macrophages (RAW 264.7 cells). Another possibility might be the choice of an early time point in

our study providing no time for translocation of the nanoparticles into the intracellular organelles.

It was interesting to find a possible direct interaction between the hematite fine and arsenopyrite ash particles enclosed within the endoplasmic reticulum with mitochondria. Since mitochondria are the major organelles involved in the production of $H_2O_2$ (Turrens, 2003), their direct interaction with the fine particles leading to the generation of oxidative stress inside the cells cannot be ruled out.

### 4.3 Analysis of the cytotoxicity of nanoparticles and fine particles

Both IMR-90 and BEAS-2B cells exposed to hematite nanoparticles demonstrated loss of cell viability after 24 h exposure. Cytotoxicity was found to be more pronounced and concentration-dependent in the IMR-90 cells at 10 and 50 µg/cm² and in the BEAS-2B cells at 50 µg/cm² particle concentrations. Wottrich *et al.* (2004) have also found 50% cell death from the hematite nanoparticles in lung epithelial and macrophage cells at 50 µg/cm$^2$ particle concentration after 24 h time point. In IMR-90 cells a second cytotoxic effect was found at 72 h time point which was also concentration-dependent but less in magnitude compared to that observed after 24 h exposure time. While a complete reduction of cytotoxicity was observed in the BEAS-2B cells after 48 and 72 h exposure time points, the IMR-90 showed an increase in cell viability only at 48 h. The cytotoxic effect produced by hematite nanoparticles in the IMR-90 cells was higher in magnitude compared to that in the BEAS-2B cells.

An exposure to hematite fine particles for different time points induced a high and distinct cytotoxic effect in the BEAS-2B cells compared to that in IMR-90 cells. A concentration- and time-dependent loss of cell viability was observed until 48 h exposure time in the BEAS-2B cells. Guilianelli *et al.* (1993) have studied the effect of hematite particles on rabbit tracheal epithelial cells and found a high cytotoxic effect at the concentration of 50 µg/cm² and the 24 h time point. In the IMR-90 cells a high cytotoxic effect was initially observed at 24 h which remained stable at the particle concentrations of 10 and 50 µg/cm². The cells showed a reduction of cytotoxicity at 48 h followed by a second effect at 72 h.

$TiO_2$ nanoparticles proved to be non-toxic in the BEAS-2B cells while producing a significant cytotoxic effect in the IMR-90 cells. In IMR-90 cells exposed to $TiO_2$ nanoparticles a gain of cell viability at the 48 h time point followed by a second higher loss of cell viability at 72 h was found similar to the hematite nanoparticles exposure. Cytotoxic effects from $TiO_2$ nanoparticle exposures in different biological systems have also been observed in several studies in the past (Donaldson *et al.,* 1998; Gilmour *et al.,* 1997; Oberdörster *et al.,* 1996). In contrast to our finding in the BEAS-2B cells, Sayes *et al.* (2006) have demonstrated cytotoxicity in A549 epithelial cells from exposure to native Anatase nanoparticles. The concentrations of nanoparticles applied to the cells were very high, however.

Exposure to DQ12 particles resulted in an elevated level of cytotoxicity at the lower concentrations (2 and 5 µg/cm²), while at higher concentrations it remained relatively non-toxic at the 24 h time point. A concentration-dependent loss of cell viability was observed at 72 h in IMR-90 cells and at 48 h in BEAS-2B cells. Geh *et al.* (2006) have studied the cytotoxic properties of DQ12 in IMR-90 cells and have found a relatively low cytotoxicity. They have also observed the highest effect at a concentration of 50 µg/cm², but at the shorter time point of 24 h. The delayed and milder cytotoxic effect in our study can be related to the age of the quartz sample. While Stone *et al.* (2004) have suggested a role of the cation exchange on the surface of the DQ12 particles in their delayed and low activity, Fubini *et al.* (1995) have found the ‘‘fresh’’ quartz samples more reactive than ‘‘aged’’ samples.

Exposure to arsenopyrite ash particles in both cell lines was found to induce a cytotoxic effect after 24 h exposure. While, the effect was more concentration-independent at 24 h, it was found to be concentration-dependent at longer exposures. In both cell lines the highest cytotoxicity was observed at 50 µg/cm² particle concentration. After exposure for 72 h to the particles the IMR-90 cells demonstrated the highest loss of cell viability, specially at the 50 µg/cm² particle concentration. A trend towards a reduced cytotoxic effect from the particles was observed in the BEAS-2B cells at the same time point of 72 h.

The cytotoxicity analyses presented quite unique results demonstrating different responses from the cells to different particles. This is particularly surprising in the case of iron-containing hematite nanosized, hematite fine and arsenopyrite ash particles, as all three particles were chemically similar ($Fe_2O_3$).

The results also demonstrated that the lung epithelial cells had a higher tolerance for particulate insult compared to lung fibroblasts. The results demonstrated a cumulative effect from the physico-chemical attributes of the individual particle type. All the particles were found cytotoxic specially at the high concentrations between 10 and 50 µg/cm² in both cell lines. It was interesting to observe that in most of the particle exposures two distinct cytotoxic events were found after exposures for 24 and 72 h time periods. These two events were separated by a gain in cell viability at 48 h. A possible factor that might lead to the increase in cell viability at 48 h exposure time might be related to the proliferation of IMR-90 and BEAS-2B cells after 24 h (Hornberg *et al.,* 1996) along with the disintegration of the dead cells followed by the process of late apoptosis / secondary necrosis. This process of disintegration is also known as 'cell blebbing'.

The flow cytometric analysis of apoptosis/ necrosis in the IMR-90 cells exposed to different particles at 10 µg/cm² concentration and the 24 h time point showed that most of the cells were at the late apoptotic/ secondary necrotic stage. The highest percentage of late apoptotic/ secondary necrotic cells was found following exposure to the arsenopyrite particles followed by hematite fine and nanoparticles. The results demonstrated that the iron-containing particles were capable of high cytotoxicity. It was also interesting to note such a high number of cells at the late apoptotic/ secondary necrotic stage which is normally followed by nuclear fragmentation and cell blebbing leading to the formation of 'apoptotic bodies'. Under *in vivo* conditions, this may lead to the phagocytosis of the dead cells by macrophages and to the recycling of biomolecules. The following study also gave a clue for the increased number of viable cells at the 48 h time point following particle exposures, comprehending that these late apoptotic/ secondary necrotic cells would bead to the generation of apoptotic bodies. However, the study failed to show if the dead cells had passed through the apoptotic/ necrotic pathway before reaching the cell blebbing/ nuclear fragmentation stage.

### 4.4 Analysis of genotoxicity of nanoparticles compared to fine particles

The exposure to hematite nanoparticles induced the strongest genotoxic effects after 24 h of exposure in the IMR-90 cells at 10 and 50 µg/cm² particle

concentrations, and in the BEAS-2B cells at 50 µg/cm² particle concentration. The magnitude of genotoxic effect observed in the IMR-90 cells at this time point was fivefold higher compared to BEAS-2B cells. These effects were found to get reduced in both cell lines after 48 h exposure to the particles. At 72 h, a minute genotoxic effect was found in both cell lines.

The exposure to hematite fine particles produced a significant genotoxic effect in both IMR-90 and BEAS-2B cell lines. In IMR-90 cells, the observed genotoxic effect was half compared to the magnitude of the genotoxic effect induced by hematite nanoparticles at the same 10 and 50 µg/cm² particle concentrations. In the BEAS-2B cells, the maximum effect was found after 24 h and at 10 µg/cm² particle concentration. The effect almost corresponded to that found in hematite nanoparticles at 50 µg/cm² particle concentration. Following the exposure to hematite fine particles a reduction of the genotoxic effect was found at 48 h which was comparable in both cell lines. Later at 72 h, when a second milder effect was found in the IMR-90 cells, the particles were found to be completely non-genotoxic in the BEAS-2B cells. Garry *et al.* (2004) have exposed 4 different cell lines to hematite fine particles and observed a negligible effect in the comet assay. Garry *et al.* (2003) have found that hematite fine particles though were non-genotoxic; they did enhance the genotoxic effects of benzo-a-pyrene coated onto them by generating free radicals.

The exposure of the IMR-90 cells to DQ12 fine particles induced significant genotoxicity. These genotoxic effects were however confined only to the high 10 and 50 µg/cm² particle concentrations and the exposure time of 24 h. DQ12 particles demonstrated a reduction of genotoxicity in the IMR-90 cells at the longer time points of 48 and 72 h. It produced however a late genotoxic effect in the BEAS-2B cells. Several studies have demonstrated that the DQ12 particles were quite capable of inducing genotoxicity in lung cells. Cakmak *et al.* (2004) and Knaapen *et al.* (2002a) have demonstrated that DQ12 induced DNA damage in human and rat lung epithelial cells, respectively. Geh *et al.* (2006a) have also demonstrated genotoxic effects of quartz using DQ12 in the IMR-90 cells. They have however used micronucleus assay parameters for determining genotoxicity. Recently, Li *et al.* (2007) have demonstrated that the DQ12 fine particles induced DNA damage in the rat epithelial

cells through the generation of oxidative stress within the cells. It is not necessary for these particles to enter the nucleus directly.

The exposure to the $TiO_2$ nanoparticles in both cell lines failed to induce any genotoxicity, proving them to be non-genotoxic in IMR-90 and BEAS-2B cells. Previous experiments performed with anatase $TiO_2$ nanoparticles have proven them to be non-genotoxic in the Chinese hamster lung fibroblast cells (V79) (Bhattacharya *et al.,* 2008 – Appendix 11).

Arsenopyrite ash particles induced a very minute but statistically significant genotoxic effect in the IMR-90 cells at the time point of 24 h, but failed to invoke any genotoxicity in the BEAS-2B cells.

From the genotoxicity assay it was established that similar to the cytotoxic effects observed after particle exposures, IMR-90 cells were also found to show stronger genotoxic effects compared to the BEAS-2B cells. This observation further strengthened the hypothesis that the lung epithelial (BEAS-2B) cells have a higher tolerance level towards a particulate insult compared to lung fibroblast (IMR-90) cells. The results also demonstrated that in the majority of the particle exposures a high genotoxic effect was observed at the high concentrations between 10 and 50 µg/cm² and the initial time period of 24 h, which was followed by a relaxation in the effect at 48 h. In some cases, a second mild effect was found at 72 h. It can be hypothesized that the initial effect at 24 h was a direct particle effect. The reduction of genotoxicity at 48 h can be related to the activation of a DNA repair mechanism during the 24 h cell cycle of both cells (Hornberg *et al.,* 1996). Cells that are not able to repair their DNA damage go through the process of apoptosis. Our findings of a high number of late apoptotic/ secondary necrotic cells after 24 h particle exposure in the flow cytometric assay strengthen this assumption. Furthermore, the apoptotic and necrotic cells form ‘Hedgehog comets’ due to nuclear fragmentation. These cells are not counted during comet analysis. The type of genotoxicity analysed in our study was ‘primary genotoxicity’, that is dependent upon the generation of ROS by particles (Schins *et al.,* 2002a).

### 4.5 Acellular and cellular reactive oxygen species production by the particles

ROS can be generated by the particles either directly depending upon the physico-chemical properties of the particle or by stimulating the cells to generate the

radicals. It has been observed that environmental particles, including asbestos, crystalline silica, heavy metal containing dusts, oil fly ash, coal fly ash and ambient particles have the ability to generate ROS themselves and cause oxidative stress in biological systems (Bergamini *et al.*, 2006; Li *et al.*, 2007; Leanderson *et al.*, 1992; Roberts *et al.*, 2007; Aust *et al.*, 2002; Alaghmand *et al.*, 2007).

For the analysis of acellular ROS generation by the particles, they were treated with an oxidizing agent ($H_2O_2$) and with reducing agents (ascorbic acid and whole cell lysate). Biologically, reduction of Fe(III) to Fe(II) have been observed with NADH (Luo 1993), ascorbic acid (Miller and Aust 1989), and NaOH (Zhou *et al.,* 2006). The major source of $H_2O_2$ inside the cells is the mitochondria, which produce it as a part of metabolism (Turrens, 2003).

Hematite nanoparticles were found to generate insignificant amounts of ROS under a normal oxidizing condition. However, when they were pre-treated with ascorbic acid or whole cell lysate they generated the highest amount of $OH^{\bullet}$ radicals independent of the time points and the applied concentration. The results pointed towards the property of agglomeration by the nanoparticles along with the alteration of surface Fe(III) ions to Fe(II). He *et al.* (2007) have demonstrated that smaller particles in the nanosize range tend to agglomerate when suspended in a low pH liquid. Therefore, the increase in the size of agglomerates at lower pH was directly proportional to the size of the particles. As observed in our study treatment of hematite nanoparticles by a reducing agent led to an alteration of the nanoparticle surface ion composition and surrounding pH. This would cause the nanoparticles to separate from their agglomerates and produce an increased surface area and highest generation of acellular ROS.

In contrast to the hematite nanoparticles, the fine particles generated significant amounts of $OH^{\bullet}$ radicals under both oxidizing and reducing conditions. Garry *et al.* (2004) have implicated the hematite fine particles of enhancing the toxicity of B(a)P coated on its surface by generating oxidative stress. Henle *et al.* (1997) have proposed a direct reaction between Fe(III) and $H_2O_2$ leading to the generation of free radicals (Reaction 15)–

$$3Fe(III) + 2H_2O_2 \rightarrow 2FeOOH^{2+} + Fe(II) + 2H^{+} + O_2^{\bullet-} \quad \text{(Reaction 15)}$$

Treatment of the hematite fine particles with ascorbic acid followed by $H_2O_2$ led to a twofold increase in the generation of acellular ROS initially at a high particle concentration. Ascorbic acid reduces the particle surface bound Fe(III) ions into Fe(II) while itself is oxidized into dehydroascorbic acid (Reaction 16). These Fe(II) ion further reacted with $H_2O_2$ generating $OH^{\bullet}$ radicals by Fenton reaction (Reaction 1, page 11).

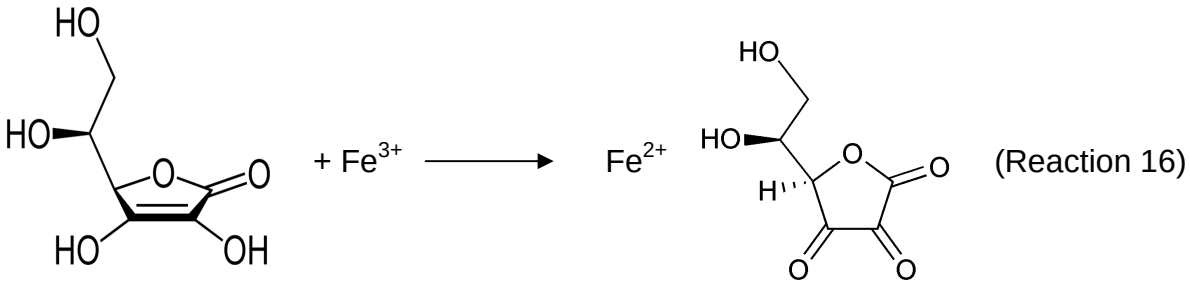


(Reaction 16)

(Ascorbic Acid) (Dehydroascorbic Acid)

This acellular ROS generation by hematite fine was later found to get reduced significantly. A probable reason for this reduction could be the maximal conversion of the Fe(II) bound on the surface of the particles to Fe(III) following the Fenton reaction.

Arsenopyrite ash particles were found capable of generating highest amount of acellular $OH^{\bullet}$ radicals under oxidizing condition and amounts equal to that generated by the hematite nanoparticles under reducing condition. However, due to their origin from an industrial process and due to the presence of several elements beside Fe(III) in high percentage it was difficult to frame any hypothesis related to a specific element capable of reacting with the $H_2O_2$ directly or indirectly following reduction and generation of $OH^{\bullet}$ radicals.

DQ12 fine particles yielded $OH^{\bullet}$ radicals that were approx. equal to that generated by hematite fine particles following treatment with $H_2O_2$. No difference in $OH^{\bullet}$ radicals generation was observed after treatment of the particles with ascorbic acid and $H_2O_2$. Previously, researchers have demonstrated that the surface characteristics of quartz were involved in the generation of ROS in an acellular environment (Vallyathan *et al.,* 1991; Schins *et al.,* 2002) as well as in the induction and persistence of pulmonary inflammation (Albrecht *et al.,* 2004).

$TiO_2$ nanoparticles were found to generate negligible amounts of acellular ROS under all tested conditions. Braydich-Stolle *et al.* (2007) have stated that under normal conditions $TiO_2$ nanoparticles were capable of generating a small quantity of acellular ROS. They have also observed that the nanoparticles form aggregates when dispersed in water and serum free media with the largest aggregates found in the serum free media.

In an effort to elucidate the acellular reaction occurring on the surface of the particles after their uptake in the cells and translocation into the cytoplasm the nanoparticles were treated with whole cell lysate and $H_2O_2$. It was found that the amount of acellular ROS generated by hematite nanoparticles was the highest amongst all particles followed by arsenopyrite ash particles and similar to that observed with ascorbic acid treatment. While $TiO_2$ nanoparticles demonstrated no difference in their acellular ROS level, DQ12 and hematite fine particles showed a subdued generation of ROS.

Based on the previous observations made after treating the particles with/without ascorbic acid and $H_2O_2$ treatment, it was found that hematite nanoparticles were indeed capable of generating high amount of acellular ROS following activation under a reducing condition that they might find inside the cytoplasm of the cells. Arsenopyrite ash particles generated acellular ROS under all conditions, but the quantity was much lower after reacting with the proteins from the cell lysate. Similarly, hematite and DQ12 fine particles also showed a drastic reduction in their acellular ROS generation capacity. This might be related to the complete covering of the particle surface area with the proteins leaving little space for $H_2O_2$ to react with the Fe(II) ions. It can be further stated that the resulting reduction of Fe(III) to Fe(II) can occur only on the surface of the particles as no chelable Fe(III) content was found in the particles with the 1,10 phenanthroline chloride test. Gao *et al.* (2007) studying $Fe_3O_4$ nanoparticles had found that the conversion of Fe(III) to Fe(II) ions took place on the surface rather than through the chelation of transition metals from it and the following catalytic activity of these nanoparticles were similar to the peroxidase enzymes. Miller *et al.* (1989) have demonstrated a high incidence of lipid peroxidation on conversion of Fe(III) to Fe(II).

Inside lungs ROS are generated endogenously during a specific and deliberate synthesis by various cell types, including vascular endothelial cells and

lung epithelial cells (Pezerat, 1991; Duffin *et al.*, 2007). Studies have indicated that the lung epithelial cells generated ROS intracellularly through processes in which mitochondrial respiration and activation of NAD(P)H-like enzyme systems were involved after exposure to fly ash, DEP, PM and quartz particles (Arroyo *et al.*, 1990; Guo *et al.*, 1995).

Our study of the intracellular ROS generation in BEAS-2B cells using $H_2$DCFDA dye showed that the $TiO_2$ nanoparticles exposure caused the maximum generation of intracellular ROS even though it failed to produce any cyto- and genotoxic effects in the cells, along with a substantial generation of acellular ROS. $TiO_2$ nanoparticles have been shown to exhibit strong cytotoxicity when exposed to UVA radiation, but are regarded as a biocompatible material in the absence of photoactivation. In contrast to this concept and similar to our study, Gurr *et al.* (2005) and Singh *et al.* (2007) have also found that $TiO_2$ nanoparticles induce oxidative DNA damage, lipid peroxidation, micronuclei formation, and increased ROS ($H_2O_2$ and $NO^{\bullet}$) production in BEAS-2B cells in the absence of photoactivation. Previously, we have found a mild and statistically insignificant induction of intracellular ROS in V79 cells exposed to $TiO_2$ nanoparticles (Bhattacharya *et al.,* 2008 – Appendix 11). But the parameters used for that analysis were based on detecting lipid peroxidation of the cell membrane. In the present study, we measured a direct generation of free radicals inside the cells by the oxidation of fluorescent dye.

Hematite nanoparticles generated the lowest amount of intracellular ROS as compared to the other particles. The effect was also found to be a late one starting from 12 h onwards. This delay in intracellular ROS generation might be related to the uptake and translocation within the cells followed by a direct interaction with the biomolecules present inside the cell. From our uptake and acellular ROS generation results it can be inferred that inside the cell hematite nanoparticles were present as large agglomerates which acted as big particles providing very little surface area for reaction. After coming in contact with neutral to alkaline pH and reducing agents inside the cell, these nanoparticles separated into smaller agglomerates and individual entities and generated ROS similar to that observed with the acellular ROS generation. Zelmanov and Semiat (2007) have observed that in the presence of $H_2O_2$ hematite nanoparticles get reduced and cause a Fenton type reaction. Gao *et al.* (2007) have also demonstrated the catalytic activity of Fe(III) nanoparticles similar to

peroxidase enzymes following their conversion to Fe(II) using $Fe_3O_4$ nanoparticles. They have stated that the reactions take place on the surface of the nanoparticles themselves rather than through the chelation of transition metals, similar to our finding.

All fine particles led to a spontaneous generation of ROS. We found that the generation of intracellular ROS by the DQ12 particles remained fairly constant, irrespective of time and concentration. In contrast, a reduction was observed in hematite fine particles at longer exposure times. Pezerat *et al.* (1991) have shown that DQ12 particles have a characteristic to generate ROS intracellularly. They have proposed that the negatively charged surface of the DQ12 particles reacts with $H_2O_2$ leading to the generation of $OH^{\bullet}$ radicals. Surface-generated ROS have also been implicated as the key element in the development of fibrosis and lung cancer (Fubini, 1998). Duffin *et al.* (2001) have also related the reactivity of the DQ12 particles to the presence of transition metals on its surface. Fontecave *et al.* (1990) have demonstrated malondialdehyde generation by oxidation of the lipid peroxisome on exposure to hematite particles. Unlike the hematite fine particles arsenopyrite ash particle exposure to the BEAS-2B cells showed a high generation of intracellular ROS only at the 24 h time point followed by a reduction later. This delayed effect from the arsenopyrite ash particles might be related to their small size as had been observed with the hematite nanoparticles exposure. Similar to the observation made after the treatment of fine particles with whole cell lysate, reduction in the ROS generating capacity of the hematite fine and arsenopyrite ash particles might be related to their interaction with the native proteins of the cells reducing the availability of surface area on the particles for generation of free radicals.

Co-treatment of the particles with deferoxamine demonstrated only a minor effect. It reduced the ROS generation only at one time point and at the lowest concentration of $TiO_2$ nanoparticles and at two concentrations of hematite fine particles, both at the 12 h exposure time point. At all other applied particle concentrations and at the other time points deferoxamine was found to increase the level of intracellular ROS generation. Deferoxamine is an iron chelator that has been used for the removal of excess iron from the blood of patients suffering from iron overload. However, deferoxamine has also been found to generate nitrous oxide ($NO^{\bullet}$) free radicals in the cells (Walker *et al.,* 1985). Davies *et al.* (1987) have

described the generation of free radicals by deferoxamine in a neutral condition following reaction with superoxide. Deferoxamine ($Df^-$) contains three ionized hydroxamic acid (-NOH) groups which react with superoxide (Reaction 17 and 18) and $OH^\bullet$ radicals (Reaction 19) leading to the generation of $OH^\bullet$ and $H_2O_2$ radicals, respectively.

$$O_2^{\bullet-} + Df^- \xrightarrow{2H^+} H_2O_2 + DfNO^\bullet \qquad \text{(Reaction 17)}$$

$$O_2^{\bullet-} + H^+ \rightarrow HO_2^\bullet \qquad \text{(Reaction 18)}$$

$$HO_2^\bullet + DfNO^- \xrightarrow{2H^+} H_2O_2 + DfNO^\bullet \qquad \text{(Reaction 19)}$$

These $NO^\bullet$ radicals can react further with $O_2^{\bullet-}$ creating reactive peroxynitrite ($ONOO^-$) radicals which would be detected by the $H_2$DCFDA dye intracellularly.

DNA is the genetic code of life. The chemical basis for the effects of radicals on DNA is probably due to oxidation and chemical modifications of the bases. Such point mutations, if transcripted and translated, will lead to modified protein structures and altered functionality finally leading to diseases. One of the major products of free radical attack is the formation of 8-OHdG adducts. Therefore, the detection of oxidative DNA damage by analyzing DNA adducts is another important parameter. Among all these base adducts 8-OHdG is the most studied one because of its highly mutagenic nature (it base pairs relatively well with adenine) (Orren, 2005).

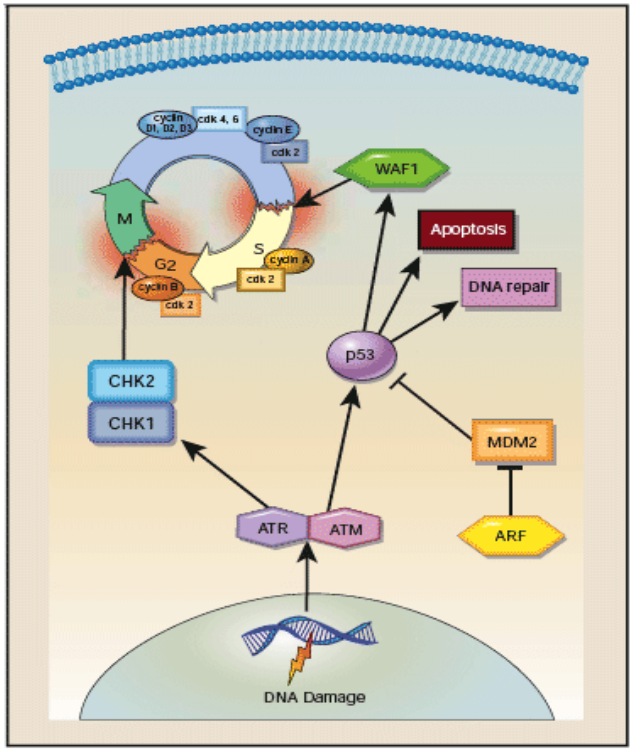


Molecules with decreased expression or function are colored in green. Molecules with increased expression are colored in orange.
Abbreviations: ATM = ataxia telangiectasia; CDK = cyclin-dependent kinase; CHK = checkpoint kinase

**Figure 45** – Cell cycle checkpoints following DNA damage in a cell.
Green represents – Down-regulation
Figure adapted from Fernàndez *et al.* (2005)

In our study we found that both

$TiO_2$ nanoparticles and hematite fine particles were capable of generating 8-OHdG adducts in the IMR-90 cells following their exposure for 24 h. Generation of 8-OHdG adducts by the hematite fine and $TiO_2$ nanoparticles can be related to the high generation of intracellular ROS as had been detected with the $H_2$DCFDA dye assay. Gurr *et al.* (2005) have found $TiO_2$ nanoparticles to induce generation of hydrogen peroxide and nitric oxide leading to lipid peroxidation and oxidative DNA damage in BEAS-2B cells. In addition to the indirect generation of 8-OHdG by causing oxidative stress hematite fine particle can also react directly with the DNA radical leading to the generation of DNA adducts (Reaction 4, page 13) (Henle *et al.,* 1997).

The other particles did not generate any 8-OHdG adducts, at all the concentrations and the time points measured. However, it might be possible that the particles generated oxidative stress which again formed other types of DNA adducts. Henle *et al.* (1997) have stated that an attack by the $OH^{\bullet}$ radicals on the DNA bases can generate 50 different base alterations. Since, this assay was designed only to detect 8-OHdG adducts by using specific antibodies no other adduct would be detected. Another possibility for the negative result can only be due to interferences from the particle themselves. The presence of a significant surface charge on the particles can interfere with the negatively charged 8-OHdG nucleotides causing them to adhere to the particle surface (Kumar *et al.,* 2007).

### 4.6 Up-regulation of genetic damage repair mechanisms after particle exposure

The analysis of DNA damage repair signalling in IMR-90 cells demonstrated a high up-regulation of genes that directed specifically towards apoptosis and oxidative DNA base damage repair.

The delays that cells experience in $G_1$, S or $G_2$ phases of the cell cycle after DNA damage are called DNA integrity checkpoints. The cell cycle is dependent upon 4 major kinases (ATM, ATR and CHEK family). In IMR-90 cells, on exposure to both types of hematite (fine and nanosize) and arsenopyrite ash particles we found an up-regulation of the major cell cycle control gene ATM (Ataxia telangiectasis mutated gene) and only in the case of hematite and arsenopyrite ash particles exposure an up-regulation of the ATR gene up-regulation. The proteins encoded by both of these genes belong to the phosphatidylinositol kinase-related kinase (PIKK) family.

ATM genes are involved in the production of a single protein with a high molecular weight of 370-kDa predominantly confined to the nucleus of human fibroblasts. Under normal conditions, ATM protein levels and localization remain constant throughout all stages of the cell cycle (Brown *et al.,* 1997). The involvement of ATM in both up-regulation of p53 and other molecular machinery required for chromosomal exchange has been demonstrated by Hawley and Friend (1996). An enhanced phosphorylation of p53 by ATM in response to DNA damage has been observed by Banin *et al.* (1998) and Canman *et al.* (1998). Involvement of ATM in the phosphorylation of BRCA1 gene has been demonstrated by Cortez *et al.* (1999). It can be therefore concluded that phosphorylation might play a critical role in the response to DNA double-strand breaks.

Wang *et al.* (2000) have found that the BRCA1 gene is part of a large multisubunit protein complex of tumour suppressors, DNA damage sensors, and signal transducers. They named this complex BASC for 'BRCA1-associated genome surveillance complex.' Other members of this complex were ATM, MSH2, MLH1, and the RAD50-MRE11-NBS1 complex. The BASC complex may therefore serve as a sensor for abnormal DNA structures or as a regulator for post-replication repair processes. Involvement of ATM in the phosphorylation of NBS1 has been directly related to the DNA damage repair response at the S phase checkpoint by Zhao *et al.* (2000).

ATR genes, similar to the ATM genes, have also been found to be involved in the detection of DNA damage, the controlling of cell cycle progression, and the DNA recombination (Cimprich e*t al.,* 1996; Enoch *et al.,* 1995). The proteins coded by ATR and ATM genes, together as well as individually, have been found to be very important cell cycle checkpoint kinases that phosphorylate and regulate a wide variety of downstream proteins, including the tumour suppressor proteins TP53 and BRCA1, the checkpoint kinases CHEK1 and CHEK2, the checkpoint proteins RAD17 and RAD9A, and the DNA repair protein NBS1.

Bao *et al.* (2001) have found a direct regulatory linkage between RAD17 and the checkpoint kinases encoded by the ATM and ATR genes. Treatment of human cells with genotoxic agents induced ATM/ATR-dependent phosphorylation of RAD17 at serine-635 and serine-645. Over-expression of a RAD17 mutant bearing alanine substitutions at both phosphorylation sites abrogated the DNA damage-induced G2-

checkpoint and sensitized human fibroblasts to genotoxic stress. In contrast to wild-type RAD17, the RAD17 mutant showed no ionizing radiation-inducible association with RAD1, a component of the RAD1-RAD9A-HUS1 checkpoint complex. These findings demonstrated that the ATR/ATM-dependent phosphorylation of RAD17 is a critical early event during checkpoint signalling in DNA-damaged cells. In the present study, all the proposed genes regulating apoptosis were found to be up-regulated, namely ATM, TP53, BRCA1, ABL1, CHEK1 (in hematite and arsenopyrite ash particles), and CHEK2 along with 5 other apoptosis regulating genes.

CHEK2 has been found to stabilize TP53, a key player in regulating the prolonged $G_1$ arrest checkpoint. Bell *et al.* (1999) have identified CHEK2 as the gene implicated in a small number of families with the cancer predisposition Li-Fraumeni syndrome and having germ line mutations in TP53. Kumar *et al.* (2007) have found that mouse cells deficient in CHEK2 had lost both TP53-dependent responses (such as apoptosis) and TP53-independent responses (such as the $G_2$ damage checkpoint).

The ABL1 (v-abl Abelson murine leukemia viral oncogene homolog-1) gene is considered to be a proto-oncogene encoding for cytoplasmic and nuclear tyrosine kinase proteins related to cell division and adhesion (Bell *et al.,* 1999). This gene has also been found to encode a protein that binds to p73 forming a component for the mismatch repair-dependent apoptosis pathway. This gene was found to be over-expressed in the IMR-90 cells after exposure to all particles. The highest activity of this ABL1 gene was found in the cells exposed to the arsenopyrite ash particles which were twofold higher compared to the control (untreated cell).

Other genes expressed in the IMR-90 cells following particle exposure were found to encode for proteins involved in the identification and repair of damaged DNA sites. The high expression of these genes pointed towards a stress-related DNA damage that occurred within the 48 h time point of particle exposure to the cells. The repair mechanisms that were found to be activated in the particle exposed cells were base excision repair, double-stranded break repair, mismatch repair and removal of oxidative-stress induced base adducts.

Base excision repair in a cell is manifested through a DNA glycosylase which recognises the damaged base and cleaves its glycolic bond. In the IMR-90 cells exposed to gypsum and hematite fine particles, 5 and 4 DNA glycosylase genes,

respectively, were found up-regulated. Of these two important DNA-glycosylase genes up-regulated in the IMR-90 cells following gypsum particle exposure were MPG (Methyladenine DNA Glycosylase) and UNG (Uracil-DNA Glycosylase)**,** both are involved in the removal of damaged purine bases that might lead to a conversion of AT↔ GC.

Genes involved in the non-homologous type of double-stranded break repair mechanism were found to be up-regulated in the IMR-90 cells exposed to the hematite fine and gypsum particles. These genes were RAD50, RAD21, FEN1, MRE11A, and XRCC6. All these genes were required in the non-homologous DNA repair mechanism forming different complexes between the proteins they encode for the activation of the repair function (Paullan and Gellert, 1998; Lin *et al.,* 2007).

DNA mismatch repair is a system for recognizing and repairing erroneous insertion, deletion and misincorporation of bases that can arise during DNA replication and recombination as-well as for repairing some forms of DNA damage (Joseph *et al.,* 2006). An up-regulation of the TREX1 (3-Prime repair exonuclease1) gene in the IMR-90 cells exposed to arsenopyrite ash particles was observed. This gene is involved in the mismatch repair of the cells by encoding a major 3'->5' DNA exonuclease enzyme. This protein is a non-processive exonuclease that has a proofreading function for a human DNA polymerase. Two mismatch repair genes MLH1 and MSH2 were found up-regulated in the IMR-90 cells following exposure to all three types of particles. These genes encode proteins involved in the removal of oxidized DNA bases, specially of 8-OHdG.

Two genes that are directly involved in the repair of oxidative DNA adducts were found to be over-expressed in the IMR-90 cells exposed to hematite fine, gypsum and arsenopyrite ash particles. Of these, NTHL1 (Endonuclease III) was found activated in the cells exposed to hematite fine and gypsum particles, while OGG1 (8-Hydroxyguanine DNA glycosylase) was found over-expressed in the cells exposed to arsenopyrite ash particles. Both these genes are involved in the removal of apurinic and apyrimidinic sites. NTHL1 encodes a 34.3 kDa exonuclease enzyme involved in the removal of 8-oxoguanine from 8-oxoguanine/guanine mispairs in DNA occurring due to oxidative DNA damage (O'Brien *et al.,* 2003) along with 5-formyluracil, 5-hydroxymethyluracil and thymine glycol in human cells (van Gent and van der Burg*,* 2007). OGG1 on the other hand is a DNA glycosylase gene similar to

the MPG and UNG genes, but is solely involved in the repair of 8-OHdGs. The protein encoded by this gene has a molecular weight of 47 kDa. Polymorphism in this gene has been related to the formation of cancers following oxidative DNA damages (Wu *et al.,* 2008).

Unfortunately, owing to a considerable loss of mRNA in the cells due to the uptake, translocation followed by continuous interference by the hematite nanoparticles during cell lysis and mRNA extraction, no data could be retrieved from the IMR-90 cells exposed to these nanoparticles.

## CONCLUSION

The results revealed that the effects from fine and nanoparticles were not solely dependent up on their chemical composition but were induced as a cumulative effect of all their physico-chemical properties. Furthermore, the toxic effects were also dependent upon the type of cells exposed to these particles. Based upon the uptake study, it was found that both the fine and nanoparticles were taken up by the lung epithelial cells using different methods such as filopodia assisted phagocytosis, micropinocytosis and endocytosis in coated pits. While all the particles were found capable of reaching the peri-nuclear region enclosed within an ER, the nanoparticles demonstrated a potential to translocate into the cytoplasm of cells enclosed within a vesicle or directly passing through the intracellular membrane.

Assessment of the toxic potential of different fine and nanoparticles demonstrated that even though particles such as hematite fine and nanosized had a similar chemical composition. The nanoparticles were more cyto- and genotoxic compared to their finer counterpart. The DQ12 particles were found to be cyto- and genotoxic compared to the $TiO_2$ nanoparticles that were found to be non-toxic to the lung cells epithelial cells and showed an effect only in the lung fibroblast cells.

Similarly, through the acellular ROS generation assay it was observed that the nanoparticles did not generate significant amount of acellular ROS following a reaction with $H_2O_2$ in contrast to the fine particles. However, the positive charge of hematite was found to get activated following a pre-treatment with reducing agent and resorted to the generation of highest amount of ROS thereafter as a reaction with the $H_2O_2$. However, the $TiO_2$ nanoparticles were found unaltered in their generation of acellular ROS. This demonstrated an importance of the surface area charge and chemical composition of nanoparticles. However, compared to the acellular ROS generation by the hematite nanoparticle they were found to generate relatively low amount of intracellular ROS and at longer exposure time as compared to the fine particles and the $TiO_2$ nanoparticles, which produced the highest amount of ROS inside the cells.

Furthermore, the $TiO_2$ nanoparticles were found to produce the highest amount of 8-OHdG adducts as compared to the other particles. The microarray analysis of the cells exposed to the fine hematite particles demonstrated induction of genomic instability which was several fold high compared to the control cells and led to an

activation of the DNA damage repair and apoptotic mechanisms. Genes that represented the base excision and mismatch repair pathways were specially found to be up-regulated along with the genes responsible for apoptotic cell death.

Arsenopyrite ash particles produced as a residue from a company contained particles between the size of $PM_{2.5}$ and $PM_{0.1}$. Chemically they were same as the hematite particles, but were also found to contain several other elements in high percentage. These particles were found to be generating very low toxic effects along with intracellular ROS generation inside the lung cells exposed to them. However, they were found capable of generating significant amount of acellular ROS similar to the hematite fine and nanoparticles after a pre-treatment of reductant and following a direct oxidation with $H_2O_2$. These particles were also found to be significantly up-regulating the expression of apoptotic and DNA damage repair genes similar to the hematite fine particles.

We conclude from this study that a simple variation in one of the physico-chemical properties of particles such as size can drastically alter their capabilities to react within a biological system. While, DQ12 is well known for its toxicity, it was interesting to find the $TiO_2$ nanoparticles capable of generating high amount of intracellular ROS and induction of 8-OHdG DNA adducts in the cells. Both, Fe(III) containing fine and nanoparticles demonstrated a significant difference in their mode of action within the cellular system and the smaller nanoparticles were found to induce higher cyto- and genotoxic effect. It can be further stated that the positively charged nanoparticles need special reducing conditions to get activated which they can easily find inside the cytoplasm of the cell following their direct translocation causing their toxicity to increase several folds higher compared to that of fine particles.

Finally, iron-containing particles cannot be considered to be safe due to their capability to generate ROS and to cause cyto- and genotoxicity along with their ability to cause genomic instability which is an important finding owing to the fact that there is an increased usage of these nanoparticles with the advancements in nanotechnology in medical applications such as magnetic resonance imaging and cancer cell drug targeting.

## 5. SUMMARY

Epidemiological studies have repeatedly reported a positive correlation between the level of particulate air pollution and increased morbidity and mortality rates in both adults and children. The fraction of nanoparticles in the ambient air has been hypothesized to be more toxic than the fraction of larger size particles. The aim of the present study was to investigate the toxicological effects of both fine particles and nanoparticles.

The entire study can be summarized as follows -

- The toxic effects of particles are not only dependent upon their physico-chemical composition but also on the type of cells that are exposed to them. We found that lung epithelial cells had a higher tolerance against the induction of cyto- and genotoxicity resulting from the particulate insult than lung fibroblasts.
- Both fine and nanoparticles were found to be taken up by the BEAS-2B cells using filopodia. Different mechanisms of uptake were observed in the cells such as filopodia-assisted phagocytosis, micropinocytosis, and endocytosis in coated pits. But only nanoparticles were found capable of translocating directly through the intracellular membrane of ER into the cytoplasm of the cell. This translocation through the cell membrane is dependent upon the size of the nanoparticles which allows them to penetrate through the membrane pore channels. The presence of a positive charge on the surface is also important, as it is responsible for the interaction between the hydrophobic (negatively charged) membrane proteins and the particles.
- The Fe(III) nanoparticles were found to be more cyto- and genotoxic compared to the Fe(III) fine, DQ12 fine and $TiO_2$ nanoparticles. Owing to the capability of the Fe(III) nanoparticles to penetrate into the cytoplasm of the cells the cyto- and genotoxic effect from the hematite nanoparticles can occur through a direct reaction of the biomolecules on the surface of the cells with Fe(III) ions present on the particle surface. It was also found that the effects were mostly confined to the concentrations beyond 10 µg/cm² and the 24 h time point. At longer time periods activation of mechanism related to the DNA repair and apoptosis reduced the number of affected cells.

- Acellular ROS generation by the nanoparticles was found to be negligible under an oxidizing condition due to the possible agglomeration of the particles. However, when they were treated with a reducing agent, hematite nanoparticles were found to generate a high amount of ROS. In the fine particles, all of them were capable of generating acellular ROS under oxidizing conditions. But when they were also treated with reducing agent (ascorbic acid) hematite fine particles generated a high quantity of ROS for a very short time, while arsenopyrite ash particles generated high amount of ROS continuously. On the other hand, such a treatment was found to have no affect on the quantity of ROS being generated by the DQ12 fine and $TiO_2$ nanoparticles. Treatment with whole cell lysate also led to a significant generation of acellular ROS by the hematite nanosize and arsenopyrite ash particles, whereas, hematite fine, DQ12 fine and $TiO_2$ nanoparticles generated very low quantities of acellular ROS due to a possible coating of the particles with native proteins.
- Intracellularly, $TiO_2$ nanoparticles induced the highest amount of ROS generation, followed by the hematite and DQ12 fine particles. Arsenopyrite ash and hematite nanoparticles failed to induce significant amounts of intracellular ROS. Treatment with an iron chelator resulted only in a minor reduction in the generation of intracellular ROS. In most of the cases the iron chelator itself led to overgeneration of ROS.
- Overexpression of intracellular ROS by the cells exposed to hematite fine and $TiO_2$ nanoparticles lead to the generation of DNA adducts. The result demonstrated that even though $TiO_2$ nanoparticles were found to be non-cyto- and genotoxic, they had a very high potential of causing point mutations inside the cells.
- The particles led to an oxidative-stress related induction of genomic instability that was visible from the activation of the DNA damage repair and apoptotic mechanisms. The DNA damage repair mechanisms were found to be specifically involved in the removal of DNA adducts in base excision and mismatch repair. Genes coding for proteins directly involved in the removal of oxidized guanine bases (8-OHdG) were found to be active in the cells exposed to hematite fine and arsenopyrite ash particles.

- The high expression of genes controlling cell cycle checkpoints and apoptosis demonstrated an up-regulation in the apoptotic activity of the cells after exposure to fine particles.

In conclusion, the results demonstrate that nanoparticles are more toxic than fine particles, even if they have the same chemical composition. The toxicity of a particle within a single cellular system is dependent on several properties including shape, size, chemical composition, and surface charge along with the intrinsic biological pathways activated in a cell following their uptake.

The higher toxicity by nanoparticles compared to fine particles having the same chemical composition is due to the higher density of surface molecules presenting them with a higher surface charge and a larger surface area to react. A Fe(III) nanoparticle behaves like a catalyst providing the space and the proper environment for the biomolecules to react with oxidizing elements.

Due to the special properties nanoparticles retain. Their utilization will increase leading to the advancement of nanotechnology in almost every industrial sector. In view of the potential toxic effects of these particles it must be recommended, that special care should be taken during their production to minimize the exposure of workers. Special emphasis should be laid on the charge and intracellular retention properties when nanoparticles are used for medical purposes such as thermal imaging and cancer drug targeting. This recommendation should be specially implemented for the poorly soluble nanoparticles made out of inorganic compounds such as the iron-containing nanoparticles.

## REFERENCES


**1.** Adams, L.K., Lyon, D.Y., McIntosh, A., Alvarez, P.J. (2006). Comparative toxicity of nano-scale $TiO_2$, $SiO_2$ and ZnO water suspensions. Water Sci Technol. **54,**327–334.

**2.** Alaghmand, M. and Blough, N. V. (2007). Source-dependent variation in hydroxyl radical production by airborne particulate matter. Environ.Sci.Technol. **41**, 2364-2370 Alaghmand, M., Blough, N. V. (2007). Source-dependent variation in hydroxyl radical production by airborne particulate matter. Environ.Sci.Technol. **4**, 2364-2370.

**3.** Albrecht, C., Schins, R.P.F., Höhr, D., Becker, A., Shi, T., Knaapen, A.M., Borm, P.J.A. (2004). Inflammatory time course following quartz instillation: role of TNFα and particle surface. *Am J Respir Cell Mol Biol.* **31**, 292–301.

**4.** American Conference of Governmental Industrial Hygienists. TLVs. Threshold limit values and biological exposure indices for 1992-1993. Cincinnati, OH. **35.**1992. (Report)

**5.** Andrew, A. S., Warren, A. J., Barchowsky, A., Temple, K. A., Klei, L., Soucy, N. V., O'Hara, K. A., Hamilton, J. W. (2003). Genomic and proteomic profiling of responses to toxic metals in human lung cells. *Environ. Health Persp.* **111**(6), 825-835.

**6.** Arroyo, C. M., Carmichael, A. J., Bouscarel, B., Liang, J. H., Weglicki, W. B. (1990). Endothelial cells as a source of oxygen-free radicals. An ESR study. *Free Radic.Res.Commun.* **9**, 287-296

**7.** Aust, A. E., Ball, J. C., Hu, A. A., Lighty, J. S., Smith, K. R., Straccia, A. M., Veranth, J. M., Young, W. C. (2002). Particle characteristics responsible for effects on human lung epithelial cells. *Res.Rep.Health Eff. Inst.* **1**, 65

**8.** Bakkenist CJ, Kastan MB.(2003). DNA damage activates ATM through intermolecular autophosphorylation and dimer dissociation. *Nature* **421**(6922), 499-506.

**9.** Ball, J. C., Straccia, A. M., Young, W. C., Aust, A. E. (2000). The formation of reactive oxygen species catalyzed by neutral, aqueous extracts of NIST ambient particulate matter and diesel engine particles. *J Air Waste Manag. Assoc.* **50**(11), 1897-1903.

**10.** Bammler, T. *et al.,* (2005). Standardizing global gene expression analysis between laboratories and across platforms. *Nat. Methods* **2**(5), 351-356.

**11.** Banin, S., Moyal, L., Shieh, S.Y., Taya, Y., Anderson, C.W., Chessa, L., Smorodinsky, N.I., Prives, C., Reiss, Y., Shiloh, Y., Ziv, Y. (1998). Enhanced phosphorylation of p53 by ATM in response to DNA damage. *Science* **281**,1674-1677.

**12.** Bao, S., Tibbetts, R.S., Brumbaugh, K.M., Fang, Y., Richardson, D.A., Ali, A.,

Chen, S.M., Abraham, R.T., Wang, X.F. (2001). ATR/ATM-mediated phosphorylation of human Rad17 is required for genotoxic stress responses. *Nature* **411**, 969-974.

**13.** Barchowsky, A., O'Hara, K. A. (2003). Metal-induced cell signaling and gene activation in lung diseases. *Free Radic. Biol. Med.* **34**(9), 1130-1135.

**14.** Bass, D. A., Parce, J. W., Dechatelet, L. R., Szejda, P., Seeds, M. C., Thomas, M. (1983). Flow cytometric studies of oxidative product formation by neutrophils: a graded response to membrane stimulation. *J Immunol.* **130**(4), 1910-1917.

**15.** Bayram, H., Devalia, J. L., Khair, O. A., Abdelaziz, M. M., Sapsford, R. J., Sagai, M., Davies, R. J. (1998). Comparison of ciliary activity and inflammatory mediator release from bronchial epithelial cells of nonatopic nonasthmatic subjects and atopic asthmatic patients and the effect of diesel exhaust particles in vitro. *J Allergy Clin. Immunol.* **102**(5), 771-782.

**16.** Bell, D. W., Varley, J. M., Szydlo, T. E., Kang, D. H., Wahrer, D. C., Shannon, K. E., Lubratovich, M., Verselis, S. J., Isselbacher, K. J., Fraumeni, J. F., Birch, J. M., Li, F. P., Garber, J. E., Haber, D. A. (1999). Heterozygous germ line hCHK2 mutations in Li-Fraumeni syndrome. *Science* **286**(5449), 2528-2531.

**17.** Bergamini, C., Fato, R., Biagini, G., Pugnaloni, A., Giantomassi, F., Foresti, E., Lesci, G. I., Roveri, N., Lenaz, G. (2006). Mitochondrial changes induced by natural and synthetic asbestos fibers: studies on isolated mitochondria. *Cell Mol. Biol. (Noisy. -le-grand)* **52**, OL905-OL913.

**18.** Bhattacharya, K., Alink, G., Dopp, E. (2007). Oxidative stress and changed gene expression profiles in fiber-/ particle- induced carcinogenesis. *Int. J of Hum. Gen.* **7**(1), 1-21.

**19.** Bhattacharya, K., Cramer, H., Zimmermann, U., Yadav, S., Geh, S., Shokouhi, B., Albrecht, C., Rahman, Q., Rettenmeier, A., Dopp, E. (2008). Ultrafine titanium dioxide particles coated with vanadium pentoxide induce cellular damage and micronucleus formation in V79-cells. *J. Toxicol. Environ. Health* (In Print).

**20.** Bhattacharya, K., Dopp, E., Kakkar, P., Jaffery, F. N., Schiffmann, D., Jaurand, M. C., Rahman, I., Rahman, Q. (2005). Biomarkers in risk assessment of asbestos exposure. *Mutat. Res.* **579**(1-2), 6-21.

**21.** Bishop, J.O., Selman, G.G., Hickman, J., Black, L., Saunders, R.D., Clark, A.J. (1985). The 45-kb unit of major urinary protein gene organization in a gigantic imperfect palindrome. *Mol. Cell. Biol.* **5**, 1591-1600.

**22.** Bockmann, J., Lahl, H., Eckert, T., Unterhalt, B. (2000). Blood titanium levels before and after oral administration titanium dioxide. *Pharmazie* **55**(2), 140-143.

**23.** Boldo, E., Medina, S., LeTertre, A., Hurley, F., Mucke, H. G., Ballester, F., Aguilera, I., Eilstein, D. (2006). Apheis: Health impact assessment of long-term

exposure to PM (2.5) in 23 European cities. *Eur. J Epidemiol.* **21**(6), 449-458.

**24.** Bonner, J. C. (2007). Lung fibrotic responses to particle exposure. *Toxicol. Pathol.* **35**(1), 148-153.

**25.** Borm, P. J. A., Robbins, D., Haubold, S., Kuhlbusch, T., Fissan, H., Donaldson, K., Schins, R. P., Stone, V., Kreyling, W., Lademann, J., Krutmann, J., Warheit, D., Oberdörster, E. (2006). The potential risks of nanomaterials: a review carried out for ECETOC. *Part Fibre. Toxicol.* **3**(11), 1-35.

**26.** Borm, P. J., Kreyling, W. (2004). Toxicological hazards of inhaled nanoparticles--potential implications for drug delivery. *J Nanosci. Nanotechnol.* **4**(5), 521-531.

**27.** Boulton SJ, Jackson SP. (1996) Saccharomyces cerevisiae Ku70 potentiates illegitimate DNA double-strand break repair and serves as a barrier to error-prone DNA repair pathways. *EMBO J.* **15**(18), 5093-103.

**28.** Brackbill, R. M., Thorpe, L. E., DiGrande, L., Perrin, M., Sapp, J. H., Wu, D., Campolucci, S., Walker, D. J., Cone, J., Pulliam, P., Thalji, L., Farfel, M. R., Thomas, P. (2006). Surveillance for World Trade Center disaster health effects among survivors of collapsed and damaged buildings. *MMWR Surveill Summ.* **55**(2), 1-18.

**29.** Braydich-Stolle, L.K., Schaeublin, N.M., Murdock, R.C., Szczublewski, K ., Schlager1, J.J., Jiang, J., Biswas, P., Hussain, S.M. (2007). The Effect of Titanium Dioxide Nanoparticles Mouse Keratinocytes (HEL-30 cells). International Congress of Nanobiotechnology & Nanomedicine 2007, San Francisco. (Abstract)

**30.** Brown, D.M., Stone, V., Findlay, P., MacNee, W., Donaldson, K. (2000). Increased inflammation and intracellular calcium caused by ultrafine carbon black is independent of transition metals or other soluble components. *Occup. Environ. Med.* **57**(10), 685-691.

**31.** Brown, K.D., Ziv, Y., Sadanandan, S.N., Chessa, L., Collins, F.S. Shiloh, Y., Tagle, D.A. (1997). The ataxia-telangiectasia gene product, a constitutively expressed nuclear protein that is not up-regulated following genome damage. *Proc. Nat. Acad. Sci.* **94**, 1840-1845.

**32.** Budman, J., Chu G. (2005). Processing of DNA for nonhomologous end-joining by cell-free extract. *EMBO J.* **24**(4), 849-60.

**33.** Cakmak, G.D., Schins, R.P., Shi, T., Fenoglio, I., Fubini, B., Borm, P.J. (2004). In vitro genotoxicity assessment of commercial quartz flours in comparison to standard DQ12 quartz. *Int. J Hyg. Environ. Health* **207**(2), 105-113.

**34.** Calderon-Garciduenas, L., Reed, W., Maronpot, R.R., Henriquez-Roldan, C., gado-Chavez, R., Calderon-Garciduenas, A., Dragustinovis, I., Franco-Lira, M., ragon-Flores, M., Solt, A. C., Altenburg, M., Torres-Jardon, R., Swenberg, J. A. (2004). Brain inflammation and Alzheimer's-like pathology in individuals

exposed to severe air pollution. *Toxicol. Pathol.* **32**(6), 650-658.

**35.** Campen, M. J., McDonald, J. D., Gigliotti, A. P., Seilkop, S. K., Reed, M. D., Benson, J. M. (2003). Cardiovascular effects of inhaled diesel exhaust in spontaneously hypertensive rats. *Cardiovasc. Toxicol.* **3**(4), 353-361.

**36.** Canman, C.E., Chen, C.Y., Lee, M.H., Kastan, M.B., (1994). DNA damage response: p53 induction, cell cycle perturbations and apoptosis. *Cold Spring Harb. Symp. Quant.Biol.* **59**, 277-286.

**37.** Canman, C.E., Lim, D.S., Cimprich, K.A., Taya, Y., Tamai, K., Sakaguchi, K., Appella, E., Kastan, M.B., Siliciano, J.D. (1998). Activation of the ATM kinase by ionizing radiation and phosphorylation of p53. *Science* **281**,1677-1679

**38.** Chalupa, D. C., Morrow, P. E., Oberdörster, G., Utell, M. J., Frampton, M. W. (2004). Ultrafine particle deposition in subjects with asthma. *Environ. Health Persp.* **112**(8), 879-882.

**39.** Chance, B., Sies, H., Boveris, A. (1979). Hydroperoxide metabolism in mammalian organs. *Physiol Rev.* **59**(3), 527-605.

**40.** Chang, L. P., Tsai, J. H., Chang, K. L., Lin, J. J. (2007). Water-soluble inorganic ions in airborne particulates from the nano to coarse mode: a case study of aerosol episodes in southern region of Taiwan. *Environ. Geochem. Health*. (Epublished before print)

**41.** Chen, M., von Mikecz, A. (2005). Formation of nucleoplasmic protein agglomerates impairs nuclear function in response to SiO2 nanoparticles. *Exp. Cell Res.* **305**(1), 51-62.

**42.** Chestnut, L. G., Schwartz, J., Savitz, D. A., Burchfiel, C. M. (1991). Pulmonary function and ambient particulate matter: epidemiological evidence from NHANES I. *Arch. Environ. Health* **46**(3), 135-144.

**43.** Cimprich, K.A., Shin, T.B., Keith, C.,T., Schreiber, S.L. (1996). cDNA cloning and gene mapping of a candidate human cell cycle checkpoint protein. *Proc. Nat. Acad. Sci.* 93, 2850-2855.

**44.** Clechet, P., Martelet, C., Martin, J. R., Olier, R. (1979). Photoelectrochemical behaviour of TiO2 and formation of hydrogen peroxide. *Electrochem. Acta.* **24**, 457.

**45.** Collins, A. R. (2004). The comet assay for DNA damage and repair: principles, applications, limitations. *Mol. Biotech.* **26**(3), 249-261.

**46.** Collins, A.R. (1999). Oxidative DNA damage, antioxidants and cancer. *BioEssays*. **21**, 238-246.

**47.** Colvin, V. L. (2003). The potential environmental impact of engineered nanomaterials. *Nat. Biotech.* **21**(10), 1166-1170.

**48.** Colvin, V. L., Kulinowski, K. M. (2007). Nanoparticles as catalysts for protein

fibrillation. *Proc. Natl. Acad. Sci. U. S. A* **104**(21), 8679-8680.

**49.** Conhaim, R. L., Rodenkirch, L. A. (1998). Functional diameters of alveolar microvessels at high lung volume in zone II. *J Appl. Physiol* **85**(1), 47-52.

**50.** Cortez, D., Wang, Y., Qin, J., Elledge, S.J. (1999). Requirement of ATM-dependent phosphorylation of Brca1 in the DNA damage response to double-strand breaks. *Science* **286**,1162-1166.

**51.** Dankovic, D., Kuempel, E., Wheeler, M. (2007). An approach to risk assessment for TiO2. *Inhal. Toxicol.* **19**(1), 205-212.

**52.** Das, B., Khatoon, N., Srivastava, R.C., Viswanathan, P.N., Rahman, Q. (1983). Biochemical studies on the toxicity of hematite dust. *Environ Res.* **32**(2):372-81.

**53.** Davies, M. J., Donkor, R., Dunster, C. A., Gee, C. A., Jonas, S., Willson, R. L. (1987). Desferrioxamine (Desferal) and superoxide free radicals. Formation of an enzyme-damaging nitroxide. *Biochem J* **246**(3), 725-729.

**54.** Dellinger, B., Pryor, W. A., Cueto, R., Squadrito, G. L., Hegde, V., Deutsch, W. A. (2001). Role of free radicals in the toxicity of airborne fine particulate matter. Chem Res.Toxicol. **14**, 1371-1377.

**55.** Demple, B., Harrison, L. (1994). Repair of oxidative damage to : Enzymology and biology. *Ann. Rev. Biochem.* **63**, 915-948.

**56.** DFG-Deutsche Forschungsgemeinschaft (2007) List of MAK and BAT values 2007. Commission for investigation of health hazards of chemical compounds in work area. Report No. – 43.

**57.** Donaldson, K., Li, X. Y., MacNee, W. (1998). Ultrafine (nanometre) particle mediated lung injury. *J. Aerosol Sci.* **29,** 553–560.

**58.** Donaldson, K., Stone, V., Borm, P. J., Jimenez, L. A., Gilmour, P. S., Schins, R. P., Knaapen, A. M., Rahman, I., Faux, S. P., Brown, D. M., MacNee, W. (2003). Oxidative stress and calcium signaling in the adverse effects of environmental particles (PM10). *Free Radic. Biol. Med.* **34**(11), 1369-1382.

**59.** Donaldson, K., Stone, V., Seaton, A., MacNee, W. (2001). Ambient particle inhalation and the cardiovascular system: potential mechanisms. *Environ. Health Persp.* **109**(4), 523-527.

**60.** Donaldson, K., Stone, V., Tran, C.L., Kreyling, W., Borm, P.J. (2004). Nanotoxicology. *Occup Environ Med.* **61**(9), 727-8.

**61.** Donaldson, K., Tran, C. L. (2002). Inflammation caused by particles and fibers. *Inhal. Toxicol.* **14**(1), 5-27.

**62.** Dopson, M., Lindstrom, E. B., Hallberg, K. B. (2001). Chromosomally encoded arsenical resistance of the moderately thermophilic acidophile Acidithiobacillus

caldus. *Extremophiles.* **5**(4), 247-255.

**63.** Duffin, R., Clouter, A., Brown, D., Tran, C. L., MacNee, W., Stone, V., et al., (2002). The importance of surface area and specific reactivity in the acute pulmonary inflammatory response to particles. *Ann. Occup. Hyg.* **46**(1), 242-245.

**64.** Duffin, R., Gilmour, P. S., Schins, R. P., Clouter, A., Guy, K., Brown, D. M., MacNee, W., Borm, P. J., Donaldson, K., Stone, V. (2001). Aluminium lactate treatment of DQ12 quartz inhibits its ability to cause inflammation, chemokine expression and nuclear factor-kappaB activation. *Toxicol. Appl. Pharmacol.* **176**(1), 10-17.

**65.** Duffin, R., Tran, L., Brown, D., Stone, V., Donaldson, K. (2007). Proinflammogenic effects of low-toxicity and metal nanoparticles in vivo and in vitro: highlighting the role of particle surface area and surface reactivity. *Inhal., Toxicol.* **19**(10), 849-856.

**66.** Dye, J. A., Lehmann, J. R., McGee, J. K., Winsett, D. W., Ledbetter, A. D., Everitt, J. I., Ghio, A. J., Costa, D. L. (2001). Acute pulmonary toxicity of particulate matter filter extracts in rats: coherence with epidemiologic studies in Utah Valley residents. *Environ. Health Persp..* **109** (3), 395-403.

**67.** El-Sayed, M. A. (2001). Some interesting properties of metals confined in time and nanometer space of different shapes. *Acc. Chem Res.* **34**(4), 257-264.

**68.** Enoch, T., Norbury, C. (1995). Cellular responses to DNA damage: cell-cycle checkpoints, apoptosis and the roles of p53 and ATM. *Trends Biochem. Sci.* **20**, 426-430.

**69.** Fernàndez, V. *et al.* (2005). Pathogenesis of mantle-cell lymphoma: all oncogenic roads lead to dysregulation of cell cycle and DNA damage response pathways. J Clin Oncol. **23**, 6364-69.

**70.** Fontecave, M., Jaouen, M., Mansuy, D., Costa, D., Zalma, R., Pezerat, H. (1990). Microsomal lipid peroxidation and oxy-radicals formation are induced by insoluble iron-containing minerals. *Biochem Biophys Res Commun.* **173**(3):912-8.

**71.** Frampton, M. W., Ghio, A. J., Samet, J. M., Carson, J. L., Carter, J. D., Devlin, R. B. (1999). Effects of aqueous extracts of PM(10) filters from the Utah valley on human airway epithelial cells. *Am. J Physiol.* **277**(5 Pt 1), L960-L967.

**72.** Fubini, B. (1998). Surface chemistry and quartz hazard. *Ann. Occup. Hyg.* **42**(8), 521-530.

**73.** Fubini, B., Bolis, V., Cavenago, A., Volante, M. (1995). Physicochemical properties of crystalline silica dusts and their possible implication in various biological responses. *Scand. J Work Environ. Health* **21**(Suppl 2), 9-14.

**74.** Fubini, B., Giamello, E., Volante, M., Bolis, V. (1990). Chemical functionalities

at the silica surface determining its reactivity when inhaled. Formation and reactivity of surface radicals. *Toxicol. Ind. Health* **6**(6), 571-598.

**75.** Fubini, B., Hubbard, A. (2003). Reactive oxygen species (ROS) and reactive nitrogen species (RNS) generation by silica in inflammation and fibrosis. *Free Radic. Biol. Med.* **34**(12), 1507-1516.

**76.** Gao, L., Zhuang, J., Nie, L., Zhang, J., Thang, Y., Gu, N., Wang, T., Yang, D., Perrett, S., Yan, X. (2007). Intrinsic peroxidase-lke activity of ferromagnetic nanoparticles. *Nature Nanotech.* **2**, 577-583.

**77.** Garry, S., Nesslany, F., Aliouat, e. M., Haguenoer, J. M., Marzin, D. (2003). Potent genotoxic activity of benzo[a]pyrene coated onto hematite measured by unscheduled DNA synthesis in vivo in the rat. *Mutagen.* **18**(5), 449-455.

**78.** Gavett, S. H. (2003). World Trade Center fine particulate matter--chemistry and toxic respiratory effects: an overview. *Environ. Health Persp.* **111**(7), 971.

**79.** Garry, S., Nesslany, F., Aliouat, E., Haguenoer, J.M., Marzin, D. (2004). Hematite (Fe2O3) acts by oxydative stress and potentiates benzo[a]pyrene genotoxicity. *Mutat. Res*. **563**(2), 117-129.

**80.** Geh, S., Shi, T., Shokouhi, B., Schins, R. P., Armbruster, L., Rettenmeier, A. W., Dopp, E. (2006a). Genotoxic potential of respirable bentonite particles with different quartz contents and chemical modifications in human lung fibroblasts. *Inhal. Toxicol.* **18**(6), 405-412.

**81.** Geh, S., Yucel, R., Duffin, R., Albrecht, C., Borm, P. J., Armbruster, L., Raulf-Heimsoth, M., Bruning, T., Hoffmann, E., Rettenmeier, A. W., Dopp, E. (2006b). Cellular uptake and cytotoxic potential of respirable bentonite particles with different quartz contents and chemical modifications in human lung fibroblasts. *Arch. Toxicol.* **80**(2), 98-106.

**82.** Geiser, M., Rothen-Rutishauser, B., Kapp, N., Schurch, S., Kreyling, W., Schulz, H., Semmler, M., Im, H., V, Heyder, J., Gehr, P. (2005). Ultrafine particles cross cellular membranes by nonphagocytic mechanisms in lungs and in cultured cells. *Environ. Health Persp.* **113**(11), 1555-1560.

**83.** Ghio, A. J. (2004). Biological effects of Utah Valley ambient air particles in humans: a review. *J Aerosol Med.* **17**(2), 157-164.

**84.** Gilmour, P., Brown, D. M., Beswick, P. H., Benton, E., MacNee, W., Donaldson, K. (1997). Surface free radical activity of PM10 and ultrafine titanium dioxide: A unifying factor in their toxicity? *Ann. Occup. Hyg.* **41**(Suppl. 1), 32–38.

**85.** Gogniat, G., Dukan, S. (2007). TiO2 photocatalysis causes DNA damage via fenton reaction-generated hydroxyl radicals during the recovery period. *Appl. Environ. Microbiol.* **73**(23), 7740-7743.

**86.** Gong, J.G., Costanzo, A., Yang, H.Q., Melino, G., Kaelin, W.G. Jr., Levrero, M., Wang, J.Y. (1999). The tyrosine kinase c-Abl regulates p73 in apoptotic

response to cisplatin-induced DNA damage. *Nat.* **399**(6738), 806-809.

**87.** Gosset, P., Garcon, G., Casset, A., Fleurisse, L., Hannothiaux, M. H., Creusy, C., Shirali, P. (2003). Benzo(a)pyrene-coated onto $Fe_0O_3$ particles-induced apoptotic events in the lungs of Sprague-Dawley rats. *Toxicol. Letters* **143**(2), 223-232.

**88.** Grawunder U, Wilm M, Wu X, Kulesza P, Wilson TE, Mann M, Lieber MR. (1997). Activity of DNA ligase IV stimulated by complex formation with XRCC4 protein in mammalian cells. *Nature*. **388**, 495-498.

**89.** Gregory, J. (1970). A survey of pneumoconiosis at a Sheffield steel foundry. *Arch. Environ. Health* **20**(3), 385-400.

**90.** Guilianelli, C., Baezasquiban, A., Boisvieuxulrich, E., Houcine, O., Zalma, R., Guennou, C., Pezerat, H., Marano, F. (1993). Effect of Mineral Particles Containing Iron on Primary Cultures of Rabbit Tracheal Epithelial-Cells - Possible Implication of Oxidative Stress. *Environ. Health Persp.* **101**(5), 436-442.

**91.** Guo, F. H., De Raeve, H. R., Rice, T. W., Stuehr, D. J., Thunnissen, F. B., Erzurum, S. C. (1995). Continuous nitric oxide synthesis by inducible nitric oxide synthase in normal human airway epithelium in vivo. *Proc.Natl.Acad.Sci.U.S.A* **92**, 7809-7813.

**92.** Gurr, J.R., Wang, A.S., Chen, C.H., Jan, K.Y. (2005). Ultrafine titanium dioxide particles in the absence of photoactivation can induce oxidative damage to human bronchial epithelial cells. *Toxicol.* **213**(1-2), 66-73.

**93.** Haase, H., Maret, W. (2005). Protein tyrosine phosphatases as targets of the combined insulinomimetic effects of zinc and oxidants. *Biometals* **18**(4), 333-338.

**94.** Hawley, R., Friend, S.H. (1996). Strange bedfellows in even stranger places: the role of ATM in meiotic cells, lymphocytes, tumors, and its functional links to p53. *Genes Dev.* **10**, 2383-2388.

**95.** He Y.T., Wan, J., Tokunga, T. (2008). Kinetic stability of hematite nanoparticles: the effect of particle. *J Nanop Res..* **10**(2),321-332

**96.** Heinrich J, Hoelscher B, Jacob B, Wjst M, Wichmann HE. . (1999). Trends in allergies among children in a region of former East Germany between 1992-1993 and 1995-1996*Eur J Med Res.* **26- 4**(3),107-13.

**97.** Heinrich, J. *et al.,* (2005). In: *Health effects of transport - related air pollution* pp. 125-183. (Book)

**98.** Helbock, H. J., Beckman, K. B., Shigenaga, M. K., Walter, P. B., Woodall, A. A., Yeo, H. C., Ames, B. N. (1998). DNA oxidation matters: the HPLC-electrochemical detection assay of 8-oxo-deoxyguanosine and 8-oxo-guanine. *Proc. Natl. Acad. Sci. U. S. A.* **95**(1), 288-293.

**99.** Henle, E. S., Linn, S. (1997). Formation, prevention and repair of DNA damage by iron/hydrogen peroxide. *J. Biol. Chem.* **272**(31), 19095-19098.

**100.** Hensley, K., Floyd, R. A. (2002). Reactive oxygen species and protein oxidation in aging: a look back, a look ahead. *Arch. Biochem. Biophys.* **397**(2), 377-383.

**101.** Hermans, C., Bernard, A. (1999). Lung epithelium-specific proteins: characteristics and potential applications as markers. *Am. J Respir. Crit Care Med.* **159**(2), 646-678.

**102.** Hershko, C., Abrahamov, A., Konijn, A.M., Breuer, W., Cabantchik, I.Z., Pootrakul, P., Link, G. (2003). Objectives and methods of iron chelation therapy. *Bioinorg Chem Appl.* 151-168

**103.** Hiroto, H., Kim, D. L., Hideko, K. (1981). Effect of temperature on normal and SV40-transformed human fibroblasts. *Biochim. et Biophy. Acta.* **673**, 37-45.

**104.** Hiura, T. S., Kaszubowski, M. P., Li, N., Nel, A. E. (1999). Chemicals in diesel exhaust particles generate reactive oxygen radicals and induce apoptosis in macrophages. *J Immunol.* **163**(10), 5582-5591.

**105.** Hornberg, C., Maciuleviciute, L., Seemayer, N.H. (1996). Human bronchoepithelial cells in vitro as a tool for detection of genotoxic activity of airborne particulates*. J. Aero. Sci.* **27**(1), 35-36.

**106.** IARC (International Agency for Research on Cancer). (1997). Monograph on the evaluation of carcinogenic risk of chemicals to humans. Silica, some silicates, coal dust and para-aramid fibrils. Lyon: *IARC.* 68 (Report)

**107.** Jimenez, L. A., Thompson, J., Brown, D. A., Rahman, I., Antonicelli, F., Duffin, R., Drost, E. M., Hay, R. T., Donaldson, K., MacNee, W. (2000). Activation of NF-kappaB by PM(10) occurs via an iron-mediated mechanism in the absence of IkappaB degradation. *Toxicol.Appl.Pharmacol.* **166**, 101-110

**108.** Joseph, N., Duppatla, V., Rao, D.N. (2006). Prokaryotic DNA mismatch repair. *Prog. Nucleic Acid Res. Mol. Biol.* **81**, 1–49.

**109.** Joshi, H., Ghosh, A. K., Singhal, D. C., Kumar, S. (2003). Arsenic contamination in parts of Yamuna sub-basin, West Bengal., *Indian J Environ. Health* **45**(4), 265-274.

**110.** Khandoga, A., Stampfl, A., Takenaka, S., Schulz, H., Radykewicz, R., Kreyling, W., Krombach, F. (2004). Ultrafine particles exert prothrombotic but not inflammatory effects on the hepatic microcirculation in healthy mice in vivo. *Circul.* **109**(10), 1320-1325.

**111.** Kim, J. H., Johannes, L., Goud, B., Antony, C., Lingwood, C. A., Daneman, R., Grinstein, S. (1998). Noninvasive measurement of the pH of the endoplasmic reticulum at rest and during calcium release. *Proc. Natl. Acad. Sci. U. S. A* **95**(6), 2997-3002.

**112.** King, R.J. (2002). Minerals explained – Arsenopyrite. *Geology today*. **18**(2), 72-75.

**113.** Klungland, A., Rosewell, I., Hollenbach, S., Larsen,E., Daly, G., Epe, B., Seeberg, E., Lindahl, T., Barnes, D.E. (1999). Accumulation of premutagenic DNA lesions in mice defective in removal of oxidative base damage. *Proc. Natl. Acad.Sci. U.S.A.* **96**:13300-13305.

**114.** Knaapen, A. M., Albrecht, C., Becker, A., Hohr, D., Winzer, A., Haenen, G. R., Borm, P. J., Schins, R. P. (2002a). DNA damage in lung epithelial cells isolated from rats exposed to quartz: role of surface reactivity and neutrophilic inflammation. *Carcinogen.* **23**(7), 1111-1120.

**115.** Knaapen, A. M., Shi, T., Borm, P. J., Schins, R. P. (2002b). Soluble metals as well as the insoluble particle fraction are involved in cellular DNA damage induced by particulate matter. *Mol. Cell Biochem.* **234-235**(1-2), 317-326.

**116.** Kress, H., Stelzer, E.H., Holzer, D., Buss, F., Griffiths, G., Rohrbach, A. (2007). Filopodia act as phagocytic tentacles and pull with discrete steps and a load-dependent velocity. *Proc Natl Acad Sci U S A.* **104**(28), 11633-8.

**117.** Kreuter, J., Shamenkov, D., Petrov, V., Ramge, P., Cychutek, K., Koch-Brandt, C., Alyautdin, R. (2002). Apolipoprotein-mediated transport of nanoparticle-bound drugs across the blood-brain barrier. *J Drug Target* **10**(4), 317-325.

**118.** Kreyling, W. G., Semmler, M., Erbe, F., Mayer, P., Takenaka, S., Schulz, H., Oberdörster, G., Ziesenis, A. (2002). Translocation of ultrafine insoluble iridium particles from lung epithelium to extrapulmonary organs is size dependent but very low. *J Toxicol. Environ. Health A* **65**(20), 1513-1530.

**119.** Kreyling, W. G., Semmler, M., Moller, W. (2004). Dosimetry and toxicology of ultrafine particles. *J Aerosol Med.* **17**(2), 140-152.

**120.** Kumar, A., Sahoo, B., Montpetit, A., Behera, S., Lockey, R. F., Mohapatra, S. S. (2007). Development of hyaluronic acid-Fe2O3 hybrid magnetic nanoparticles for targeted delivery of peptides. *Nanomed.* **3**(2), 132-137.

**121.** Lahermo, P., Alfthan, G., Wang, D. (1998) Selenium and arsenic in the environment in Finland. *J Environ Pathol Toxicol Oncol.* **17**(3-4):205-16.

**122.** Leanderson, P., Tagesson, C. (1992). Hydrogen peroxide release and hydroxyl radical formation in mixtures containing mineral fibres and human neutrophils. *Br. J Ind. Med.* **49**(11), 745-749.

**123.** Lee, S., Russell, A. G., Baumann, K. (2007). Source apportionment of fine particulate matter in the southeastern United States. *J Air Waste Manag. Assoc.* **57**(9), 1123-1135.

**124.** Leonard, S. S., Harris, G. K., Shi, X. (2004). Metal-induced oxidative stress and signal transduction. *Free Radic. Biol. Med.* **37**(12), 1921-1942.

**125.** Lewin, M., Carlesso, N., Tung, C. H., Tang, X. W., Cory, D., Scadden, D. T., Weissleder, R. (2000). Tat peptide-derivatized magnetic nanoparticles allow in vivo tracking and recovery of progenitor cells. *Nat. Biotechnol.* **18**(4), 410-414.

**126.** Li, H., Haberzettl. P., Albrecht, C., Höhr, D., Knappen, A.M., Borm, P.J., Schins, RP. (2007). Inhibition of the mitochondrial respiratory chain function abrogates quartz induced DNA damage in lung epithelial cells. *Mutat. Res.* **617**(1-2), 46-57.

**127.** Li, H., van, B. D., Shi, T., Speit, G., Knaapen, A. M., Borm, P. J., Albrecht, C., Schins, R. P. (2007). Curcumin protects against cytotoxic and inflammatory effects of quartz particles but causes oxidative DNA damage in a rat lung epithelial cell line. *Toxicol. Appl. Pharmacol.* **227**(1):115-24.

**128.** Li, N., Karin, M. (1999). Is NF-kappaB the sensor of oxidative stress? *FASEB J* **13**(10), 1137-1143.

**129.** Li, N., Sioutas, C., Cho, A., Schmitz, D., Misra, C., Sempf, J., Wang, M., Oberley, T., Froines, J., Nel, A. (2003). Ultrafine particulate pollutants induce oxidative stress and mitochondrial damage. *Environ. Health Persp.* **111**(4), 455-460.

**130.** Limbach, L. K., Li, Y., Grass, R. N., Brunner, T. J., Hintermann, M. A., Muller, M., Gunther, D., Stark, W. J. (2005). Oxide nanoparticle uptake in human lung fibroblasts: effects of particle size, agglomeration, diffusion at low concentrations. *Environ. Sci. Technol.* **39**(23), 9370-9376.

**131.** Lin, J., Sun, T., Ji, L., Deng, W., Roth, J., Minna, J., Arlinghaus, R. (2007). Oncogenic activation of c-Abl in non-small cell lung cancer cells lacking FUS1 expression: inhibition of c-Abl by the tumor suppressor gene product Fus1. *Oncogene* **26**(49), 6989-6996.

**132.** Linse, S., Cabaleiro-Lago, C., Xue, W. F., Lynch, I., Lindman, S., Thulin, E., Radford, S. E., Dawson, K. A. (2007). Nucleation of protein fibrillation by nanoparticles. *Proc. Natl. Acad. Sci. U. S. A.* **104**(21), 8691-8696.

**133.** Lipfert, F. W., Wyzga, R. E. (1997). Air pollution and mortality: the implications of uncertainties in regression modeling and exposure measurement. *J Air Waste Manag. Assoc.* **47**(4), 517-523.

**134.** Liu, Y.T., Chen, Z. (1996). A retrospective lung cancer mortality study of people exposed to insoluble arsenic and radon. *Lung Cancer***. 14**(1), S137-48.

**135.** Lodish,H., Berk, A., Matsudaira, P., Kaiser, C.A., Krieger, M., Scott, M.P., Zipursky, L., Darnell, J. (1986) *Molecular Cell Biology* ed. Bentley, D. and Toroian-Raymond, A. by W.H. Freeman and Company. **5,** 821- 823.

**136.** Luo, H. Y., Liu, Y., Yang, X. L. (2007). Particle deposition in obstructed airways. *J Biomech.* **40**(14), 3096-3104.

**137.** Luo, Y. Charecterization of Fenton oxidants and DNA damage. (1993).

University of California, Berkeley. (Thesis work)

**138.** Matsumoto, Y., Zhang, Q. M., Takao, M., Yasui, A., Yonei, S. (2001). Escherichia coli Nth and human hNTH1 DNA glycosylases are involved in removal of 8-oxoguanine from 8-oxoguanine/guanine mispairs in DNA. *Nucleic Acids Res.* **29**(9), 1975-1981.

**139.** McDonald, J. C., McDonald, A. D., Hughes, J. M., Rando, R. J., Weill, H. (2005). Mortality from lung and kidney disease in a cohort of North American industrial sand workers: an update. *Ann. Occup. Hyg.* **49**(5), 367-373.

**140.** Meyers, R. A. (2000). Inductively coupled plasma mass spectrometry in environmental analysis. In *Encycl. of anal. Chem.* (S.I.Yamasaki, Ed.), 2000 ed., pp. 2672-2692. John Wiley and Sons Ltd.

**141.** Miller, D. M., Aust, S. D. (1989). Studies of ascorbate-dependent, iron-catalyzed lipid peroxidation. *Arch-Biochem-Biophys.* **271**(1), 113-119.

**142.** Monteiller, C., Tran, L., MacNee, W., Faux, S., Jones, A., Miller, B., Donaldson, K. (2007). The pro-inflammatory effects of low-toxicity low-solubility particles, nanoparticles and fine particles, on epithelial cells in vitro: the role of surface area. *Occup. Environ. Med.* **64**(9), 609-615.

**143.** Moore JK, Haber JE. (1996). Cell cycle and genetic requirements of two pathways of nonhomologous end-joining repair of double-strand breaks in Saccharomyces cerevisiae. *Mol Cell Biol.* **16**(5), 2164-73.

**144.** Nagelschmidt, G. (1960). The relation between lung dust and lung pathology in pneumoconiosis. *Br. J Ind. Med.* **17**, 247-259.

**145.** Nehls, P., Seiler, F., Rehn, B., Greferath, R., Bruch, J. (1997). Formation and persistence of 8-oxoguanine in rat lung cells as an important determinant for tumor formation following particle exposure. *Environ. Health Perspect.* **105**(5), 1291-1296.

**146.** Nel, A. E., az-Sanchez, D., Li, N. (2001). The role of particulate pollutants in pulmonary inflammation and asthma: evidence for the involvement of organic chemicals and oxidative stress. Curr.Opin.Pulm.Med. **7**, 20-26.

**147.** Nel, A., Xia, T., Madler, L., Li, N. (2006). Toxic potential of materials at the nanolevel. *Science* **311**(5761), 622-627.

**148.** Nemery, B., Hoet, P. H., Nemmar, A. (2001). The Meuse Valley fog of 1930: an air pollution disaster. *Lancet* **357**(9257), 704-708.

**149.** Nemmar, A., Hoet, P. H., Vanquickenborne, B., Dinsdale, D., Thomeer, M., Hoylaerts, M. F., Vanbilloen, H., Mortelmans, L., Nemery, B. (2002). Passage of inhaled particles into the blood circulation in humans. *Circulation* **105**(4), 411-414.

**150.** Nemmar, A., Hoylaerts, M. F., Hoet, P. H., Nemery, B. (2004). Possible mechanisms of the cardiovascular effects of inhaled particles: systemic

translocation and prothrombotic effects. *Toxicol. Lett.* **149**(1-3), 243-253.

**151.** Nemmar, A., Nemery, B., Hoet, P. H., Vermylen, J., Hoylaerts, M. F. (2003). Pulmonary inflammation and thrombogenicity caused by diesel particles in hamsters: role of histamine. *Am. J Respir. Crit Care Med.* **168**(11), 1366-1372.

**152.** Nichols, W. W., Murphy, D. G., Cristofalo, V. J., Toji, L. H., Greene, A. E., Dwight, S. A. (1977). Characterization of a new human diploid cell strain, IMR-90. *Science* **196**, 60-63

**153.** NIOSH (National Institute for Occupational Safety and Health). Health effects of occupational exposure to respirable crystalline silica 2002. Bethesda, MD: Department of Health and Human Services Centres for Disease Control and Prevention National Institute for Occupational Safety and Health DHHS (NIOSH). 2002(129). 2002. (Report)

**154.** Nolan, R. P., Langer, A. M., Harington, J. S., Oster, G., Selikoff, I. J. (1981). Quartz hemolysis as related to its surface functionalities. *Environ.Res.* **26**, 503-520

**155.** Oberdörster, G. (1996). Significance of particle parameters in the evaluation of exposure-dose-response relationships of inhaled particles. *Inhal. Toxicol.* **8,** 73–89.

**156.** Oberdörster, G. (2002). Toxicokinetics and effects of fibrous and nonfibrous particles. *Inhal., Toxicol.* **14**(1), 29-56.

**157.** Oberdörster, G., Ferin, J., Gelein, R., Soderholm, S. C., Finkelstein, J. (1992). Role of the alveolar macrophage in lung injury: studies with ultrafine particles. *Environ.Health Perspect.* **97**, 193-199

**158.** Oberdörster, G., Ferin, J., Lehnert, B. E. (1994). Correlation between particle size, in vivo particle persistence and lung injury. *Environ. Health Perspect.* **102**(5), 173-179.

**159.** Oberdörster, G., Maynard, A., Donaldson, K., Castranova, V., Fitzpatrick, J., Ausman, K., Carter, J., Karn, B., Kreyling, W., Lai, D., Olin, S., Monteiro-Riviere, N., Warheit, D., Yang, H. (2005a). Principles for characterizing the potential human health effects from exposure to nanomaterials: elements of a screening strategy. *Part Fibre. Toxicol.* **2**, 8.

**160.** Oberdörster, G., Oberdörster, E., Oberdörster, J. (2005b). Nanotoxicology: an emerging discipline evolving from studies of ultrafine particles. *Environ. Health Perspect.* **113**(7), 823-839.

**161.** Oberdörster, G., Sharp, Z., Atudorei, V., Elder, A., Gelein, R., Kreyling, W., Cox, C. (2004). Translocation of inhaled ultrafine particles to the brain. *Inhal., Toxicol.* **16**(6-7), 437-445.

**162.** O'Brien, P. J., Ellenberger, T. (2003). Human alkyladenine DNA glycosylase uses acid-base catalysis for selective excision of damaged purines.

*Biochemistry* **42**, 12418-12429.

**163.** Ogami, A., Morimoto, Y., Myojo, T., Oyabu, T., Murakami, M., Nishi, K., Kadoya, C., Tanaka, I. (2007). Histopathological changes in rat lung following intratracheal instillation of silicon carbide whiskers and potassium octatitanate whiskers. *Inhal., Toxicol.* **19**(9), 753-758.

**164.** Orren, D.K. (2005). The irresistible resistance of nonsense: Evolutionary adaptation of termination codons to minimize the effects of common DNA damage. *DNA Rep.* **4**(10), 1208-1212.

**165.** Ostling, O., Johanson, K. J. (1984). Microelectrophoretic study of radiation-induced DNA damages in individual mammalian cells. *Biochem.Biophys.Res.Commun.* **123**, 291-298

**166.** Paull, T. T., Gellert, M. (1998). The 3-prime to 5-prime exonuclease activity of Mre11 facilitates repair of DNA double-strand breaks. *Molec. Cell* 1: 969-979.

**167.** Pekarkova, I., Parara, S., Holecek, V., Stopka, P., Trefil, L., Racek, J. and Rokyta, R. (2001). Does exogenous melatonin influence the free radicals metabolism and pain sensation in rat? *Physiol Res.* **50**(6), 595-602.

**168.** Peretz, A., Checkoway, H., Kaufman, J. D., Trajber, I., Lerman, Y. (2006). Silica, silicosis and lung cancer. *Isr. Med. Assoc. J.* **8**(2), 114-118.

**169.** Peters, A., Doring, A., Wichmann, H. E., Koenig, W. (1997). Increased plasma viscosity during an air pollution episode: a link to mortality? *Lancet* **349**(9065), 1582-1587.

**170.** Pezerat, H. (1991). The surface activity of mineral dusts and the process of oxidative stress. In *Mechanisms of fibe carcinogenesis* (R.C.Brown, J.A.Hoskin and N.F.Johnson, Eds.), pp. 387-395. Plenum Press, New York.

**171.** Pisanic, T. R., Blackwell, J. D., Shubayev, V. I., Finones, R. R., Jin, S. (2007). Nanotoxicity of iron oxide nanoparticle internalization in growing neurons. *Biomat.* **28**(16), 2572-2581.

**172.** Pope, C. A., III (1991). Respiratory hospital admissions associated with PM10 pollution in Utah, Salt Lake and Cache Valleys. *Arch. Environ. Health* **46**(2), 90-97.

**173.** Pope, C. A., III, Burnett, R. T., Thun, M. J., Calle, E. E., Krewski, D., Ito, K., Thurston, G. D. (2002). Lung cancer, cardiopulmonary mortality and long-term exposure to fine particulate air pollution. *JAMA* **287**(9), 1132-1141.

**174.** Pope, C. A., III, Burnett, R. T., Thurston, G. D., Thun, M. J., Calle, E. E., Krewski, D. and Godleski, J. J. (2004). Cardiovascular mortality and long-term exposure to particulate air pollution: epidemiological evidence of general pathophysiological pathways of disease. *Circul.* **109**(1), 71-77.

**175.** Pott, F., Huth, F., Friedrichs, K.H. (1974). Tumorigenic effect of fibrous dusts

in experimental animals. *Environ. Health Persp.* **9**, 313-5.

**176.** Prahalad, A. K., Inmon, J., Dailey, L. A., Madden, M. C., Ghio, A. J., Gallagher, J. E. (2001). Air pollution particles mediated oxidative DNA base damage in a cell free system and in human airway epithelial cells in relation to particulate metal content and bioreactivity. *Chem Res. Toxicol.* **14**(7), 879-887.

**177.** Pyenson, H., Tracy, P. H. (1945). A 1,10 Phenanthroline method for the determination of iron in powdered milk. *J of Dairy Sci.* **28**(5), 401-412.

**178.** Raab, A., Feldmann, J. (2005). Arsenic speciation in hair extracts. *Anal., Bioanal., Chem.* **381**(2), 332-338.

**179.** Rahman, Q., Lohani, M., Dopp, E., Pemsel, H., Jonas, L., Weiss, D. G., Schiffmann, D. (2002a). Evidence that ultrafine titanium dioxide induces micronuclei and apoptosis in Syrian hamster embryo fibroblasts. *Environ.Health Perspect.* **110**, 797-800.

**180.** Rejman, J., Oberle, V., Zuhorn, I. S., Hoekstra, D. (2004). Size-dependent internalization of particles via the pathways of clathrin- and caveolae-mediated endocytosis. *Biochem. J* **377**(Pt 1), 159-169.

**181.** Ridley, M. K., Machesky, M. L., Wesolowski, D. J., Finnegan, M. P., Palmer, D. A. (2001). Surface Charge and Ion Sorption Properties of Titanium Dioxide. *American Geophysical Union, Fall Meeting 2001*(Abstract).

**182.** Rimai D.S., Quesnel D.J., Busnaia A.A. (2000). The adhesion of dry particles in the nanometer to micrometer –size range. *Colloids Surf A Physicochem Eng Aspects.* **165**, 3-10.

**183.** Risom, L., Moller, P., Loft, S. (2005). Oxidative stress-induced DNA damage by particulate air pollution. *Mutat. Res,* **592:**119-37.

**184.** Roberts, J. R., Young, S. H., Castranova, V., Antonini, J. M. (2007). Soluble metals in residual oil fly ash alter innate and adaptive pulmonary immune responses to bacterial infection in rats. *Toxicol. Appl. Pharmacol.* **221**(3), 306-319.

**185.** Ross, H. F., King, E. J., Yoganathan, M., Nagelschmidt, G. (1962). Inhalation experiments with coal dust containing 5 per cent, 10 per cent, 20 per cent and 40 per cent quartz: tissue reactions in the lungs of rats. *Ann. Occup. Hyg.* **5**, 149-161.

**186.** Sagai, M., Saito, H., Ichinose, T., Kodama, M., Mori, Y. (1993). Biological effects of diesel exhaust particles. I. In vitro production of superoxide and in vivo toxicity in mouse. *Free Radic. Biol. Med.* **14**(1), 37-47.

**187.** Salvi, S., Holgate, S. T. (1999). Mechanisms of particulate matter toxicity. *Clin. Exp. Allergy* **29**(9), 1187-1194.

**188.** Sayes, C. M., Wahi, R., Kurian, P. A., Liu, Y., West, J. L., Ausman, K. D., Warheit, D. B., Colvin, V. L. (2006). Correlating nanoscale titania structure with

toxicity: a cytotoxicity and inflammatory response study with human dermal fibroblasts and human lung epithelial cells. *Toxicol.Sci.* **92**, 174-185.

**189.** Schaumann, F., Borm, P. J., Herbrich, A., Knoch, J., Pitz, M., Schins, R. P., Luettig, B., Hohlfeld, J. M., Heinrich, J., Krug, N. (2004). Metal-rich ambient particles (particulate matter 2.5) cause airway inflammation in healthy subjects. *Am. J Respir. Crit Care Med.* **170**(8), 898-903.

**190.** Schins, R. P. *et al.(*2002a). Surface modification of quartz inhibits toxicity, particle uptake and oxidative DNA damage in human lung epithelial cells. *Chem. Res. Toxicol.* **15**(9), 1166-1173.

**191.** Schins, R. P., Knaapen, A. M., Cakmak, G. D., Shi, T., Weishaupt, C., Borm, P. J. (2002b). Oxidant-induced DNA damage by quartz in alveolar epithelial cells. *Mutat. Res.* **517**(1-2), 77-86.

**192.** Schwartz, J. (1999). Air pollution and hospital admissions for heart disease in eight U.S. counties. *Epidemiol.* **10**(1), 17-22.

**193.** Schwartz, J., Marcus, A. (1990). Mortality and air pollution in London: a time series analysis. *Am. J Epidemiol.* **131**(1), 185-194.

**194.** Seaton, A., Cherrie, J., Dennekamp, M., Donaldson, K., Hurley, J.F., Tran, C.L. (2005). The London Underground: dust and hazards to health. *Occup Environ Med.* **62**(6):355-62.

**195.** Seaton, A., MacNee, W., Donaldson, K., Godden, D. (1995). Particulate air pollution and acute health effects. *Lancet* **345**(8943), 176-178.

**196.** Seiler, F., Rehn, B., Rehn, S., Hermann, M., Bruch, J. (2001). Quartz exposure of the rat lung leads to a linear dose response in inflammation but not in oxidative DNA damage and mutagenicity. *Am. J Respir. Cell Mol. Biol.* **24**(4), 492-498.

**197.** Semmler, M., *et al.* (2004). Long-term clearance kinetics of inhaled ultrafine insoluble iridium particles from the rat lung, including transient translocation into secondary organs. *Inhal. Toxicol.* **16**(6-7), 453-459.

**198.** Serpone, N., Salinaro, A., Emeline, A. (2001). Deleterious Effects of Sunscreen Titanium Dioxide Nanoparticles on DNA. Efforts to Limit DNA Damage by Particle Surface Modification, Nanoparticles & Nanostructured Surfaces - Novel Reporters with Biological Applications. In *SPIE* (C.J.Murphy, Ed.), 2 ed., pp. 86-98.

**199.** Service, R. F. (2004). Nanotoxicology. Nanotechnology grows up. *Science* **304**(5678), 1732-1734.

**200.** Shi, T., Knaapen, A. M., Begerow, J., Birmili, W., Borm, P. J., Schins, R. P. (2003). Temporal variation of hydroxyl radical generation and 8-hydroxy-2'-deoxyguanosine formation by coarse and fine particulate matter. *Occup.*

*Environ. Med.* **60**(5), 315-321.

**201.** Sies, H. (1986). Biochemistry of oxidative stress. *Angew Chem Int. Ed.* **25**, 1058-1071.

**202.** Singh, S., Shi, T., Duffin, R., Albrecht, C., van, B. D., Hohr, D., Fubini, B., Martra, G., Fenoglio, I., Borm, P. J., Schins, R. P. (2007). Endocytosis, oxidative stress and IL-8 expression in human lung epithelial cells upon treatment with fine and ultrafine TiO2: role of the specific surface area and of surface methylation of the particles. *Toxicol. Appl. Pharmacol.* **222**(2), 141-151.

**203.** Sorescu, D., Griendling, K. K. (2002). Reactive oxygen species, mitochondria and NAD(P)H oxidases in the development and progression of heart failure. *Congest. Heart Fail.* **8**(3), 132-140.

**204.** Soukup JM, Ghio AJ, Becker S. (2000). Soluble components of Utah Valley particulate pollution alter alveolar macrophage function in vivo and in vitro. *Inhal Toxicol.***12**(5):401-14.

**205.** Squadrito, G. L., Cueto, R., Dellinger, B., Pryor, W. A. (2001). Quinoid redox cycling as a mechanism for sustained free radical generation by inhaled airborne particulate matter. *Free Radic.Biol.Med.* **31**, 1132-1138

**206.** Stearns, R. C., Paulauskis, J. D., Godleski, J. J. (2001). Endocytosis of ultrafine particles by A549 cells. *Am. J. Respir. Cell Mol. Biol.* **24**(2), 108-115.

**207.** Stikinger, H.E., A review of world literature finds iron oxides noncarcinogenic. *Am. Ind. Assoc. J.* **45**(2), 127-133.

**208.** Stoeger, T., Reinhard, C., Takenaka, S., Schroeppel, A., Karg, E., Ritter, B., Heyder, J., Schulz, H. (2006). Instillation of six different ultrafine carbon particles indicates a surface area threshold dose for acute lung inflammation in mice. *Environ. Health Persp.* **114**(3), 328-333.

**209.** Stokinger, H. E. (1984). A review of world literature finds iron oxides noncarcinogenic. *Am. Ind. Hyg. Assoc. J* **45**(2), 127-133.

**210.** Stone, V., Johnston, H., Clift, M. J. (2007). Air pollution, ultrafine and nanoparticle toxicology: cellular and molecular interactions. *IEEE Trans. Nanobioscience.* **6**(4), 331-340.

**211.** Stone, V., Jones, R., Rollo, K., Duffin, R., Donaldson, K., Brown, D. M. (2004). Effect of coal mine dust and clay extracts on the biological activity of the quartz surface. *Toxicol.Lett.* **149**, 255-259.

**212.** Taira, M., Sasaki, K., Saitoh, S., Nezu, T., Sasaki, M., Kimura, S., Terasaki, K., Sera, K., Narushima, T., Araki, Y. (2006). Accumulation of element Ti in macrophage-like RAW264 cells cultured in medium with 1 ppm Ti and effects on cell viability, SOD production and TNF-alpha secretion *Dent Mater J.* **25**(4), 726-32.

**213.** Tal, T. L., Graves, L. M., Silbajoris, R., Bromberg, P. A., Wu, W., Samet, J. M.

(2006). Inhibition of protein tyrosine phosphatase activity mediates epidermal growth factor receptor signaling in human airway epithelial cells exposed to Zn2+. *Toxicol. Appl. Pharmacol.* **214**(1), 16-23.

**214.** The relevance of the rat lung response to particle overload for human risk assessment: a workshop consensus report. ILSI Risk Science Institute Workshop Participants. *Inhal. Toxiclo.* **12**, 1-17

**215.** Tinkle, S. S., Antonini, J. M., Rich, B. A., Roberts, J. R., Salmen, R., DePree, K., Adkins, E. J. (2003). Skin as a route of exposure and sensitization in chronic beryllium disease. *Environ. Health Persp.* **111**(9), 1202-1208.

**216.** Turkez, H., Geyikoglu, F. (2007). An in vitro blood culture for evaluating the genotoxicity of titanium dioxide: the responses of antioxidant enzymes. *Toxicol. Ind. Health* **23**(1), 19-23.

**217.** Turrens, J. F. (2003). Mitochondrial formation of reactive oxygen species. *J. Physiol.* **552**(Pt 2), 335-344.

**218.** Vallyathan, V., Kang, J. H., Van, D. K., Dalal, N. S., Castranova, V. (1991). Response of alveolar macrophages to in vitro exposure to freshly fractured versus aged silica dust: the ability of Prosil 28, an organosilane material, to coat silica and reduce its biological reactivity. *J Toxicol. Environ. Health* **33**(3), 303-315.

**219.** Vallyathan, V., Mega, J. F., Shi, X., Dalal, N. S. (1992). Enhanced generation of free radicals from phagocytes induced by mineral dusts. *Am. J Respir. Cell Mol. Biol.* **6**(4), 404-413.

**220.** Vallyathan, V., Shi, X. L., Dalal, N. S., Irr, W., Castranova, V. (1988). Generation of free radicals from freshly fractured silica dust. Potential role in acute silica-induced lung injury. *Am. Rev. Respir. Dis.* **138**(5), 1213-1219.

**221.** van Gent, D,C,, van der Burg, M. (2007). Non-homologous end-joining, a sticky affair. *Oncogene.* **26**, 7731-7740.

**222.** Vinzents, P. S., Moller, P., Sorensen, M., Knudsen, L. E., Hertel, O., Jensen, F. P., Schibye, B., Loft, S. (2005). Personal exposure to ultrafine particles and oxidative DNA damage. *Environ. Health Perspect.* **113**(11), 1485-1490.

**223.** Walker, J. A., Sherman, R. A., Eisinger, R. P. (1985). Thrombocytopenia associated with intravenous desferrioxamine. *Am. J Kidney Dis.* **6**(4), 254-256.

**224.** Wang, H., Perrault, A.R., Takeda, Y., Qin, W., Wang, H., Iliakis, G. (2003). Biochemical evidence for Ku-independent backup pathways of NHEJ. *Nucleic Acids Res.* **31**(18):5377-88.

**225.** Wang, H., Rosidi, B., Perrault, R., Wang, M., Zhang, L., Windhofer, F., Iliakis, G. (2005). DNA ligase III as a candidate component of backup pathways of nonhomologous end joining. *Cancer Res.* **65**(10), 4020-4030.

**226.** Wang, J.J., Sanderson, B. J., Wang, H. (2007). Cyto- and genotoxicity of

ultrafine TiO2 particles in cultured human lymphoblastoid cells. *Mutat. Res.* **628**(2), 99-106.

**227.** Wang, Y., Cortez, D., Yazdi, P., Neff, N., Elledge, S.J., Qin, J. (2000). BASC, a super complex of BRCA1-associated proteins involved in the recognition and repair of aberrant DNA structures. *Genes Dev.* **14**, 927-939.

**228.** Warheit, D. B., Borm, P. J., Hennes, C., Lademann, J. (2007). Testing strategies to establish the safety of nanomaterials: conclusions of an ECETOC workshop. *Inhal. Toxicol.* **19**(8), 631-643.

**229.** Warheit, D.B. (2004). Nanoparticles health impacts? *Mat. Today.* **7**, 32-35.

**230.** Warheit, D.B., Webb, T.R., Reed, K.L., Frerichs, S., Sayes, C.M. (2007). Pulmonary toxicity study in rats with three forms of ultrafine-$TiO_2$ particles: differential responses related to surface properties. *Toxicology.* **230**, 90–104.

**231.** Warheit, D.B., Webb, T.R., Sayes, C.M., Colvin, V.L., Reed, K.L. (2006). Pulmonary instillation studies with nanoscale $TiO_2$ rods and dots in rats: toxicity is not dependent upon particle size and surface area. *Toxicol Sci.* **91**, 227–236.

**232.** Wiessner, J. H., Mandel, N. S., Sohnle, P. G., Mandel, G. S. (1989). Effect of particle size on quartz-induced hemolysis and on lung inflammation and fibrosis. *Exp. Lung Res.* **15**(6), 801-812.

**233.** Wilson, M. R., Lightbody, J. H., Donaldson, K., Sales, J., Stone, V. (2002). Interactions between ultrafine particles and transition metals in vivo and in vitro. *Toxicol. Appl. Pharmacol.* **184**(3), 172-179.

**234.** Wilson, T.E., Lieber, M.R. (1999). Efficient processing of DNA ends during yeast nonhomologous end joining. Evidence for a DNA polymerase beta (Pol4)-dependent pathway. *Biol Chem.* **274**(33), 23599-609.

**235.** Woo, K., Lee, H.J.H.J. (2004). Synthesis and magnetism of hematite and maghemite nanoparticles. *J Mag Mag Mat* **272-276**(1), E1155-E1156

**236.** Wottrich, R., Diabate, S., Krug, H. F. (2004). Biological effects of ultrafine model particles in human macrophages and epithelial cells in mono- and co-culture. *Int. J Hyg. Environ. Health* **207**(4), 353-361.

**237.** Wu, M., Che, W., Zhang, Z. (2008). Enhanced sensitivity to DNA damage induced by cooking oil fumes in human OGG1 deficient cells. *Environ Mol Mutagen.* [Epubublished ahead of print]

**238.** Yamamoto, F., Kasai, H., Bessho, T., Chung, M. H., Inoue, H., Ohtsuka, E., Hori, T., Nishimura, S. (1992). Ubiquitous presence in mammalian cells of enzymatic activity specifically cleaving 8-hydroxyguanine-containing DNA. *Jpn. J Cancer Res.* **83**(4), 351-357.

**239.** Yamano, Y., Kagawa, J., Hanaoka, T., Takahashi, T., Kasai, H., Tsugane, S., Watanabe, S. (1995). Oxidative DNA damage induced by silica in vivo. *Environ.*

*Res.* **69**(2), 102-107.

**240.** Yokohira, M., Takeuchi, H., Yamakawa, K., Saoo, K., Matsuda, Y., Zeng, Y., Hosokawa, K., Imaida, K. (2007). Bioassay by intratracheal instillation for detection of lung toxicity due to fine particles in F344 male rats. *Experimental and Toxicologic Pathology* **58**(4), 211-221.

**241.** Yu, Z., Chen, J., Ford, B.N., Brackley, M.E., Glickman, B.W. (1999). Human DNA repair systems: An overview. *Envion. Mol. Mutagen.* **33**, 3-20.

**242.** Zhao, S., Weng, Y.C., Yuan, S.S.F., Lin, Y.T., Hsu, H.C., Lin, S.C.J., Gerbino, E., Song, M., Zdzienicka, M.Z., Gatti, R.A., Shay, J.W., Ziv, Y., Shiloh, Y., Lee, E.Y.H.P. (2000). Functional link between ataxia-telangiectasia and Nijmegen breakage syndrome gene products. *Nature* **405**, 473-477.

**243.** Zhou, N., Qiu, T., Yang-Ping, L., Yang, L. (2006). Superoxide anion radical generation in the NaOH/H(2)O(2)/Fe(III) system: a spin trapping ESR study. *Magn Reson. Chem.* **44**(1), 38-44.

**Table 1:** Chart for dosage calculation from stock solution

| **Stock solution*. [mg/ml]** | **Area of cell culture flask [$cm^2$]** | | | | | | | | | |
|---|---|---|---|---|---|---|---|---|---|---|
| 5 | 150 | | 75 | | 25 | | 12.5 | | 9.62 | |
| **Final concentration [µg/$cm^2$]** | **Absolute in culture [µg]** | **Applied Volume [µl]** | **Absolute in culture [µg]** | **Applied Volume [µl]** | **Absolute in culture [µg]** | **Applied Volume [µl]** | **Absolute in culture [µg]** | **Applied Volume [µl]** | **Absolute in culture [µg]** | **Applied Volume [µl]** |
| 500 | 75000 | 15000 | 37500 | 7500 | 12500 | 2500 | 6250 | 1250 | 4810 | 962 |
| 50 | 7500 | 1500 | 3750 | 750 | 1250 | 250 | 625 | 125 | 481 | 96.2 |
| 10 | 1500 | 300 | 750 | 150 | 250 | 50 | 125 | 25 | 96.2 | 19.24 |
| 5 | 750 | 150 | 375 | 75 | 125 | 25 | 62.5 | 12.5 | 48.1 | 9.62 |
| 2 | 300 | 60 | 150 | 30 | 50 | 10 | 25 | 5 | 19.24 | 3.84 |

*in 0.9% NaCl/ PBS

## Appendix 2

**Table 2:** List of chemicals used

| Name | Source (Supplier/Company) |
|---|---|
| 1,10- Phenanthroline Chloride | Merck |
| 2- Propanol | Sigma |
| 2,7 Dihydrodichloroflurescein diacetate | Invitrogen |
| 5,5-dimethylpyrroline-N-oxide (DMPO) | Sigma |
| Acrodisc 45-mm syringe filter | Pall Gelman Laboratory |
| Active Coal | Merck |
| Ammonium Acetate | Merck |
| Ammonium Carbonate | Sigma |
| Annexin V – FITC | Beckman Coulter GmbH |
| Arsenic (III) oxide | Sigma Aldrich |
| Arsenopyrite Ash /Cinder | Süd Chemie GmbH. Germany |
| Ascorbic Acid | Sigma |
| Defined – KSFM | Gibco |
| Defined – KSFM (Epithelial Growth Supplement) | Gibco |
| DMSO | Fluka |
| Earl's Modified Eagle Medium | C-C Pro GmbH |
| EDTA | Fluka |
| Ethanol | Riedel De Hään |
| Ethylene glycol tetra acetic acid (EGTA) | Sigma |
| Fetal Bovine Serum | Gibco |
| Gelatine | Sigma |
| Gelbond Film | Cambrel |
| Gentamycin | C-C Pro GmbH |
| Glacial Acetic Acid | Sigma |
| Glutaraldehyde | EMS. Hatfield. USA |
| Glycine | Sigma |
| Haemocytometer | Neubauer |
| Hank's Buffered Salt Solution | Gibco |
| HEPES | C-C Pro GmbH |
| Highly Sensitive 8-OHdG check ELISA kit | Gentaur |

| | |
|---|---|
| Hydrochloric Acid | Sigma |
| Hydrogen Peroxide | Sigma |
| Hydroxyammonium Chloride | Merck |
| L-Glutamine | C-C Pro GmbH |
| Low Melting Agarose | Amersham Biosciences |
| Magnesium Chloride | Sigma |
| Methyl Cellulose | Sigma |
| N- Laurysarcosine | Sigma |
| Nitric Acid | Sigma |
| Non-essential Amino acid | C-C Pro GmbH |
| Nuclease P1 | Sigma |
| Paraformaldehyde (EM Grade) | EMS. Hatfield. USA |
| Phosphate Buffer Solution | Invitrogen |
| Piperazine-N-bis(2-ethanesulfonic acid) | GFS Chemicals. USA |
| Potassium Peroxodisulfate | Merck |
| Propidium Iodide | Sigma |
| Protein Assay Kit | Bio-Rad Laboratories |
| Proteinase K | Sigma |
| RNAse A | Sigma |
| Sodium Chloride | Sigma |
| Sodium Hydroxide | Sigma |
| Sodium Iodide | Sigma |
| Sodium Pyruvate | C-C Pro GmbH |
| Sucrose | Sigma |
| SYBR Green I Nucleic Acid Stain | Fluka |
| Titanium Dioxide | Degussa GmbH. Germany |
| Tris – HCl | Merck |
| Triton X | Merck |
| Trypan Blue | Fluka |
| Trypsin – EDTA | C-C Pro GmbH |
| Trypsin Neutralizing Solution | Promo Cell GmbH |

## Appendix 3

**Table** List of instruments used

| | |
|---|---|
| $CO_2$ Incubator | Forma Scientific |
| Platform Model | TSI Inc. (Model No: 3080) |
| Scanning Mobility Particle Sizer | TSI Inc. (Model: 3936) |
| Differential Mobility Analyzer | TSI Inc. (Model: 3081) |
| Condensation Particle Sizer | TSI Inc. (Model: 3786) |
| Aerodynamic Particle Sizer | TSI Inc. (Model: 3321) |
| Scanning Electron Microscope | LEO 1530 Gemini instrument. |
| HPLC Column | Hamilton (Model: PRP-X-100) |
| ICP-MS | Agilent Technologies. Germany (Model : Agilent 7500a) |
| MilliQ Elix & RiOs System | Millipore |
| Unicam UV/Vis Spectrometer | ATI Unicam |
| Ultracut UCT cryotome | Leica Microsystem. Germany |
| Cryotrim 45º Diamond Knife | Diatome. Hatield. USA |
| Transmission Electron Microscope | Zeiss (Model: EM10) |
| Leica Fluorescence Microscope | Leica (Model: DMLS) |
| Comet Assay IV software | Perspective Instruments |
| Incubator with the Greiner/ Falcon tube part inserted | Biometra |
| EPR spectrometer | Magnettech. Germany (Model: Miniscope MS 100) |
| FACS Calibur | Becton Dickinson |

## Appendix 4

### 1. Determination of Fe (III) concentration in the particles

- **Stock Solutions –**
  - **Iron Standard Stock Solution–**20 mg of $FeCl_3.6H_2O$ in 1 l of MilliQ $H_2O$.
  - **Iron Standard Solutions –**

| Standards (mg/ml) | Stock Solution (ml) | MilliQ $H_2O$ (ml) |
|---|---|---|
| 1 | 5 | 95 |
| 2 | 10 | 90 |
| 3 | 15 | 85 |
| 4 | 20 | 80 |
| 5 | 25 | 75 |

  - **Potassium Peroxodisulphate –**4 g in 100 ml MilliQ $H_2O$.
  - **Ammonium Acetate -** 40 g in 50 ml of Glacial Acetic Acid and final volume adjusted to 100 ml with MilliQ $H_2O$.
  - **1.10 Phenanthroline Chloride -** 0.5 g in 100 ml of MilliQ $H_2O$.
  - **Hydroxyl Ammonium Chloride –** 10 g in 100 ml of MilliQ $H_2O$.
  - **Aqua Regia -**65% $HNO_3$ and 25% HCl.

### 2. Transmission Electron Microscopy for studying the uptake of the particles

- **4% Paraformaldehyde –** 4 ml of Paraformaldehyde in 100 ml of MilliQ $H_2O_2$.
- **0.1% Glutaraldehyde –** 100 µl of Glutaraldehyde in 100 ml of MilliQ $H_2O_2$.
- **0.1M PHEM buffer –** 60 mM piperazine-N-bis (2-ethanesulfonic acid), 20 mM HEPES, 2 mM $MgCl_2$, 10 mM ethylene glycol tetra-acetic acid.

### 3. Genotoxicity test (Comet assay)

- **1M EDTA solution (pH10) –** 37.2 g EDTA dissolved in 1 l aqua bidest.
- **1M EDTA solution (pH 8) –** 37.2 g EDTA dissolved in 1 l aqua bidest.

- **1 M NaOH solution** - 40 g NaOH dissolved in 1 l aqua bidest.
- **1M Tris solution** - 157.6 g Tris.HCl dissolved in 1 l aqua bidest.
- **1 lt Electrophoresis solution (pH 12.7) -** Mix 300 ml NaOH (1M), 1 ml of 1M EDTA (pH10) and 1M Tris.HCl. Make the final volume 1 l.
- **Lysis solution -**
    - Solution A – Mix 10 ml of 1M Tris.HCl, 146.1 g of NaCl, 100 ml 1M EDTA (pH10), 10 g of N-Laurysarcosine and make up the final volume to 890 ml.
    - Solution B – Mix 100 ml DMSO with 10 ml of Triton X.
    - ***For final Solution - mix A and B prior to use: 11 ml A and 89 ml B.***
- **Neutralisation solution (pH 7.5)** - 400 ml of 1M Tris.HCl.
- **SYBR-Green nuclei staining solution -** SYBR-Green in TAE buffer $1:10^4$
- **50x TAE buffer –** Mix 242 g of Tris.HCl with 57.1 ml of Glacial Acetic Acid.

**3. <u>Acellular / Cellular Reactive Oxygen Species Measurement (Electron Paramagnetic Resonance)</u>**

- **Preparation of (DMPO) dye:**

**Materials required-**

- Freshly prepared AAS water.
- Incubator with the Greiner/ Falcon tube part inserted and prewarmed at 35ºC.
- 15ml Falcon tube wrapped in aluminium foil.

**Procedure –**

Frozen DMPO is thawed (approx. 1 h) and transferred to an aluminium foil-covered 15ml tube. 7.5 ml of AAS water is added to it (final volume). Two hundred and twenty five mg of active coal (Merck) is added to this DMPO solution and it is incubated for 20 min at 35ºC in the incubator with a special rotating attachment for the Falcon tube. The whole solution is then centrifuged for 10 min at 3000 rpm (RT) and the supernatant is filtered through a 0.2 µm syringe filter and transfer to a fresh Falcon tube.

To measure the concentrations of DMPO take 3 readings at 234 nm absorbance after diluting the DMPO solution 10.000x (prepare 2 eppendorf tubes with 990µl AAS. transfer 10 µl DMPO solution into the first one, vortex, then transfer 10 µl from the diluted DMPO solution into the second eppendorf tubes), vortex. To calculate the molarity of DMPO use the formula

$$\text{Molarity} = \frac{\text{Absorption at 234nm}}{7700} \times 10.000$$

Values between 0.95 and 1.05 M are acceptable; if the concentration is too high it has been adjusted using AAS water. Aliquots of the prepared DMPO are frozen in eppendorf tubes at -20ºC.

- **Preparation of Hypotonic Solution:**

Mix 10 mM HEPES (pH 7.5), 5 mM KCl, 1.5 mM $MgCl_2$, 0.2 mM PMSF and 0.5 mM DTT.

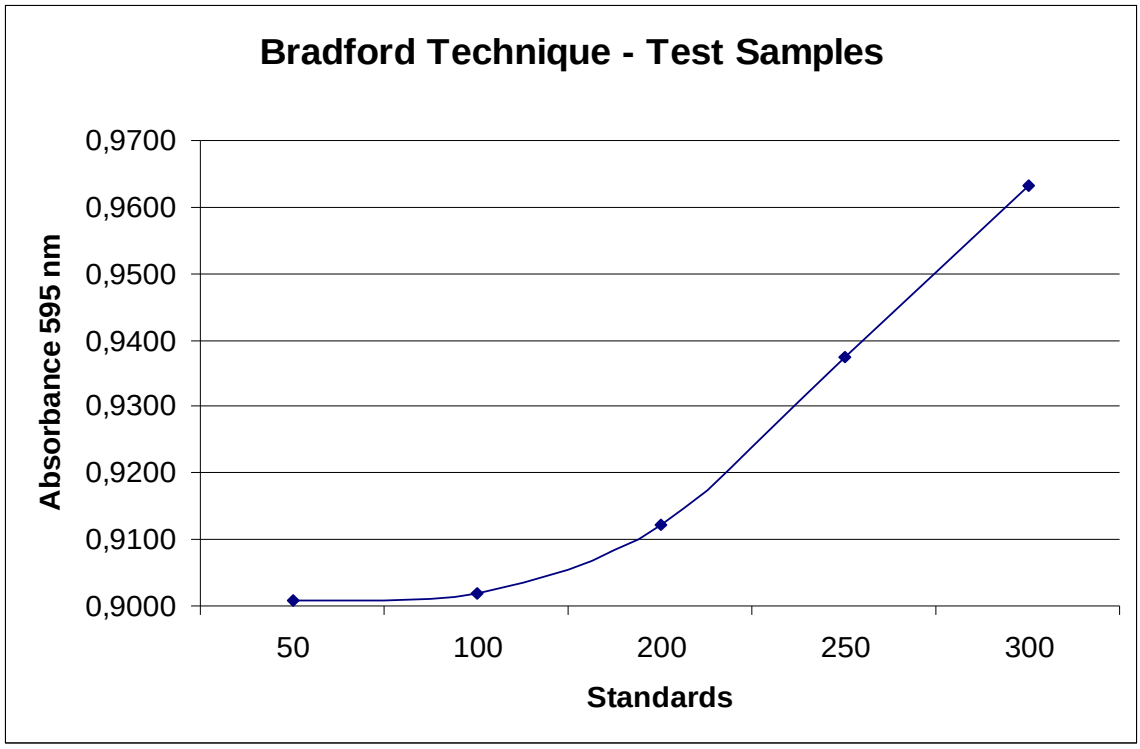


**Figure 46 –** Bradford analysis for protein estimation in whole cell lysate.

**4. Cellular Reactive Oxygen Species Measurement (2', 7' Dihydrodichlorofluoresceine diacetate)**

- **Stock Solution -** Measure 1.2 mg of $H_2$DCFDA powder and dissolve in 25 µl of DMSO and make the final volume of this to 25 ml (100µM concentration of $H_2$DCFDA).

- **Working Solution -** Take 100 µl in 1 ml of PBS / HBSS (10 µM concentration).

## 5. 8-Hydroxy-2-deoxyguanosine (8-OHdG) Detection

- **Cell Lysis Solution –** Mix 1% Triton X, 0.32 M Sucrose, 5 mM $MgCl_2$, 10 mM Tris- HCl (pH 7.5).
- **Enzyme Reaction Buffer –** Mix 1% SDS, 5 mM EDTA-$Na_2$, 10 mM Tris HCl (pH 7.5).
- **RNAse A (Stock Solution) –** Dissolve 20 µg/ml.
- **Proteinase K –** Dissolve 17 mg/ml.
- **Sodium Iodide Solution –** Mix 7.6 M Sodium Iodide, 20 mM EDTA-$Na_2$ and 40 mM Tris-HCl.
- **Tris - EDTA Buffer –** Mix 10 mM Tris HCl (pH 7.5), 1 mM EDTA and make the final volume 1 l with MilliQ $H_2O$.

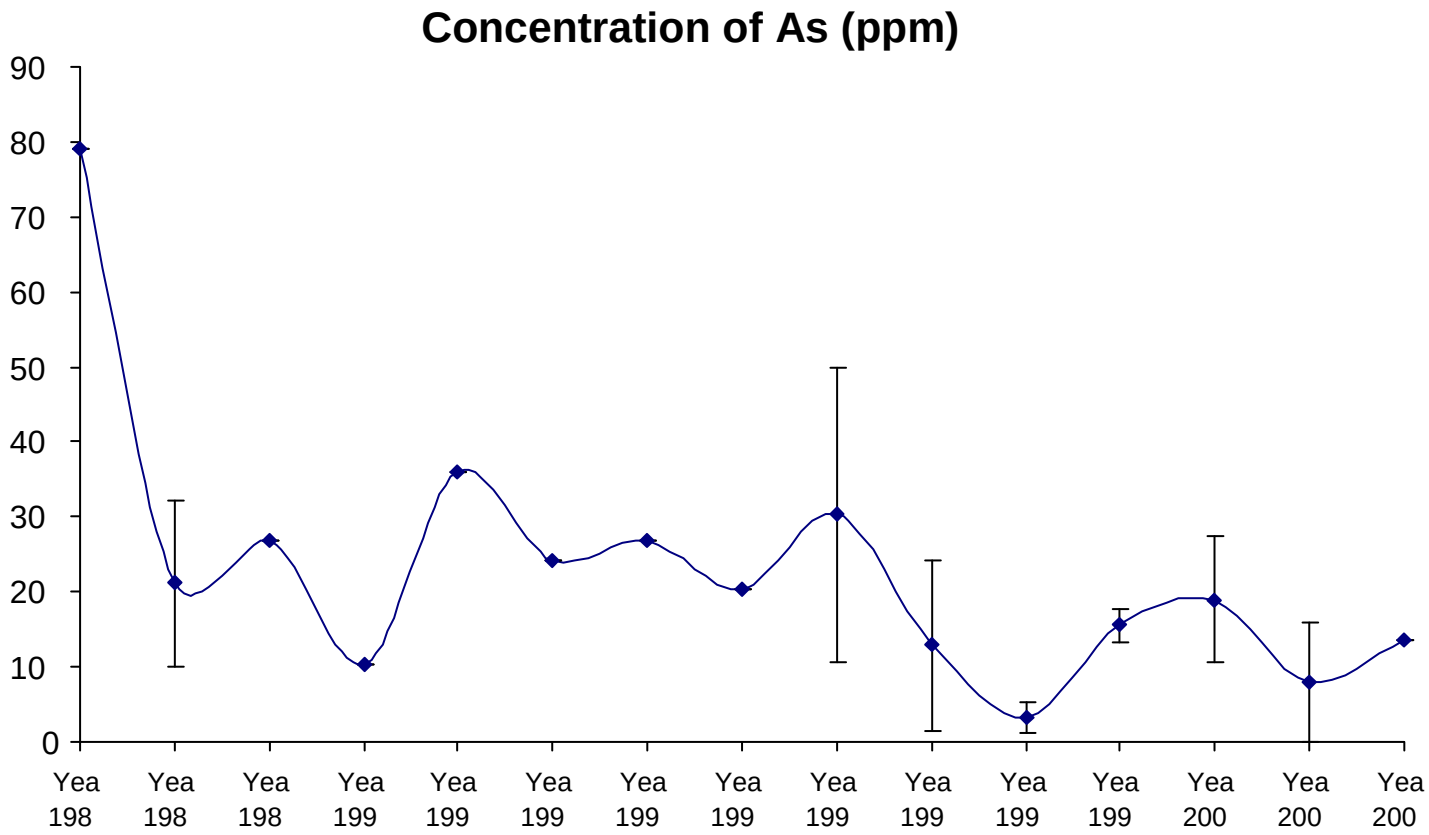


**Figure 47 –** Year wise analysis of $As_2O_3$ content in the arsenopyrite ash particle samples using atomic absorption spectrometry

## Appendix 6

**Table 1:** Cytotoxicity analysis in IMR-90 cells using Trypan blue assay

| IMR-90 cells | | | |
|---|---|---|---|
| **Hematite (Fine particles)** | **24 h** | **48 h** | **72 h** |
| **Control** | 92 | 81 ± 2.1 | 81 ±1.4 |
| **2 µg/cm$^2$** | 73 ± 5.4 | 70 ± 9.19 | - |
| **5 µg/cm$^2$** | 68 ± 8.9 | 64 ± 7.2 | - |
| **10 µg/cm$^2$** | 70 ± 3.5 | 73 ± 3.5 | 50 |
| **50 µg/cm$^2$** | 69 ± 1 | 55 | 53 |
| | | | |
| **Hematite (Nanoparticles)** | **24 h** | **48 h** | **72 h** |
| **Control** | 92 | 81 ± 2.1 | 81 ±1.4 |
| **2 µg/cm$^2$** | 82 ± 3.4 | 76 ± 14.7 | - |
| **5 µg/cm$^2$** | 74 ± 1.1 | 64 ± 13.3 | - |
| **10 µg/cm$^2$** | 60 ± 1.4 | 75 ± 2.8 | 58 ± 4.2 |
| **50 µg/cm$^2$** | 40 | 75 ± 3.8 | 44 |
| | | | |
| **Titanium dioxide (Nanoparticles)** | **24 h** | **48 h** | **72 h** |
| **Control** | 96 | 97 ± 2.3 | 92 ± 2.4 |
| **2 µg/cm$^2$** | 90 ±5.9 | 94 ± 4.1 | 91 ± 1.8 |
| **5 µg/cm$^2$** | 87 | 94 ± 2.5 | 76 ± 9.7 |
| **10 µg/cm$^2$** | 82 ± 6.4 | 88 | 57 ± 6.4 |
| **50 µg/cm$^2$** | 58 ± 3 | 89 ± 1 | 33 |
| | | | |
| **DQ12 (Fine particles)** | **24 h** | **48 h** | **72 h** |
| **Control** | 92 | 81 ± 2.1 | 81 ±1.4 |
| **2 µg/cm$^2$** | 69 ± 2.3 | 69 ± 2.1 | - |
| **5 µg/cm$^2$** | 74 ± 10.1 | 78 ± 9 | - |
| **10 µg/cm$^2$** | 83 ± 2.3 | 51 ± 0.2 | 57 ± 1.6 |
| **50 µg/cm$^2$** | 83 ± 2.6 | 54 ± 1.8 | 35 ± 2.5 |
| | | | |
| **Arsenopyrite ash particles** | **24 h** | **48 h** | **72 h** |
| **Control** | 92 | 81 ± 2.1 | 81 ±1.4 |
| **2 µg/cm$^2$** | 74 ± 5.1 | 69 ± 5.4 | - |
| **5 µg/cm$^2$** | 80 ± 6.4 | 68 ± 7.9 | - |
| **10 µg/cm$^2$** | 69 ± 2 | 68 ± 1 | 57 |
| **50 µg/cm$^2$** | 70 | 51 ± 0.3 | 46 ± 1.9 |

**Table 2:** Cytotoxicity analysis in BEAS-2B cells using Trypan blue assay

| BEAS-2B cells | | | |
|---|---|---|---|
| **Hematite (Fine particles)** | **24 h** | **48 h** | **72 h** |
| **Control** | 93 ± 1 | 86 ± 2.4 | 79 ± 1.4 |
| **2 µg/cm$^2$** | 84 ± 3.7 | 74 ± 17.7 | - |
| **5 µg/cm$^2$** | 83 ± 10 | 67 ± 9.6 | - |
| **10 µg/cm$^2$** | 72 | 57 ± 5.3 | 69 ± 2.1 |
| **50 µg/cm$^2$** | 71 ± 2 | 51 ± 5.7 | 63 ± 17.3 |
| | | | |
| **Hematite (Nanoparticles)** | **24 h** | **48 h** | **72 h** |
| **Control** | 92 ± 1 | 86 ± 2 | 79 |
| **2 µg/cm$^2$** | 90 | 67± 2 | - |
| **5 µg/cm²** | 88 | 75 | - |
| **10 µg/cm²** | 81 ± 2 | 77 ± 5 | 68 ± 3 |
| **50 µg/cm²** | 63 ± 3 | 66 | 63 ± 3.9 |
| | | | |
| **Titanium dioxide (Nanoparticles)** | **24 h** | **48 h** | **72 h** |
| **Control** | 97 | 99 | 99 ± 0.2 |
| **2 µg/cm²** | 96 | 98 | 93 ± 7.4 |
| **5 µg/cm²** | 97 ± 2 | 97 ± 1.2 | 98 |
| **10 µg/cm²** | 96 | 94 ± 3.6 | 98 |
| **50 µg/cm²** | 89 ± 4 | 91 ± 4.2 | 95 ± 1.6 |
| | | | |
| **DQ12 (Fine particles)** | **24 h** | **48 h** | **72 h** |
| **Control** | 92.7 ± 1 | 86 ± 2.5 | 79 ± 1.4 |
| **2 µg/cm²** | 72.8 ± 11 | 77 ± 4.5 | - |
| **5 µg/cm²** | 62.8 ± 6 | 7 ± 5.5 | - |
| **10 µg/cm²** | 79.00 ± 11 | 62 ± 5.7 | 65 ± 2.8 |
| **50 µg/cm²** | 68.75 | 60 ± 7.4 | 43 |
| | | | |
| **Arsenopyrite ash particles** | **24 h** | **48 h** | **72 h** |
| **Control** | 93 ± 1 | 86 ± 2.5 | 79 ± 1.4 |
| **2 µg/cm²** | 77 ± 5 | 67.9 ± 33 | - |
| **5 µg/cm²** | 65 ± 2.1 | 68 ± 8 | - |
| **10 µg/cm²** | 75 ± 4.9 | 65 ± 1.7 | 61 |
| **50 µg/cm²** | 51 | 50 ± 5 | 51 ± 5.7 |

**Table 1:** Olive tail moment being produced by the IMR-90 cells after exposure to different particles and analyzed by comet assay

| IMR -90 cells | Control | 2 µg/cm² | 5 µg/cm² | 10 µg/cm² | 5 0 µg/cm² |
|---|---|---|---|---|---|
| **Hematite fine particle** | | | | | |
| **24 h** | 1.1 | 1.6 ±0.4 | 2.2 ± 0.7 | 7.59 ± 0.28 | 6.58 ± 0.11 |
| **48 h** | 1.2 | 0.8 | 0.64 ± 0.08 | 0.95 ± 0.05 | 0.92 ± 0.04 |
| **72 h** | 1 | 3.8 ± 0.2 | 3.36 ± 0.10 | 2.38 ± 0.07 | 2.81 ± 0.24 |
| | | | | | |
| **Hematite nanoparticle** | | | | | |
| **24 h** | 1.12 | 3.14 ± 0.17 | 2.25 ± 0.58 | 12.21 ± 0.12 | 9.43 ± 0 .8 |
| **48 h** | 1.17 | 1.01 ± 0.01 | 1.19 ± 0.01 | 1.38 ± 0.07 | 1.42 ± 0.3 |
| **72 h** | 1.08 | 1.4 ± 0.02 | 1.0 ± 0.02 | 1.54 ± 0.01 | 0.72 ± 0.16 |
| | | | | | |
| **Titanium dioxide nanoparticle** | | | | | |
| **24 h** | 1.1 | 0.22 ± 0.06 | 0.26 ± 0.03 | 0.36 ± 0.15 | 0.23 ± 0.0 1 |
| **48 h** | 0.12 | 0.07 ± 0.01 | 0.12 ± 0.02 | 0.10 | 0.119 |
| **72 h** | 0.10 | 0.11 ± 0.04 | 0.15 ± 0.01 | 0.17 ± 0.02 | 0.26 ± 0.0 1 |
| | | | | | |
| **DQ12** | | | | | |
| **24 h** | 1.12 | 1.46 ± 0.4 | 1.44 ± 0.3 | 6.3 ± 0.1 | 5.43 ± 1.2 |
| **48 h** | 1.17 | 0.87 | 1.04 ± 0.1 | 1.01 ± 0.1 | 0.94 |
| **72 h** | 1.08 | 1.19 | 1.21 ± 0.1 | 1.04 ± 0.1 | 0.59 ± 0.1 |
| | | | | | |
| **Arsenopyrite ash** | | | | | |
| **24 h** | 1.12 | 2.49 ± 0.1 | 1.86 ± 0.3 | 2.16 ± 0.1 | 1.88 |
| **48 h** | 1.17 | 0.33 | 0.44 ± 0.1 | 0.77 ± 0.1 | 0.65 |
| **72 h** | 1.08 | 0.92 | 1.0 ± 0.2 | 1.41 ± 0.1 | 0.17 |

**Table2:** Olive tail moment being produced by the BEAS-2B cells after exposure to different particles and analyzed by comet assay

| BEAS-2B cells | Control | 2 µg/cm² | 5 µg/cm² | 10 µg/cm² | 50 µg/cm² |
|---|---|---|---|---|---|
| **Hematite fine particle** | | | | | |
| **24 h** | 0.06 | 0.85 ± 0.3 | 0.67 ± 0.1 | 1.13 ± 0.7 | 0.18 ± 0.1 |
| **48 h** | 0.23 | 0.25 | 0.25 | 0.29 | 0.30 |
| **72 h** | 0.27 ± 0.1 | 0.48 ± 0.2 | 0.22 | 0.22 ± 0.1 | 0.21 ± 0.1 |
| | | | | | |
| **Hematite nanoparticle** | | | | | |
| **24 h** | 0.06 | 0.13 ± 0.1 | 0.04 | 0.07 | 1.16 ± 0.8 |
| **48 h** | 0.23 | 0.27 ± 0.1 | 0.22 | 0.39 ± 0.1 | 0.40 ± 0.1 |
| **72 h** | 0.27 ± 0.1 | 0.31 | 0.34 ± 0.1 | 0.40 | 0.51 ± 0.5 |
| | | | | | |
| **Titanium dioxide nanoparticle** | | | | | |
| **24 h** | 0.11 | 0.1 | 0.1 | 0.09 | 0.11 |
| **48 h** | 0.14 ± 0.081 | 0.09 | 0.16 | 0.1 | 0.14 ± 0.1 |
| **72 h** | 0.12 | 0.21 ± 0.1 | 0.14 | 0.12 | 0.12 |
| | | | | | |
| **DQ12** | | | | | |
| **24 h** | 0.06 | 0.17 ± 0.1 | 0.15 | 0.16 | 0.24 ± 0.1 |
| **48 h** | 0.23 | 0.19 | 0.20 | 0.21 ± 0.1 | 1.19 ± 0.5 |
| **72 h** | 0.27 ± 0.1 | 0.35 ± 0.3 | 0.30 | 0.33 ± 0.1 | 0.69 ± 0.3 |
| | | | | | |
| **Arsenopyrite ash** | | | | | |
| **24 h** | 0.06 | 0.05 | 0.1 | 0.03 | 0.1 |
| **48 h** | 0.23 | 0.29 | 0.32 | 0.27 | 0.32 ± 0.1 |
| **72 h** | 0.27 ± 0.1 | 0.22 ± 0.3 | 0.31 | 0.33 | 0.38 ± 0.3 |

## Appendix 8

**Table 1:** Acellular ROS production by the particles after treatment with $H_2O_2$ and spin trap – DMPO

| | Mean | SD |
|---|---|---|
| **Blank** | 0 | 0 |
| **$TiO_2$ (Nanoparticles) <100nm** | 747 | 10 |
| **DQ12 (Fine) <5µm** | 3327 | 347 |
| **Hematite (Fine) <5µm** | 2800 | 448 |
| **Hematite (Nanoparticles) <100nm** | 252 | 0 |
| **Arsenopyrite ash particles** | 8398 | 1203 |

**Table 2:** Acellular ROS measurement with electron paramagnetic resonance (EPR) after treatment of particles with ascorbic acid and $H_2O_2$ treatment

| Exposure Time | | 2 h | 4 h | 6 h |
|---|---|---|---|---|
| **Blank** | | 0 | 0 | 0 |
| **Hematite (Fine particles)** | **10 µg/cm$^2$** | 1067 | 2080 ± 280 | 487 ± 689 |
| | **50 µg/cm$^2$** | 4040 ± 1085 | 1663 ± 1020 | 601 ± 849 |
| **Hematite (Nanoparticles)** | **10 µg/cm$^2$** | 11049 | 20242 ± 4398 | 19053 ± 908 |
| | **50 µg/cm$^2$** | 1040 | 525 ± 536 | 4420 ± 685 |
| **$TiO_2$ (Nanoparticles)** | **10 µg/cm$^2$** | 919 ± 333 | 400 ± 486 | 649 ± 186 |
| | **50 µg/cm$^2$** | 891 | 524 ± 606 | 840 ± 261 |
| **DQ12 (Fine particles)** | **10 µg/cm$^2$** | 26 ± 37 | 559 ± 512 | 965 ± 713 |
| | **50 µg/cm$^2$** | 3593 ± 1155 | 3258 ± 908 | 3575 ± 1809 |
| **Arsenopyrite ash particles** | **10 µg/cm$^2$** | 11878 ± 1676 | 9627 ± 1076 | 14877 ± 1270 |
| | **50 µg/cm$^2$** | 19063 ± 823 | 16650 ± 1031 | 21138 ± 1384 |

**Table 3:** Acellular ROS measurement with electron paramagnetic resonance (EPR) after treatment of particles with cell lysate and $H_2O_2$ treatment

| Exposure Time | | 2 h | 4 h | 6 h |
|---|---|---|---|---|
| **Blank** | | 0 | 0 | 0 |
| **Hematite (Fine particles)** | **10 µg/cm$^2$** | 123 ± 174 | 570 ± 547 | 136 ± 70 |
| | **50 µg/cm$^2$** | 231 | 251 ± 55 | 300 ± 239 |
| **Hematite (Nanoparticles)** | **10 µg/cm$^2$** | 0 | 4581 ± 532 | 4190 |
| | **50 µg/cm$^2$** | 11985 ± 4301 | 3584 ± 2763 | 8417 ± 2016 |
| **$TiO_2$ (Nanoparticles)** | **10 µg/cm$^2$** | 954 ± 120 | 751 | 602 ± 133 |
| | **50 µg/cm$^2$** | 1017 | 913 | 524 ± 59 |
| **DQ12 (Fine particles)** | **10 µg/cm$^2$** | 111 ± 68 | 71 ± 3 | 56 ± 71 |
| | **50 µg/cm$^2$** | 0 | 206 ± 15 | 419 |
| **Arsenopyrite ash particles** | **10 µg/cm$^2$** | 1648 | 1685 ± 187 | 873 ± 231 |
| | **50 µg/cm$^2$** | 4728 ± 1119 | 2994 ± 136 | 3321 ± 227 |

**Table1:** Intracellular ROS measurement with $H_2$DCFDA dye, after treatment with particle only and particle with desferoxamine (Iron chelator) treatment

| **Hematite Nanoparticle exposure to the BEAS-2B cells** | | | | | | **Particle and desferoxamine treatment to the BEAS-2B cells** | | |
|---|---|---|---|---|---|---|---|---|
| **Time** | 1 h | 6 h | 12 h | 24 h | 48 h | 12 h | 24 h | 48 h |
| **Control** | 15582 ± 1955 | 16545 | 16845 ± 2836 | 13460 ± 1130 | 15235 ± 984 | 18137 ± 1278 | 14545 ± 1757 | 16626 ± 1611 |
| **Desferoxamine Control** | 0 | 0 | 0 | 0 | 0 | 20534 ± 3953 | 16174 ± 590 | 12496 ± 500 |
| **2 µg/cm²** | 15790 ± 493 | 12719 | 0 | 0 | 0 | 0 | 0 | 0 |
| **5 µg/cm²** | 10643 | 9161 | 22718 ± 1576 | 25968 ± 153 | 25873 ± 128 | 18065 | 29522 ± 3614 | 30492 ± 3859 |
| **10 µg/cm²** | 8480 | 8148 | 24760 ± 621 | 22376 ± 2677 | 25025 ± 3719 | 21239 ± 2555 | 32223 ± 3295 | 32184 ± 2410 |
| **50 µg/cm²** | 6832 | 7480 | 23439 | 11216 ± 5642 | 22690 ± 9818 | 30826 ± 2055 | 33805 ± 1262 | 36363 ± 308 |

**Table 2:** Intracellular ROS measurement with $H_2$DCFDA dye, after treatment with particle only and particle with desferoxamine (Iron chelator) treatment

| Titanium dioxide nanoparticle exposure to the BEAS-2B cells | | | | | | Particle and desferoxamine treatment to the BEAS-2B cells | | |
|---|---|---|---|---|---|---|---|---|
| **Time** | 1 h | 6 h | 12 h | 24 h | 48 h | 12 h | 24 h | 48 h |
| **Control** | 18554 ± 1933 | 12907 ± 9069 | 8820 ± 4180 | 6360 ± 4718 | 5934 ± 808 | 18137 ± 1278 | 14545 ± 1757 | 16626 ± 1611 |
| **Desferoxamine Control** | 0 | 0 | 0 | 0 | 0 | 20534 ± 3953 | 16174 ± 590 | 12496 ± 500 |
| **2 µg/cm²** | 23629 ± 489 | 15663 ± 6594 | 10781 ± 5678 | 5255 ± 4073 | 7170 ± 242 | 0 | 0 | 0 |
| **5 µg/cm²** | 32598 ± 1728 | 17451 ± 9084 | 13407 ± 1046 | 11418 ± 3754 | 8828 ± 909 | 4440 ± 509 | 2799 ± 820 | 3775 ± 510 |
| **10 µg/cm²** | 37143 ± 1337 | 25809 ± 6775 | 20462 ± 992 | 22852 ± 1092 | 13519 ± 745 | 13032 ± 1617 | 5372 ± 1197 | 7933 ± 1724 |
| **50 µg/cm²** | 40390 ± 497 | 39672 ± 6261 | 32411 ± 5161 | 41147 ± 789 | 35401 ± 3594 | 24723 ± 1319 | 30761 ± 1319 | 31301 ± 5006 |

**Table 3:** Intracellular ROS measurement with $H_2$DCFDA dye, after treatment with particles only and particles with desferoxamine (Iron chelator) treatment

| **Hematite fine particle exposure to the BEAS-2B cells** | | | | | | **Particle and desferoxamine treatment to the BEAS-2B cells** | | |
|---|---|---|---|---|---|---|---|---|
| **Time** | 1 h | 6 h | 12 h | 24 h | 48 h | 12 h | 24 h | 48 h |
| **Control** | 15582 ± 1955 | 16545 ± 1205 | 16845 ± 2836 | 13460 ± 1130 | 15235 ± 984 | 18137 ± 1278 | 14545 ± 1757 | 16626 ± 1611 |
| **Desferoxamine Control** | 0 | 0 | 0 | 0 | 0 | 20534 ± 3953 | 16174 ± 590 | 12496 ± 500 |
| **2 µg/cm²** | 30079 ± 2184 | 34825 ± 128 | 0 | 0 | 0 | 0 | 0 | 0 |
| **5 µg/cm²** | 35075 ± 2363 | 38717 ± 3220 | 33650 ± 3652 | 27052 ± 2700 | 26455 ± 3387 | 19991 ± 1117 | 25537 ± 3061 | 21108 ± 405 |
| **10 µg/cm²** | 35631 ± 4074 | 35934 ± 2383 | 41021 ± 2765 | 16544 ± 1738 | 25112 ± 8089 | 26717 ± 216 | 32506 ± 1271 | 27826 ± 2073 |
| **50 µg/cm²** | 34539 ± 3922 | 34621 ± 2979 | 20478 ± 1503 | 24381 ± 4432 | 16451 ± 2769 | 27896 ± 4881 | 31714 ± 1838 | 25085 ± 5061 |

**Table 4:** Intracellular ROS measurement with $H_2$DCFDA dye, after treatment with particles only and particles with desferoxamine (Iron chelator) treatment

| Quartz (DQ12) particle exposure to the BEAS-2B cells | | | | | | Particle and desferoxamine treatment to the BEAS-2B cells | | |
|---|---|---|---|---|---|---|---|---|
| **Time** | 1 h | 6 h | 12 h | 24 h | 48 h | 12 h | 24 h | 48 h |
| **Control** | 15582 ± 1955 | 16545 ± 1205 | 16845 ± 2836 | 13460 ± 1130 | 15235 ± 984 | 18137 ± 1278 | 14545 ± 1759 | 16626 ± 1611 |
| **Desferoxamine Control** | 0 | 0 | 0 | 0 | 0 | 20534 ± 3953 | 16174 | 12496 ± 500 |
| **2 µg/cm²** | 26085 ± 1980 | 25146 ± 5190 | 0 | 0 | 0 | 0 | 0 | 0 |
| **5 µg/cm²** | 28090 ± 246 | 32070 ± 4470 | 26908 ± 10140 | 28211 ± 1100 | 28290 ± 5911 | 11541 ± 856 | 15620 ± 4005 | 14449 ± 728 |
| **10 µg/cm²** | 28612 ± 578 | 26230 ± 6739 | 37290 ± 72282 | 26433 ± 2031 | 32514 ± 5544 | 21482 ± 1282 | 23873 ± 2650 | 20551 ± 3802 |
| **50 µg/cm²** | 17334 ± 589 | 20363 ± 4584 | 35943 ± 4033 | 27999 ± 404 | 33150 ± 62233 | 27850 ± 1100 | 21772 | 13662 |

**Table 5:** Intracellular ROS measurement with $H_2$DCFDA dye, after treatment with particles only and particles with desferoxamine (Iron chelator) treatment

| **Arsenopyrite ash particle exposure to the BEAS-2B cells** | | | | | | **Particle and desferoxamine treatment to the BEAS-2B cells** | | |
|---|---|---|---|---|---|---|---|---|
| **Time** | 1 h | 6 h | 12 h | 24 h | 48 h | 12 h | 24 h | 48 h |
| **Control** | 15580 ± 1955 | 16545 ± 1205 | 16845 ± 2836 | 13460 ± 1130 | 15235 ± 984 | 18137 ± 1278 | 14545 ± 1757 | 16626 ± 1611 |
| **Desferoxamine Control** | 0 | 0 | 0 | 0 | 0 | 20534 ± 3953 | 16174 ± 590 | 12496 ± 500 |
| **2 µg/cm²** | 19884 ± 209 | 17567 ± 1073 | 32150 ± 2689 | 32150 ± 5912 | 30580 ± 1800 | 25968 ± 443 | 25968 ± 743 | 16928 ± 130 |
| **5 µg/cm²** | 21109 ± 930 | 23036 ± 4168 | 27995 ± 2546 | 27995 ± 3734 | 26621 ± 429 | 31021 ± 1099 | 31021 ± 343 | 22795 ± 1307 |
| **10 µg/cm²** | 23093 ± 3745 | 25821 ± 1067 | 25447 ± 1681 | 25447 ± 4216 | 24290 ± 1218 | 32557 ± 4870 | 32557 ± 1394 | 26617 ± 2626 |
| **50 µg/cm²** | 21554 ± 1527 | 24011 ± 3752 | 18165 ± 2789 | 18165 ± 2217 | 18639 ± 4318 | 32999 ± 142 | 32999 ± 1222 | 25325 ± 3991 |

## Appendix 10

**Table 1:**. The table provides location of a specific gene in the 3D profile graphs (Figure 39, 40 and 41) showing the fold difference in expression of each gene between the particles and negative control in the 96-well format of the PCR array.

| Gene Symbol | Location on graph | Gene Symbol | Location on graph | Gene Symbol | Location on graph | Gene Symbol | Location on graph |
|---|---|---|---|---|---|---|---|
| ABL1 | A01 | GADD45A | C01 | NTHL1 | E01 | SMC1A | G01 |
| ANKRD17 | A02 | GADD45G | C02 | OGG1 | E02 | SUMO1 | G02 |
| APEX1 | A03 | GML | C03 | PCBP4 | E03 | TP53 | G03 |
| ATM | A04 | GTF2H1 | C04 | PCNA | E04 | TP73 | G04 |
| ATR | A05 | GTF2H2 | C05 | AIFM1 | E05 | TREX1 | G05 |
| ATRX | A06 | GTSE1 | C06 | PMS1 | E06 | UNG | G06 |
| BRCA1 | A07 | HUS1 | C07 | PMS2 | E07 | XPA | G07 |
| BTG2 | A08 | IGHMBP2 | C08 | PMS2L3 | E08 | XPC | G08 |
| CCNH | A09 | IHPK3 | C09 | PNKP | E09 | XRCC1 | G09 |
| CDK7 | A10 | XRCC6BP1 | C10 | PPP1R15A | E10 | XRCC2 | G10 |
| CHEK1 | A11 | LIG1 | C11 | PRKDC | E11 | XRCC3 | G11 |
| CHEK2 | A12 | MAP2K6 | C12 | RAD1 | E12 | ZAK | G12 |
| CIB1 | B01 | MAPK12 | D01 | RAD17 | F01 | | |
| CIDEA | B02 | MBD4 | D02 | RAD18 | F02 | | |
| CRY1 | B03 | MLH1 | D03 | RAD21 | F03 | | |
| DDB1 | B04 | MLH3 | D04 | RAD50 | F04 | | |
| DDIT3 | B05 | MNAT1 | D05 | RAD51 | F05 | | |
| DMC1 | B06 | MPG | D06 | RAD51L1 | F06 | | |
| ERCC1 | B07 | MRE11A | D07 | RAD9A | F07 | | |
| ERCC2 | B08 | MSH2 | D08 | RBBP8 | F08 | | |
| EXO1 | B09 | MSH3 | D09 | REV1 | F09 | | |
| FANCG | B10 | MUTYH | D10 | RPA1 | F10 | | |
| FEN1 | B11 | N4BP2 | D11 | SEMA4A | F11 | | |
| XRCC6 | B12 | NBN | D12 | SESN1 | F12 | | |

## Personal Data:

| | |
|---|---|
| Name: | **Bhattacharya, Kunal** |
| Date of Birth: | 02.04.1977 |
| Place of Birth | Lucknow (India) |
| Family Status | Single |
| Nationality | Indian |
| Passport number | F0616108 |

## Academic Career:

| | |
|---|---|
| February, 2005 – March, 2008 | ***Ph.D. in Particle Inhalation Toxicology entitled*** **"Comparative analysis of fine and nanoparticles for cellular uptake, oxidative stress and genomic damage in human lung cells"** from Institute of Hygiene and Occupational Medicine, University Hospital Essen, Essen, Germany. |
| 1998 - 2000 | ***Master of Science*** in ***Life Sciences*** from University of Lucknow, Lucknow, India. |
| 1995 - 1998 | ***Bachelor of Science*** in ***Life Sciences*** from University of Lucknow, Lucknow, India |

## Professional Experience:

| | |
|---|---|
| September, 2005 – March, 2008 | **Scientific colleague (Wiss. Mitarbeiter) and PhD Scholar,** Institute of Hygiene and Occupational Medicine, University Hospital Essen, Essen, Germany. |
| March, 2006 - May, 2006 | **Guest Scientist,** Sub-division of Toxicology, Division of Life Sciences, University of Wageningen, The Netherlands. |
| February, 2005 – August, 2005 | **Guest Scientist**, Institute of Hygiene and Occupational Medicine, University Hospital Essen, Essen, Germany. |
| May, 2002 – October, 2004 | **Project Assistant**, Fiber Toxicology Division, Industrial Toxicology Research Centre, Lucknow, India in project "Human Risk Assessment Studies in Asbestos-based Industries in India".<br>- Determination of occupational hazards faced by the asbestos industry workers that might lead to asbestos related lung diseases using *in vitro* and *in vivo* (directly in worker) assays. |
| 2000 | Completion of dissertation "Effects of auto-exhaust and chemical effluents on *Cassia nodosa* and *Vicia faba* and study of mitotic cell - division in *Trigonella foenum – graecum*" as a part of partial fulfillment of M.Sc. |

## Advanced Training:

| | |
|---|---|
| 2000 | 2 weeks training in **Biotechnology** from **National Botanical Research Institute (N.B.R.I.),** Lucknow, India. |
| 2002 | Refresher course on **"Use of Bioinformatics in Biological Research"** jointly conducted by Council of Scientific and Industrial Research (**C.S.I.R.**) and Industrial Toxicology Research Center (**I.T.R.C.**), Lucknow, India. |

## Proficiencies:

| | |
|---|---|
| Languages Known: | **English:** Excellent<br>**Hindi:** Excellent<br>**Bengali:** Mother Language<br>**German:** Beginner |
| Computer knowledge: | **Advanced Diploma in Web Designing** from **UPTEC**, Lucknow, India |

## Techniques Known:

- Cell culture of different mammalian cell lines and in vitro and vivo culture of blood lymphocytes.
- Genotoxicity analysis using micronuclei, chromosomal aberration, kinetochore staining and alkaline comet assay techniques.
- SNP/ point mutation analysis techniques using MALDI-TOF.
- Non-invasive inflammation analysis technique (Nasal lavage in humans and bronchiolar lavage analyis in rats) and differential cell counting and cytokine analysis via ELISA (DAS).
- Polarized and phase contrast microscopy.

## Extra Curricular Activity:

Former active member of nature club **National Environmental Society,** University of Lucknow, India (a registered branch of Nature Club of India, the youth movement of **World Wide Fund for Nature – India.**)

## Publications:

- **Bhattacharya, K.**; Yadava, S.; Schiffman, D.; Rahman, Q.; **Reduction of asbestos induced genotoxicity in human peripheral blood lymphocytes by fresh garlic extract**; Toxicology Letters, 2004 Nov 28; 153(3) : 327-32. PMID: 15454308. Impact Factor - 2.784
- **Bhattacharya, K.**; Dopp E.; Kakkar, P.; Jaffery, F.N.; Schiffmann, D.; Jaurand M.C.; Rahman, I.; Rahman, Q.; **Biomarkers in the risk assessment of asbestos exposure;** Special Edition Mutation Research Fundamental and Molecular Mechanism of Mutagenesis, 2005 Aug17; 579: 6 - 21. PMID: 16112146. (Review) Impact Factor : 4.111
- Dopp. E.; Yadava, S.; Ansari, F.A.; **Bhattacharya, K.**; Recklinghausen, U.V.; Raun, U.; Rödelsperger, K.; Shokouhi, B.; Geh, S.; Rahman, Q.; **ROS-mediated genotoxicity of asbestos-cement in mammalian lungs cells *in vitro*** ; Particle and Fiber Toxicology, 2005 Oct 6; 2(1):9. PMID: 16209709.
- **Bhattacharya, K.**; Alink. G.M.; Dopp. E.; **Oxidative stress and changed gene expression profiles in fiber / particles induced carcinogenesis**, Special Issue of International Journal of Human Genetics, 2007 March; 7(1): 1-21 (Review).
- **Bhattacharya, K;** Cramer, H; Zimmermann, U; Yadav, S; Geh, S; Shokouhi, B; Albrecht, C; Rahman, Q; Rettenmeier, AW; and E. Dopp; **Ultrafine titanium dioxide particles coated with vanadium pentoxide induce cellular damage and micronucleus formation in V79-cells.** Submitted to Journal of Toxicology and Environmental Health. Impact Factor : 1.811
- **Bhattacharya, K**; Hoffmann, E; Hartmann, L.M; Albrecht, C; Rettenmeier, A.W; Dopp, E; **Cellular uptake and toxicity of inhalable arsenopyrite particles and of its natural analogue hematite** (In progress).

**Conferences and Symposiums Attended:**

- 89TH Indian Science Congress, Lucknow, India. 2002.
- Musthapa, MS; Ameen, MM; Ansari, FA; **Bhattacharya, K**; Rahman, Q; Ahmad, I; **Modulation of macromolecules by particulate air pollutants**; 10th Congress of Federation of Asian and Oceanic Biochemists at IISC, Bangalore, India. 7 – 11, December, 2003. (Abstract)**.**
- Dopp, E; Cramer, W; **Bhattacharya, K**; Yadav, S; Geh, S; Shi, T; Büsselberg, D; Shokouhi, B; **Cyto-, geno- and neurotoxic effects of natural and surface-treated ultrafine titanium dioxide particles in mammalian cells, Nanoparticle Workshop;** Combustion Generated Nanoparticles and their Health Effects:Molecular and Cellular Basics, Gustav Stresemann Institut e.V. (GSI), Bonn, Germany. May 1- 4 2005. (Abstract and Poster)
- Dopp, E; Yadav, S; **Bhattacharya, K**; Rahman, Q; **Cyto- and genotoxicity of asbestos-cement in Mammalian lung cells *in vitro*.** EPA conference on "Mechanisms of Action of Inhaled Fibers, Particles, and Nanoparticles in Lung and Cardiovascular Disease", Research Triangle Park, NC, US. October 25-28, 2005. (Abstract).
- **Bhattacharya, K**; Geh, S; Rettenmeier, AW; Dopp, E: **Cyto-, geno- and neurotoxic effects of natural and surface-treated ultrafine titanium dioxide particles in mammalian cells,** Forschungstag (Annual Function), University Hospital Essen, Essen, Germany. November 17, 2005. (Poster)
- **Bhattacharya, K**; **Use of MALDI-TOF-MS in Genomic Research,** "Workshop des Forum Proteomics" (Annual Meeting), Bommerholz, Germany. June 30 – July 1, 2006. (Presentation and Abstract).
- **Bhattacharya, K**; Cramer, H; Yadav, S; Geh, S; Shokouhi, B; Albrecht, C; Schins, R; Rahman, Q; Rettenmeier, AW; Dopp, E; **Ultrafine titanium dioxide particlesy coated with vanadium pentoxide induce cellular damage and micronucleus formation in V79- cells.** International Symposium – Annual Meeting of the German Society of Biomaterials, Essen, Germany. September 5 – 8, 2006. (Poster and Abstract).
- **Bhattacharya, K**; Hoffmann,E; Hartmann, LM; Albrecht, C; Rettenmeier, AW; Dopp, E; **Cellular uptake and toxicity of inhalable arsenopyrite particles and its natural analogue hematite.** 48. Frühjahrstagung der DGPT, Mainz, Germany. March 13 – 15, 2007. (Poster and Abstract).
- **Bhattacharya, K;** Cramer, H; Zimmermann, U; Yadav, S; Geh, S; Shokouhi, B; Albrecht, C; Rahman, Q; Rettenmeier, AW; and E. Dopp; **Ultrafine titanium dioxide particles coated with vanadium pentoxide induce cellular damage and micronucleus formation in V79-cells.** EnTox , Dortmund, Germany. May 10 – 11, 2007. (Poster and Abstract).
- Elke Dopp, **Kunal Bhattacharya**, Eik Hoffmann, Catrin Albrecht, Roel Schins, Jens Boertz, Louise M. Hartmann, Gerrit Alink, Albert W. Rettenmeier; **Enhanced cyto- and genotoxic effects of Fe(III) nanoparticles compared to Fe(III) fine particles**, International Symposium on Nanotechnology in Environmental Protection and Pollution, Florida, US. December 11 – 13, 2007. (Presentation and Abstract)
- **Kunal Bhattacharya**, Eik Hoffmann, Catrin Albrecht, Roel Schins, Gerrit Alink, Elke Dopp; **Enhanced cyto- and genotoxic effect of Fe(III) nanoparticles compared to Fe(II) fine particles in human lung cells**; 47th Annual Meeting of Society of Toxicology, Seattle, US. March 16 – 20, 2008. (Poster and Abstract)

**Awards and Grant:**

- Best Poster Award: "**Ultrafine titanium dioxide particles coated with vanadium pentoxide induce cellular damage and micronucleus formation in V79-cells."** EnTox , Dortmund, Germany. May 10 – 11, 2007
- Grant: **Deutsche Forschungsgemeinschaft (DFG) travel grant** for visiting 47th Annual Meeting of Society of Toxicology, Seattle, US. March 16 – 20, 2008.

## Referees:

**Priv. Doz. Dr. Elke Dopp,**
Invitro Toxicology Division,
Institute of Hygiene and Occupational Medicine,
University Hospital Essen,
Hufelandstrasse 55,
45147 – Essen
Germany.
Email – elke.dopp@uni-due.de
Phone – 0049 201 723 4548

**Prof. (Dr.) A.W. Rettenmeier,**
Director,
Institute of Hygiene and Occupational Medicine,
University Hospital Essen,
Hufelandstrasse 55,
45147 – Essen
Germany.
Email – Albert.Rettenmeier@uni-due.de
Phone – 0049 201 723 4574 / 75

**Prof. (Dr.) Qamar Rahman,**
Emeritus Scientist,
Industrial Toxicology Research Centre, Lucknow, India
Professor Jamia Hamdard University, New Delhi, India
Visiting Professor Rostock University, Rostock, Germany.
Email- qamar_15@sify.com
Phone – 0091 522 2890730 / 812

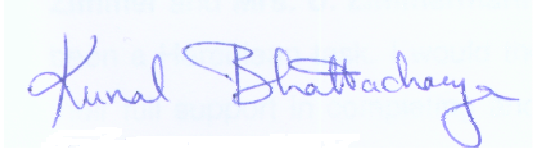

Essen, 2nd April. 2008.

**Kunal Bhattacharya:** *Institute of Hygiene and Occupational Medicine, University Hospital Essen, Hufelandstrasse55, 45147 - Essen, Germany.*
*Official ☎: +49 (0)201-7234510 Personal ☎ +49 (0)201-6955948*
*Email:* kunal.bhattacharya@uk-essen.de*;* kunal.bhattacharya@uni-due.de

## ACKNOWLEDGEMENT

*Words are never enough to pay my regards and gratitude to all the people who contributed their help in completing my doctoral work.*

With a profound sense of gratitude, I express my appreciation for the academic guidance, patience and encouragement rendered by my project supervisor **PD Dr. Elke Dopp**. Her constructive ideas, informative, fruitful and provocative discussion inspired me to work towards my objective. She is a kind hearted and generous lady who helped me in all possible ways during my stay in Germany and gave me guidance through all my troubles during this time.

I am extremely thankful to **Prof. A.W. Rettenmeier** for giving me the opportunity to do this interesting research work in the Institute of Hygiene and Occupational Medicine and helping me in the thesis work with productive discussions.

I also acknowledge the help and guidance of **Prof. G. Alink, Dr. T. Kuhlbusch, Prof. H. Grosse-Wilde Dr. R. Schins and Dr. C. Albrecht** for giving me the opportunity to work at their respective institutes and providing me proper guidance during experiments. I give special thanks to **Mr. E. Hoffmann** and **Ms. C. Katier** for helping me in doing electron microscopic uptake studies and comet assay analysis experiments.

I would also like to thank **Mr. J. Boertz, Dr. U. Recklinghausen, Dr. S. Geh, Dr. F. Petrat, Dr. S. Spanke, Dr. G. Muller** and **Dr. F. Mosel** for helping me with relevant discussions pertaining to experimental setups and data analysis.

I would like to express my deep gratitude to the dedicated team of technicians **Ms. G. Zimmer** and **Mrs. U. Zimmermann**. Without their support this PhD work would have been a Herculean task. I would therefore like to specially thank them for giving me their full support in completing and solving problems pertaining to experiments and help in maintaining good environment during my project.

I wish to thank **Prof. H. Esche**, for providing all the essential information regarding the Ph.D. procedure.

I also acknowledge to all other members of my institute for their help in different ways during my project work.

I specially thank all my friends **Ashish, Aparna, Janapriya, Manoj, Meenakshi, Savita, Satyendra and Sreenath** for helpful suggestions, morale boosting and encouragement.

Lastly, I am humbly thankful to my parents for their unending morale support and understanding. It is difficult to express my feelings and thankfulness in words for them. Their love and prayers have been a source of inspiration. Without their support and love, it is difficult to imagine anything in life.

**Erklärung:**
Hiermit erkläre ich, gem. § 6 Abs. 2, Nr. 7 der Promotionsordnung der Fachbereiche 6 bis 9 zur Erlangung des Dr. rer. nat., dass ich das Arbeitsgebiet, dem das Thema: "Comparative analysis of fine and nanoparticles for cellular uptake, oxidative stress and genomic damage in human lung cells" zuzuordnen ist, in Forschung und Lehre vertrete und den Antrag von Herrn Kunal Bhattacharya befürworte.

Essen, den 2. April 2008


**Erklärung:**
Hiermit erkläre ich gem. § 6, Abs. 2, Nr. 6 der Promotionsordnung der Fachbereiche 6 bis 9 zur Erlangung des Dr. rer. nat., dass ich die vorliegende Arbeit selbständig verfasst und mich keiner anderen als der angegebenen Hilfsmittel bedient habe.

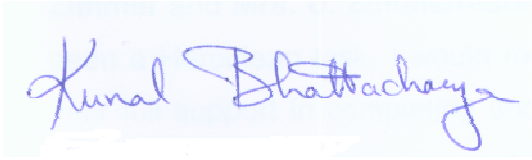

Essen, den 2. April 2008 Kunal Bhattacharya

**Erklärung:**
Hiermit erkläre ich gem. § 6, Abs. 2, Nr. 8 der Promotionsordnung der Fachbereiche 6 bis 9 zur Erlangung des Dr. rer. nat., dass ich keine anderen Promotionen bzw. Promotionsversuche in der Vergangenheit durchgeführt habe und dass diese Arbeit von keiner anderen Fakultät abgelehnt wurde.

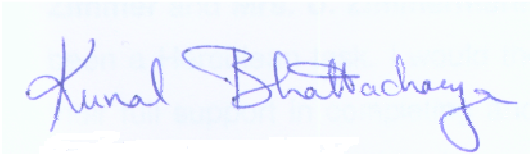

Essen, den 2. April 2008 Kunal Bhattacharya

**Appendix 11**

**Research paper and Review**